Design of new hybrid materials: study of its application in new detection formats and in controlled release

ESTELA CLIMENT TEROL

EDITORIAL
UNIVERSITAT POLITÈCNICA DE VALÈNCIA

UNIVERSITAT POLITÈCNICA DE VALÈNCIA

ESCOLA TÈCNICA SUPERIOR D'ENGINYERIA DEL DISSENY

Design of new hybrid materials: Study of its application in new detection formats and in controlled release applications.

PhD. THESIS

Submitted by

Estela Climent Terol

PhD. Supervisors:

Prof. Ramón Martínez Máñez
Dr. María Dolores Marcos Martínez

Valencia 2012

This editorial is member of the UNE, which guarantees the diffusion and commercialization of its publications at national and international level.

ISBN: 978-84-9048-015-1 (printed version)

Instituto Interuniversitario de Reconocimiento Molecular y Desarrollo Tecnológico

Escuela Técnica Superior de Ingeniería del Diseño

RAMÓN MARTÍNEZ MÁÑEZ, PhD in Chemistry and Professor at the Universitat Politècnica de València, and MARÍA DOLORES MARCOS MARTÍNEZ, PhD in Chemistry and Lecturer at the *Universitat Politècnica de València*.

CERTIFY:

That the work *"Design of new hybrid materials: Study of its application in new detection formats and in controlled release applications"* has been developed by Estela Climent Terol under their supervision in the Centro de Reconocimiento Molecular y Desarrollo Tecnológico de la *Universitat Politècnica de València*, as a thesis Project in order to obtain the degree of PhD in Chemistry at the *Universitat Politècnica de València.*

Valencia, November 23th 2012.

Prof. Ramón Martínez Máñez Dr. Mª Dolores Marcos Martínez

Als meus pares,

als meus germans, i a Victor.

“Tellus superata, Sidera donat”. Boecio

"Modelando la materia, crea estrellas"

Epitafio del sepulcro de Händel en la Abadía de Westminster

Acknowledgements.

Agraïments. Agradecimientos

Passet a passet, amb paciència i dedicació i no sense una miqueta d'esforç, tot allò que comença arriba a la seua fi. I és que per arribar fins ací el camí ha sigut una miqueta llarg i costós, però, sense cap dubte, ha sigut molt més fàcil gràcies a tots els que m'han acompanyat. Tots sabem que durant els anys en els que una Tesi Doctoral es realitza es genera un gran treball científic, però, a banda, m'agradaria destacar que també es genera un gran vincle amb tots aquells que, dia a dia t'ajuden a avançar, no sols com investigadora, sinó com a persona. Tots ells han fet possible que hui estiga ací escrivint aquestes paraules, i és per això que vos vull dir a tots, GRÀCIES!!

En primer lugar, me gustaría darles las gracias a mis directores de tesis, Loles y Ramón. Gracias a los dos por darme la oportunidad de hacer la tesis en vuestro grupo de investigación, por guiarme y aconsejarme, por enseñarme multitud de cosas sobre materiales, y por enseñarme a hacer investigación. Junto con vosotros, gracias Félix, por ayudarme en todo momento, por estar siempre ahí y por intentar solucionar cualquier duda en todo momento. Juan, muchas gracias por tus buenos consejos y por tu ayuda en la realización de modelos y cálculos de constantes. Gràcies JV, primerament per tindre el meu currículum en compte mentre buscaves gent, però sobretot per els teus consells i per la teua ajuda. Luís, gracias por tus buenas ideas y por tu agradable compañía en el lab, alegrándonos los ratos con tus creaciones de jazz. Ángel Maquieira, muchas gracias por tus consejos y por tu ayuda durante mi primer contacto con los anticuerpos, y Teresa, Ángel, Rafa y Fina, gracias por vuestros consejos durante mis prácticas docentes.

I would like to thank Dr. Knut Rurack for giving me the opportunity to stay in his research group nine months in Berlin within 2010-2012 and helping me with all, inside and outside the lab, without forgetting the nice moments outside the lab, showing me interesting and nicest places in Berlin! On the other hand, I would also like to say thank you to the awesome people of your research group, from

Jenny, Dominik or Ensar during their work in their Diplomarbeit or Erasmus periods, since research technicians, phD students or post-Doctoral researchers. Wei, Shengchao, Mustafa, Karin, Carsten, Tobias, Mandy and Delia, thanks for your help! Tobias, many thanks for your patience trying to help me with my measurements, and Karin and Mandy, thanks for your effort loading MCM-41 materials with dyes. Delia, muchísimas gracias por todo, dentro y fuera del laboratorio, por ayudarme con mis experimentos y por tu grata compañía, ¡y por las comidas al sol en el parque escondido del BAM! I would also say thanks to Asdrid for her help with my work with antibodies, and Jonas, for his help preparing strips. An alle, vielen Dank für eure Hilfe!!

Y como no, gracias a todos mis compañeros del Lab 2.6, desde todos aquellos que ya no están, todos los que han estado conmigo desde el primer día y todos los que están conmigo desde hace poco. Creo que, de un modo sencillo, podría definir a nuestro laboratorio como un pequeño puzle en el que cada uno somos como una pieza que encaja a la perfección. Somos un montón, y por ello somos muy diferentes, pero entre todos, y durante todos estos años, hemos conseguido crear una calidad humana increíble. Me gustaría daros las gracias a todos por vuestra amistad, por escucharme en todo momento, por ayudarme, y sobre todo por apoyarme, animarme y ayudar a levantarme en algún que otro momento.

¿Por donde empezar? Pues primero, a todos los que estaban cuando llegué. Gracias Hanoi, por ser la alegría del laboratorio, y por tus buenos consejos. Rosa, amb tu vaig aprendre algunes cosetes de materials i algunes cosetes més. Gràcies per tot! Pilar, esa cordobesa-valenciana con la que aprendí a bifuncionalizar nanopartículas, muchísimas gracias por todo lo que hemos compartido, y por todo lo que me has enseñado. Merche, mil gracias por estar siempre ahí. Santi (o Jaume), gràcies per tot el que m'has ensenyat i per tot el que hem compartit. Tati!! La artista del grupo… ¡gracias por los buenos momentos y por las risas que hemos compartido! Elena, Elena… que dirt-te, floreta? Simplement gràcies. Per fer de "mestra", per escoltar-me, per aconsellar-me, per ajudar-me sempre que no sabia com fer alguna coseta, en fi,…. gràcies perquè sempre que t'ho he demanat, o no, sempre, has estat ahí. I agafadeta de tu de la mà…. Carmen. Perla, a tu et toca el mateix! Gràcies perquè, pobretes meues, a les dos vos he acrivillat a

preguntes! Gracies per ajudar-me i escoltar-me en tot moment. I bé, per a completar el trio *la la la* falta la madrilenya-valenciana, que arribà tan sols tres mesets abans que jo. Andrea carinyet, gracias por ser mi compañera de viaje durante estos años en el lab, bueno y mi compañera en ingles, gym, en las cañitas… porque tu pobre Forfi seguro que me añora…. Gracias por estar siempre ahí, por escucharme y por ayudarme en todo momento.
Y, de igual modo, gracias a todos a los que os vi empezar. Cris S., compi de viaje en este camino durante la tesis y la diseñadora oficial del grupo, gracias por ser la más molona y ofrecernos cada día tu simpatía. Inma Candel, poliglota oficial del grupo, gracias por todo, entre otras cosas por ser embajadora de la EOI en el lab y por ofrecernos tus candeladas en todo momento. ¡Inma Campos! Gracias por tus buenos consejos y por "hacernos aburrir" contigo. Yoli, mil gracias por ofrecernos cada día tu alegría y tus risas. Por estar ahí dando tus buenos consejos y por los buenos ratitos que hemos compartido. María, más conocida como la organizadora pacífica oficial del lab, gracias por tu simpatía y por tus consejos. Laura, mil gracias por tus consejos, y por tus buenas ideas. Édgar! Gracietes per transmetre'ns eixa simpatía i alegría que sols tu ens saps donar. Alessandro, grazie per tutto! Por tus sabios consejos, tus risas y tu compañía. Maria Sapiña, gracietes per la teua companyía! Núria, tant dolçeta com els pastissos eixos tan bons que fas, gràcies per transmetre al lab la teua alegría. Cris G, valldalbaidina com jo! Gracietes per tindre una miqueta de paciència amb servidora, per escoltarme i per estar ahí. Luis Enrique, gracias por ofrecernos tu serenidad y simpatía. Roman, gràcies per ajudar-nos a reparar cosetes elèctriques, que d'això nosaltres anem venudes… i per transmetre la teua serenitat al grup. Sameh… ¡gracias por las pinceladas que nos ofreces de tus costumbres! Carolina, ¡gracias por transmitirnos tu simpatía! Patri, gràcies per oferir-nos la teua simpatía i ajudar-nos sempre que t'ho demanem, i bé, als que fa menys temps que vos conec, Lluís, Mar, Cris de la Torre, Miriam i Salva, mil gràcies perquè amb la vostra joventut heu aportat nous aires al lab! Gràcies per la vostra companyia i per la vostra ajuda!

Por otro lado, me gustaría dar las gracias a todas las personas que trabajan en el edificio 5M, especialmente a mis compañeros del laboratorio del grupo de Angel Maqueira, que me han acogido como una más al mudarme a la primera planta,

especialmente a Patricia, Eva, Núria, Tania, Dolors, Chelo, Sara y Diana. También daros las gracias a los compañeros del 2.2 y 2.5, desde Belén, Raúl, Carlos, Nacho, Pavel, Dani, Neus, Paula, Sergio, Murty, Maykel, Mireia, Roberto, Rafa, David y todos los demás, gracias por vuestra ayuda y por vuestras risas fuera del lab. A Quique, gracias por tu ayuda en los papeleos! Y a mis compañeros de Burjassot, en especial a Andrea y Almudena, con las que he compartido algún que otro ratito, muchas gracias por vuestra ayuda y compañía!

I bé, a banda de tots vosaltres, fóra del lab també hi ha molta gent a la que m'agradaria donar-vos les gràcies per estar ahí durant aquestos anys. Als meus amics, en especial la meua pastissereta Adri, gracietes per preocupar-te sempre per mi. També, gràcietes a un altra amiga especial, a la música i a tota la gent què m'envolta gràcies a ella. Als meus companys de la BACM i de Clarialba, a tots ells i a la meua amiga de sis forats, gràcies, perquè en molts moments m'heu donat la possibilitat de fer un "canvi de xip" total. També, i com molt be diu el refrany, "quien canta su mal espanta", i amb vosaltres n'he aconseguit espantar uns quants.

Finalment, també m'agradaria agraïr, d'una manera especial, a aquells que sempre, haja passsat el que haja passat, han estat ahí, preguntant-me moltes vegades que com anava la cosa, o mostrant interés moltes vegades sense acabar d'entendre el rollet que els estava contant, sempre amb l'objectiu d'intentar ajudar. Ells són la meua familia. Als meus pares, perquè sóc tot el que vosaltres m'heu donat. Gràcies als dos pel vostre esforç, per cuidar-me sempre i ajudar-me a créixer dia a dia. Gràcies per estar, cadascú des d'on esteu, sempre presents. Als meus germans, gràcies per estar sempre ahí i per ajudar-me en tot moment, tenint una miqueta de paciència amb mi. Al meu iaio, gràcies pels teus savis consells, tots ells en poesíes que encara recordes de l'escola, i com no, gràcies a tu Vic, gràcies per tindre la paciència i la serenitat que et caracteritzen, per intentar entendre'm i per donar-me eixa miqueta de llum quan moltes vegades ho veig tot negre. Gràcies per espentar del carro durant tots aquestos anys!

Resumen

La presente tesis doctoral titulada “Diseño de nuevos materiales híbridos: Estudio de su aplicación en nuevos formatos de detección y en procesos de liberación controlada” está centrada en el desarrollo de nuevos materiales híbridos orgánico-inorgánicos funcionales basados en la combinación de los principios de la Química Supramolecular y la Ciencia de los Materiales.

La primera parte de la tesis se centra en el diseño y la preparación de nuevos materiales que poseen la habilidad de modular el acceso a su superficie empleando conceptos de Química Supramolecular. Estos sistemas están diseñados pensando en soportes silíceos que contienen dos grupos diferentes, un grupo que actúa como centro reactivo capaz de reaccionar con un colorante (observando un cambio de color o fluorescencia) y un segundo grupo que modula el acceso del colorante al centro reactivo en función de alguna modificación producida en el medio o de la presencia de alguna especie química. Teniendo en cuenta este sistema, seleccionamos a las escuaridinas como colorante y a los grupos tiol como centro reactivo, debido a que la reacción de ambos grupos produce un cambio de color de azul a incoloro. Por otro lado, seleccionamos primeramente grupos poliamina como agentes modulantes, con la finalidad de detectar especies aniónicas. La coordinación de las poliaminas con aniones modula el acceso de la escuaridina a los tioles anclados en la superficie de sílice, y, con ello, se consigue reconocer a estas especies en disolución, detectando pirofosfato y heparina de forma selectiva. Basándonos en el mismo protocolo de reconocimiento se preparó otro material híbrido para el reconocimiento de surfactantes aniónicos en agua, utilizando en este caso grupos imidazol como agentes coordinantes.

Por otro lado, el resto de la Tesis se basa en el diseño, síntesis y caracterización de nuevos materiales híbridos que actúan como puertas moleculares para la detección de especies químicas empleando soportes mesoporosos. Los materiales preparados pueden almacenar un colorante dentro de los poros. Después de la

aplicación de un estímulo externo que module las propiedades de las moléculas que bloquean los poros del material, como la presencia de especies pequeñas, el colorante se libera a la disolución. Teniendo en cuenta este concepto, en el segundo capítulo se reporta la síntesis de un nuevo nanodispositivo para la detección de metilmercurio, diseñando un sólido híbrido teniendo en cuenta la gran afinidad que posee el metilmercurio por los grupos tiol. En el tercer capítulo se han preparado tres nuevos materiales híbridos orgánicos inorgánicos teniendo en cuenta la afinidad que presenta un antígeno por un anticuerpo. Con estos materiales se pudieron detectar los antígenos sulfatiazol (un antibiótico de la familia de las sulfonamidas), finastéride (un inhibidor de la 5α-reductasa) y TATP (un explosivo). Finalmente, y teniendo en cuenta la hibridación del ADN, el último capítulo muestra un nuevo material que libera un colorante debido al reconocimiento entre dos oligonucleótidos complementarios.

En resumen, se puede decir que los nuevos materiales híbridos orgánico-inorgánicos preparados en esta tesis ofrecen nuevos formatos de detección para las especies químicas. Por otro lado, la preparación de materiales híbridos para la liberación controlada en presencia de anticuerpos o oligonucleótidos ofrece la posibilidad de aplicar estos nanodispositivos en diferentes áreas, como la química analítica, biotecnología o en el campo del diagnóstico clínico.

Resum

La present Tesi doctoral titulada "Disseny de nous materials híbrids: Estudi de la seva aplicació en nous formats de detecció i en processos de lliberació controlada" està centrada en el desenvolupament de nous materials híbrids orgànic-inorgànics funcionals basats en la combinació dels principis de la Química Supramolecular i la Ciència dels Materials.

La primera part de la Tesi es centra en el disseny i la preparació de nous materials que tenen l'habilitat de modul·lar l'accés a la seua superfície utilitzant conceptes de Química Supramolecular. Aquestos sistemes estan dissenyats pensant en suports silicis que contenen dos grups diferents: Un grup que actua com centre reactiu capaç de reaccionar amb un colorant (observant un canvi de color o de fluorescència) i un segon grup que modul·la l'accés del colorant al centre reactiu en funció d'alguna modificació produïda al medi o de la presència d'alguna espècie química. Tenint en compte aquest sistema, decidírem sel·leccionar com a colorant a les esquaridines i als grups tiol com a centre reactiu, degut a que la reacció entre ambdós grups produeix un canvi de color de blau a incolor. Per altra banda, seleccionàrem, en un primer treball, grups poliamines com agents modul·lants, amb la finalitat de detectar espècies aniòniques. La coordinació de les poliamines amb anions modul·la l'accés de la esquaridina als tiols ancorats a la superficie de sílice. Amb açò, es conseguí reconéixer aquestes espècies en dissolució, detectant pirofosfat i heparina de forma selectiva. Basant-nos en el mateix protocol de reconeixement, es preparà un altre material híbrid per al reconeixement de surfactants aniònics en aigua, utilitzant en aquest cas grups imidazol com agents coordinants.

Per altra banda, la resta de la Tesi es basa en el disseny, síntesi i caracterització de nous materials híbrids que actuen com portes moleculars per a la detecció d'espècies químiques utilitzant suports mesoporosos. Els materials preparats poden emmagatzemar un colorant al seu interior. Després de l'aplicació d'un estímul extern que modul·le les propietats de les mol·lècules que bloquejen els

pors del material, com la presencia d'espècies xicotetes, el colorant es llibera a la dissolució. Tenint en compte aquest concepte, en el segon capítol s'ha preparat un nou sòlid híbrid basant-nos amb la gran afinitat que poseeix el metilmercuri per els grups tiol. Al tercer capítol s'han preparat tres nous materials híbrids orgànic-inorgànics tenint en compte l'afinitat que presenta un antígen per un anticòs. Amb aquestos materials es poguéren detectar els antígens sulfatiazol (un antibiòtic de la familia de les sulfonamides), finastèride (un inhibidor de la 5α-reductassa) i TATP (un explosiu). Finalment, i tenint en compte la hibridació de l'ADN, l'últim capítol mostra un nou material que llibera un colorant degut al reconeixement entre dos oligonucleòtids complementaris.

Abstract

This thesis entitled " Design of new hybrid materials: Study of its application in new detection formats and in controlled release applications", is focused on the development of new functional hybrid organic-inorganic materials based on the combination of Supramolecular Chemistry and Materials Science principles.

The first part of the thesis is focused on the design and preparation of new materials with the ability to control the access to their surface using concepts of Supramolecular Chemistry. These systems are based on silica supports containing two different groups, one group that act as a reactive center, and it is able to produce a measurable change in color or fluorescence upon reaction with a selected dye. The other group modulates the access of dye to the surface upon a change in the media or after addition of certain target species. Bearing in mind this proposed system, we selected squaraines as reporter molecules and thiols as reactive centers, due to the change in color produced upon reaction between both species. On the other hand, the first host selected was polyamines as binding sites in order to detect anionic species. Coordination of polyamines with anions modulates the access of squaraine to the thiols anchored onto silica surface and, with this, detection of these species in solution is achieved. Using the same recognition protocol, another hybrid material for the colorimetric detection of anionic surfactants in water is prepared, using in this case imidazolium groups as binding sites.

The other part of the thesis is focused on the design, synthesis and characterization of new hybrid materials than acts as molecular gates for the detection of chemical species. Prepared materials can store a dye inside of the pores. Upon application of a stimulus that triggers the release, such as the presence of small molecules, dye can be released to the solution. Using this concept, in the second chapter is reported the synthesis of a novel probe device for methylmercury detection, using a molecular gated hybrid solid, bearing in mind the strong affinity between methylmercury and thiol moieties. In the third

chapter, three hybrid organic-inorganic mesoporous materials that are triggered by antigen-antibody immunological process are showed, allowing the detection of the antigens sulfathiazole (an antibiotic of the sulfonamides family), finasteride (a 5α-reductase inhibitor) and TATP (an explosive). Finally, and bearing in mind DNA hybridisation process, the last chapter presents a material in which the release is triggered by recognition between two oligonucleotides.

In summary, the new hybrid organic-inorganic solids described in this thesis offers new detection format for chemical species. On the other hand, preparation of hybrid materials for controlled guest release in the presence of antibodies or oligonucleotides offers the possibility to apply these nanodevicess in analytical chemistry, biotechnology or in clinical diagnostic field.

Results of this thesis and other contributions have resulted in the following scientific publications:

Rosa Casasús, Estela Climent, María Dolores Marcos, Ramon Martínez Mañez, Félix Sancenón, Juan Soto, Pedro Amorós, Joan Cano, Eliseo Ruiz, *Dual aperture control on pH- and anion-driven supramolecular nanoscopic hybrid gate-like ensembles*, J. Am. Chem. Soc., 2008, 130, 1903 - 1917.

Estela Climent, Rosa Casasús, María Dolores Marcos, Ramón Martínez-Mañez, Félix Sancenón, Juan Soto, *Chromo-fluorogenic sensing of pyrophosphate in aqueous media using silica functionalised with binding and reactive units,* Chem. Commun., 2008, 6531 – 6533.

Estela Climent, Pilar Calero, María Dolores Marcos, Ramón Martínez-Máñez, Félix Sancenón, Juan Soto, *A selective chromo-fluorogenic sensing of heparin using functionalised silica nanoparticles containing binding sites and a signalling reporter,* Chemistry a European Journal, 2009, 15, 1816 – 1820.

Estela Climent, Rosa Casasús, María Dolores Marcos, Ramón Martínez-Máñez, Félix Sancenón, Juan Soto, *Colorimetric sensing of pyrophosphate in aqueous media using bis-functionalised silica surfaces,* Dalton Transactions, 2009, 4806 – 4814.

Estela Climent, Andrea Bernardos, Ramón Martínez-Máñez, Angel Maquieira, María Dolores Marcos, Nuria Pastor-Navarro, Rosa Puchades, Félix Sancenón, Juan Soto, Pedro Amorós, *Controlled Delivery Systems Using Antibody-Capped Mesoporous Nanocontainers*, J. Am. Chem. Soc., 2009, 131, 14075 – 14080.

Estela Climent, María Dolores Marcos, Ramón Martínez-Máñez, Félix Sancenón, Juan Soto, Knut Rurack, Pedro Amorós*, The Determination of Methylmercury in Real Samples Using Organically Capped Mesoporous Inorganic Materials Capable of Signal Amplification,* Angew. Chem. Int. Ed., 2009, 48, 8519 – 8522.

Estela Climent, Almudena Martí, Santiago Royo, Ramón Martínez-Máñez, María Dolores Marcos, Félix Sancenón, Juan Soto, Ana M. Costero, Salvador Gil, Margarita Parra. *Chromogenic Detection of Nerve Agent Models by Mass Transport Control at the Surface of Bifunctionalized Silica Nanoparticles,* Angew. Chem. Int. Ed., 2010, 49, 5945 – 5948.

Estela Climent, Ramón Martínez-Máñez, Félix Sancenón, María Dolores Marcos, Juan Soto, Angel Maquieira, Pedro Amorós, *Controlled Delivery Using Oligonucleotide-Capped Mesoporous Silica Nanoparticles*, Angew. Chem. Int. Ed., 2010, 49, 7281 – 7283.

Estela Climent, Cristina Giménez, María Dolores Marcos, Ramón Martínez-Máñez, Félix Sancenón, Juan Soto*, Selective and Sensitive chromo-fluorogenic sensing of anionic surfactants in water using functionalized silica nanoparticles*, Chem. Comm., 2011, 47, 6873 – 6875.

Inmaculada Candel, Andrea Bernardos, Estela Climent, María Dolores Marcos, Ramón Martínez-Máñez, Félix Sancenón, Juan Soto, Ana Costero, Salvador Gil, Margarita Parra, *Selective opening of nanoscopic capped mesoporous inorganic materials with nerve agent simulants; an application to design chromo-fluorogenic probes,* Chem. Comm., 2011, 47, 8313 – 8315.

Yolanda Salinas, Estela Climent, Ramón Martínez-Mañez, Félix Sancenón, María Dolores Marcos, Juan Soto, Ana Costero, Salvador Gil, Margarita Parra, Alberto Perez de Diego.*Highly selective and sensitive chromo-fluorogenic detection of the Tetryl explosive using functional silica nanoparticles.* Chem. Comm., 2011, 47, 11885 – 11887.

Estela Climent, Ramón Martínez-Máñez, Ángel Maquieira, Félix Sancenón, María Dolores Marcos, Eva María Brun, Juan Soto, Pedro Amorós. *Antibody-Capped Mesoporous Nanoscopic Materials: Design of a Probe for the Selective Chromo-*

Fluorogenic Detection of Finasteride. Chemistry Open, 2012, in press, DOI: 10.1002/open.20.

Estela Climent, Delia Gröninger, Mandy Hecht, M. Astrid Walter, Ramón Martínez-Máñez, Michael G. Weller, Félix Sancenón, Pedro Amorós, and Knut Rurack, *Selective and sensitive detection of TATP with antibody-gated dye delivery from mesoporous hybrid nanoparticles in a lateral flow assay*, submitted.

Luis E. Santos-Figueroa, María E. Moragues, Estela Climent, Alessandro Agostini, Ramón Martínez-Máñez, Félix Sancenón, Chem. Soc. Rev., *Chromogenic and fluorogenic chemosensors and reagents for anions. A comprehensive review of the years 2010-2011,* **2012,** submitted.

Estela Climent, María Dolores Marcos, Ramón Martínez-Mañez, Félix Sancenón, Juan Soto, "Sistema de liberación controlada activado por oligonucleótidos", Patent application P201000900. Date: 12th July 2010.

Abbreviations

ADP	Adenosine Diphosphate
APC group	2,4-Bis(4-Dialkylaminophenyl)-3-Hydroxy-4-Alkylsulfanylcyclobut-2-Enone
AS	Anionic Surfactant
ATP	Adenosine Triphosphate
AuNPs	Gold Nanoparticles
BET	Brunauer, Emmett and Teller Model
BJH	Barret, Joyner and Halenda Model
BSA	Bovine Serum Albumin
CB[n]	Cucurbit[n] uril Rings
$CBPQT^{4+}$	Cyclobis(Paraquat-P-Phenylene)
CD	Cyclodextrine
CHES	N-Cyclohexyl-2-Aminoethanesulfonic Acid
CS-PMAA	Chitosan-Polymethacrylic Acid
CTAB	Hexadecyltrimethylammonium Bromide
DB24C8	Dibenzo[24]Crown-8
DNA	Deoxyribonucleic acid
DNPD	Dioxynaphthalene
DTT	Dithiotheritol
ELISA	Enzyme Linked Immunosorbent Assay
Fmoc	Fluorenylmethoxycarbonyl
HPLC	High Performance Liquid Chromatography
ICSs	Ion-Channel Sensors
IEDs	Improvised Explosive Devices
IR	Infra Red
$Ir(ppy)_3$	Iridium, tris(2-phenylpyidine)
KLH	Keyhole Limpet Hemocyanin
LS	Lauryl Sulfate
LCST	Lower Critical Solution Temperature

MCM	Mobile Crystalline Material
ME	Mercaptoethanol
MIPs	Molecular Imprinted Polymers
MO	Methyl Orange
MPTS	Mercaptopropyltrimethoxysilane
MSN	Mesoporous Silica Nanoparticles ()
MUA	16-Mercaptoundecanoic Acid
N3TS	3-[2-(2-Aminoethylamino)Ethylamino]Propyltrimethoxysilane
NMR	Nuclear Magnetic Resonance
PAA	Poly(Acrylic) Acid
PBEs	Peroxide-Based Explosives
PBS	Phosphate-Buffered Saline
PDDA	Poly-(Dimethyldiallylammonium Chloride
PMOs	Periodic Mesoporous Organosilicas
PNIPAAm	N-Isopropylacrylamide
PXRD	Powder X-Ray Diffraction
$Ru(bipy)_3^{2+}$	Tris(2,2'bipyridyl)Ruthenium(II)
SAMs	Self-Assembled Monolayer Surfaces
SBA	Santa Barbara Amorphous Material
SMP	Silica Mesoporous Material
Squaraine I (sq)	4-(Bis(2-(2-Methoxyethoxy)Ethyl))Aminophenyl Squaraine
STZ	Sulfathiazole
TATP	Triacetone Triperoxide
$TEAH_3$	Triethanolamine
TEM	Transmission Electron Microscopy
TEOS	Tetraethylorthosilica
TGA	Termogravimetric Analysis
TLCT	True Liquid-Crystal Templating Mechanism
TMOS	Tetramethylorthosilica
TTF	Tetratuiafulvalene
UV	Ultraviolet
UVM	Universidad Valencia Material

Content

General introduction

1.1 **Supramolecular Chemistry.**

Chemistry, is the science that studies the nature, structure, properties, and composition of matter. Chemistry also studies how matter undergoes changes during reactions and the energetic balance in these processes. The main basis of chemistry is the creation of molecular assemblies employing a controlled formation or breaking of covalent bonds. In the same context, supramolecular chemistry examines the weaker and reversible noncovalent interactions between molecules. These forces include hydrogen bonding, metal coordination, hydrophobic forces, van der Waals forces, π-π interactions and electrostatic effects, [1] with the aim to easily generate unique nanostructured supermolecules

[1] Taylor & Francis Group, Encyclopedia of Supramolecular Chemistry, Vols. 1, 2 (Ed.: Atwood, J.L.; Steed, J.W.), LLC, New York, 2004.

that presented different properties (often better) than the sum of the properties of each individual component.[2]

Supramolecular chemistry appears during the decade of 1960 with the pioneering works of Pedersen, Cram and Lehn, who's received the Nobel Prize in 1987 for their contributions to the development of this new area inside chemistry. According to Dr. Lehn, who introduced the term, a *supermolecule* is an organized complex entity that is created from the association of two or more chemical species held together by intermolecular forces, whereas the term *Supramolecular Chemistry* may be defined as *"chemistry beyond the molecule"*, focusing on the organized entities of higher complexity that result from the association of two or more chemical species held together by intermolecular forces.[3]

Development of Supramolecular Chemistry was inspired primarily by Nature, which displays a wide variety of complex nanostructures originated during processes that occur in biology, such as substrate binding to a receptor protein, enzymatic reactions, assembling of protein-protein complexes, immunological antigen-antibody association, intermolecular reading, translation and transcription of the genetic code, signal induction by neurotransmitters, etc.

The emergence of supramolecular chemistry has a deep effect on how efficiently chemists prepare structures of different sizes and shapes with dimension in the range of 1 to 100 nm. Molecules can be associated by their geometric or electronic affinity yielding supramolecular aggregates that presented new properties and characteristics that are very difficult to achieve by the isolated molecular entities. Due to this fact, incorporation of molecules onto materials offers new developments in the area of nanoscience and nanotechnology.

[2] K. Ariga, T. Kunitake, *Supramolecular Chemistry-Fundamentals and application*, Springer-Verlag Heidelberg.

[3] J. -M. Lehn, Supramolecular Chemistry, Ed. VCH, 1995; J.-M. Lehn, Nobel lecture, **1987**

1.2 **Molecular recognition: Molecular chemical sensors.**

Molecular recognition can be defined as the selective interaction between a host or receptor molecule and a guest or substrate through *non-covalent interactions*. In order to form a supermolecule, the receptor and guest must have mutual spatial and electronically complementary binding sites, or, in other words, they must follow the *lock and key principle*, (Figure 1) in which the guest has a geometric size or shape complementary to the receptor or host. This concept laid the basis for *molecular recognition*; i.e. the discrimination by a host between a number of different guests.

If, in addition to binding sites, the receptor also bears reactive groups, it may produce a chemical transformation on the bound substrate, thus behaving as a supramolecular reagent or catalyst. Thus, molecular recognition, transformation and translocation represent the basic functions of supramolecular species.

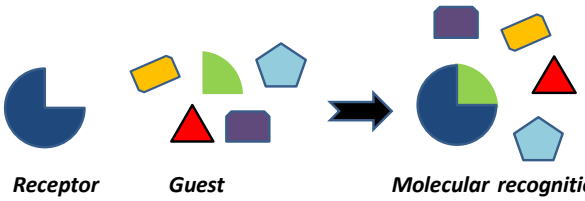

Figure 1. Scheme of a molecular recognition event by an specific host-guest interaction.

Bearing in mind this concept, in order to design a suitable receptor for a specific guest, some factors of the guest should be considered, as for example, the size, charge, geometry, hydrophilicity or lipophilicity or the possible formation of hydrogen bonds. On this basis, a myriad of receptors that mimic the behavior of biological systems have been described. These synthesized abiotic receptors are able to recognize cations, anions and neutral molecules.[4]

[4] a) M. D. Best, S. L. Tobey, E. V. Anslyn, *Coord. Chem. Rev.*, **2003**, *240*, 3. b) J. M. Llinares, D. Powell, K. Bowman-James, *Coord. Chem. Rev.*, **2003**, *240*, 57. c) K. A. Schug, W. Lindner, *Chem. Rev.*, **2005**, *105*, 67. d) J. Yoon, S. K. Kim, N. J. Singh, K. S. Kim, *Chem. Soc. Rev.*, **2006**, *35*, 355. e) P. Blondeau,

One of interesting applications of these receptors is their use for the development of molecular chemical sensors. A *molecular sensor* or *chemosensor* is a molecule than interacts with an analyte producing a detectable signal. Chemosensors combine molecular recognition events with the generation of a macroscopic signal (by a reporter molecule) that revealed the presence of the guest.[5] This phenomenon should be selective, reversible and fast, in order to be applicable. Whereas chemical sensors or chemosensors usually refer to systems that typically used coordinative forces for guest binding the term reagents or chemodosimeter is related with the use of specific irreversible reactions involving guests.[6]
A molecular sensor or chemosensor usually contains two units:

- ✓ A *receptor subunit*, which is the responsible of recognition and also of the efficiency of the interaction with the selected substrate. The receptor subunit must be designed with the aim of achieve a selective coordination with the target guest. In order to achieve selectivity a high degree of complementarity between the receptor and the guest (in terms of size, shape, charge, etc.) is mandatory.

- ✓ A *signaling subunit*, which acts as a signal transducer, and informs of the recognition process that occurs at molecular level with a measurable macroscopic signal. Traditionally, changes in colour, fluorescence or redox potential have been used as signal outputs.

Chromo-fluorogenic sensors offers significative advantages over other analytical methods such as: It is a non-destructive detection method, uses simple and extended instrumentation, needs small amounts of samples and allow, in some

M. Segura, R. Pérez-Fernández, J. de Mendoza, *Chem. Soc. Rev*., **2007**, *36*, 198. f) Z. Xu, S. K. Kim J. Yoon, *Chem. Soc. Rev*., **2010**, *39*, 1457. g) J. W. Steed, Chem. Soc. Rev., **2009**, 38, 506. h) V. Amendola, L. Fabbrizzi, Chem. Commun., **2009**, 513.

[5] W. C. Rogers, M. O. Wolf, *Coord. Chem. Rev.,* **2002**, *233*, 341

[6] a) R. Martínez-Máñez, F. Sancenón, *Chem. Rev.*, **2003**, *103*, 4419. b) M. Moragues, R. Martínez-Máñez, F. Sancenón, *Chem. Soc. Rev.*, **2011**, *40*, 2593.

cases, in situ detection and in real-time measurements. Colorimetric sensors induced noticeable color changes, observable with the naked eye, and can be used for rapid qualitative determinations. On the other hand, fluorogenic sensors have a high degree of sensitivity and specificity due to the possibility of specifying excitation and emission wavelengths, and normally allow to achieve lower detection limits when compared with colorimetric techniques.

Practically, all the reported examples of chromo-fluorogenic chemosensors described in the literature are constructed by the application of one of the three main approaches described below (see also Figure 2):

- ✓ *Binding site–signalling subunit approach*: Chemosensors constructed using this approach are formed by two subunits namely a "binding site" and a "signaling subunit" linked through a covalent bond. The interaction of target molecule with the binding site changes the electronic properties of the signaling subunit (a dye or a fluorophore) resulting in a sensing event via color or emission modulation.[7]

- ✓ *The displacement approach*: This approach also uses binding sites and signaling subunits but in this case these are not covalently bonded but forming a molecular ensemble. The sensing paradigm relies on a displacement reaction because the coordination of the target molecule with the binding site induced the release of the signalling subunit. An optical response is obtained because the color or emission of the signaling subunit in the sensing ensemble are different than those presented when it is free in solution.[8]

[7] a) T. Gunnlaugsson, M. Glynn, G. M. Tocci, P. E. Kruger, F. M. Pfeffer, *Coord. Chem. Rev*., **2006**, *250*, 3094. b) V. Amendola, D. Esteban-Gómez, L. Fabbrizzi, M. Lichelli, *Acc. Chem. Res*., **2006**, *39*, 343.
c) T. Gunnlaugsson, H. D. P. Ali, M. Glynn, P. E. Kruger, G. M. Hussey, F. M. Pfeffer, C. M. G. Dos Santos, J. Tierney, J. *Fluoresc*., **2005**, *15,* 287.

[8] a) S. L. Wiskur, H. Ait-Haddou, J. J. Lavigne, E. V. Anslyn, *Acc. Chem. Res*., **2001**, *34*, 963. b) B. T. Nguyen, E. V. Anslyn, *Coord. Chem. Rev*., **2006**, *250*, 3118.

- ✓ The *''chemodosimeter'' approach*: This approach takes advantage of target induced chemical reactions that generate fluorescence or color changes.[9]

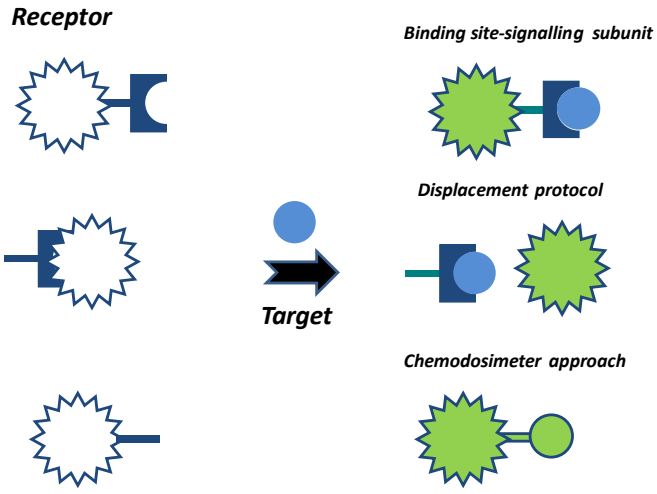

Figure 2. Representative scheme of the three main approaches used in the development of optical chemosenors.

Scientists working in the field of supramolecular chemistry are interested in the topology and arrangement of functional groups within molecules, always with the same aim: improve the properties (such as selectivity) of these molecular devices.[10] For these, processes of *translocation* (changes in position of molecules or ions in a controlled fashion) or *self-assembly* (where simple structural molecular units self-organize to yield macromolecular aggregates of nano and micrometric dimensions with new properties) have been used in the design of new chemosensors. Also, these concepts and processes have been applied for desingning novel "hetero-supramolecular" hybrid organic-inorganic materials for their use in signalling applications. These hybrid organic-inorganic materials have

[9] Z. Xu, X. Chen, H. N. Kim, J. Yoon, *Chem. Soc. Rev*., **2010**, *39*, 127–137.

[10] P. D. Beer, P. A. Gale, *Angew. Chem. Int. Ed.* **2001**, *40*, 486.

been constructed by the anchoring of certain molecular receptors (synthesized bearing in mind the supramolecular chemistry concepts) in the surface of selected 2D or 3D inorganic scaffoldings.

1.3 **Organic-inorganic hybrid materials.**

The development of organic-inorganic hybrid materials started with the aim to synthesize complex systems with innovative synergic effects, which are impossible to achieve with simple molecular receptors, and improved features.[11] These materials are easily obtained by the covalent anchoring of molecular (organic) receptors into nanoscopic inorganic materials as supporting platforms.[12]

Hybrid organic inorganic materials are not simply physical mixtures. They can be broadly defined as molecular or nano-composites with (bio)organic and inorganic components, intimately mixed where at least one of the component domains has a dimension ranging from a few Å to several nanometers. Consequently the properties of hybrid materials are not only the sum of the individual contributions of both phases, but the role of their inner interfaces could be predominant.[13] Incorporation of organic molecules on solid supports by covalent bonding offers certains advantages:

- ✓ Receptors can be organized in a more or less compact monolayer (depending on the degree grade of the surface functionalization), and, due to this, the movement of the different sensors is reduced and this generates new collective proceses that improve the features of the sensing process, such as "surface chelate effect" with monodentate ligands or an increase on the "effective concentration" on the solids.

[11] a) *Coord. Chem. Rev.*, Ed P. A. Gale, **2006**, *250*. b) J. F. Callan, A. P. de Silva, D. C. Magri, *Tetrahedron,* **2005**, *61*, 8551. c) G. J. Mohr, *Sens. Actuators B,* **2005**, *107*, 2.

[12] K. Rurack, R. Martínez-Máñez, *The supramolecular chemistry of organic-inorganic hybrid materials*, **2010**, ed. John Wiley & Sons.

[13] C. Sánchez, *J. Mater. Chem.*, **2005**, 15, 3557.

- ✓ It is possible to realize subsequent anchoring processes to obtain a solid surface functionalized with different organic molecules and thus modulate their properties according with the nature of the anchored molecules.

- ✓ Leaching processes involving the receptor are avoided.

- ✓ If the solid support is functionalized with a receptor that could give reversible coordination processes it can be reused several times without lost of their sensing features.

As we have cited before, the combination of supramolecular principles and nanoscopic solid structures enables the design of new hybrid sensing ensembles with improved sensitivity and/or selectivity for the targeting of analytes for which selectivity is hard to achieve by conventional methods.[14] Some relevant examples, taking into account their functional aspects, will be detailed bellow.

1.3.1 Effect of pre-organization onto surfaces.

One of the most common ways to obtain hybrid materials at the nanoscopic scale is to anchor certain functional molecular units on the surface of nanoscopic inorganic scaffoldings. As a consequence, an enhancement of guest recognition, compared to the free receptor in solution, is observed. This phenomenon is produced due to the pre-organization of the receptor molecule on the surface of the inorganic scaffold. This pre-organization leads to the formation of a dense monolayer of binding/coordination sites arranged in specific positions in order to maximize the interaction with the target analyte.

[14] a) A. Verma, V.M. Rotello, *Chem. Commun.*, **2005**, 303. b) U. Drechsler, B. Erdogan, V. M. Rotello, *Chem. Eur. J.*, **2004**, *10*, 5570. c) A. B. Descalzo, R. Martínez-Máñez, F. Sancenón, K. Hoffmann, K. Rurack, *Angew. Chem. Int. Ed.*, **2006**, *45*, 5924. d) F. Mancin, E. Rampazzo, P. Tecilla, U. Tonellato, *Chem. Eur. J.*, **2006**, *12*, 1844. e) I. Willner, B. Basnar, B. Willner, *Adv. Funct. Mater.*, **2007**, *17*, 702.

Gold or silica are the most commonly used surfaces for the grafting of organic moieties due to the easy and known process of functionalization. On the other hand, a large number of chemicals with several organic groups used for modification of surfaces are commercially available. Examples of surface-assisted enhancement of recognition have been mainly reported for gold nanoparticles (AuNPs) functionalized with thiols containing binding sites, yielding hybrid materials with organic moieties anchored onto the surface. Mayor and Zhu described AuNPs containing 16-mercaptohexadecanoic acid (MHA) as a ligand, in order to form mono and bidentate complexes with Cu^{2+} cation.[15] Using modified AuNPs with MHA, autors prepared layer assemblies by first attaching a monolayer of 16-mercaptohexadecanoic acid (HS-$(CH_2)_{15}$-COOH) to a gold substrate. In order to estimate the magnitude of the surface chelate effect, the authors compared the stability constant for surface complexation with the stability constants in solution, bearing in mind that succinic acid (HOOC-$(CH_2)_2$-COOH) and glutaric acid (HOOC-$(CH_2)_3$-COOH) are able to chelate bivalent metal ions by forming seven- and eight-membered rings, respectively. At this respect, the ratio K_{surf}/K_{soln} for Cu^{2+} complexation for succinic and glutaric acid showed values of 119 and 213, respectively. These higher stability constants for hybrid materials were ascribed to the fact that after the coordination of Cu^{2+} with one surface carboxylic group, there was a great propensity for the metal ion to bind to one of the six neighboring carboxylic groups present on the monolayer.

The same effect was observed by Beer et al. They prepared AuNPs functionalized with disulfide-containing zinc metalloporphyrins (See Figure 3).[16] These hybrid AuNPS were able to coordinate with chloride and $H_2PO_4^-$ anions in DMSO, with association constants (log *K*) of 4.3 and 4.1, respectively. These constant values were 2-fold higer when compared with the free metalloporpyrin in solution (log $K<2$ for chloride and 2.5 for $H_2PO_4^-$). This enhacend coordination was ascribed also to the pre-organization of binding sites in an inorganic support.

[15] R. C. Major, X. -Y. Zhu, *J. Am. Chem. Soc.*, **2003***, 125*, 8454.

[16] P. D. Beer, D. P. Cormode, J. J. Davis, *Chem. Commun.,* **2004**, 414.

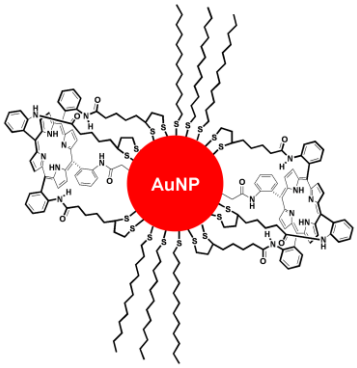

Figure 3. AuNPs functionalized with disulfide-containing zinc metalloporphyrins for the binding of anions.

As well as the increase in the stability constants, pre-organization on solid surfaces can also produce macroscopic signal amplifications when organic entities are organized on a suitable surface as they can respond collectively to a binding event. One illustrative example of this effect was reported by Montalti's group. These researchers prepared silica nanoparticles covered with dansyl moieties on the surface and used them for pH determination.[17] At this respect, protonation of few dansyl moieties induced a remarkable quenching of both the protonated and the surrounding unprotonated fluorophores showing chemical amplification of the signal. In another work, the same authors also developed other representative model using silica nanoparticles that were functionalized with a dansyl-polyamine-appended molecule as binding and signalling unit.[18] Addition of Cu^{2+}, Co^{2+} and Ni^{2+} to suspesions of this hybrid materials resulted in a strong quenching of the fluorescence at nanomolar concentrations because coordination of a single cation quenched several fluorophores located in their close proximity. In this work, enhanced signalling was demonstrated by the fact that a single Cu^{2+} cation was able to induce an emission decrease which corresponded to quenching of 13 dansyl moieties (see Figure 4).

[17] M. Montalti, L. Prodi, N. Zaccheroni, J. Fallini*, J. Am. Chem. Soc.,* **2002**, *124*, 13540.

[18] M. Montalti, L. Prodi, N. Zaccheroni*, J Mater Chem*, **2005**, *15*, 2810.

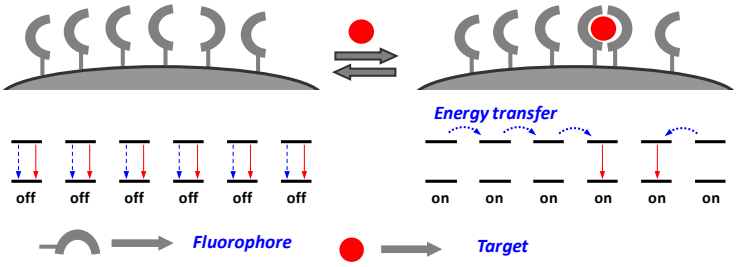

Figure 4. General scheme of signal amplification produced onto functionalized surfaces. *Adapted from Supramolecular Chemistry: From Molecules to Nanomaterials.* Copyright © 2012 John Wiley & Sons.

Other examples were reported by Ding's group. They anchored dansyl fluorophores with dietilentriamine ligands onto glass surfaces in order to detect Cu^{2+}.[19] On the other hand, the first example of amplification in the case an off–on chemosensor was reported by Mancin et al. They prepared silica nanoparticles functionalized with a 6-methoxy-8-(*p*-toluensulfonamide)quinoline derivative that acted as a binding site and signalling unit and used the hybrid material for Zn^{2+} detection.[20] Coordination of Zn^{2+} induced fluorescence enhancement of surrounding non-coordinated fluorophores.

Bearing in mind these works, several researchers began to anchor binding sites and signalling units independently in close proximity into the surface, in order to study possible additional cooperative effects. One of the first works was reported by Tecilla and Tonellato. They prepared a fluorescent sensor for Cu^{2+} using silica nanoparticles functionalized with dansylamide fluorophores and picolinamide binding sites for the selective coordination of this metal cation. The emission of dansylamide fluorophore is quenched in the presence of the paramagnetic guest.[21,22] Using this mechanism is possible to detect Cu^{2+} concentrations down to

[19] L. Ding, X. Cui, Y.Han, F.Lu, Y.Fang, *J Photochem Photobiol A*, **2007**, *186*, 143.

[20] S. Bonacchi, E. Rampazzo, M. Montalti, L. Prodi, N. Zaccheroni, F. Mancin, P. Teolato, *Langmuir*, **2008**, *24*, 8387.

[21] E. Brasola, F. Mancin, E. Rampazzo P. Tecilla, U. Tonellato, *Chem. Commun.*, **2003**, 3026.

the nanomolar level in DMSO-water solutions. Some years later the same research group reported the sensing of Pb^{2+} with a hybrid material prepared by the independent anchoring of thiol groups (binding sites) and dansyl fluorophores (signalling units) onto silica nanoparticles.[23] Using the same approach (the independent anchoring of binding sites and signalling subunits), other examples for TNT[24] and ATP[25] detection have been published very recently. In this latter work, silica nanoparticles were functionalized with two fluorescent dyes; an indicator functionalized with a Zn(II)-dipicolylamine complex as ATP receptor (1-Zn) and a rhodamine derivative used as reference dye (see Figure 5). The fluorescence of aqueous suspenions of bifuctionalized silica nanoparticles was measured in the presence of nucleotides (ATP, GTP, UTP and CTP) and only ATP was able to induce changes. At this respect ATP induced an enhancement in the emission of the indicator fluorophore due to the formation of a complex with 1-Zn.

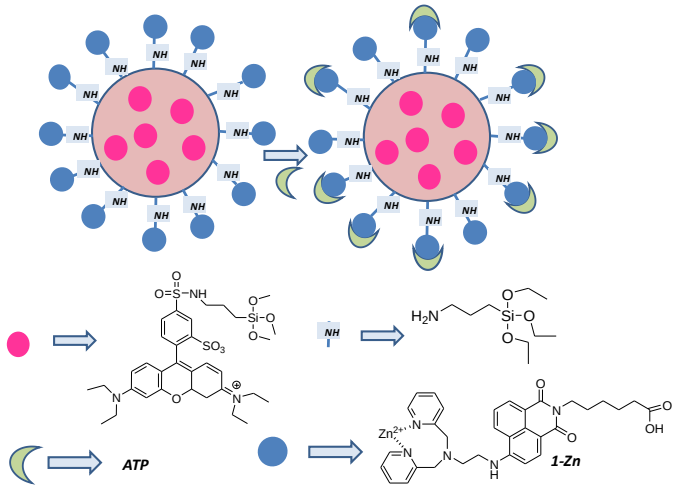

Figure 5. Detection of ATP using bi-functionalised silica nanoparticles.

[22] E. Rampazzo, E.Brasola, S. Marcuz, F. Mancin, P. Tecilla, U. Tonellato, *J. Mater. Chem.,* **2005**, *15*, 2687.

[23] M. Arduini, F. Mancin, P. Tecilla, U. Tonellato, *Langmuir*, **2007**, *23*, 8632.

[24] D. Gao, Z. Wang, B. Liu, L. Ni, M. Wu, Z. Zhang, *Anal. Chem*., **2008,** *80*, 8545.

[25] A. J. Moro, J. Schmidt, T. Doussineau, A. Lapesta-Fernandez, J. Wegener, G. J. Mohr, *Chem. Commun.*, **2011**, *47*, 6066.

The effect of improved signalling by independent anchoring and pre-organization of receptors and signalling units is not unique for silica nanoparticles, and other examples employing the same strategy have been reported using sol-gel films,[26] polymeric nanoparticles,[27] micellar systems[28] and extended surfaces.[29]

1.4 **Mesoporous materials.**

Microporous and mesoporous materials, due to their large internal surface area, are attracting considerable research attention for applications in catalysis,[30] filtration and separation,[31] gas adsorption and storage,[32] enzyme immobilization,[33] biomedical tissue regeneration,[34] drug delivery,[35] and chemical/biochemical sensing.[36] Typical microporous materials are crystalline framework solids, such as zeolites,[37] but the largest pore dimensions where compressed between the 10-12

[26] M. Montalti, L. Prodi, N. Zaccheroni, G. Battistini, S. Marcuz, F. Mancin, E. Rampazzo, U. Tonellato, *Langmuir*, **2006**, *22*, 5877.

[27] a) R. Méallet-Renault, R. Pansu, S. Amigoni-Gerbier, C. Larpent, *Chem. Commun.*, **2004**, 2344. b) F. Gouanvé, T. Schuster, E. Allard, R. Méallet-Renault, C. Larpent, *Adv. Funct. Mater.*, **2007**, *17*, 2746.

[28] E. L. Doyle, C. A. Hunter, H. C. Philips, S. J. Webb, N. H. Williams, *J. Am. Chem. Soc.*, **2003**, *125*, 4593.

[29] Y. Zheng, J. Orbulescu, X. Ji, F. M. Andreopoulos, S. M. Pham, R. M. Leblanc, *J. Am. Chem. Soc.*, **2003**, *125*, 2680.

[30] D.E. De Vos, M. Dams, B.F. Sels, P.A. Jacobs, *Chem. Rev.,* **2002**, *102*, 3615.

[31] X. Liu, Y. Du, Z. Guo, S. Gunasekaran, C. -B. Ching, Y. Chen, S .S .J. Leong, Y. Yang, *Microporous Mesoporous Mater.,* **2009**, *122*, 114.

[32] a) M. Kruk, M. Jaroniec, *Chem. Mater.*, 2001, 13, 3169. b) A. Corma, M. Moliner, M. J. Diaz-Cabanas, P. Serna, B. Femenia, J. Primo, H. Garcia, *New J. Chem.*, **2008**, *32*, 1338. c) C. Ispas, I. Sokolov, S. Andreescu, *Anal. Bioanal. Chem.,* **2009**, *393*, 543.

[33] M. Vallet-Regi, M. Colilla, I. J. Izquierdo-Barba, *Biomed. Nanotechnol.*, **2008**, *4*, 1.

[34] I. I. Slowing, B. G. Trewyn, S. Giri, V. S. –Y. Lin, *Adv. Funct. Mater.*, **2007**,*17*, 1225.

[35] a) M. Vallet-Regi, F. Balas, D. Arcos, *Angew. Chem., Int. Ed.*, **2007**, *46*, 7548. b) K. A. Kilian, T. Bocking, K. Gaus, J. King-Lacroix, M. Gal, J. J. Gooding, *Chem. Commun.,* **2007**, 1936.

[36] a) K. A. Kilian, T. Boecking, K. Gaus, M. Gal, J. J. Gooding, *ACS Nano* **2007**, *1*, 355. b) A. Jane, R. Dronov, A. Hodges, N. H. Voelcker, *Trends Biotechnol.* **2009**,*27*, 230.

[37] M. E. Davis, C. Saldarriaga, C. Montes, J. Garces, C. Crowder, *Nature,* **1988***, 331,* 698.

Å presented by certain metallophosphates[38] and the 14 Å of cacoxenite.[39] In 1992, researchers of the Mobil Company reported the synthesis of new mesoporous silica family known as M41S phases,[40] and, since this report, these silica mesoporous supports (SMP) have been extensively used as inorganic scaffoldings in the development of nanoscopic materials. The best-known representatives of this class of materials include the silica solid MCM-41 (Mobile Crystalline Material with a hexagonal arrangement of the mesopores), MCM-48 (with a cubic arrangement of mesopores) and MCM-50 (with a lamellar structure). This class of materials posees homogeneous pore size, ranging from approximately 2 to 10 nm, a high pore volume (in the order of 1 $cm^3 g^{-1}$) and a very high specific surface area between 500 and 1000 $m^2 g^{-1}$. In addition, these types of materials are inert and posees high thermal stability. On the other hand, their synthesis requires inexpensive and nonhazardous precursors that are simple enough for large-scale production and that can be chemically modified using the well-known silicon oxide functionalisation chemistry.[41] Due to all of these characteristics, these materials are ideal supports for the adsorption processes of molecules, and, until now, these materials are the most commonly used supports to study the controlled release of species from inorganic matrices upon exposition to an external stimulus.

1.4.1 Synthesis of mesoporous materials.

Research on mesoporous materials was initially motivated by the desire for ordered silica/alumina supports with pores of larger dimensions than those found in microporous zeolites for their use in petrochemical catalysis. As we cited above, the first successful studies on surfactant–organised mesoporous materials were carried out on silica, and to date still remains the most studied system.

[38] M. Estermann, L. B. McCusker, C. Baerlocher, A. Merrouche, H. Kessler, *Nature,* **1991**, *352*, 320.

[39] P. B. Moore, J. Shen, *Nature,* **1983***, 306*, 356.

[40] a) C. T. Kresge, M. E. Leonowicz, W. J. Roth, J. C. Vartuli, J. S. Beck, *Nature*, **1992**, *359*, 710. b) J. S. Beck, J. C. Vartuli, W. J. Roth, M. E. Leonowicz, C. T. Kresge, K. D. Schmitt, C. T. W. Chu, D. H. Olson, E. W. Sheppard, *J. Am. Chem. Soc.*, **1992**, *114*, 10834.

[41] F. Hoffmann, M. Cornelius, J. Morell, M. Fröba, *Angew. Chem. Int. Ed.*, **2006**, *45*, 3216.

From the literature it is obvious that the formation of ordered mesoporous materials largely depend on parameters related with the specific chemistry and chemical interactions involved in the studied system, but also on the physical conditions employed in their synthesis. Some of these parameters are, for example, the type of inorganic material and its propensity to crystallise in the walls, type of precursors used and the kinetics of their hydrolysis and condensation, type of surface-active molecules, the respective and relative concentrations of surfactant and inorganic species, pH, temperature, synthesis time, type of solvent, etc.

Generally, the synthesis of these inorganic silica based scaffolds is accomplished by the use of a template such as a surfactant, that acts as a structure-directing agent, and is able to form micelles in water solution. Depending on factors described above, such as concentration and dimensions of the surfactant, temperature, pH solution, ionic force, etc. different kind of micelles can be obtained. These micelles organize themselves into supermicellar structures and depending on the same factors reported before different kind of supermicellar aggregates can be obtained. In the synthesis of silica based ordered inorganic scaffolds, oligomeric silicates, wich are present in the reaction mixture, are able to condensate around the template, obtaining as a result a mesoporous solid that contains in its pores larger quantities of surfactant molecules. The subsequent elimination of the surfactant from the pores of the materials gives the desired inorganic mesoporous scaffold. The surfactant elimination can be carried out by aerobic high temperature calcination or by extraction with adequate solvents.

Researchers have found that two different mechanisms are involved on the formation process of these composite materials. In the first mechanism, named as true liquid-crystal templating (TLCT) mechanism, the concentration of the surfactant is very high and, as a consequence, a lyotropic liquid-crystalline phase is formed without requiring the presence of the precursor inorganic framework

materials (normally tetraethyl- (TEOS) or tetramethylorthosilica (TMOS)).[42] The other mechanism considers that liquid-crystalline phase is formed even at lower concentrations of surfactant molecules, for example, in a cooperative self assembly of the template molecules and the added inorganic species.[43]

Using these processes, the original approach has been extended by a number of variations. As an example, the use of triblock copolymer templates under acidic conditions was employed to prepare the so-called SBA (Santa Barbara Amorphous) silica phases,[44] whereas the use of cationic surfactants, such as hexadecyltrimethylammonium bromide (CTAB) was originally used in the synthesis of the first M41S materials, obtaining the hexagonal (MCM-41), the cubic (MCM-48) and lamellar (MCM-50) forms described above.

Bearing in mind these types of materials, MCM-41 is one of the best known and most widely studied. The MCM-41 synthesis is schematically represented in Figure 6. As it can be observed the synthesis deals with the polymerization of tetrahethylortosilicate (TEOS), used as inorganic siliceous precursor, around super-micellar-template previously formed in basic water solution. As explained before, removal of surfactant by aerobic high temperature calcination or by extraction with adequate solvents allow us to obtain the final mesoporous inorganic scaffold, wich presents cylindrical unidirectional empty channels of approximately 3 nm of diameter (when CTAB is used as surfactant) arranged in a hexagonal distribution. The final solid presented a delicate structural order that is very difficult to obtain following traditional synthetic routes. The principal advantage of this synthetic method is that the high grade of homogeneity of the initial elements is transmitted to the final material, showing a system of pores not only homogeneously in size but also in form and regularity.

[42] G. S. Attard, J. C. Glyde, C. G. Göltner, *Nature,* **1995**, *378*, 366.

[43] A. Monnier, F. Scheth, Q. Huo, D. Kumar, D. Margolese, R. S. Maxwell, G. Stucky,M. Krishnamurty, P. Petroff, A. Firouzi, M. Janicke, B. Chmelka, *Science*, **1993**, *261*, 1299.

[44] a) D. Zhao, J. Feng, Q. Huo, N. Melosh, G.H. Fredrickson, B.F. Chmelka, G.D. Stucky, *Science*, **1998**, *279*, 548. b) D. Zhao, Q. Huo, J. Feng, B.F. Chmelka, G.D. Stucky, *J. Am. Chem. Soc.*, **1998**, *120*, 6024.

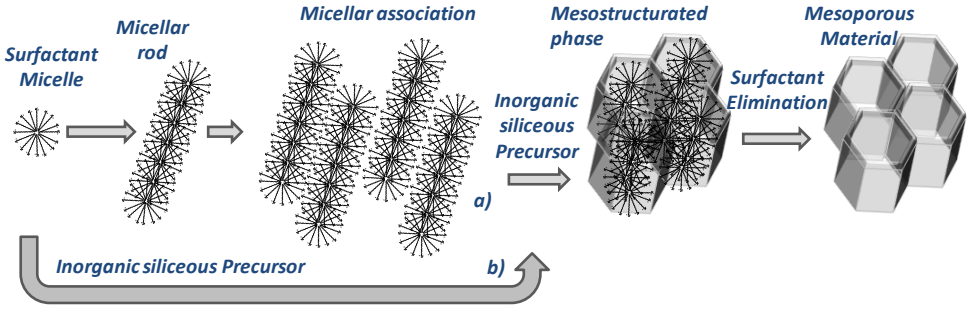

Figure 6. Schematic representation of MCM-41 synthesis by structure-directing agents: a) true liquid-crystal template mechanism, in wich the liquid crystal phase is intact before the inorganic precursor is added b) cooperative liquid-crystal mechanism, in wich addition of the inorganic precursor mediates the ordering of the surfactant micelles.

Other advantage of this type of material is its versatility, since it is possible to modify their final features making small changes in the synthetic process. For instance, the pore size can be easily tuned by varying the structure directing agent,[45] obtaining silica mesoporous supports with pore diameter ranging from 2 up to 50 nm. On the other hand, the original synthetic methods yield large particles of hexagonally packed mesoporous silicate, but the particle morphology can also be tuned from micrometric and heterogeneous particles to create various forms, including thin films, nanoparticles or monoliths.[46] Furthermore, this approach has been extended to non-silica oxides, such as TiO_2 and ZrO_2, using

[45] S. A. Bagshaw, E. Prouzet, T. J. Pinnavaia, *Science*, **1995**, *269*, 1242.

[46] a) H. B. S. Chan, P. M. Budd, T. D. V. Naylor, *Journal of Materials Chemistry*, **2001**, *11*, 951. b) Q. Cai, Z.-S. Luo, W.-Q. Pang, Y.-W. Fan, X.-H. Chen and F.-Z. Cui, *Chem. Mater.*, **2001,** *13*, 258. c) S. Huh, J. W. Wiench, J.-C. Yoo M. Pruski, V. S.-Y. Lin, *Chemistry of Materials*, **2003**, *15*, 4247. d) S. P. Naik, W. Fan, T. Yokoi, T. Okubo, *Langmuir*, **2006**, *22*, 6391. e) J. Kobler, K. Moller, T. Bein, *ACS Nano*, **2008**, *2*, 791.

several types of templating agents, including non-ionic surfactants and block copolymers.[47]

1.4.2 Functionalization of MCM-41 scaffolds: Obtention of organic-inorganic hybrid materials.

Soon after discovery of MCM-41, there was much interest in order to incorporate organic groups into these materials. This would be easily achieved bearing in mind the structure of mesoporous materials and the fact that it presents a high concentration of structural defects in the form of silanol (Si-OH) groups. These silanols can easily react with trialkoxysilane derivatives ($(R'O)_3$-Si-R) to give a nucleofilic aliphatic substitution and generate a novel class of organic–inorganic nanocomposites known as "*organic-inorganic hybrid materials*". In these *"hybrid materials",* the chemical nature of the fragment R can be selected in order to include specific groups onto inorganic framework. In addition, this R groups can contain one or more reactive atoms, which can be later chemically modified.

Two procedures for the synthesis of porous hybrid materials based on organosilica units are available:[41,48]

- ✓ *Grafting procedure*: In this case a post functionalization of the inorganic silica material with selected trialkoxysilanes takes place. With this mechanism, a superficial modification is usually obtained.[49] This method of modification has the advantage that, under the synthetic conditions used, the mesostructure of the starting silica phase is usually retained. However, if the organosilanes react preferentially at the pore openings during the initial stages of the

[47] a) P. Yang, D. Zhao, D. I. Margolese, B. F. Chmelka, G. D. Stucky, *Nature*, **1998**, *396*, 152. b) J. Y. Ying, C. P. Mehnert and M. S. Wong, *Angew. Chem., Int. Ed.*, 1999, **38**, 56. c) A. Sayari, B.-H. Han, Y. Yang, *J. Am. Chem. Soc.*, **2004**, *126*, 14348.

[48] Vinu, A.; Hossain, K. Z.; Ariga, K., *Nanosci. Nanotech.,* **2005**, *5*, 347.

[49] a) A. Stein, B. J. Melde, R. C. Schroden, *Adv. Mater*. **2000**, *12*, 19, 1403. b) F. Juan, E. Ruiz-Hitzky, *Adv. Mater.* **2000**, *12*, 6, 430.

synthetic process, the diffusion of further molecules into the center of the pores can be impaired. This could lead to a non-homogeneous distribution of the organic groups within the pores and a lower degree of occupation.

- ✓ *Co-condensation procedure or direct synthesis*: In this case a simultaneous condensation of corresponding silica and organosilica precursors takes place. This method allows to obtain an internal and external covalent modification of the scaffold, and organic units are generally more homogeneously distributed compared with the grafting process. However, several disavantadges have been found using this procedure:

    - The degree of mesoscopic order of the final materials decreases when concentration of organic silane increases. At this respect, when the organic functionality exceeds 40% mol disordered materials are obtained.

    - Homocondensation reactions between silane groups are increased. As a consequence, the proportion of terminal organic groups that are incorporated into the pore-wall network is generally lower than would correspond to the starting concentration in the reaction mixture. Also the homogeneous distribution of different organic functionalities in the framework cannot be guaranteed.

    - The incorporated organic groups can lead to a reduction in the pore diameter, pore volume, and specific surface areas.

    - Commonly only extractive methods can be used to remove the template. Calcination is not suitable, in most cases, in order to avoid the organic functionality destruction during removal of the surfactant.

Another way to incorporate organic compounds onto silicas is the production of *Periodic Mesoporous Organosilicas (PMOs*), but, using this method, a disordered

pore system is obtained. This procedure allows to incorporate organic groups as bridging components directly and specifically into the pore walls by the use of bis-silylated single-source organosilica precursors. In contrast to the organically functionalized silica phases, which are obtained by postsynthetic or direct synthesis, the organic units in this case are incorporated in the three-dimensional network structure of the silica matrix through two covalent bonds and thus distributed homogeneously in the pore walls. These materials, which are obtained as porous aero- and xerogels, can have large inner surface areas (up to 1800 $m^2 g^{-1}$) as well as high thermal stability but generally exhibit completely disordered pore systems.[50]

A schematic representation of the two procedures for the functionalization of inorganic mesoporous materials is shown in Figure 7.

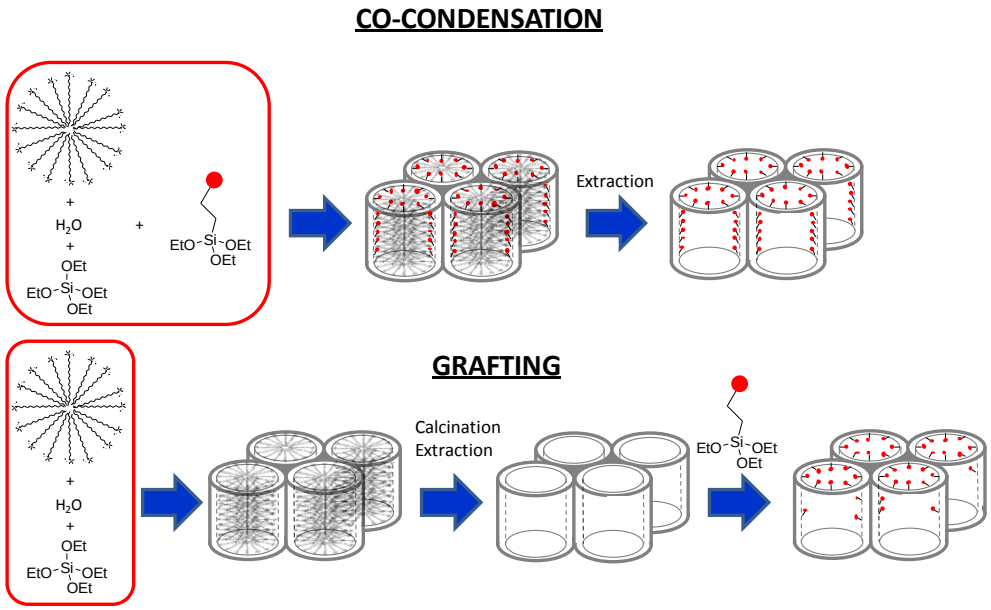

Figure 7. A Schematic representation of the functionalization of MCM-41. Modified from *E. Aznar PhD Thesis.*

[50] B. Hatton, K. Landskron, W. Whitnall, D. Perovic, G. A. Ozin, *Acc. Chem. Res.*, **2005**, *38*, 305.

1.4.3 Applications of Organic-Inorganic Mesoporous Hybrid Materials.

Mesoporous silica materials have been used as effective scaffoldings for the entrapment of (bio)molecules due to their important properties, such as chemical inertness, three dimensional structure, high external surface, high load capacity, biocompatibility etc. They posses uniform pore systems that grants a large load capacity of chemical species.[51] Mesoporous solids, functionalized through both methodologies, have been employed in different scientific fields developing stimuli-responsive gatekeepers materials that are able to transport molecules to specific locations,[52] or, on the other hand, they are able to produce a controlled release in response to target molecules or certain stimuli.[53]

This PhD thesis deals just with the design, synthesis and application of organic-inorganic mesoporous materials for the controlled delivery of their cargo in the presence of target species. Because of this, a briew description of the concept and some relevant applications of these stimuli-responsive capped materials will be described.

1.4.4 Molecular Gates

One of the most appealing concepts in nature is related with channels that act as gates and are able to control mass transport. Inspired by this example, many researchers have been involved in the preparation of hybrid materials that mimics these channels, developing stimuli-responsive nanoscopic gated systems that are

[51] a) M. Vallet-Regi, A. Rámila, R. P. del Real, J. Pérez-Pariente, *J. Chem. Mater.* **2001**, *13*, 308. b) B. Muñoz, A. Rámila, J. Pérez-Pariente, I. Díaz, M. Vallet-Regi, *Chem. Mater.* **2003**, *15*, 500.

[52] a) J. M. Rosenholm, E. Peuhu, L. T. Bate-Eya, J. E. Eriksson, C. Sahlgren, M. Linden, *Small*, **2010**, *6*, 1234. b) M. Liong, J. Lu, M. Kovochich, T. Xia, S. G. Ruehm, A. E. Nel, F. Tamanoi, J. I. Zink, *ACS Nano*, **2008**, *2*, 889.

[53] K.K. Cotí, M. E. Belowich, M. Liong, M. W. Ambrogio, Y. A. Lau, H. A. Khatib, J. I. Zink, N. M. Khashab, J. F. Stoddart, *Nanoscale,* **2009**, *1*, 16.

commonly reported as "*molecular gates*".[54] Thus, a molecular o supramolecular gate can be defined as a nanoscopic system in which mass transport or delivery can be triggered by a target external stimulus that controls the state of the gate (closed or open) on-command. At this respect, a molecular gate contains a suitable inorganic support that includes molecules in the inner of the pores that are able to be delivered, and certain molecular or supramolecular entity, usually grafted in the external surface, which is the responsible of mass transport and delivery control from the pores to the solution. A schematic representation of a gate-like superstructure is shown in Figure 8. The scheme shows inorganic scaffolding loaded with an entrapped guest and with a suitable molecule anchored in the pore outlets (molecular gate). The application of an extermal stimulus allows the release of the entrapped guest due to changes in the molecule than acts as gate.

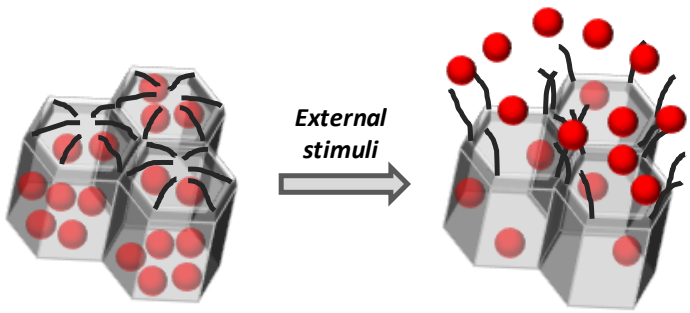

Figure 8. Schematic representation of the operation principle of a molecular gate.

Since the first example of molecular gate reported by Fujiwara and coworkers in 2003,[55] several nanoscopic gated systems using mesoporous hybrid scaffoldings

[54] A. B. Descalzo, R. Martínez-Máñez, F. Sancenón, K. Hoffmann, K. Rurack, *Angew. Chem. Int. Ed.,* **2006**, *45*, 5924.

[55] a) N. K. Mal, M. Fujiwara, Y. Tanaka, Y. *Nature,* **2003**, *421*, 350. b) N. K. Mal, M. Fujiwara, Y. Tanaka, T. Taguchi, M. Matsukata, *Chem. Mater.* **2003**, *15*, 3385-3394.

have been described. For example, inorganic nanoparticles,[56] polymers,[57] and larger supramolecular assemblies[58] have been used as blocking caps that controls the opening/closing of pore entrances in mesoporous scaffolds. On the other hand, different stimuli, such as pH,[59] light,[60] redox potential,[61] temperature[62] and target molecules[63] have been applied as "triggers" for uncapping the pores and

[56] a) C.-Y. Lai, B. G. Trewyn, D. M. Jeftinija, K. Jeftinija, S. Xu, S. Jeftinija, V. S.-Y. Lin, *J. Am. Chem. Soc.* **2003**, *125*, 4451. b) S. Giri, B. G. Trewyn, M. P. Stellmaker, V. S.-Y. Lin, *Angew. Chem., Int. Ed.*, **2005**, *44*, 5038. c) E. Aznar, M . D. Marcos, R. Martinez-Manez, F. Sancenon, J. Soto, P. Amoros, P. Guillem, *J. Am. Chem. Soc.*, **2009**, *131*, 6833. d) J. L. Vivero- Escoto, I. I. Slowing, C. Wu, V. S.-Y. Lin, *J. Am. Chem. Soc.* **2009**, *131*, 3462.

[57] a) R. Liu, X. Zhao, T. Wu., P. Y. Feng, *J. Am. Chem. Soc*. **2008**, *130*, 14418. b) C. L. Zhu, X. Y. Song, W. H. Zhou, H. H. Yang, X. R. Wang, *J. Mater. Chem.,* **2009**, **19**, 7765.

[58] a) T. D. Nguyen, Y. Liu, S. Saha, K. C. F. Leung, J. F. Stoddart, J. I. Zink, *J. Am. Chem. Soc.* **2007**, *129*, *626*. b) R. Liu, Y. Zhang, P. Y. Feng, *J. Am. Chem. Soc.* **2009**, *131*, 15128.

[59] a) R. Casasus, M. D. Marcos, R.Martínez-Máñez, J. V. Ros-Lis, J. Soto, L. A. Villaescusa, P. Amorós, D. Beltrán, C. Guillem, J. Latorre, *J. Am. Chem. Soc.,* **2004**, *126*, 8612. b) A. Bernardos, E. Aznar, C. Coll, R. Martínez-Máñez, J. M. Barat, M. D. Marcos, F. Sancenón, J. Soto, *J. Control. Rel.*, **2008**, *131*, 181. c) Q.Yang, S. Wang, P. Fan, L. Wang, Y. Di, K. Lin, F. –S. Xiao, *Chem. Mater.,* **2005**, *17*, 5999. d)V. Cauda, C. Argyo, A. Schlossbauer, T. J. Bein, *J. Mater. Chem.*, **2010**, *20*, 4305. e) S. Angelos, Y. –W. Yang, K. Patel, J. F. Stoddart, J. I. Zink, *Angew. Chem. Int. Ed.*, **2008**, *47*, 2222. f) H. Meng, M. Xue, T. Xia, Y. –L. Zhao, F. Tamanoi, J. F. Stoddart, J. I. Zink, E. A. Nel, *J. Am. Chem. Soc.*, **2010**, *132*, 12690. g) Y. Klichko, N. M. Khashab, Y. –W. Yang, S. Angelos, J. F. Stoddart, J. I. Zink, *Micropor. Mesopor. Mater.*, **2010**, *132*, 435. h) J. Liu, X. Du, *J. Mat. Chem.*, **2010**, *20*, 3642. i) W. Guo, J. Wang, S. -J. Lee, F. Dong, S. S. Park, C. –S. Ha, *Chem. Eur. J.*, **2010**, *16*, 8641. j) A. Popat, J. Liu, G. Q. Lu, S. Z. Qiao, *J. Mater. Chem.,* **2012**, *22*, 11173.

[60] a) E. Johansson, E. Choi, S. Angelos, M. Liong, J. I. Zink, *Sol-Gel Sci. Technol.*, **2008**, *46*, 313. b) Q. Lin, Q. Huang, C. Li, C. Bao, Z. Liu, F. Li, L. Zhu, L. *J. Am. Chem. Soc.*, **2010**, *132*, 10645. c) J. Lai, X. Mu, Y. Xu, X. Wu, C. Wu, C. Li, J. Chen, Y. Zhao, *Chem. Commun.,* **2010**, *46*, 7370.

[61] a) R. Hernandez, H. –R. Tseng, J. W. Wong, J. F. Stoddart, J. I. Zink, *J. Am. Chem. Soc.*, **2004**, *126*, 3370. b) R. Liu, X. Zhao, T. Wu, P. Feng, *J. Am. Chem. Soc.*, **2008**, *130*, 14418. c) R. Mortera, J. Vivero-Escoto, I. I. Slowing, E. Garrone, B. Onida, V. S.-Y. Lin, *Chem. Commun.,* **2009**, 3219.

[62] a) C. Liu, J. Guo, W. Yang, J. Hu, C. Wang, S. Fu, *J. Mat. Chem.*, **2009**, *19*, 4764. b) J. Lai, X. Mu, Y. Xu, X. Wu, C. Wu, C. Li, J. Chen, Y. Zhao, *Chem. Commun.,* **2010**, *46*, 7370. c) C. R. Thomas, D. P. Ferris, J. –H. Lee, E. Choi, M. H. Cho, E. S. Kim, J. F. Stoddart, J. –S. Shin, J. Cheon, J. I. Zink, *J. Am. Chem. Soc.,* **2010**, *132*, 10623.

releasing the guest molecules from mesoporous scaffolds. Most recently, design of stimuli-responsive nanoscopic gated systems involving biomolecules became an important field. Thus, some biomolecules, specially enzymes,[64] have been used as stimuli to uncap the gated-scaffolds, whereas other biomolecules, such as sachharides,[65] peptides,[66] aptamers for ATP recognition[67a,b] or DNA,[67c,d] have been reported as capping supramolecules.

The controlled release of bioactive molecules is a very interesting issue, from a pharmaceutical point of view, because it opens new possibilities to direct the nanoscopic vehicle to specific cell using a particular surface functionalization and/or can prevent the internal entrapped cargo degradation due to the normal

---

[63] a) R. Casasús, E. Aznar, M. D. Marcos, R. Martínez-Máñez, F. Sancenón, J. Soto, P. Amorós, *Angew. Chem.Int. Ed.*, **2006,** *45*, 6661. b) C. Coll, R. Casasús, E. Aznar, M. D. Marcos, R. Martínez-Máñez, F. Sancenón, J. Soto, P. Amorós, *Chem. Commun.*, **2007**, 1957. c) R. Casasús, E. Climent, M. D. Marcos, R. Martínez-Máñez, F. Sancenón, J. Soto, P. Amorós, J. Cano, E. Ruiz, *J. Am. Chem. Soc.,* **2008***, 130*, 1903. d) E. Aznar, C. Coll, M. D. Marcos, R. Martínez-Máñez, F. Sancenón, J. Soto, P. Amorós, J. Cano, E. Ruiz, *Chem. Eur. J.*, **2009**, *15*, 6877. e) Y. Zhao, B. G. Trewyn, I. I. Slowing, V. S.-Y. Lin, *J. Am. Chem. Soc.,* **2009***, 131*, 8398. f) Y. L. Choi, J. Jaworsky, M. L. Seo, S. J. Lee, J. H. Jung, *J. Mater. Chem.,* **2011**, *21*, 7882. g) A. Schulz, R. Woolley, T. Tabarin, C. McDonagh, *Analyst*, **2011**, *136*, 1722. h) J. Lee, J. Lee, S. Kim, C. –J. Kim, S. Lee, B. Min, Y. Shin, C. Kim, *Bull. Korean Chem. Soc.*, **2011**, 32, 1357. i) I. Candel, A. Bernardos, E. Climent, M. D. Marcos, R. Mart_nez-MaÇez, F. Sancenon, J. Soto, A. Costero, S. Gil, M. Parra, *Chem. Commun*. **2011**, *47*, 8313.

[64] a) K. Patel, S. Angelos, W. R. Dichtel, A. Coskun, Y. –W. Yang, J. I. Zink, J. F. Stoddart, *J. Am. Chem. Soc.,* **2008***, 130*, 2382. b) A. Schlossbauer, J. Kecht, T. Bein, *Angew. Chem. Int. Ed.*, **2009**, *48*, 3092. c) A. Bernardos, E. Aznar, M. D. Marcos, R. Martínez-Máñez, F. Sancenón, J. Soto, J. M. Barat, P. Amorós, P. *Angew. Chem. Int. Ed.*, **2009**, *48*, 5884. d) C. Park, H. Kim, S. Kim, C. Kim, *J. Am. Chem. Soc.,* **2009***, 131*, 16614. e) P. D. Thornton, A. Heise, *J. Am. Chem. Soc.,* **2010**, *132*, 2024.

[65] A. Bernardos, L. Mondragón, E. Aznar, M. D. Marcos, R. Martínez-Máñez, F. Sancenón, J. Soto, J. M. Barat, E. Pérez-Payá, C. Guillem, P. Amorós, *ACS Nano*, **2010**, *4*, 6353.

[66] a) C. Coll, L. Mondragón, R. Martínez-Máñez, F. Sancenón, M. D. Marcos, J. Soto, P. Amorós, E. Pérez-Payá, *Angew*. *Chem*. *Int*. *Ed*., **2011**, 50, 2138. b) F. Porta, G. E. M. Lamers, J. I. Zink, A. Kros, *Phys. Chem. Chem. Phys.,* **2011**, *13*, 9982.

[67] a) C. -L. Zhu, C. –H. Lu, X. –Y. Song, H. –H. Yang, X. –R. Wang, *J. Am. Chem. Soc.*, **2011**, *133*, 1278. b) V. C. Özalp, T. Schäfer, *Chem. Eur. J.,* **2011**, *17*, 9893.c) A. Schossbauer, S. Warncke, P. M. E. Gramlich, J. Kecht, A. Manetto, T. Carell, T. Bein, *Angew. Chem.Int. Ed.*, **2010**, *49*, 4734. d) Y. Zhang, Q. Yuan, T. Chen, X. Zhang, Y. Chen, W. Tan, *Anal. Chem.*, **2012**, *84*, 1956.

metabolic processes. However, there are few examples in which the cargo released are biomolecules or drugs, and ever fewer works related with the use of nanoscopic gated materials for release in intracellular media.[68] Most of the reported works release dyes from the inner of the pores because it allows an easy monitorization of the proper function of the gating ensemble.

In the following part of this introduction some examples of gated materials will be presented, according to the stimulus employed to induce the release of the entrapped guest.

1.4.4.1 *Light-Driven Molecular Gates*

Grafting of photoresponsive organic molecules in mesoporous silica supports is a well-established method for the preparation of hybrid gated materials. Bearing in mind the photoisomerization of coumarin derivatives, Fujiwara and coworkers reported the first example of molecular gate in 2003,[55] showing that the uptake, storage and release of organic molecules in MCM-41 could be regulated through the photocontrolled and reversible intermolecular dimerization of coumarin derivatives attached to the pore outlets. The authors prepared a releasing nanodevice by grafting 7-[(3-triethoxysilyl)propoxy]coumarin (that can undergo [2+2] electrocyclic photoisomerization to give the more hindered cyclobutane derivatives upon irradiation with $\lambda > 310$ nm) onto an MCM-41 support. Figure 9 shows a schematic representation of the process. The MCM-41 was previously loaded with cholestane to monitor the efficiency of the system. Thus, irradiaton at wavelengths higher than 310 nm induced the formation of the cyclobutane derivatives, which were bulkier than the starting monomers, preventing the delivery of the cargo entrapped in the pores of the scaffold. On the other hand, irradiation at 250 nm induced the cleavage of the dimer, showing cholestane release (77% of the total loaded).

[68] a) E. Aznar, R. Martínez-Máñez, F. Sancenón, *Expert Opin. Drug Deliver.,* **2009**, *6*, 643. b) J. L. Vivero-Escoto, I. I. Slowing, B. G. Trewyn, V. S.-Y. Lin, *Small*, **2010**, 6, 1952.

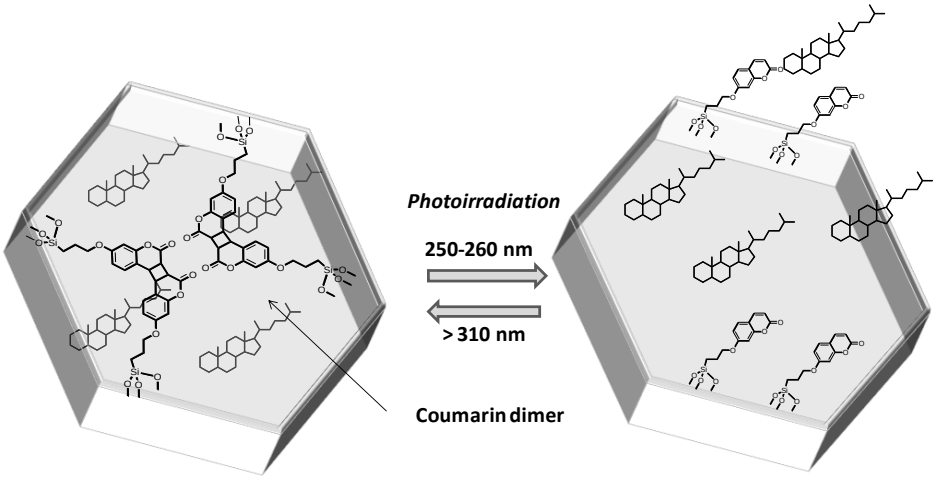

Figure 9. Schematic representation of a light-driven molecular gate. Coumarin fotoisomerization reaction ($\lambda > 310$ nm) induced the formation of a cyclobutane dimer that inhibit cargo release. Irradiation with UV light (250-260 nm) induced the photo-opening of cyclobutane ring with the subsequent cargo delivery.

Similar light-driven gated materials were reported by the groups of Brinker,[69] Zink[70] and Stoddart,[71] using azobenzene moieties as photoactivable molecules. The first example of a two-input (photochemical and chemical) gated hybrid system operative in water was reported by Martínez-Máñez et al.[72] This nanodevice consisted of a MCM-41 solid containing the dye $Ru(bipy)_3^{2+}$ onto the pores and spiropyran photochrome units attached to the external surface of the inorganic support. This molecule could be transformed reversibly between two forms, the neutral spirocyclic and the positively charged merocyanine, upon the application of UV-light. To achieve the controlled release, negatively charged G1.5

[69] a) N. G. Liu, Z. Chen, D. R. Dunphy, Y. –B. Jiang, R. A. Assink, C. J. Brinker, *Angew. Chem. Int. Ed.*, **2003**, *42*, 1731. b) N. G. Liu, D. R. Dunphy, P. Atanassov, S. D. Bunge, Z. Chen, G. P. Lopez, T. J. Boyle, C. J. Brinker, *Nano Lett.*, **2004**, *4*, 551.

[70] a) S. Angelos, E. Choi, F. Vögtle, L. De Cola, J. I. Zink, *J. Phys. Chem.*, **2007**, *111*, 6589. b) J. Liu, E. Choi, F. Tamanoi, J. I. Zink, *Small*, **2008**, *4*, 421.

[71] D. P. Ferris, Y. –L. Zhao, N. M. Khashab, H. A. Khatib, J. F. Stoddart, J. I. Zink, *J. Am. Chem. Soc.*, **2009**, *131*, 1686.

[72] E. Aznar, R. Casasús, B. García-Acosta, M. D. Marcos, R. Martínez-Máñez, F. Sancenón, J. Soto, P. Amorós, *Adv. Mater.*, **2007**, *19*, 2228.

PAMAM dendrimers (G1.5) were used as molecular stoppers, due to the coulombic interaction between the negatively charged G1.5 PAMAM dendrimer and the positively charged merocyanine. At this respect, no release of the dye was observed upon irradiation with UV-light. However, irradiation with visible light induced the transformation of the merocyanine isomer to the neutral spirocyclic form (wich do not have any affinity for the negatively charged dendrimers) allowing the release of the entrapped dye to the solution. Furthermore, the functional task of the dendrimers was also switched on/off by simple adjustment of the pH, due to the protonation of their carboxylate moieties. At acidic pH (pH ca. 2) G1.5 PAMAM dendrimers are protonated and are unable to interact with the charged merocyanine isomer with the subsequent dye release. At neutral pH, interaction of G1.5 PAMAM dendrimers with the merocyanine inhibits dye release. Figure 10 shows a schematic representation of the gated system.

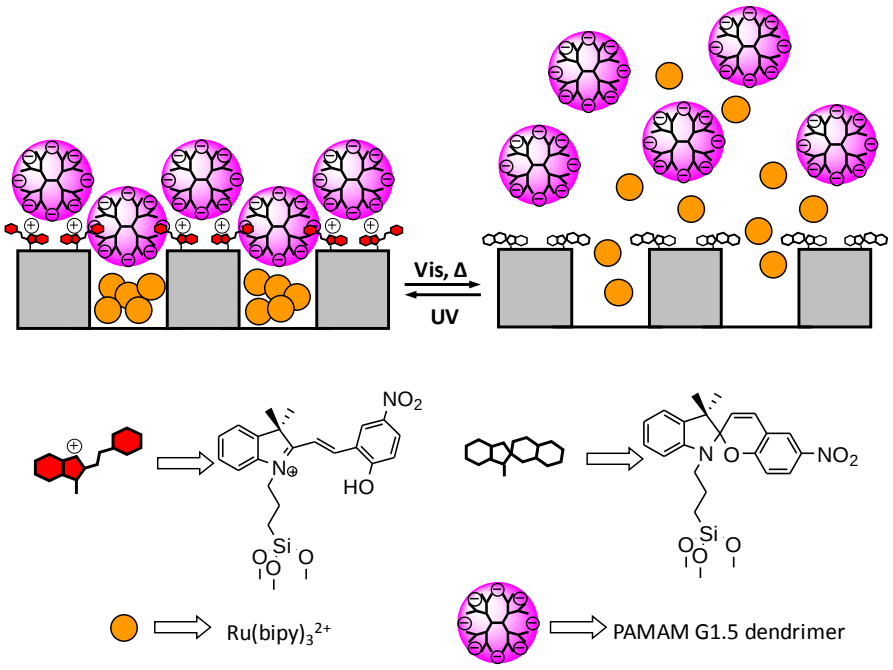

Figure 10. Schematic representation of an MCM-41 support functionalized with spirobenzopyran derivatives and capped with PAMAM G1.5 dendrimers. Adapted from *Adv. Mater.*, ***2007***, *19,* 2228. Copyright 2007 John Wiley & Sons.

Other light-driven gated materials have been reported by Lin's and Kim's research groups. Lin's group prepared gold nanoparticle-capped mesoporous silica materials (SMP) for the release of the hydrophobic anticancer drug paclitaxel into cells.[56d] In this hybrid material gold nanoparticles acted as capping agents by their attachment to the SMP material through a photoresponsive linker. This linker is photo-cleaved upon irradiation with 365 nm light with the subsequent release of the hosted molecules. In a very similar approach, Kim et al. prepared mesoporous silica particles that contains calcein as guest molecules, *o*-nitrobenzyl ester moieties as a photocleavable linker and β-cyclodextrins (β-CD) as "gatekeepers".[73] Irradiation at 350 nm induced the rupture of *o*-nitrobenzyl ester moiety that detaches the β-cyclodextrins gatekeepers with the subsequent calcein release.

Very recently, Zhao et al. prepared mesoporous silica nanoparticles containing $Ru(bipy)_3^{2+}$ dye inside the pores and thymine derivatives grafted onto the outer surface, as shown in Figure 11.[74] Photodimerization of tymine, upon UV irradiation at 365 nm, induced the formation of a cyclobutane dimer that inhibits dye release. Irradiation with UV light (240 nm) induced the cleavage of the cyclobutane dimer, allowing the release of the entrapped guest molecules. In addition, and bearing in mind that fluorescence of $Ru(bipy)_3^{2+}$ can be quenched in presence of oxygen, the authors also employed this light-responsive system as a light-switchable oxygen sensor.

[73] C. Park, K. Lee, C. Kim, C. *Angew. Chem. Int. Ed.*, **2009**, *48*, 1275.

[74] D. He, X. He, K. Wang, J. Cao, Y. Zhao, *Langmuir,* **2012**, *28*, 4003.

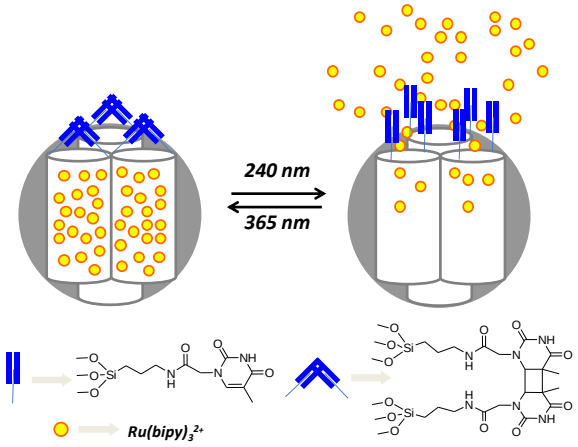

Figure 11. Schematic representation of the light-driven hybrid material functionalized with thymine derivatives.

Finally, other light-switchable supramolecular nanovalves based on cucurbituril CB[7]-cinnamamides have been recently reported,[75] and their sustained controlled-release of model compounds in biological media have been tested.

1.4.4.2 *Redox-Driven Molecular Gates.*

The use of redox reactions for the development of gated mesoporous hybrid materials opens the possibility to employ electrochemical stimuli to regulate mass transport. This type of hybrid materials are very attractive because they can be used for intracellular controlled release thanks to the in-cell presence of redox active molecular pairs such as NAD^+-NADH or lipoic-dihydrolipoic acid.

A large number of examples have been described during the last decade, but they can be summarized into two groups: (i) systems based in the rupture of disulfide bonds (that linked the capping molecule to the mesoporous scaffold) or (ii) systems where the movement of certain molecules induces the change in the state of the molecular gate (open-closed).

[75] a) Y. Kim, Y. H. Ko, M. Jung, N. Selvapalam, K. Kim, *Photochem. Photobiol. Sci.* **2011**, *10*, 1415. b) Y. –L. Sun, B. –J. Yang, S. X.- A. Zhang, Y.-W. Yang, *Chem. Eur. J.,* **2012**, 18, 9212.

Lin's group reported several hybrid materials characterized by the use of different nanoparticles anchored to the surface of SMP through different covalent linkers able to be broken by the addition of certain redox agents, and allowing, as a consequence, the release of the entrapped guests. The first example was presented in 2003.[56a] In this case the authors loaded the pores of the MCM-41 scaffold with bioactive molecules (vancomycin or ATP) and functionanalized the external surface of the solid with with 2-(propyldisulfanil)ethylene diamine. In order to block the pores the authors used 2 nm CdS nanocrystals derivatized with mercaptoacetic acid. The CdS nanoparticles were attached to the modified scaffold through an amidation reaction between the carboxylic acids and the amine group anchored into the solid surface. The addition of reductors, such as dithiotheritol (DTT) or mercaptoethanol (ME), induced the breaking of the disulfide bridges that linked the CdS nanoparticles with the hybrid materials, with the subsequent uncapping and cargo release. In a very similar work, the same authors loaded the pores of a MCM-41 material with fluorescein dye and grafted onto MCM-41 surface 3-(propyldisulfanyl)propionic acid groups. [56b] In order to cap the pores, they used Fe_3O_4 magnetic nanoparticles functionalized with 3-aminopropyltriethoxysilyl groups. An amidation reaction between the carboxylic acids grafted in the inorganic support and the amine of the Fe_3O_4 nanoparticles leads to pore closure. Addition of a reducing agent allowed the rupture of the disulfide linkage and the release of fluorescein. A schematic representation of the system can be observed in Figure 12. In addition, Fe_3O_4 offered the possibility to magnetically direct these nanodevices to the place of interest, and the authors tested their nanoparticles in HeLa cells.

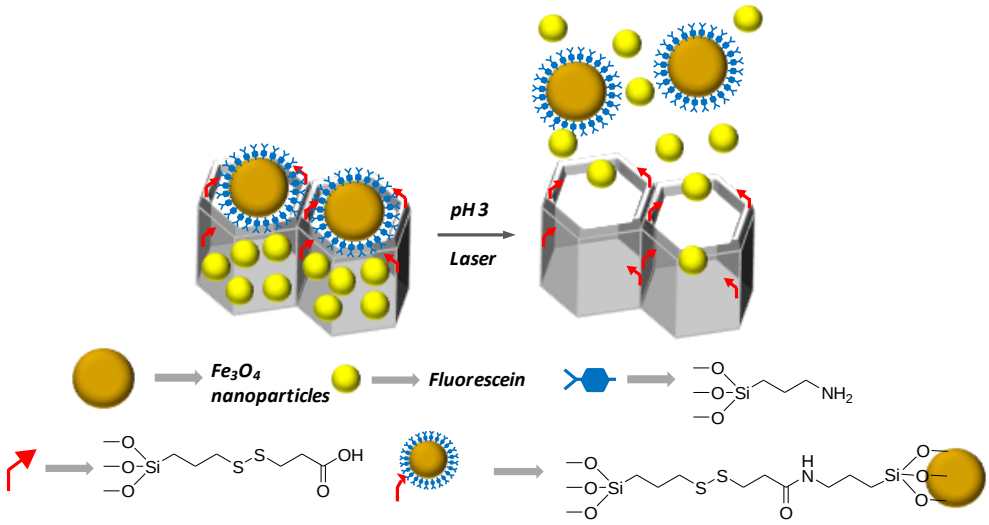

Figure 12. Schematic representation of the stimuli-responsive delivery system based on mesoporous silica nanorods capped with superparamagnetic iron oxide nanoparticles.

Bearing in mind the same mechanism, the authors also reported new mesoporous materials capped with gold nanoparticles and containing a DNA gene and their chemical inducer β-oestradiol in the inner of the porous network.[76] This hybrid material is able to deliver, simultaneously, DNA fragments and the chemical inducer needed for transgene expression into plant cells.

Recently the first hybrid material in which an extracellular matrix component is employed for both cell-specific targeting and redox-responsive controlled drug release has been described.[77] This hybrid system is based on mesoporous silica nanoparticles (MSN) capped with collagen and loaded with a fluorescent dye. Collagen was immobilized on the exterior surface of the MSN through disulfide linkages. On the other hand, lactobionic acid (LA), which bears a galactose group, was also grafted in the outer surface as targeting moiety. Cleavage of disulfide moieties with various reducing agents, such as dithiothreitol (DTT) present inside of the cells, allowed the release of the fluorescent dye in the cellular medium.

[76] F. Torney, B. G. Trewyn, V. S.-Y. Lin, K. Wang, *Nature Nanotechnol.*, **2007**, *2*, 295.

[77] Z. Luo, K. Cai, Y. H. –L. Zhao, P. Liu, L. Duan, W. Yang, *Angew. Chem. Int. Ed.* **2011**, *50*, 640

The other approach used in the development of electrochemical-driven molecular gates is based on the stabilization/destabilization of supramolecular complexes via the oxidation/reduction of suitable groups. The first example of electrochemical-driven molecular gates that used this approach was the work reported by Zink and Stoddart.[61a] The authors synthesized a mesostructured silica thin film with a luminescent molecule in the inner of the pores ($Ir(ppy)_3$) and a [2]pseudorotaxane, formed by 1,5-dioxynaphthalene (DNPD) encircled, through non-covalent interactions, with a cyclobis(paraquat-*p*-phenylene) ($CBPQT^{4+}$) macrocycle, anchored onto surface (see Figure 13). Addition of the reducing agent $NaCNBH_3$ produced a reduction of the DNPD with the subsequent dethreading $CBPQT^{4+}$ ring and the release of the entrapped complex.

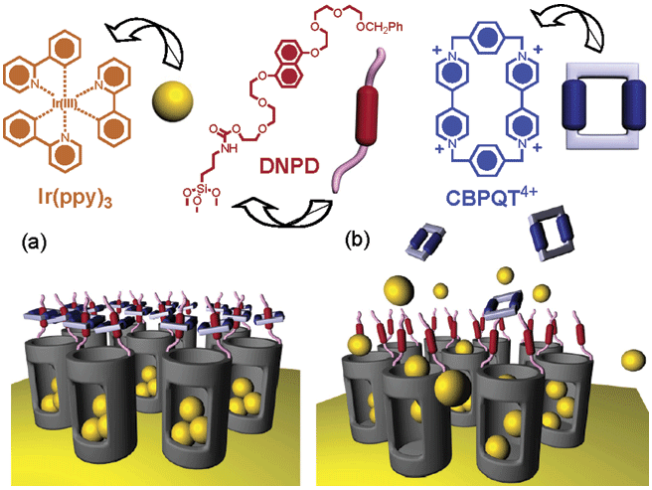

Figure 13. Schematic representation of the operation of redox nanovalves due to the destabilization of the supramolecular complex produced between $CBPQT^{4+}$ and DNPD. Adapted from *J. Am. Chem. Soc.*, **2004**, *126*, 3370. Copyright © 2004 American Chemical Society.

On the other hand, pseudorotaxanes and rotaxanes have been used as gatting molecules in the development of redox-driven hybrid materials. Most of these systems have been reported by Stodart's and Zink's research groups. The *IUPAC Compendium of Chemical Terminology* defines rotaxanes as molecules in which a

ring encloses another rod-like molecule having end-groups too large to pass through the ring opening, whereas the pseudorotaxanes can be defined as rotaxane-like molecular assembly in which the threading component has ends small enough to permit threading or dethreading of the macrocyclic molecule.[78] Bearing this in mind, pseudorotaxanes stability arises from spatially hindered dethreading of their components and also from the interaction between the threading and the macrocyclic components (donor-acceptor, electrostatic, etc.).

Using these concepts, these authors reported a reversible molecular valve based on a double redox-active bis-stable [2]rotaxane.[79] The [2]rotaxane contains DNPD and tetratuiafulvalene (TTF), as redox centers connected through a oligoethyleneglycol chain with a rigid terphenylene space, and $CBPQT^{4+}$ as movable molecule. The redox-induced movement was dependent on the addition of oxidant or reducing species that changed the oxidation state of TTF and, consequently, the preference of $CBPQT^{4+}$ for TTF or DNPD groups. With this movement the state of the gate was changed from closed to open at will.

Another interesting nanodevice was reported by Feng's group, which prepared the first hybrid material that used polymers as a redox-driven gate.[57a] At this respect, they attached the polymer poly(*N*-acryloxysuccinimide) onto the surface of MCM-41 silica nanoparticles containing rhodamine B inside of the pores. Addition of cystamine induced the formation of disulfide linkages between the polymer chains with the subsequent pore capping. Addition of DTT induced the cleavage of the disulfide bond, allowing the release of the cargo. Later, the same authors, improve the system using poly(*N*-acryloxysuccinimide) polymer functionalized with β-cyclodextrin (β-CD) (through disulfide bonds).[58b] The

[78] A. D. McNaught, A. Wilkinson, IUPAC. *Compendium of Chemical Terminology*, 2nd ed. (the "Gold Book"). Blackwell Scientific Publications, Oxford, **1997**. XML on-line corrected version: M. Nic, J. Jirat, B. Kosata; updates compiled by A. D. Jenkins, http://goldbook.iupac.org, 2006 created by M. Nic, J. Jirat, B. Kosata; updates compiled by A. D. Jenkins.

[79] T. D. Nguyen, H. –R. Tesng, P. C. Celestre, A. H. Flood, Y. Liu, J. F. Stoddart, J. I. Zink, *Proc. Natl. Acad. Sci. U.S.A.*, ***2005***, *102*, 10029.

capping of the pores was achieved by the addition of a diazo compound, able to form inclusion complexes with the β-CD, that linked several polymer chains leading to the formation of a dense network surrounding the pore outlets. The pore opening is achieved by UV irradiation (isomerization of *trans*-azobenzene into *cis*-azobencene that is unable to coordinate with β-CD), by competitive binding (with β-CD) or through the rupture of disulfide bonds (that linked the polymers with β-CD macrocycles) by adding DTT. This hybrid material showed that several triggering stimuli could be selected in order to open the gate according to particular requirements.

1.4.4.3 *pH-driven Molecular Gates*

Organic molecules that contains protonable atoms or functional groups that are able to give protonation processes have been employed for the design and preparation of pH-driven molecular gate-like scaffoldings. Changes in their size/shape or attraction/repulsion interactions with other charged species due to proton addition or abstraction can induce an open-close process. pH-driven molecular gates can offer some advantages. At this respect, most of the published examples are, in principle, reversible and show a response in aqueous media (vide infra). Furthermore, it is possible to finely control the pH at which the gate is opened/closed easily selecting a suitable pH sensitive molecular unit that is anchored on the outer surface of the silica support. On the other hand, these systems can be applied to intracellular level, due to the pH difference between the extracellular environment (pH 7) and endosomes and lisosomes (pH 5).

In this field R. Martínez-Máñez and coworkers developed the first pH driven molecular gate in 2004.[59a] This new hybrid material consists of a particular solid support belonging to the MCM-41 family, (UVM-7) which was functionalized on the surface with 3-[2-(2-aminoethylamino)ethylamino]propyltrimethoxysilane and in the inner of the pores with thiol groups. To verify the correct pH dependent open-close paradigm, a squaraine dye was added to the reaction mixture, because this particular dye is characterized by an intense light blue color that is lost when

reacts with thiols yielding a colorless derivative.[80] At acidic pH the polyamines are in their protonated form adopting a rigid-like conformation pushed away toward the pore opening. This inhibited dye access to the pores and the solution remained blue. However, when the pH was increased to neutral, the polyamines were partially deprotonated, allowing the access of squaraine to the pores in order to react with the thiols, giving a colorless solution. Bearing in mind this system, the same group reported a similar hybrid material for anion recognition and signaling. For this, the pores of an MCM-41 solid support were loaded with $Ru(bipy)_3^{2+}$ dye and then the same polyamine reported above was anchored on the outer surface.[63a] The designed material was able to diferenciate GMP from ATP and ADP due to the dye delivery inhibition induced by the differential coordination of the polyamines with these nucleotides. Some years later, the behavior of the same material at different pH and in the presence of several anions (of different sizes, shapes and charge), was studied. These hybrid material acted as pH-driven and anion-controlled nano-supramolecular gate-like system. [63c] A representative scheme is shown in Figure 14.

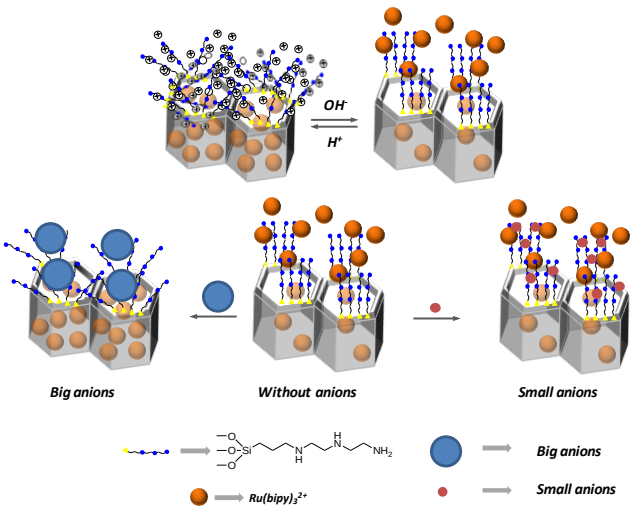

Figure 14. Schematic representation of pH-driven and anion-controlled nano-supramolecular gate-like material.

[80] J. V. Ros-Lis, B. García-Acosta, D. Jiménez, R. Martínez-Máñez, F. Sancenón, J. Soto, F. Gonzalvo, M. C. Valldecabres, *J. Am. Chem. Soc.,* **2004,** *126*, 4064.

Finally the same authors reported the use of this pH-controlled gate-like scaffolding as a prototype for the selective delivery of riboflavin at the intestine.[59b] The idea relies on the different pH at stomach (acid pH) and intestine (basic pH) in order use this hybrid material as an applicable delivery system designed to protect the cargo from the acidic conditions of the stomach.

Whereas the systems previously reported were able to deliver the cargo at neutral pH, Xiao et al. reported a molecular gate able to release vancomycin at acidic pH by anchoring carboxylates on porous SBA-15 silica rods and using the positively charged poly-(dimethyldiallylammonium chloride) (PDDA) as blocking agent. [59c] At acidic pH the protonation of carboxylates resulted in the disruption of the electrostatic interactions with the positively charged polyelectrolyte PDDA allowing the release of the vancomycin.

Pseudorotaxanes and rotaxanes have been also used as gatting molecules in the development of pH-driven hybrid materials. Using this molecules, Stoddart and Zink reported the first pH-responsive nanovalve based on [2]pseudorotaxanes (rotaxane formed within a linear molecule upon which is threaded a single macrocycle) formation via the encirclement of dialkylammonium cations (grafted in the outer surface of a mesoporous material that was previously loaded with coumarin 460) with the macrocyclic polyether dibenzo[24]crown-8 (DB24C8), through hydrogen-bonding interactions.[81] The formation of the 1:1 complex between the ammonium cation and the macrocycle leads the pore closure, whereas addition of a base produced the dethreading of the [2]pseudorotaxane due to the deprotonation of the dialkylammonium groups, releasing the coumarin 460 from the pores to the solution. In further studies, the same authors found that addition of other cationic species (fluorodialkylammonium salts and metal ions) were able to activate the delivery of the probe molecules by competitive binding with the macrocycle, producing a shift of the equilibrium between the ring and the stalk. [82] A representative scheme is shown in Figure 15.

[81] T.D. Nguyen, K.C.-F. Leung, M. Liong, C.D. Pentecost, J.F. Stoddart, J.I. Zink, *Org. Lett.* **2006**, *8*, 3363.

[82] K. C. -F. Leung, T. D. Nguyen, J. F. Stoddart, J. I. Zink, *Chem. Mater.* **2006**, *18*, 5919.

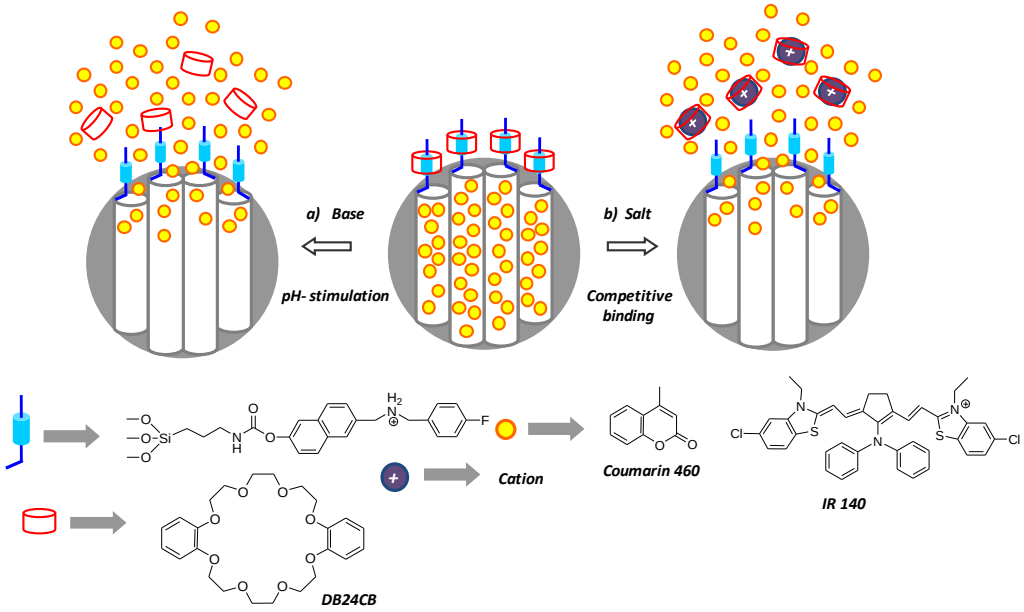

Figure 15. Graphical representation of the operating supramolecular nanovalves from DB24C8/dialkylammonium tethered MCM-41 porous silica particles.

Following with the same concepts other gated systems that incorporate amine and ferrocene stalks, wich form inclusion complexes with cyclodextrins (CD) or cucurbit[n]uril rings (CB[n]), have been reported. CD and CB[n] have the ability to form inclusion complexes that can be reversibly dissociated by external stimuli such as pH change. Bearing these molecules in mind, Kim's group reported a pH-responsive pseudorotaxane-based gated material.[83] In this work they loaded silica mesoporous support with calcein and anchored polyethyleneimine (PEI) stalks on the outer surface. Then, the pores were closed by addition of α- and γ-cyclodextrins at pH 11.0 due to the formation of inclusion complexes with PEI polymer (of 1:1 PEI:α-CD and 2:1 PEI:γ-CD stoichiometries). The new gated system prevented the release of calcein at pH 11.0 whereas when pH was fixed at 5.5,

[83] C. Park, K. Oh, S.C. Lee, C. Kim, *Angew. Chem. Int. Ed.* **2007**, *46*, 1455

calcein release was observed due to amine protonation and subsequent dethreading of the polypseudorotaxanes.

Zink and Stoddart also reported several works employing CD and CB[n] molecules[84] as nanovalves that remained closed at neutral pH levels but opened under mildly acidic conditions for biological applications,[85] and incorporating some of these systems to silica thin films.[59g] In 2010, Du et al. described another new pH-driven supramolecular nanovalve also based on the use of pseudorotaxanes[59h] using mesoporous silica nanoparticles functionalized with 1,4-butanediamine stalks and cucurbit[7]uril units that were able to form a supramolecular complex with the protonated stalks. The pores of the support were loaded with calcein and the gate-like system was opened via deprotonation of the stalks, and also using simple cationic molecules such as cetyltrimethylammonium bromide or 1,6-hexanediamine that were able to bind the cucurbit[7]uril rings. Other gated materials employing the supramolecular interactions between anilines and oxygen-containing macrocycles (i.e. β-cyclodextrin, dibenzo-24-crown-8 and cucurbit[6]uril) as caps have been described recently. These supermolecules were used to prepare pH-responsive materials based in mesoporous organosilica hollow nanospheres (as alternative inorganic supports).[86]

Very recently, a stimulated release of size-selected cargos in succession from mesoporous silica nanoparticles containing the large Hoechst 33342 and the smaller *p*-coumaric acid dyes was reported. This system is able to release both dyes by the application of two different stimuli, first, lowering the pH, and then by adding a reducing agent.[87] The hybrid material contained β-CD rings covalently

[84] a) M. M. Khashab, M. E. Belowich, A. Trabolsi, D. C. Friedman, C. Valente, Y. Lau, H. A. Khatib, J. I. Zink, J. F. Stoddart, *Chem.Commun.*, **2009**, 5371. b) N. M. Khashab, A. Trabolsi, Y. A. Lau, M. W. Ambrogio, D. C. Friedman, H. A. Khatib, J. I. Zink, J. F. Stoddart, *Eur.J. Org. Chem.*, **2009**, 1669.

[85] a) S. Angelos, N. M. Khashab, Y. –W. Yang, A. Trabolsi, H. A. Khatib, J. F. Stoddart, J. I. Zink, *J. Am. Chem. Soc.*, **2009**, *131*, 12912. b) L. Du, S. Liao, H. A. Khatib, J. F. Stoddart, J. I. Zink, *J. Am. Chem. Soc.*, **2009**, *131*, 15136.

[86] W. Guo, J. Wang, S. –J. Lee, F. Dong, S. S. Park, C. –S. Ha, *Chem. Eur. J.*, **2010**, *16*, 8641.

[87] C. Wang, Z. Li, D. Cao, Y. –L. Zhao, J. W. Gaines, O. A. Bozdemir, M. W. Ambrogio, M. Frasconi, Y. Y. Botros, J. I. Zink, J. F. Stoddart, *Angew. Chem. Int. Ed.,* **2012***, 51*, 5460.

attached onto MCM-41 surface through a linker that encloses disulfide units. The β-CD cavities can be plugged with methyl orange (MO), which was able to form reversible inclusion complexes with β-CD rings in response to changes in pH. In this gated material, the small molecules of *p*-coumaric acid were released after protonation of MO (due to the displacement of MO from the β-CD rings), and the large ones Hoechst 33342 were released after cleavage of the disulfide bonds upon addition of mercaptoethanol (ME). Thus, β-CD rings not only acted as gatekeepers for the larger molecules but they also allow small molecules to diffuse to the solution when pH was decreased and MO was moved out of their cavities. Figure 16 show a schematic representation of the dual-cargo release process.

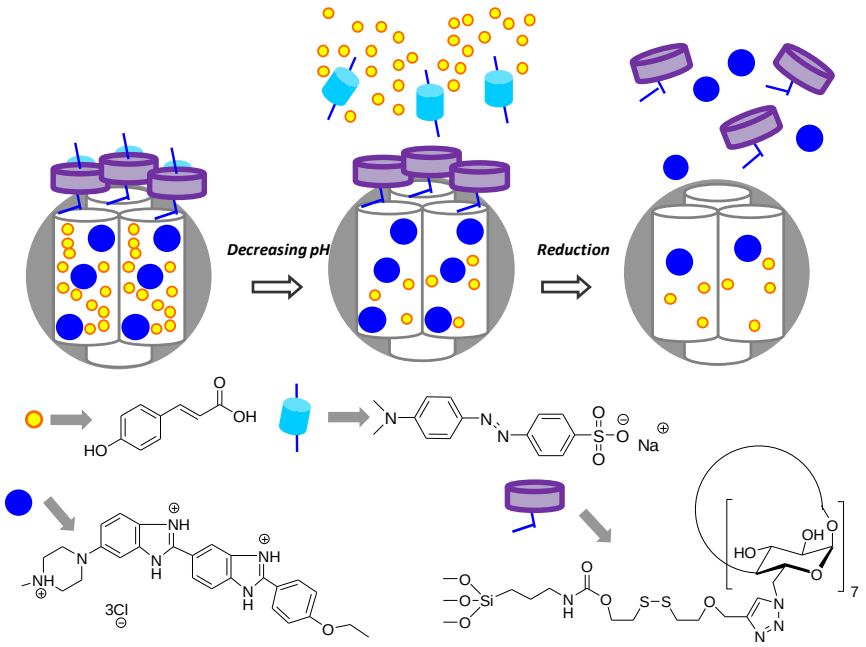

Figure 16. Schematic representation of the dual-cargo release process. The dual cargos can be released one step at a time by, first of all, lowering the pH and then adding mercaptoethanol.

Apart from the use of rotaxanes and pseudorotaxanes as capping systems, pH-driven nanogates have also been described taking advantage of pH-responsive

hydrogels located on the outer surface of mesoporous silica supports. One of the first examples used poly(acrylic acid) (PAA) for the controlled release of bovine serum albumin (BSA) from an SBA-15 material[88] and fluorescein from silica mesoporous nanoparticles.[89] In both cases, at acidic pH, PAA remained contracted preventing guest release, whereas when pH was increased to >7.4, the carboxylic acids of PAA suffered a deprotonation process and the polymer chains adopted a rigid conformation that enables cargo release. Most recently, the same polymer has been used for the preparation of mesoporous silica nanoparticles loaded with doxorubicin and coated with PAA. This synthesized pH-responsive controlled drug delivery system was tested in HeLa cells, in order to study their application in cancer therapy.[90] Appart from PAA, other pH-responsive polymer shells, such as chitosan/polymethacrylic acid (CS-PMAA), have been used as coatings of mesoporous silica nanoparticles (MSN) loaded with doxorubicin and ibuprofen.[91] On the other hand, very recently, Lee and co-workers have demonstrated the introduction of inorganic calcium phosphate (CaP) as a novel pore blocker by enzyme-mediated mineralization on the MSN. This material is able to release doxorubicin from the CaP blocked materials under pH control.[92]

The use of gold nanoparticles as caps on silica mesoporous supports for the development of pH-triggered systems has also been reported.[56c] In this case, MCM-41 material was functionalized with a polialcohol derivative that interacts with boronic acid coated gold nanoparticles giving a pH-labile boronate ester linkage. Dye safranine O was retained in the pore voids at pH higher than 5 but was delivered at pH 3. In addition, this new nanogate can also be opened using light input thanks to the ability of the gold nanoparticles to raise their temperature locally by irradiation with a laser (1064 nm). In a similar way, Feng et

[88] S. –W. Song, K. Hidajat, S. Kawi, *Chem. Commun.*, **2007**, 4396.

[89] C. –Y. Hong, X. Li, C. –Y. Pan, *J. Mat. Chem.,* **2009***, 19,* 5155.

[90] L. Yuan, Q. Tang, D. Yang, J. Z. Zhang, F. Zhang, J. Hu, , *J. Phys. Chem. C.*, **2011**, *115*, 9926.

[91] a) H. Tang, J. Guo, Y. Sun, B. Chang, Q. Ren, W. Yang, *Int. J. Pharm.*, **2011**, *421*, 388. b) A. Popat, J. Liu, G. Q. Lu, S. Z. Qiao, *J. Mater. Chem.,* **2012**, *22*, 11173. c) F. Chen, Y. Zhu, *Micropor. Mesopor. Mater.*, **2012**, *150*, 83.

[92] H. P. Rim, K. H. Min, H. J. Lee, S. Y. Jeong, S. C. Lee, *Angew. Chem. Int. Ed.* **2011**, *50*, 8853.

al. developed a new pH-responsive gate using gold nanoparticles as caps and an acid-labile acetal linker.[93] At neutral pH no release of dye was observed whereas at acidic pH the hydrolysis of the acetal linker detached the gold nanoparticles from the surface allowing dye delivery.

Finally, pH-driven system using quadruplex DNA-capped silica nanocontainers have been described by Qu's group.[94] In this work, the authors controlled cargo release using quadruplex DNA as caps onto pore oulets of mesoporous silica nanoparticles loaded with rhodamine B. Simple conformational changes of this DNA motiv induced by raisning the pH above 8 resulted in rhodamine B release.

The above described examples show the potential applicability of pH as external stimuli for cargo release triggering. pH is one of the more studied stimuli for the development of gate-like materials due to their easy measurement and modification. For all of these issues pH-triggered nanodevices will find promising applications in different scientific and technological fields in the near future.

1.4.4.4 *Temperature-Driven Molecular Gates*

The first temperature-controlled nanoscopic gated hybrid material was reported using modified SMP functionalized with the well-known temperature sensitive polymer *N*-isopropylacrylamide (PNIPAAm). This polymer exhibits a hydrophilic–hydrophobic transition at a "lower critical solution temperature" (LCST) of about 32 °C in water. At temperatures below the LCST, the polymer is in the coil conformation (hydrated), while above the LCST it is in the globule or collapsed state (dehydrated). Using this concept, several autors designed different approaches to for the preparation of thermally responsive hybrid mesoporous materials using the polymer descrived above.[95]

---

[93] R. Liu, Y. Zhang, X. Zhao, A. Agarwal, L. J. Mueller, P. Feng, *J. Am. Chem. Soc.,* **2010**, *132*, 1500.

[94] C. Chen, F. Pu, Z. Huang, Z. Liu, J. Ren, X. Qu, *Nucleic Acids Res.*, **2011**, *39*, 1638.

[95] a) Q. Fu, G. V. R. Rao, L. K. Ista, Y. Wu, B. P. Andrzejewski, L. A. Sklar, T. L. Ward, G. P. López, *Adv. Mat.*, **2003***, 15*, 1262. b) Q. Fu, G. V. R. Rao, T. L. Ward, Y. Lu, G. P. López, *Langmuir*, **2007**, *23*, 170. c) Y. –Z. You, K. K. Kalebaila, S. L. Brock, D. Oupicky, *Chem. Mater.,* **2008***, 20*, 3354.

Aznar and co-workers prepared a new family of paraffin-capped mesoporous silica nanoparticles as thermoresponsive-driven hybrid system.[96] These materials were prepared using MCM-41 supports functionalized with octadecyltrimethoxysilane and paraffins, which are able to form a hydrophobic layer around the pore outlets that inhibits cargo release. An increase of the temperature above the paraffin melting point results in the release of the entrapped guest. With this mechanism a finely tuned tailor-made temperature triggered delivery was achieved. Bearing in mind the possibility to select a wide range of paraffins with specific melting points over a wide range of temperatures, these systems are suitable for applications that demand zero release before stimulus implementation and render them important for delivery applications triggered by selected global or local temperature changes. A schematic mechanism of the function of these temperature-responsive systems is depicted in Figure 17.

DNA sequences have been used recently as capping molecules. At this respect, Bein and co-workers reported the first DNA-based temperature-controlled gated material.[67a] The authors attached biotin-labeled DNA double strands on the pore outlets of colloidal mesoporous silica nanoparticles through a click chemistry reaction and then loaded the material with fluorescein. Finally, the pores were closed by adding the protein avidin through the formation of the strong biotin-avidin complex. The authors found fluorescein delivery upon heating up to the specific melting temperature of the double stranded DNA sequence.

[96] E. Aznar, L. Mondragón, J. V. Ros-Lis, F. Sancenón, M. D. Marcos, R. Martínez-Máñez, J. Soto, E. Pérez-Payá, P. Amorós, *Angew. Chem. Int. Ed.,* **2011**, 50, 11172.

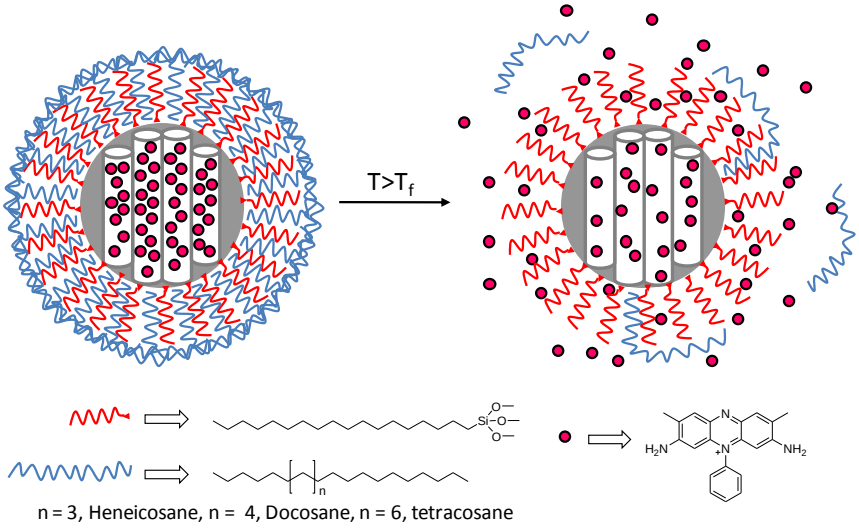

Figure 17. Schematic representation of the gated material functionalized with octadecyltrimethoxysilane and capped with paraffins. The delivery of the entrapped guest (safranine O) is triggered when temperature rises above paraffin melting point. Adapted from *Angew. Chem. Int. Ed.,* **2011**, *50*, 11172. Copyright © 2011 WILEY-VCH Verlag GmbH & Co. KGaA, Weinheim.

1.4.4.5 *Chemical triggers: Bio-molecules and small ionic species.*

In the last few years new bio-controlled molecular gates have been developed, and many authors designed and prepared new hybrid materials able to deliver the internal cargo upon application of biological stimulus. Among different possibilities, some of the most commonly used bio-molecules for the development of bio-gated hybrid materials are enzymes. This is a promising research field taking into account that the use of tailor-made molecular sequences and specific enzymes is envisioned to have a large potential that may provide exquisite selectivity in the design of advanced gate-opening devices.

The first example of gated mesoporous system that responds to an enzyme was described by Stoddart et al. and consisted in a mesoporous support with a [2]rotaxane capped with an ester-linked adamantyl stopper.[64a] Upon addition of porcine liver esterase the bulky adamantyl stopper was released allowing cargo

delivery. Bein and co-workers reported another example using enzyme protease.[64b] In this case, biotinylated mesoporous silica nanoparticles loaded with fluorescein were prepared. The pores were capped by addition of avidin, due to avidin-biotin complex formation. No delivery of the dye was observed in the absence of the protease trypsin whereas the addition of this enzyme induced the hydrolysis of the attached protein avidin and the release of the entrapped dye.

Martínez-Máñez and co-workers demonstrated that the attachment of a lactose derivative as gatekeeper on the surface of silica mesoporous supports provided a suitable method for the design of mesoporous systems that were able to deliver entrapped guests by a bio-controlled uncapping using β-D-galactosidase, due to the enzymatic hydrolysis of the glycosidic bond in the anchored lactose.[64c] In order to improve the efficiency of this system, the authors prepared nanoscopic MCM-41 silica supports loaded with a dye and functionalized, on the pore outlets, with different commercially available hydrolyzed starch derivatives.[65] These materials are tested for the controlled release in intracellular media using HeLa and LLC-PK1 cells. Figure 18 shows a representative scheme of the gated mechanism.

Kim and co-workers reported the preparation of silica nanoparticles functionalized with β-cyclodextrins as gatekeepers and loaded with calcein dye. [64d] Addition of α-amylase induced the release of calcein due to hydrolysis of the cyclodextrin core. The hybrid material contained an *o*-nitrobenzyl ester in the linker that connected β-cyclodextrins with the inorganic scaffold and, due to this, addition of lipase enzyme (able to hydrolize the ester group) induced a delivery of calcein. Moreover this material was able to deliver its cargo upon irradiation with UV light due to the presence of the photocleavable *o*-nitrobenzyl ester moiety.

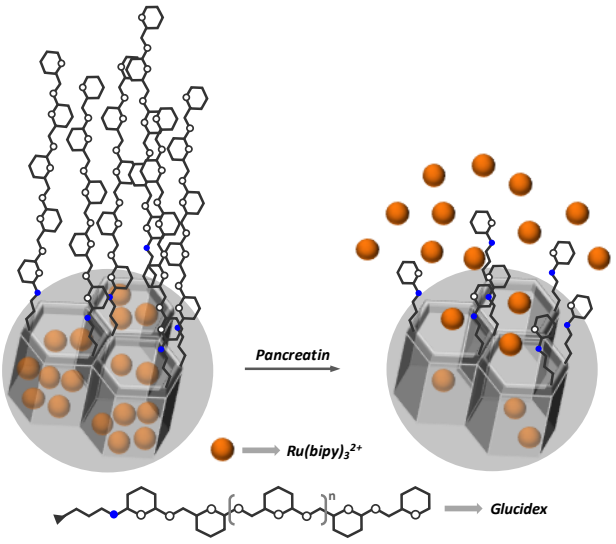

Figure 18. Schematic representation of the gated material capped with hydrolyzed starch derivatives (Glucidex 47, Glucidex 39 and Glucidex 29) and their opening in the presence of pancreatin.

Very recently, highly specific delivery system using peptide-coated mesoporous silica nanoparticles have been reported by Heise and co-workers[64e] and Martinez-Máñez et al.[66a] Heise et al. loaded silica nanoparticles with fluorescein-conjugated dextran molecules and grafted, onto the external surface, a specific peptide sequence containing terminal bulky fluorenylmethoxycarbonyl (Fmoc) fragments. The final material was able to release their cargo only upon addition of thermolysin to the aqueous suspensions of the hybrid nanoparticles. Addition of this enzyme induced the cleavage of the peptide sequence that removed the bulky Fmoc groups and, as a consequence, delivery of the dye was observed. Martínez-Máñez et al. prepared a MCM-41 loaded with the dye $Ru(bipy)_3^{2+}$ and containing onto their surface peptide sequences anchored by click chemistry (see Figure 19). Aqueous solutions of this material are unable to release the entrapped dye, whereas addition of targeted proteolytic enzymes induced the enzymatic hydrolisys of the peptide sequences with the subsequent diffusion of the ruthenium complex.

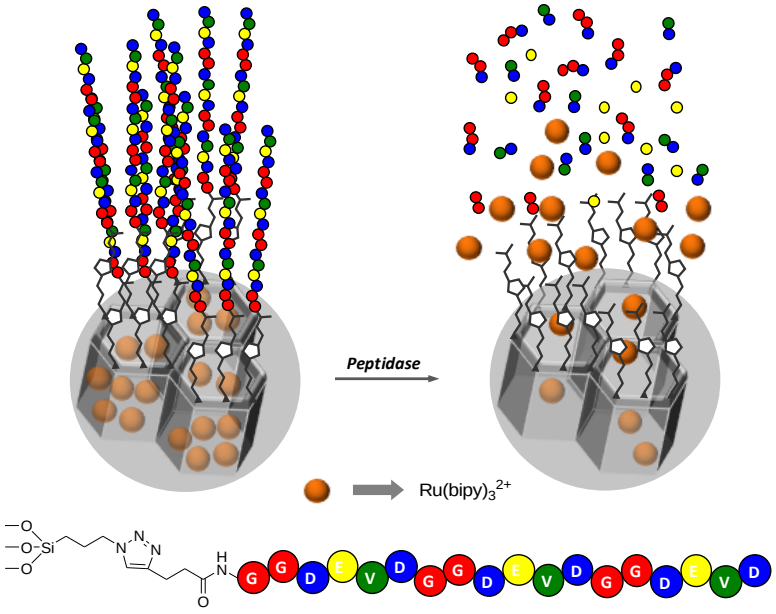

Figure 19. Shematic representation of the gated material capped with peptide sequences (through a click reaction). The release of the loaded $Ru(bipy)_3^{2+}$ dye was achieved through enzymatic cleavage at the C-terminus amide bonds of the negatively charged amino acids (D and E) contained in the peptide sequence.

Besides of the use of enzymes for uncapping mesoporus supports, other bio-molecules have also been used for the design of hybrid materials for delivery applications. At this respect, Lin et al. reported the synthesis of glucose-responsive mesoporous silica nanoparticles-based double delivery system for both insulin and cAMP.[63e] The prepared material is a mesoporous support containing cAMP, in the inner of the pores, and a boronic ester with gluconic acid-modified insulin (G-Ins) anchored onto surface. Bearing in mind that certain carbohydrates are able to form more stable cyclic boronic esters than G-Ins, addition of glucose induced the release of both G-Ins and cAMP from the material. Fructose was also tested, showing enhanced release when compared with glucose due to the fact that phenylboronic acid has a strong preference for binding with the hydroxyls of saccharides in their furanose forms (fructose has 25% of furanose in water whereas glucose contains only 0.14%). However, the authors suggested that this

system was suitable for glucose-responsive insulin release because contents of glucose in blood are higher than fructose. The system was also tested in four different cell lines, showing good viability, proliferation and an efficient intracellular release of cAMP. Other related material that also used saccharidddes as trigger was reported recently by Kim and co-workers.[63h] The authors prepared a mesoporous material loaded with calcein and with boronic acid moieties grafted in the outer surface. Addition of cyclodextrins induced pore capping due to the formation of cyclic boronate esters between the grafted boronic acid and the hydroxyl moieties of the cyclic sacharidddes. The cyclodextrin gatekeeper is removed when glucose or fructose are added to the suspensions of the hybrid material (due to displacement of the cyclodextrins) with the subsequent release of the entrapped calcein.

Concering small ionic species, one of the first examples was the sensing of long-chain carboxylates through the use of size- and polarity-controlled gate-like scaffoldings. The hybrid materials consisted in a mesoporous systems containing $Ru(bipy)_3^{2+}$ dye inside the pores and imidazolium cations anchored on the outer surface.[63b] Coordination between the anchored imidazolium cations and certain carboxylates induced the capping of the gate-like ensemble. This open–closed protocol was related with the size of the carboxylates and with the hydrophilic/hydrophobic nature of the formed monolayer. Small or medium carboxylates, such as octanoate or smaller, were unable to inhibit dye release from the pores to the bulk solution, whereas dodecanoate formed, upon coordination with the imidazolium groups, a highly hydrophobic layer around the pore outlets that inhibited the delivery of the dye. Bearing in mind this work, some years later the same authors reported a similar material for the detection of ionic surfactants in water.[97] At this respect, two hybrid materials were prepared. The first material contained imidazolium cations (in order to coordinate with anionis surfactants) grafted in a silica gel support, whereas the second material used the same support but functionalized with sulfonate anions (in order to

[97] C. Coll, J. V. Ros-Lis, R. Martínez-Máñez, M. D. Marcos, F. Sancenón, J. Soto, *J. Mater. Chem.*, **2010**, *20*, 1442.

interact with cationic surfactants). The self-assembly of the anionic and cationic surfactants on the corresponding surface produced hydrophobic layers that were able to extract, in a second step, the dyes methylene blue (for anionic surfactants) and patent blue (for cationic surfactants). The amount of dye extracted was directly related with the surfactant present in the surface of the hybrid material.

In other work, the same research group prepared an MCM-41 mesoporous support containing the $Ru(bipy)_3^{2+}$ dye in the inner of the pores and functionalised with saccharides at the pore outlets for the selective chromogenic detection of borate in water at neutral pH.[63d] The formation of the corresponding boroester derivative, due to the selective reaction of borate with the anchored saccharides, in the solid produced an inhibition of the delivery of the dye. In addition, the system was also triggered by pH stimulus, releasing dye at acidic pH (due to hydrolysis of boroester moieties), and remaining closed at neutral pH. Scheme 20 shows a paradigm of the sensing mechanism.

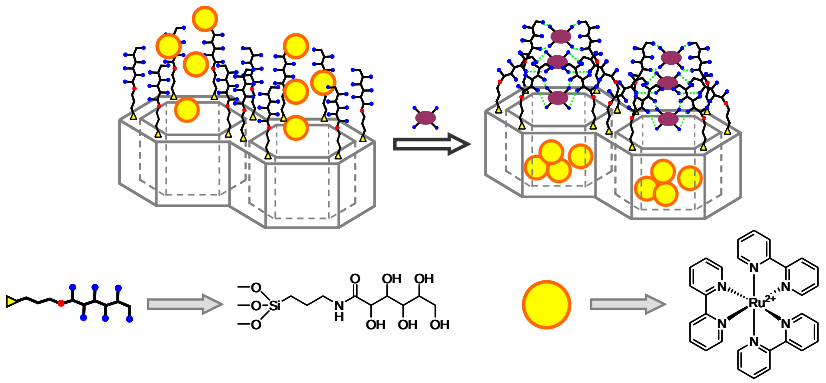

Figure 20. Chromogenic detection of borate anion through the inhibition of dye release from a hybrid mesoporous material functionalized with sacharidddes. Adapted from *Chem. Eur. J.,* **2009**, *15*, 6877. Copyright © 2009 WILEY-VCH Verlag GmbH & Co. KGaA, Weinheim

Recently, a hybrid material capped with disulfide-linked PEG polyetilenglicol (PEG) gatekeepers have been reported for glutathione detection in cells.[98] The authors

[98] a) Y. Cui, H. Dong, X. Cai, D. Wang, Y. Li, *Appl. Mater. Interfaces*, **2012**, *4*, 3177.

loaded then pores of MCM-41 nanoparticles with fluorescein dye, and anchored PEG units onto the surface through disulfide-linkers. These PEG molecules are selectively detached from the surface in the presence of glutathione, due to the cleavage of the disulfide bond, with the subsequent release of the encapsulated dye.

Finally, a hybrid material that responds to the presence of Cs^+ and K^+ has been prepared very recently.[63f] The authors functionalized an MCM-41 material loaded with curcumin (one of the best characterized chemopreventive agents) with a 18-crown-6 derivative in order to prepare a cation-responsive release system. Addition of Cs^+ to suspensions of the hybrid material inhibited curcumin release due to the formation of sandwich type complexes (2:1 18-crown-6:Cs^+) between the bulky cation and the anchored macrocycle. Addition of K^+ cation (smaller than Cs^+ and with high stability constant with the grafted marocycle) induced the displacement of the bulky Cs^+ with the subsequent curcumin release. A schematic representation of the K^+-driven gated material is depicted in Figure 21.

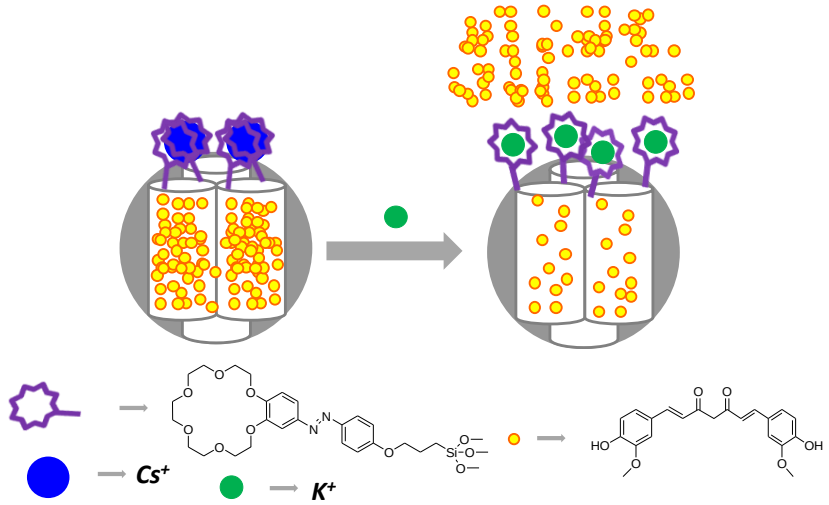

Figure 21. K^+-driven hybrid material for the release of curcumin. The pores of the hybrid materials are closed in the presence of bulky Cs^+ cation (formation of sandwich complexes with 2:1 macrocycle-cation stoichiometry), whereas are opened upon addition of K^+ (formation of 1.1 macrocycle-cation stoichiometry complexes).

From the examples cited before, it is apparent that most of the guest-release systems with gate-like scaffoldings described used light, redox potential, temperature or pH changes as stimulus for controlled mass transport. In contrast there are few hybrid materials in which a small molecule or a biomolecule are used as chemical triggers, specially when this thesis started. For this reason, our aim was to prepare hybrid materials for the detection of chemical species, allowing, in some cases, a control release and involving, in most of the cases, certain biomolecules.

1. Control Access to silica surfaces. An approximation to ion-channels

1.1 **Introduction.**

Most of the functional objects that perform active task in living organisms are nanometric or micrometric in size and are built from very simple molecules such as amino acids, sugars, nucleobases or certain inorganic materials. Due to this, it is not then surprising that chemists have attempted to make use of concepts and strategies from nature to enhance "bottom-up" approaches in order to develop complex nanometric ensembles able mimic biological structures and functions.[1] According to this, Otto H. Schmitt defined the term biomimetics in 1969,[2] as a part of the science that studies and imitates nature's methods, mechanisms and processes.[3,4] This broad area has been reflected by many lines of research related

[1] P. Fratzl, *J. R. Soc. Interface*, **2007**, *4*, 637.

[2] O. H. Schmitt, Proc. 3rd Intl. Biophysics Congress (Boston, MA, 29 Aug. to 3 Sept. 1969) p 297.

[3] Y. Bar-Cohen, *Bioinsp. Biomim.*, **2006**, *1*, 1.

[4] J. F. V. Vincent, O. A. Bogatyreva, N. R. Bogatyrev, A. Bowyer, A.-K. Pahl, *J. R. Soc. Interface*, **2006**, *3*, 471.

to biomimetic chemistry aspects, and chemistry researchers have focused their study on the development of biomimetic hybrid materials in an attempt to prepare abiotic systems that simulate solid biological structures showing increasing complex hierarchical organization.[5]

Bearing in mind this concept, in this chapter systems that attempt to mimic ion channels present in nature are described.[6,7,8,9] The ion channel is a very general system in biological entities and are used, for instance, in the conversion of extracellular events into intracellular signals via hormones, in transfer of information in nerve systems, etc. The unique feature of ion channels in biological cell membranes is a selective recognition of substrates. This recognition induces a conformational change that allows the opening of an ion-specific channel with the subsequent permeation of great amount of ions across the membrane following an electrochemical potential gradient.

Umezawa et al.[10] described in 1987 an electrochemical detection system that mimicked the ion channels present in biological membranes, calling this type of systems as ion-channel sensors (ICSs).[11,12] These sensors are normally electrochemical, and consist of an electrode that contains a monolayer of molecules anchored on its surface than act as receptors. These receptors are able to react specifically with different analytes, and coordination with these analytes modulates the accessibility of redox markers (molecules with defined and reversible oxidation-reduction processes) to the electrode surface. As a result, an electrochemical detection induced by analyte coordination with surface receptors

[5] C. Sanchez, H. Arribart, M. M. G. Guille, *Nat. Mater.*, **2005**, *4*, 277.

[6] M. Montal, *Annu. Rev. Biophys. Biomol. Struct.*, **1995**, *24*, 31.

[7] T. J. Jentsch, V. Stein, F. Weinreich, A. A. Zdebik, *Physiol. Rev.*, **2002**, *82*, 503.

[8] S. Morbach, R. Krämer, *ChemBioChem*, **2002**, *3*, 385.

[9] J. A. Wemmie, M. P. Price, M. J. Welsh, *Trends Neurosci.*, **2006**, *29*, 578.

[10] M. Sugawara, K. Kojima, H. Sazawa, Y. Umezawa, *Anal. Chem*. **1987**, *59*, 2842.

[11] L. M. Goldenberg, M. R. Bryce, M. C. Petty, *J. Mater. Chem.*, **1999**, *9*, 1957.

[12] Y. Umezawa, H. Aoki, *Anal. Chem.*, **2004**, *76*, 320A.

is observed. These type of sensors have a function of channel switching by the following sequence: in the absence of a stimulus (analyte), the channel is closed and, therefore, marker ions (monitoring ions) cannot permeate through the "membrane". On the other hand, when the stimulus is present, the channel is opened, and a large amount of marker ions are allowed to permeate through the membrane, which are immediately detected electrochemically at an underlying electrode. The amount of marker ions thus detected is a direct but much amplified measure of the amount of analyte.

Depending on the mechanism of response it is possible to difference between two types of ion channel sensors, as shown in Figure 1.1. In the first case (Figure 1.1a), the analyte molecules form complexes with the receptors on the electrode, blocking the access of the marker to the electrode surface. This approach attempts to mimic the ion channels formed by proteins, and it could be use for the detection of neutral species or analytes which are not able to produce oxidation-reduction processes. In the second case (Figure 1.1b), the response mechanism is based on electrostatic attraction or repulsions. When the analyte (an ionic target) interacts with the receptor anchored into the electrode, produces an alteration in total charge of the monolayer, and, with this, it is possible to adjust the oxidation or reduction of electroactive ions (markers) on the surface of the electrode.

The main point in the design of the sensor "membranes" is that they need to provide receptor functions for selective recognition of analytes and, at the same time, the analyte need to provide gated permeability changes in order to produce a swiching access for redox marker ions to the surface. Uncharged receptor formed by self-assembled monolayers (SAMs) are generally not void-free, and the marker ions can permeate to a degree, but in the case of charged receptors, the marker ion with the same charge is repelled from the receptor surface due to the electrostatic repulsion, allowing minimum permeability. For this reason, a redox marker with a negative or positive charge (often $[Fe(CN)_6]^{3-/4-}$ or $[Ru(NH_3)_6]^{3+/2+}$) is selected according to the "membrane" charge.

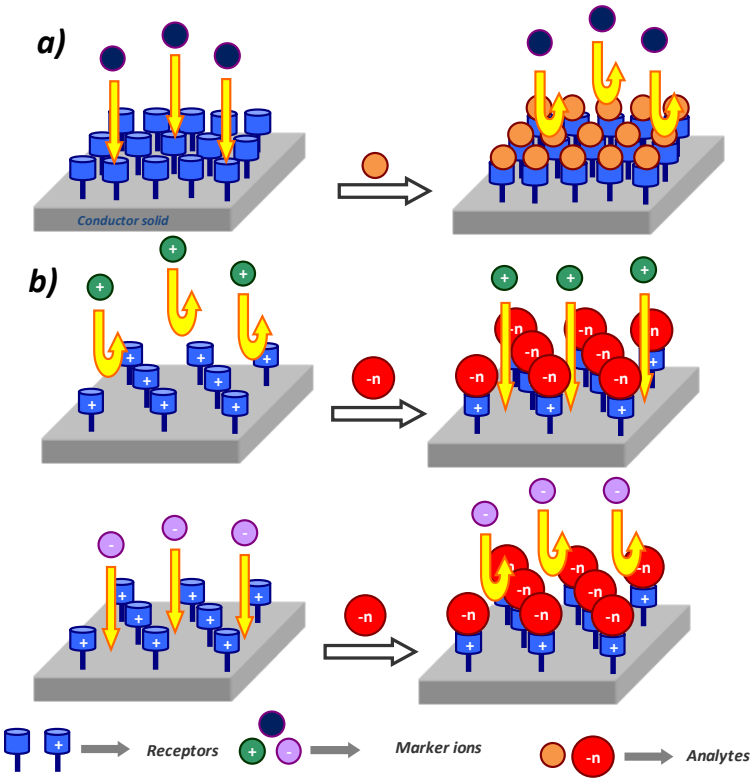

Figure 1.1.- Scheme of two different mechanisms of ICSs based on synthetic receptors.

One advantage of these ion channel systems is the signal amplification produced. In an ideal case, a single analyte can open or close more than one channel, and, as a consequence, a number of molecules that act as markers can diffuse through the chanels, and a signal produced by the presence of the analyte is observed.[13,14] Another advantage offered by this type of sensor is that receptors can be synthetic, but it is possible to use biological receptors, such as antibodies or proteins. Furthermore, we should also consider that the mode of signal

[13] P. Bühlmann, H. Aoki, K. P. Xiao, S. Amemiya, K. Tohda, Y. Umezawa, *Electroanalysis*, **1998**, *10*, 1149.

[14] M. Sugawara, A. Hirano, P. Bühlmann, Y. Umezawa, *Bull. Chem. Soc. Jpn.*, **2002**, *75*, 187.

transduction does not change when the pair analyte-receptor changes, due to the fact that signal is produced only by the control access of the redox markers to the electrode surfaces in order to produce an oxidation or reducción reaction.[12]

Some of the earliest examples, in which ICSs were described, contained multilayer "membranes" of anionic phospholipids, macrocyclic polyamines and cyclodextrin with ammonium groups[10,15] as receptors. In order to prepare ICSs, these receptors were fixed on a glassy carbon (GC) electrode by the Langmulr-Blogdett method. In the first case, the phospholipid layer blocked the access of redox marker $Fe(CN)_6^{4-}$ to the electrode surface, and oxidation was not able to be produced. Complexation between phospholipids and the cationic analyte added (for instance Ca^{2+}), via electrostatic interactions, induced a decrease in the repulsion between the marker and the surface, and with this, the marker could access from the solution to the electrode surface producing the oxidation of $Fe(CN)_6^{4-/3-}$. With the aim of improving the stability of monolayer generated in the electrode surface using the Langmuir-Blodgett technique, Nakashima and coworkers prepared the first biomimetic ion channel sensor based on self-assembled monolayer surfaces (SAMs), consisting of a monolayer of a thiol-containing phosphate lipid by the spontaneous assembly onto gold electrodes.[16]

In another case, gold electrodes were modified by SAMs of thioctic acid for the detection of protamine (a polycation used to neutralize the anticoagulant activity of heparin) using $[Ru(NH_3)_6]^{3+}$ and $[Fe(CN)_6]^{3-}$ as redox markers.[17] After deprotonation of thioctic acid, the carboxylate group conferred to the electrode surface a negative charge, inducing adsorption of protamine through electrostatic interactions, preventing the access of $[Ru(NH_3)_6]^{3+}$ to the electrode surface. In the absence of protamine $[Ru(NH_3)_6]^{3+}$ had free access to the electrode surface,

[15] S. Nagase, M. Kataoka, R. Naganawa, R. Komatsu, K. Odashima, Y. Umezawa, , *Anal. Chem.*, **1990**, *62*, 1252.

[16] T. Nakashima, Y. Taguchi, K. Takada, M. Fujio, O. Kunitake, J. Manabe, *J. Chem. Soc., Chem. Commun*., **1991** 232.

[17] V. P. Y. Gadzekpo, K. P. Xiao, H. Aoki, P. Bühlmann, Y. Umezawa, *Anal. Chem.*, **1999**, *71*, 5109.

yielding the reduction of $[Ru(NH_3)_6]^{3+}$ to $[Ru(NH_3)_6]^{2+}$. When we used a negatively charged marker, the detection scheme was reversed. In the absence of protamine, $[Fe(CN)_6]^{3-}$ was repelled by the SAM, but addition of protamine induced a decrease of the negative charge excess on the monolayer. This decrease of surface negative charge allowed the access of $[Fe(CN)_6]^{3-}$ to the electrode surface showing, as a consequence, a reduction process.

The same authors used an electrode coated with this polycation (protamine) to detect heparin, using in this case the control of the rate of $[Mo(CN)_8]^{4-}$ oxidation or $[Fe(CN)_6]^{3-}$ reduction.[18] Heparin, being negatively charged, is able to neutralize the charges of protamine and provides the electrode surface with an excess of negative charge. As a consequence, heparin produces a repulsion of the marker ions from the electrode surface. A representative scheme for the detection of protamine and heparin is described in Figure 1.2.

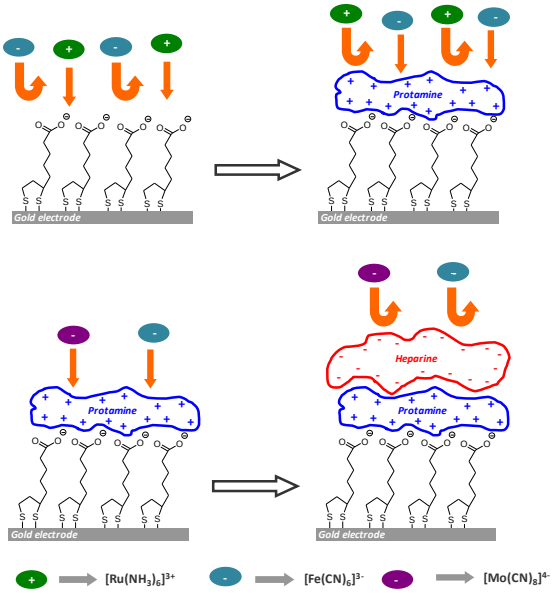

Figure *1.2.*- Scheme for protamine and heparin detection using a gold electrode modified with thiotic acid and $[Fe(CN)_6]^{3-}$, $[Ru(NH_3)_6]^{3+}$ and $[Mo(CN)_8]^{4-}$ probes as electrochemical markers.

[18] V. P. Y. Gadzekpo, P. Bühlmann, K. P. Xiao, H. Aoki, Y. Umezawa, *Anal. Chim. Acta*, **2000**, *411*, 163.

Apart from the examples described above, other materials have been prepared using the same approach in order to detect metal ions,[19–21] some analytes (via complex formation),[22,23] certain anions[24] and oligonucleotides.[25]

Mimicking ion channels is not the only strategy that chemists follow to utilize features of natural membrane systems, and other approaches that exploit their principle of operation for technological applications are the use of modified biological channels,[26] protein pores[27] via natural ionophores (such as valinomycin combinated with biomimetic membranes),[28] or under selected artificial conditions[29] in order to combine artificial ionophores with lipid membranes.[30] Other approaches that have been used are the development of artificial systems such as ionophore-polymer hybrids[31] or the use of molecular imprinted polymers (MIPs).[32]

---

[19] K. Bandyopadhyay, H. Liu, S.-G. Liu, L. Echegoyen, *Chem. Commun.*, **2000**, 141.

[20] S. Flink, H. Schönherr, G. J. Vancso, F. A. J. Geurts, K. G. C. van Leerdam, F. C. J. M. van Veggel, D. N. Reinhoudt, *J. Chem. Soc. Perkin Trans. 2*, **2000**, 2141.

[21] H. Aoki, Y. Umezawa, A. Vertova, S. Rondinini, *Anal. Sci.*, **2006**, *22*, 1581.

[22] H. Aoki, Y. Umezawa, *Analyst*, **2003**, *128*, 681.

[23] Y. Katayama, Y. Ohuchi, H. Higashi, Y. Kudo, M. Maeda, *Anal. Chem.*, **2000**, *72*, 4671.

[24] H. Aoki, K. Hasegawa, K. Tohda, Y. Umezawa, *Biosens. Bioelectron.*, **2003**, *18*, 261.

[25] a) H. Aoki, P. Bühlmann, Y. Umezawa, *Electroanal.*, **2000**, *12*, 1272. b) H. Aoki, Y. Umezawa, *Electroanal.*, **2002**, *14*, 1405. H. Aoki, Y. Umezawa, *Analyst*, **2003**, *128*, 681.

[26] H. Bayley, C. R. Martin, *Chem. Rev.*, **2000**, *100*, 2575.

[27] Y. Jung, H. Bayley, L. Movileanu, *J. Am. Chem. Soc.*, **2006**, *128*, 15332.

[28] a) A. T. A. Jenkins, N. Boden, R. J. Bushby, S. D. Evans, P. F. Knowles, R. E. Miles, S. D. Ogier, H. Schönherr, G. J. Vancso, *J. Am. Chem. Soc.*, **1999**, *121*, 5274. b) L. Rose, A. T. A. Jenkins, *Bioelectrochem.*, **2007**, *70*, 387.

[29] H. Tsukube, K. Takagi, T. Higashiyama, T. Iwachido, N. Hayama, *Inorg. Chem.*, **1994**, *33*, 2984.

[30] a) J. H. van Zanten, H. G. Monbouquette, *Biotechnol. Prog.*, **1992**, *8*, 546. b) O. Murillo, I. Suzuki, E. Abel, C. L. Murray, E. S. Meadows, T. Jin, G. W. Gokel, *J. Am. Chem. Soc.*, **1997**, *119*, 5540. c) N. Sakai, K. C. Brennan, L. A. Weiss, S. Matile, *J. Am. Chem. Soc.*, **1997**, *119*, 8726.

[31] M. F. M. Roks, R. J. M. Nolte, *Macromol.*, **1992**, *25*, 5398.

[32] P. Metilda, K. Prasad, R. Kala, J. M. Gladis, T. P. Rao, G. R. K. Naidu, *Anal. Chim. Acta*, **2007**, *582*, 147.

1.2 **Objectives**

Bearing in mind these examples we considered the possibility of design different systems for the colorimetric detection of target chemical species, based on ionic channels reported above.

Thus, the main objective of this chapter is the design and development of new organic-inorganic hybrid materials that could be able to modulate the accessibility of certain chemical species to functionalized surfaces (in particular silica surfaces), with the aim to obtain colorimetric ion-channel-like materials for the detection of target analytes.

Specifically, our aim was:

- ✓ Design and synthesis of ion-channel-like sensor systems, inspired by biological ion-channels, with the ability to detect target chemical species using a colorimetric response by the anchoring of organic molecules on silica supports.
- ✓ Characterization of new hybrid systems by the usual techniques used in material chemistry for hybrid organic-inorganic solids.
- ✓ Evaluate the hybrid materials prepared according to the chemical properties of the medium (changes in pH) or in the presence or absence of different chemical species.

1.3 **Design of the system**

The design of this new detection system is based on the use of a solid support containing two different groups. On one hand, and trying to mimic ion channels, the first group should contribute to modulate the access of different chemical species to the surface. This group should act as a receptor, or host (H), and should interact specifically with certain analytes of interest. On the other hand, the second group should act as a reactive center (R). The role of (R) is to react with a

certain reporter molecule, such a dye (D), inducing a measurable change in colour or fluorescence. The presence of certain guests (G) (such as analytes of interest which are able to coordinate with the receptor (R)) should inhibit the access of the reporter molecule (D) to the reactive center (R), and therefore any change should be observed. However, in the absence of the guests (G), the indicator (D) could access to the surface, showing a change in the optical properties of the solution due to reaction between the reporter dye (D) and the reactive center (R). Thus, the sensing protocol relies on the inhibition of the reaction between (R) and (D) when a suitable guest (G) is bound to (H), resulting in a modulation of the signal change, due to the control of dye transport from the solution to the silica surface. A schematic of the proposed approach is shown in Figure 1.3.

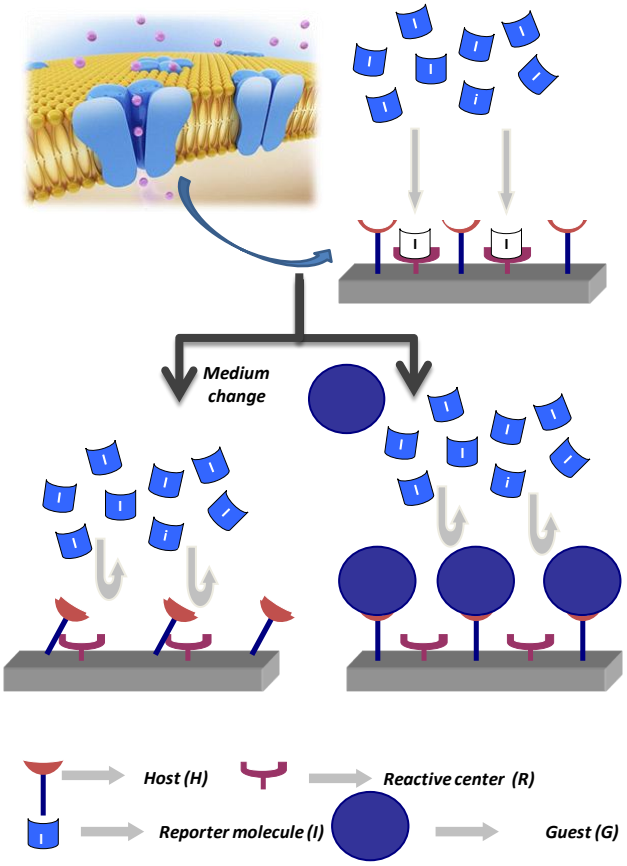

Figure 1.3.- Scheme showing the design of the new detection paradigm. The colorimetric detection is achieved by changes in the medium or by the presence of certain chemical species.

When this thesis was developed, as far as we know, neither chromogenic nor fluorogenic hybrid systems using the ion channel approach had been described in the literature. In addition, and related with ICSs described above, the designed sensory systems shoud allow us to detect several chemical species with a simple change in the receptor-indicator pair. This strategy would yield a large number of possibilities to prepare new bis-functionalized solids with improved recognition capabilities (when compared with traditional molecular receptors) with a chromo-fluorogenic response.

By using this new approach, we have prepared different materials using inorganic solids as supports for the development of new protocols of recognition. We designed colorimetric assays for pyrophosphate,[33] heparin[34] and surfactants[35] employing silica fumed and silica nanoparticles as inorganic supports. These materials are suitable inorganic supports because presented certain favourable characteristics such as inertness, ease of functionalization, and a relatively high specific surface area (ca. 200 $m^2 g^{-1}$).

1.3.1 Reactive center (R) and indicator (D) selected.

Squaraines are a class of organic dyes that shows intense absorbance and fluorescence in the red and near infrared region. They are characterized by their unique aromatic four membered ring system derived from squaric acid, and are prepared by an electrophilic aromatic substitution reaction with an aniline or another electron rich derivative in order to form a highly conjugated product. As a consequence, these dyes present very intense absorption bands (with absorption maxima wavelength between 630 and 670 and log $\varepsilon > 5$) due to a charge transfer

[33] E. Climent, R. Casasús, M. D. Marcos, R. Martínez-Máñez, F. Sancenón, J. Soto, *Chem. Commun.*, **2008**, 6531.

[34] E. Climent, P. Calero, M. D. Marcos, R. Martínez-Máñez, F. Sancenón, J. Soto, *Chem. Eur. J.*, **2009**, *15*, 1816.

[35] E. Climent, C. Giménez, M. D. Marcos, R. Martínez-Máñez, F. Sancenón, J. Soto, *Chem. Commun.*, **2011**, 6873.

between donor groups (nitrogen atoms of aniline) and acceptor groups (electron deficient four membered central ring) of squaraines. Solutions of these squaraines are also fluorescent (with emission maxima wavelength between 650–700 nm) with relatively high quantum yields even in aqueous environments.[36] Due to these impressive optical properties,[37] these dyes are commonly used as fuorescent probes and labels in the design and preparation of molecular sensors for the determination of cations,[38] anions[39] or neutral species.[40]

Moreover, the four membered central ring of squaraines is electron deficient, and it is able to react with nucleophilic species, yielding addition product. These adducts contains a sp^3 carbon, wich inhibits electronic conjugation and, as a consequence, the charge transfer band and the color dissapears. Also, reaction of squaraines with nucleophilic species is fast, take place at room temperature and in a wide pH range.

Bearing in mind our proposed design of bi-functionalised surfaces that use an indicator that change their chromo-fluorogenic properties when interacts with a reactive center, we selected squaraines as reporter molecule for the development of this new sensing approach. Then, we selected thiols as reactive centers, because are nucleophilic species that would give substitution reactions with the

[36] a) W. C. Dirk, W. C. Herndon, F. Cervantes-Lee, H. Selnau, S. Martínez, P. Kalamegham, A.Tan, G. Campos, M. Vélez, J. Zyss, I. Ledoux, L. Cheng, *J. Am. Chem. Soc.*, **1995**, *117*, 2214. b) P. V. Kamat, S. Das, G. Thomas, M. V. George, *J. Phys. Chem.*, **1992**, *96*, 195. c) K.-Y. Law, *J. Phys. Chem.*, **1987**, *91*, 5184-5193.

[37] a) P. T. Snee, R. C. Somers, G. Nair, J. P. Zimmer, M. G. Bawandi, D. G. Nocera, *J. Am. Chem. Soc.*, **2006**, *128*, 13320. b) V. S. Jisha, K. T. Arun, M. Hariharan, D. Ramaiah, *J. Am. Chem. Soc.*, **2006**, *128*, 6024. c) W. Pham, R. Weissleder, C. H. Tung, *Angew. Chem. Int. Ed.*, **2002**, *41*, 3659. d) E. U. Akkaya, S. Turkyilmaz, *Tetrahedron Lett.*, **1997**, *38*, 4513. e) K. G. Thomas, K. J. Thomas, S. Das, M. V. George, *Chem. Commun.*, **1997**, 597.

[38] a) J. V. Ros-Lis, R. Martínez-Máñez, K. Rurack, F. Sancenón, J. Soto, M. Spieles, *Inorg. Chem.*, **2004**, *43*, 5183. b) J. V. Ros-Lis, M. D. Marcos, R. Martínez-Máñez, K. Rurack, J. Soto, *Angew. Chem. Int. Ed.*, **2005**, *44*, 4405.

[39] J. V. Ros-Lis, R. Martinéz-Máñez, J. Soto, *Chem. Commun.*, **2002**, 2248-2249.

[40] J. V. Ros-Lis, R. Martínez-Máñez, J. Soto, *Org. Lett.*, **2005**, *7*, 2337-2339.

electron deficient four membered ring of the squaraines. This reaction between squaraines and thiols induced a rupture of the electronic delocalization and bleaching of the blue squaraine solution. The chromo-fluorogenic response arises from the fact that in the absence of guests, able to interact with receptors anchored onto surfaces, squaraine will react with thiols anchored to the surface and, as a consequence, a bleaching of the blue color suspension will be observed. However, in presence of certain guest, coordination with the hosts occurs with the subsequent modulation of the squaraine access to the thiols anchored onto surface. As a consequence, no decoloration or a partial decoloration will be observed. Chemical structure of a general squaraine and the addition product generated by reaction with thiols are shown in Figure 1.4.

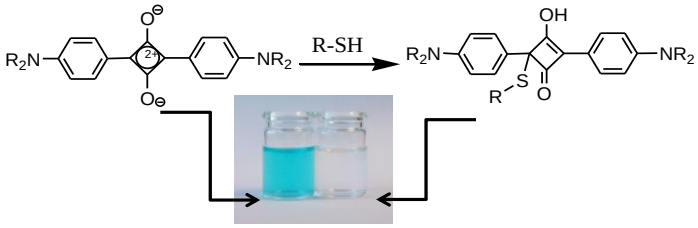

Figure *1.4.* Chemical structure of a squaraine (R can be an alkyl chain, a chain containing heteroatoms or aromatic rings) and of the addition product yielded by reaction between squaraines and thiols.

A myriad of squaraines has been synthesized in the last years. For the development of chromo-fluorogenic ion-channel sensors we selected (4-(bis(2-(2-methoxyethoxy)ethyl))aminophenyl squaraine **I** which structure is shown in Figure 1.5. The presence of two polyether chains enhances its water solubility. This is an important issue for the application of the designed hybrid materials in the detection of chemical species in aqueous media. In addition, the optical properties of this molecule are well known.[41] Nucleophilic attack of thiol to

[41] a) J. V. Ros-Lis, B. García, D. Jiménez, R. Martínez-Máñez, F. Sancenón, J Soto, F. Gonzalvo, M. C. Valldecabres, *J. Am. Chem. Soc.*, **2004**, *126*, 4064. b) J. V. Ros-Lis, R. Casasús, M. Comes, C. Coll, M. D.

squaraine **I** leads to the formation of the 2,4-bis(4-dialkylaminophenyl)-3-hydroxy-4-alkylsulfanylcyclobut-2-enone derivative (see Figure 1.5).

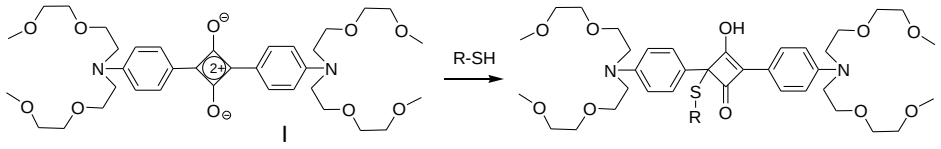

I

Figure 1.5. Chemical structure of bis (4-(bis (2 - (2-methoxyethoxy)ethyl))aminophenyl) squaraine **I** employed and addition product obtained upon reaction of squaraine I with thiols.

As discussed above, our aim is to prepare hybrid materials that allows, with a proper selection of the host (as a receptor), the recognition of different chemical species. Our initial goal was the detection of target anionic species. For this proposal, we used polyamines as binding sites (hosts) in our hybrid sensory material. The nitrogen atoms of the polyamine possess different degree of protonation at different pH values. As a consequence, polyamines (especially when the amino group is converted into ammonium cation by protonation) could interact with different anions yielding several complexes through electrostatic interactions and/or hydrogen bonds.[42] Bearing these concepts in mind, coordination of polyamines with anions could modulate the access of squaraine **I** to the thiols anchored onto silica surface and, with this, detect the presence of these species in solution. Selective targeting of pyrophosphate and heparin is reported.

Using the same recognition protocol, another hybrid material for the colorimetric detection of anionic surfactants in water was prepared. Bearing in mind previous works reported in our research group, we selected imidazolate cations as binding

---

Marcos, R. Martínez-Máñez, F. Sancenón, J. Soto, P. Amorós, J. El Haskouri, N. Garró, K. Rurack, *Chem. Eur. J.*, **2008**, *14*, 8267.

[42] a) F. Sancenón, A. Benito, J. M. Lloris, R. Martínez-Máñez, T. Pardo, J. Soto, *Helv. Chim. Acta*, **2002**, *85*, 1505. b) J. M. Lloris, R. Martínez-Máñez, M. Padilla-Tosta, T. Pardo, J. Soto, M. J. L. Tendero, *J. Chem. Soc., Dalton Trans.*, **1998**, 3657.

sites (hosts) for anionic surfactants.[43] It is well known that imidazolate cations are able to interact with several anions through electrostatic interactions or $(CH)^{+}\cdots X^{-}$ hydrogen bonds. Sulfate is one of these anions, and is present as polar head in the structure of several surfactants.[44]

The following sections discuss in detail the preparation of different hybrid materials that are based on ICSs sensors (functionalized with several binding sites and thiols as a reactive center). Characterization of these materials and studies about the anion-controlled accessibility of squaraine **I** to thiol moieties anchored onto different silica surfaces are described.

[43] a) C. Coll, R. Martinez-Mañez, M. D. Marcos, F. Sancenón, J. Soto, *Angew. Chem. Int Ed.***, 2007,** *46*, 1675. b) C. Coll, R. Martínez-Máñez, M. D. Marcos, F. Sancenón, J. Soto,R. K. Mahajan, *Eur. J. Inorg. Chem.*, **2009**, 3770.

[44] a) J. Y. Kwon, N. J. Singh, H. Kim, S. K. Kim, K. S. Kim, J. Yoon, *J. Am. Chem. Soc.*, **2004**, *126*, 8892. b) J. Yoon, S. K. Kim, N. J. Singh, J. W. Lee, Y. J. Yang, K. Chellappan, K. S. Kim, *J. Org. Chem.*, **2004**, *69*, 581. c) C. E. Willans, K. M. Anderson, P. C. Junk, L. J. Barbour, J. W. Steed, *Chem. Commun.*, **2007**, 3634. d) C. Coll, R. Casasús, E. Aznar, MD. Marcos, R. Martínez-Máñez, F. Sancenón, J. Soto, P. Amorós, *Chem. Commun*., **2007**, 1957.

Colorimetric sensing of pyrophosphate in aqueous media using bis-functionalised silica surfaces

Estela Climent, Rosa Casasús, María Dolores Marcos, Ramón Martínez Máñez, Félix Sancenón and Juan Soto

Instituto de Reconocimiento Molecular y Desarrollo Tecnológico, Centro Mixto Universidad Politécnica de Valencia-Universidad de Valencia, Spain
Departamento de Química, Universidad Politécnica de Valencia, Camino de Vera s/n, 46022 Valencia, Spain
CIBER de Bioingeniería, Biomateriales y Nanomedicina (CIBER-BNN).

Received 2nd February 2009, Accepted 1st April 2009
First published on the web 6th May 2009

Dalton Transactions, ***2009****, 4806-4814*

Abstract

Bis-functionalised silica surfaces have been designed in order to develop selective and sensitive probes for the chromo -fluorogenic detection of certain guests. The designed system consists of a siliceous support bis-functionalised with thiol and polyamine groups . Thiol groups are suitable reactive centres (R) that are know to react with squaraine dyes (D) inducing bleaching, whereas polyamines act as host sites (H) able to coordinate certain target guests (G). In the absence of G, the reactive groups (R) react with the dye resulting in a bleaching of the solution. On the contrary, the presence of certain guest (G) results in a control of the reaction kinetic between R and D and eventually in a complete reaction inhibition. Different functionalised solids **S1*x*** were prepared by reaction of the siliceous surface with different concentrations of mercaptopropyltrimethoxysilane (**MPTS**) and 3-[2-(2-aminoethylamino)ethylamino]propyl-trimethoxysilane (**N3TS**). The final materials (solids **S1a** to **S1d**) were characterized employing standard procedures. In a first step the reactivity of the signaling dye D (squaraine **I**) with the reactive centre R (thiol groups) was studied as a function of the pH using solid **S1d** that showed a most suitable response. At pH 7 and pH 5 there was a quick reaction between the squaraine and the thiol groups on the surface. On the contrary this reaction is significantly slower at pH 3 due to the different degree of protonation of the amines as a function of the pH. Additionally the reaction of **S1d** with the squaraine **I** has been studied in the presence of a range of inorganic anions with different structural dimensions and charges, including chloride, perchlorate, nitrate, sulfate, phosphate and pyrophosphate. At pH 3 the reaction of the dye with the thiol groups is still effective in the presence of chloride and perchlorate, but the reaction is highly inhibited in the presence of the anions nitrate, sulfate, phosphate and pyrophosphate. At pH 7 the squaraine **I** reacts very fast with the thiol groups in the presence of all the anions studied. In contrast, at pH 5 only pyrophosphate is able to inhibit, to a certain extent, the reaction of the squaraine with the thiols, resulting in a selective chromo-fluorogenic detection of this anion in pure water. Finally, the observed behaviour was discussed in terms of both, the kinetic rates of the reaction between the thiol and the squaraine

groups and the thermodynamic interaction reaction between the anions and the polyamine moieties.

Introduction

One recently suggested mode to advance new functionalities in connection with supramolecular concepts is to attach molecular entities on pre-organized solid structures. This approach has recently resulted in a number of new functional enhanced chemical effects.[1] Related with this issue is the anchoring of certain molecular entities on surfaces with the aim of developing controlled switchable solids *via* changes in external stimuli.[2] This interesting field of research has been focused on both (i) the control of physical properties of the material such as wettability[3], adhesive features,[4] roughness,[5] biocompatibility,[6] *etc.* and (ii) supramolecular electrochemical or photochemical control of host–guest complexation at surfaces.[7,8] For these systems, the solids are modified in most cases with switching molecules that respond to light, redox stimuli and thermal changes. This has been mainly achieved using polymers and self-assembled monolayers (SAMs) in both cases causing changes in morphologies that result in modulations or switching in the macroscopic properties of the modified surfaces. The redox and photochemical examples have been focused to control simple host –guest interactions between anchored molecules and target guests (*e.g. via* modulation of the binding efficiency or controlling assembly/disassembly) or to the fabrication of devices *via* immobilization of molecular redox or photo-active switching systems based on interlocked molecules.

In relation to recognition and signaling using functionalised surfaces, a suggestive approach involves the design of the so-called ion channel sensors. These systems consist of a conducting solid and a layer of anchored molecular entities containing certain binding sites. When certain guests coordinate the binding sites on the anchored layer there is a change in the net charge on the layer that results in a regulation of the oxidation or reduction of an electroactive ion (*i.e.* the redox marker). Thus, the coordination of guest anchored substrates guides the

accessibility of the redox marker to the electrode surface resulting in an overall guest-controlled switching functional effect.[9] The principle of ion-channels was first reported by Umezawa[10] trying to mimic membranes -containing ion-channel proteins, that are able to be opened *via* selective binding of ligands allowing guests to pass across the membranes. Based in this concept many sensors have been reported for a wide range of species from simple metal ions[11] to complex guests.[12]

Despite these interesting examples we believe that there is still plenty of room for the design of controlled responsive surfaces. For instance the development of ion-channel-mimetic sensors have been reported using electrochemical markers but as far as we know the same concept has not been applied to the design of optical probes for selective guest sensing. Following our interest in the study of supramolecular functional aspects that arise from the covalent grafting of organic molecules to solid supports,[13] we focused our attention towards the use of ion-channels for the design, for the first time, of chromo-fluorogenic probes based on a competitive access to functionalized surfaces. The new chromogenic signaling approach is shown in Scheme 1. It involves the use of a suitable support decorated with two distinctive groups. One is a suitable reactive centre (R) that is know to react with a certain dye (D) inducing bleaching, whereas the other anchored group is a host site (H) able to coordinate certain target guests (G). In the absence of G, the reactive groups will react with the dye resulting in a bleaching of the solution ("off state"). On the contrary, the presence of the guest G results in a control of the reaction kinetic between R and D and eventually in a complete reaction inhibition ("on state"). As far as we know, from the literature it is apparent that studies similar to those shown in Scheme 1 for the design of new chromo-fluorogenic probes have not been reported. Yet, we envisioned that the protocol is simple and versatile and would allow taking coordination chemistry up to new signaling applications in hybrid materials.

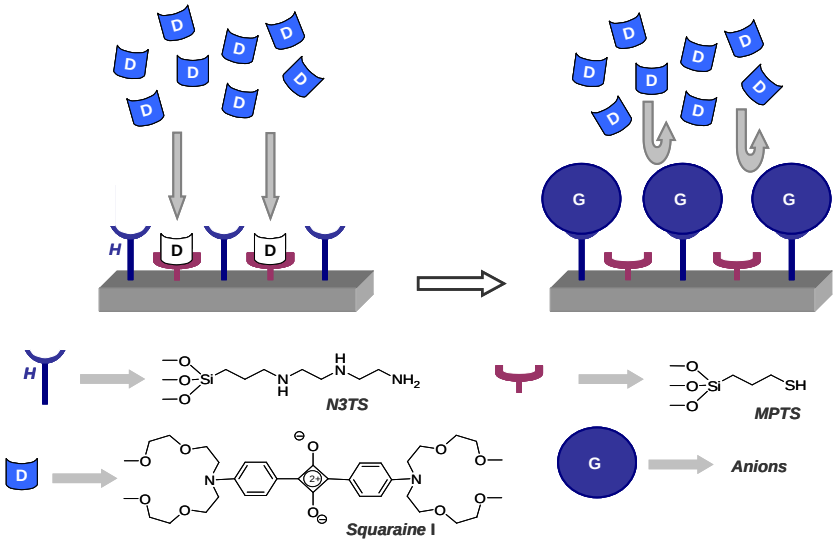

Scheme 1 Representation of the sensing paradigm for the chromogenic recognition of anions.

As a proof-of-concept in relation to the signaling protocol detailed in Scheme 1, we report herein the functionalisation of a silica surface with anion-coordinating groups (a polyamine acting as "H") and a reactive centre (a thiol, "R"). The reactivity of the thiols with a dye (a squaraine derivative, "D") is studied in the presence of certain anions (guests, "G"). The factors that control the reactive site–dye reaction have been studied. The system can be tuned (*via* pH changes) resulting in the selective sensing of certain guests.

Results and discussion

Designing the chromo -fluorogenic probe

The general development of the chromo-fluorogenic probe requires the choice of a suitable signaling reaction (the pair "R", "D" in Scheme 1) and the selection of a binding site–guest system (the pair "H", "G" in Scheme 1). As a signaling pair we have selected a thiol group ("R") and a squaraine dye ("D") based on the well-known thiol–squaraine reactivity.[14] This is a selective reaction that occurs *via* nucleophilic attack of the thiol group to the electron deficient central four-

member ring of the squaraine scaffolding resulting in a rupture of the electronic delocalization and a bleaching of the blue squaraine solutions. This is a very suitable reaction because it is rapid and it occurs at room temperature in a relatively wide pH range. Additionally, squaraines are well-known attractive dyes for chromo- and fluorogenic optical detection since they possess a very intense absorption band (log $\varepsilon > 5$) and relatively high quantum yields even in aqueous environments. Thus, for instance, the use of squaraine derivatives as signalling reporters for certain cations,[15] anions[16] and neutral guests[17] have been widely reported. The squaraine derivative **I** used is shown in Scheme 1 and it has been synthesized following literature procedures.[18] For the signaling protocol a water/CH_3CN 90:10 v/v mixture was used due to the low solubility of the squaraine **I** in pure water.

As a binding site–guest system we have selected polyamines and anions, respectively. The protonation of the amines at a certain pH is expected to result in the formation of the corresponding complexes with certain anionic species that would result in control of the reactivity or accessibility of the squaraine derivative from the solution to the thiol groups anchored on the surface. The host and spectroscopic inhibitor components have to be additionally anchored onto a suitable support. For preliminary studies, we chose here silica fumed as a simple yet suitable inorganic structure due to its inertness and ease of functionalisation.

The functionalisation of the surface

A first step consisted on the functionalisation of the silica surface. In order to avoid a non-uniform distribution of thiol and amino groups , the silica fumed solid was initially activated with HCl (see experimental details). Then, the functionalisation of the surface was carried out using the thiol and amine derivatives mercaptopropyltrimethoxysilane (**MPTS**) and 3-[2-(2-aminoethylamino)ethylamino]propyl-trimethoxysilane (**N3TS**) both containing the same trimethoxysilane moieties as reactive groups .

Different functionalised solids **S1*x*** were prepared using the following procedure; the activated starting solid (fumed silica) was suspended in anhydrous toluene,

the mixture was heated up to 140 °C and the systems distilled in order to eliminate water by azeotropic distillation . Then, different mixtures of **N3TS** and **MPTS** containing a total of 15 mmol of Si were added to the silica suspension. The final materials (solids **S1a** to **S1d**) were then filtered, washed with toluene and dried at 70 °C for 12 h. This method would allow obtaining a uniform distribution of both functional groups on the silica surface, the only expected difference between the solid would derive from the initial concentrations of **N3TS** and **MPTS**.

Materials characterization

The solids were characterized using standard procedures. After functionalisation, the infrared spectra of the solids **S1a–d** show the expected features, *i.e.*, intense bands due to the silica matrix (1250, 1087, 802, 462 cm^{-1}), vibrations of water molecules (3420 and 1620 cm^{-1}) and vibrations of C–H bonds at 2954–2850 cm^{-1} from the anchored organic moieties. The presence of thiol and amine groups could not be unambiguously confirmed because the absorptions of these group vibrations result in very weak bands.

The degree of functionalisation was determined by elemental analysis and thermogravimetric studies for the **S1a–d** solids. From elemental analysis of C, H, N, S it is possible to determine the amount of thiol and amine groups contained in the materials calculated in millimoles per gram of SiO_2 (mmol g^{-1} SiO_2) using eqn (1):

$$\alpha_A = \frac{\Delta W_i\% \times 1000}{\Delta W_{SiO_2}\% \times nM_i} \quad (1) \quad [\text{mmol g}^{-1}\ \text{SiO}_2]$$

where $\Delta W_i\%$ (i = C, N, S) are the weight percentages of carbon, nitrogen or sulfur, M_i is the corresponding atomic weight and n is the number of the corresponding atom type in one molecule. $\Delta W_{SiO2}\%$ is the inorganic SiO_2 content in weight percentage. The values of organic content as milimole of thiol (**MPTS**) and tri-amine (N3TS) per gram of SiO_2 for the solids **S1a–d** are shown in Table 1.

Table 1 Total moles and moles of **N3TS** and **MPTS** per gram of SiO_2, average coverage and interdistance between anchored groups for the **S1a–d** functionalised materials.

	α_{total} (mmol g^{-1} SiO_2)	α_{N3TS} (mmol g^{-1} SiO_2)	α_{MPTS} (mmol g^{-1} SiO_2)	β total (molecules nm^{-2})	Distance (Å)
S1a	0.504	0.472	0.032	1.33	8.68
S1b	0.498	0.434	0.064	1.35	8.59
S1c	0.438	0.363	0.075	1.22	9.07
S1d	0.431	0.343	0.089	1.20	9.15

Taking into account the contents given in Table 1 and the value of the specific surface of the silica fumed support (200 m^2 g^{-1}), the average coverage (β_A in groups nm^{-2}) of the surface of the solids **S1a–d** by thiol and triamine groups was calculated by eqn (2)

$$\beta_A = \alpha_A \times 10^{-3} \times S^{-1} \times 10^{-18} \times N_A = \alpha_A \times S^{-1} \times 602.3 \qquad (2)$$

In which α_A is the thiol or the triamine content (mmol g^{-1} SiO_2), S the specific surface (m^2 g^{-1}) of the non-functionalized silica support and N_A is Avogadro's number. From these data and eqn (2) a surface coverage in the 1.30–1.20 molecules nm^{-2} range was calculated for the **S1a–d** solids resulting in an average distance between anchored molecules of *ca.* 9 Å. In more detail, for instance solid **S1d** contains 1.20 molecules per nm^{-2} of which 0.95 and 0.25 are of **N3TS** and **MPTS** respectively.

Controlled access to the surface

In a first step, reactivity of the signaling dye D (squaraine **I**) with the reactive centre R (thiol groups) was studied as a function of the pH. From the solids prepared **S1d** shows a most suitable response in terms of selectivity (*vide infra*). For this solid the reaction of the squaraine with the thiol groups is relatively fast, whereas, at the same time, the interaction of the anchored amines with anions is able to inhibit the squarine–thiol reaction in certain circumstances (*vide infra*).

Solids containing a larger proportion of thiols result in a very fast reaction with the squaraine reported but no clear selective responses were found in the presence of anions. Additionally, solids containing larger proportions of amines result in low response times.

Studies with solid **S1d** were carried out in a range of pHs, although for the sake of clarity only results at pH 3, 5 and 7 where distinctive effects are observed, will be shown. Too basic pH was avoided in this study in order to stay away from the possible damage of the siliceous matrix at high concentration of hydroxide anions. Also very acidic or basic solutions have been reported to result in a degradation of the squaraine dye . In a typical experiment, 9 mg of **S1d** were placed in contact with water/ CH_3CN 90:10 v/v mixtures at a certain pH containing the squaraine **I** at a concentration of 5×10^{-6} mol dm^{-3}. The decrease in the absorption band at 643 nm *versus* time in the aqueous solution is indicative of the reaction of the squaraine with the thiol groups and therefore indicative of the accessibility of this neutral molecule to the silica surface. The pH-controllable effect can be seen in Fig. 1 that plots the changes in colour of the squaraine solution (squaraine band at 643 nm) at pH 3, 5 and 7. In all cases the pH was adjusted with hydrochloric acid and in all the experiments the final concentration of the chloride anion was fixed at 0.01 mol dm^{-3} (completed in each case by adding the corresponding amount of sodium chloride) in order to have in all cases similar conditions.

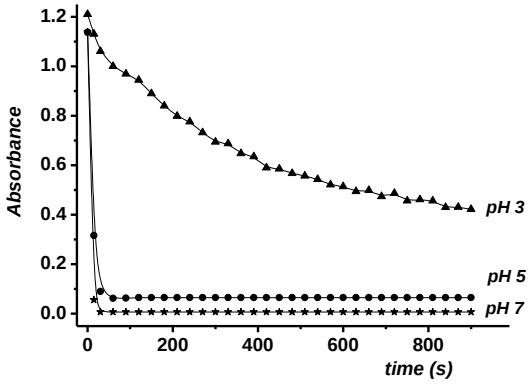

Fig. 1 Absorbance at 643 nm (squaraine band) *vs* time at pH 3, 5 and 7 for solid **S1d** in presence of Cl^- (0.01 M) in water/acetonitrile 90:10 v/v.

Fig. 1 shows that at pH 7 and pH 5 there is a quick reaction between the squaraine and the thiol groups on the surface. On the contrary this reaction is significantly slower at pH 3. The interpretation of such behavior has to be found in the different degrees of protonation of the amines. At neutral pH the amines would be poorly protonated. This would result in loose amines surrounding the thiol groups. In this picture, the approximation of a squaraine dye and reaction with the thiol groups is possible. On the contrary, at acidic pH the amines would be completely protonated giving rise to Coulombic repulsions between ammonium groups resulting in a rigidification of the tethered amines. That result in a firm polyammonium structure that would make more difficult the squaraine accessibility to the thiol groups.[19] Additionally to this cause there is an additional effect related with the electrostatic attraction between the protonated amines and the chloride anion *via* formation of amine/ammonium-chloride complexes (*vide infra*).

This pH effect is dependent on the degree of protonation. For instance the pK_a values of the diethylentriamine (H_2N-CH_2-CH_2-NH-CH_2-CH_2-NH_2), are 9.84, 9.02 and 4.23.[20] This is a similar amine to that anchored to the siliceous surface. However it is expected that the basicity behaviour of the amine would significantly change when a significant number of polyamines are anchored to the silica surface. Thus it is well known that, when closely placed, amines display decreasing values of pK_a due to the additional electric work associated to protonate an amine near an already protonated ammonium group.[21] Therefore it would be expected that the amines anchored on the solid surface would modify significantly their pK_a values. In a recent publication we have studied a similar problem and determined *via* titration experiments that the polyamine **N3TS** anchored on a MCM-41 type solid have percentages of protonation of 44, 65 and nearly 100% for the pHs 6, 4 and 2, respectively. Using a similar procedure percentages of protonation of *ca.* 26, 55 and 78 for pH 7, 5 and 3, respectively have been found from titration experiments for solid **S1d**.

We were particularly concerned with the possibility that the observed effect was not caused by the amine-containing ensemble but due to some simple change in the reactivity of the squaraine dye with the thiol groups anchored on the silica surface as a function of the pH. To eliminate this possibility, we prepared solid **S1–SH** that consists of a fumed silica material functionalised only with thiol groups. This solid displays no pH-controlled effect and a very rapid pH-independent decolouration of the dye (due to a rapid reaction with the SH groups) is found in aqueous solution indicating that the control of the reactivity observed in Fig. 1 is due to the different protonation degree of the anchored polyamine **N3TS**.

Studies in the presence of anions

The extent of dye reactivity in **S1d**, is expected to depend on a number of factors. Additionally to the pH-dependent behavior also an anion-controlled outcome is expected to occur at a certain pH. As we will see below this is a much more remarkable effect that arises from the ability of polyamines to form complexes with anions. In fact, the amines, especially when transformed into ammonium groups by protonation, have been reported to be suitable anion coordination hosts usually *via* a combination of hydrogen bonding interactions and electrostatic attractions.[22] Thus, it has been reported that amines can act as hydrogen donor elements, whereas protonated amines (*i.e.* ammonium groups) can serve as hydrogen donor elements and as a source of Coulombic attractive interactions with anions.

The reactivity of **S1d** with the squaraine **I** has been studied in the presence of a range of inorganic anions with different structural dimensions and charges, including chloride, perchlorate, nitrate, sulfate, phosphate and pyrophosphate. A clear anion-controlled effect can be seen in Fig. 2 that plots the changes in colour of the squaraine solution (squaraine band at 643 nm) at a fixed pH 3 *versus* time in the presence of the anions chloride, perchlorate, nitrate, sulfate, phosphate and pyrophosphate ($C_{anion} = 1 \times 10^{-2}$ mol dm^{-3}). It can be seen that the presence of different anions affect in a different manner to the reaction between the squaraine and the appended thiol groups . Thus, whereas the reaction of the dye

is still effective in the presence of chloride and perchlorate, the same reaction is highly inhibited in the presence of the anions nitrate, sulfate, phosphate and pyrophosphate.

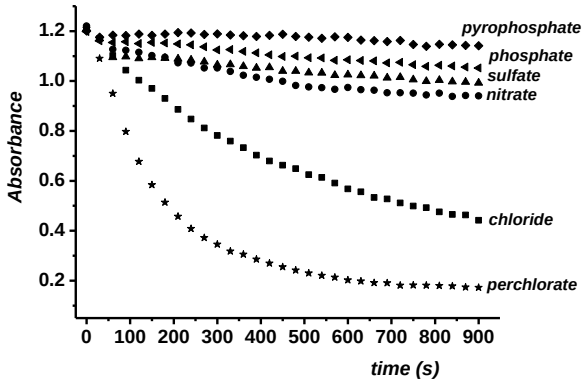

Fig. 2 Absorbance at 643 nm (squaraine band) *versus* time at pH 3 for solid **S1d** in the presence of the anions chloride, perchlorate, nitrate, sulfate, phosphate and pyrophosphate (C_{anion} = 1 × 10^{-2} mol dm^{-3}) in water/acetonitrile 90 : 10 v/v.

In order to additionally show the effect of the anion concentration, additional studies were carried out by measuring the absorption of the solution after a certain time for a given pH for increasing amounts of the corresponding anionic species. In a typical assay 9 mg of **S1d** were suspended in 13.5 ml of water containing a certain concentration of a given anion and then 1.5 mL of a solution of squaraine **I** ($C_{squaraine}$ = 5 × 10^{-5} mol dm^{-3}) in acetonitrile was added. After 15 min the mixture was filtered and the absorbance in the solution of the squaraine band measured. Although at this time the equilibrium is not completely reached we found that the variation in the absorbance is minimum in consecutive assays and very reproducible data (calibration curves) were obtained. The anion-controlled effect, *i.e.* the modulation in the reactivity of the thiol groups with the squaraine dye *via* the presence of certain anions, can clearly be seen in Fig. 3. At pH 3 a large number of anions appear to inhibit the reaction of the dye with the thiol groups most likely due to strong interactions with the polyamines. At pH 5 and 7 (see below) the behaviour is remarkably different. This anion-controlled effect can be explained in terms of formation of anion complexes with the tethered

polyamines. For the correct interpretation of the interaction of certain guests with the anchored groups, it is important to note that polyamines and also many anions display one or several stepwise protonations in water. Thus, anions that are conjugated bases of acids will accept protonation processes, and their charge will depend on their basicity constants. Also amines are basic groups that can be protonated at low pH values (see above). For instance, at pH 3, sulfate, phosphate and pyrophosphate are in solution as a mixture of SO_4^{2-}/HSO_4^-, $H_2PO_4^-/H_3PO_4$, and $H_2P_2O_7^{-2}/H_3P_2O_7^-$ species, respectively, whereas the anions chloride, perchlorate and nitrate are as Cl^-, ClO_4^- and NO_3^- species. The inhibition of the squaraine–thiol reactivity at pH 3 follows the order pyrophosphate > phosphate > sulfate > nitrate > chloride > perchlorate. From these results it is apparent that chloride or perchlorate may form very weak and labile complexes allowing the reaction of **I** with the SH groups. On the other side pyrophosphate and phosphate are able to strongly inhibit the thiol-squaraine reaction most likely due to the formation of stronger complexes with the tethered polyamines. This observed behaviour is basically in agreement with the polyamine/polyammonium literature that report that polyamines form very weak complexes with perchlorate and chloride, whereas polyamines are able to display much stronger interactions with sulfate and phosphate-derivatives.[23] It is also important to note that the stability trends of phosphate complexes with polyamines are not strictly determined by electrostatic contributions, and phosphate species have been reported to form very stable complexes with polyamines due to the ability of phosphate and phosphate-derivatives to form strong hydrogen-bonding interactions as they can behave as both hydrogen-bond acceptor and donor, in contrast to anions such as SO_4^{2-} or NO_3^- which can only act as hydrogen-bond acceptors. At neutral pH 7 (not shown), polyamines are less protonated, and their interactions with anions, both by strength and number, are drastically reduced, therefore the squaraine **I** reacts very fast with the thiol groups in the presence of all the anions studied. No changes in the apparent reaction kinetics are observed even at concentrations up to 1×10^{-2} mol dm^{-3} of the anionic guests.

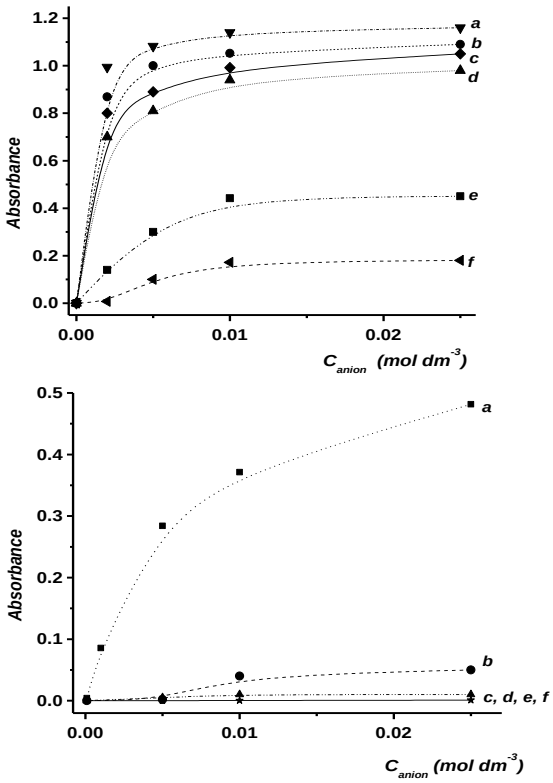

Fig. 3 Absorbance at 643 nm (squaraine band) *versus* concentration of (a) pyrophosphate, (b) phosphate, (c) sulfate, (d) nitrate, (e) chloride and (f) perchlorate at pH 3 (top) and 5 (bottom) for solid **S1d** in water/acentonitrile 90 : 10 v/v

Finally Fig. 3 (bottom) shows the response of solid **S1d** at pH 5 in the presence of increasing concentrations of different anions. As it can be observed, whereas increasing concentrations of pyrophosphate allows it to inhibit, to a certain extent, the reaction of the squaraine with the thiols the interaction of the remaining inorganic anions (*i.e.* chloride, sulfate, phosphate and nitrate) with the polyamines does not hamper bleaching of the squaraine dye. As can be seen in the figure the overall result is a highly selective colorimetric signaling of the pyrophosphate anion. Detection limits of *ca.* 1.0 x 10^{-7} mol dm^{-3} can be reached following this simple colorimetric procedure using fluorescence measurements (the quantum yield of squaraine **I** in water is 0.015, λ_{exc} = 643 nm and λ_{em} = 666

nm). A photograph showing the colorimetric selective detection of pyrophosphate is shown in Fig. 4. This highly selective colorimetric signaling of pyrophosphate with respect to other inorganic anions in mixed aqueous solutions based on a control of dye transport (squaraine) is quite unusual and would have been hardly observable using classical chemosensors. In fact, although several fluorescent chemosensors for pyrophosphate have been reported, there are very few examples of chromogenic pyrophosphate sensing in water or mixed aqueous solutions.

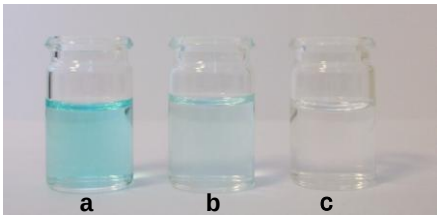

Fig. 4 Photograph of the colorimetric selective detection of pyrophosphate. The correspondent anions (5.0×10^{-3} mol dm^{-3}) were added to suspensions of solid **S1d** and **I** in water/acetonitrile 90:10 v/v mixtures. After 15 min the suspension was filtered. From left to right: pyrophosphate, phosphate and nitrate .

For instance, the first chromogenic chemosensor for pyrophosphate anion showing sensing features in aqueous solution was developed by Hong *et al.* in 2003 using a Zn^{2+} dinuclear complex of an azophenol-(bis(2-pyridylmethyl)amine) receptor that showed selective colour change from yellow to orange upon addition of the pyrophosphate anion.[24] Since then, as far as we know, only two more examples of colorimetric pyrophosphate sensing have been reported in aqueous environments. One is based on the use of an europium-chelating complex that suffers a colour modulation ascribed to cluster conformation changes upon binding of the pyrophosphate anion with the vacant coordination sites of the Eu(III) centre.[25] The other uses the chromogenic receptor dipyrrolylquinoxaline that was first functionalised with polymerizable ethylenedioxythiophene groups and then subjected to an oxidative electropolymerization to give conductive materials that showed gradual changes in colour upon addition of fluoride and pyrophosphate.[26] Two more examples

have been reported in DMSO solutions. One is an anthracene group functionalised with two *p*-nitrophenylurea moieties that show remarkable colour change upon coordination *via* hydrogen bonding with fluoride and pyrophosphate.[27] A second example uses a calixarene framework functionalised with amidourea moieties containing 4-nitrophenyl groups. Response to fluoride and pyrophosphate was observed.[28]

Kinetics and thermodynamic studies

The observed selectivity patterns can now be discussed in terms of both, the kinetic rates of the reaction between the thiol and the squaraine groups and the thermodynamic interaction reaction between the anions and the polyamine moieties. From Fig. 2 it is evident that at pH 3 the reactivity of the squaraine with the thiol groups is modulated by the presence of certain anions due to the formation of anion complexes with the anchored polyamines on the silica surface. Based on these observations, the proposed model suggests that the observed apparent rate of the reaction is proportional to both, (i) the concentration of squaraine (Sq) dye and (ii) to the fraction of anion binding centers that are not occupied by anions at a certain concentration; *i.e.*

$$-\frac{d[Sq]}{dt} = k_v(1-\Theta)[Sq]^2 \qquad (3)$$

where k_v is the absolute rate constant of the squaraine–thiol reaction, Θ is the fraction of occupied anion binding centers at the surface and [Sq] is the squaraine concentration (in mol L^{-1}). The product $k_v(1-\Theta)$ is the "apparent rate constant" that reflects that the squaraine–thiol reaction is dependent on the anion present in the solution (see Fig. 2 and 3). The interaction of the anions with the binding sites (the appended polyamines) at the silica surface can be determined using a Langmuir-type analysis. This model assumes that the isotherm coverage can be expressed in terms of the Langmuir adsorption constant (*K*) and the concentration *C* (in mol L^{-1}) of the anion at the equilibrium.

$$\Theta = \frac{KC}{1+KC} \qquad (4)$$

From these initial hypotheses, the final equation used for fitting was obtained:

$$\frac{1}{A}-\frac{1}{A_0}=\frac{k_v}{\varepsilon}\left(1-\frac{KC}{1+KC}\right)t$$

$$C=\frac{-(K(\frac{n_M}{V}-C_0)+1)}{2K}+\sqrt{\left(\frac{(K(\frac{n_M}{V}-C_0)+1)}{2K}\right)^2+\frac{C_0}{K}} \quad (5)$$

In this equation, A_0 and A are the absorbances of squaraine band (λ = 643 nm) at t = 0 and at time t, k_v is the rate constant for the squaraine–thiol reaction, K is the adsorption constant that will measure the interaction between a certain anion and the functionalized polyamine silica surface, ε is the molar extinction coefficient of the squaraine, C_0 is the added concentration of anion (in mol L^{-1}), C is the concentration (in mol L^{-1}) of the anion at the equilibrium, n_M is the maximum concentration of anion that can be adsorbed in the solid by interaction with the amines and V is the volume (in litres) in which the experiment was carried out. The formalism that leads to the deduction of this equation is given in the Experimental Section. In order to determine k_v (kinetic rate for the squaraine –thiol reaction on the surface) and K (interaction between a given anion and the polyamines at the surface) the reaction between the solid **S1d** and the squaraine **I** was studied using different concentrations of anions and a fixed concentration of squaraine. As a representative example, Fig. 5 shows the plot of 1/A *versus* time for the reaction of solid **S1d** with squaraine **I** in the presence of pyrophosphate at pH 3 at concentrations of 0.0025 mol dm^{-3} (a), 0.005 mol dm^{-3} (b), 0.01 mol dm^{-3} (c) and 0.025 mol dm^{-3} (d). The solid line shows the fit obtained with eqn (5) that resulted in the calculation of values of log k_v and log K of 2.88 and 3.25, respectively. The same procedure was applied for anions chloride, nitrate, sulfate and phosphate. The values of log K obtained using eqn (5) are shown in Table 2. It is noteworthy that from experiments carried out using different anions a very similar value of log k_v was found. This was an expected outcome bearing in mind

that the absolute kinetic constant for the reaction between the squaraine **I** and the thiol groups attached on the surface of the **S1d** solid must be a constant.

Table 2 Values of log *K* for certain anions calculated at pH 3.

Anions	log *K* (pH 3)	log *K* (pH 5)
Pyrophosphate	3.25	4.22
Phosphate	3.23	—[a]
Sulfate	3.21	—[a]
Nitrate	2.35	—[a]
Chloride	2.65	—[a]

[a] Changes in the concentration of these anions show poor changes in the reactivity of the squaraine-thiol moieties and adsorption constants could not be calculated.

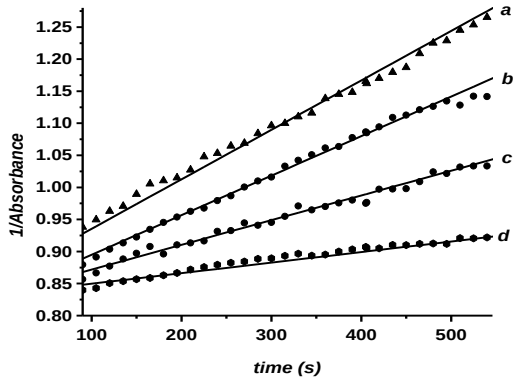

Fig. 5 Plot of a 1/*A* at 643 nm (squaraine band) *verus* time for the reactivity of the squaraine **I** with the solid **S1d** in water/acentonitrile 90:10 v/v at pH 3 in the presence of different concentrations of anion pyrophosphate. ($C = 5 \times 10^{-6}$ mol dm^{-3}). The solid straight lines were calculated using eqn (5).

Values of log *K* follow the order pyrophosphate > phosphate > sulfate > nitrate > chloride which is in agreement with the enhanced inhibition of the squaraine reactivity with solid **S1d** that follows the same order. At neutral pH 7, the reactivity of the squaraine **I** and the **S1d** solid was not changed by the presence of

anions and therefore values of *K* could not be calculated. At pH 5, the adsorption constant *K* was calculated for the anion pyrophosphate (see Table 2).

The calculation of the *K* values through the use of eqn (5) gives in-depth information on the factors that control the reactivity of solid **S1d** and the squaraine **I** in the presence of different anions. Fig. 6 shows a plot of the adsorption *K* constants for anions pyrophosphate, phosphate, sulfate, nitrate and chloride at pH 3 as a function of the charge of the anion. A good linear correlation was observed for the anions phosphate, sulfate, nitrate and chloride suggesting that the main driving force in the control of the reactivity between the squaraine **I** and the thiol groups on the surface of **S1d** are the electrostatic interactions between the corresponding anion and the protonated polyamines anchored on the silica surface. It is also noteworthy that this general lineal trend is not followed by phosphate that shows a larger constant *K* than that expected for the charge of the anion. This means that the *K* constant can not be justified by simple electrostatic polyammonium–phosphate interactions suggesting that for this anion hydrogen bonding coordinative forces with the polyamines are of importance.

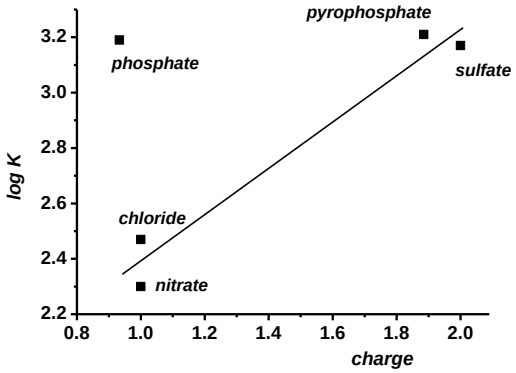

Fig. 6 Plot of the adsorption constant *K* (see eqn (5)) on **S1d** for anion pyrophosphate, phosphate, sulfate, nitrate and chloride at pH 3 as a function of the anion charge. For pH values where more than anionic species are found, the anion charge refers to the average charge, calculated as $\sum X_i q_i$ (where X_i and q_i are the molar fraction and charge of species *i*, respectively).

Conclusions

In summary, we have shown here how a biomimetic ion-channel system (*i.e.* simple silica surface functionalised with suitable "reactive centres" and polyamines) can be used for the design and development of new pyrophosphate anion recognition and colorimetric signalling systems. This example, along with others reported recently, offers new perspectives on the use of solids as hosts for the development of advanced inventive and functional hetero-supramolecular methods. This protocol shows enhanced features and displays potential that can not be considered when using classical "binding site –signalling unit" receptors. For instance, the nature of the spectroscopic inhibitor , the size and charge of the dye and the anchored binding groups can be easily changed, giving rise to a large number of potential new functionalised solids that can eventually show enhanced colorimetric selective responses towards target guests. Further studies in this line are planned in our laboratory.

Experimental

General methods

TGA analysis, IR spectroscopy, elemental analysis, and UV-visible spectroscopy techniques were employed to characterize the materials obtained. Thermo-gravimetric analyses were carried out on a TGA/SDTA 851e Mettler Toledo balance, using an oxidant atmosphere (air, 80 mL min^{-1}) with a heating program consisting of a ramp of 10 °C min^{-1} from 393 K to 1273 K. IR spectra were recorded on a Jasco FT/IR-460 Plus between 400 and 4000 (cm^{-1}) diluting the solids in KBr pellets. UV-visible spectroscopy was carried out with a Lambda 35 UV/Vis Spectrometer (Perkin Elmer Instruments). Nonporous amorphous Fumed silica, with a surface area of *ca.* 200 m^2 g^{-1} was provided by Aldrich. The organosiloxane derivatives 3-[2-(2-aminoethylamino)ethylamino]propyl-trimethoxysilane and 3-mercaptopropyltrimethoxysilane for the synthesis of the solids **S1a–d** were provided by Aldrich.

*Synthesis of **S1a–d***

In a typical synthesis, 1.00 g of activated Silica Fumed was suspended in 50 mL of anhydrous toluene inside a round-bottomed flask connected to a Dean–Stark (trap) apparatus in an inert atmosphere. The suspension was refluxed (110 °C) in azeotropic distillation collecting 10 mL in the trap in order to remove the adsorbed water. After this, different mixtures of 3-[2-(2-aminoethylamino)ethylamino]propyl-trimethoxysilane (**N3TS**) and mercaptopropyltrimethoxysilane (**MPTS**) containing a total of 15 mmol of Si were added to the silica suspension at room temperature. The mol/mol ratio between **N3TS** and **MPTS** measured for the four different solids (**S1a–d**) are listed in Table 1. The mixture was stirred for 5.5 h. Finally, the different solids **S1a–d** were filtered off, washed with 30 ml of toluene and dried at 70 °C for 12 h.

Squaraine–solid interaction studies

9 mg of **S1d** were suspended in 13.5 ml of water containing a certain concentration of a given anion and then 1.5 mL of a solution of squaraine **I** (C = 5 × 10^{-5} mol dm^{-3}) in acetonitrile was added. After 15 min the mixture was filtered and the absorbance in the solution of the squaraine band measured. The reaction of the squaraine dye with the solid was monitorized *via* changes in the squaraine band centered at 643 nm.

Thermodynamic/kinetic model of controlled switchable access to the surface

The kinetic model for the study the reaction between squaraine and thiol groups modulated by the interaction between a certain anion in the solution and the binding sites anchored on the silica surface is based on the concept that the rate of the reaction is proportional both, (i) the concentration of squaraine (Sq) dye and (ii) to the fraction of the free anion binding centers by the corresponding anion at a certain concentration.

$$-\frac{d[Sq]}{dt} = k_v(1-\Theta)[Sq]^2 \qquad (6)$$

where k_v is the rate constant of the Sq-thiol reaction, Θ is the of occupied anion binding centers at the surface and [Sq] is the squaraine concentration (in mol L^{-1}). The interaction of the anions with the binding sites (in this case amines) at the silica surface can be determined using a Langmuir-type analysis. This model assumes that, (i) the anion (the absorbate) forms a monolayer, (ii) there are 0 or 1 molecules adsorbed at each site, (iii) all the binding sites have the same energy and (iv) the interaction between sites is negligible. In Langmuir analysis the isotherm coverage is dependent of both the temperature and the concentration of the adsorbate. If the temperature is fixed, then the coverage is only function of the concentration of the anionic guest C:

$$\Theta = \frac{n_A}{n_M} = \frac{KC}{1+KC} \qquad (7)$$

where n_A is he number of moles of the adsorbed anion and n_M the maximum moles of anion that can be adsorbed on the monolayer. Alternatively Θ can be expressed in terms of the Langmuir adsorption constant (*K*) and the concentration *C* (in mol L^{-1}) of the anion at the equilibrium. Taking into account that the total amount of anion (n_0) is the sum of the moles of anion monolayer (n_A) and those remaining in the solution (*n*), i.e.

$$n_0 = n + n_A \qquad (8)$$

then

$$n_A = n_0 - n = n_M \Theta = \frac{n_M KC}{1+KC} \qquad (9)$$

Dividing by the volume of the solution (*V*, in liters), we obtain:

$$C_0 - C = \frac{\frac{n_M}{V} KC}{1+KC} \qquad (10)$$

then

$$KC^2 (K(\frac{n_M}{V} - C_0) + 1)C - C_0 = 0 \qquad (11)$$

and finally

$$C = \frac{-(K(\frac{n_M}{V} - C_0) + 1)}{2K} + \sqrt{\left(\frac{(K(\frac{n_M}{V} - C_0) + 1)}{2K}\right)^2 + \frac{C_0}{K}} \qquad (12)$$

Additionally the reaction between the squaraine dye and the thiol groups in the surface is easily monitored by the decrease of the squaraine blue band at 641 nm. Therefore the concentration of squaraine at any time can be calculated from the simple measurement of the absorbance (A) following the Lambert-Beer law.

$$[Sq] = \frac{A}{\varepsilon} \qquad (13)$$

where *A* is the absorbance of the squaraine band at 641 nm and ε is the molar extinction coefficient of the squaraine. Bearing in mind eq 7, 8 and 14 we can write:

$$-\frac{dA}{A^2} = \frac{k_v}{\varepsilon}\left(1 - \frac{KC}{1+KC}\right)dt \qquad (14)$$

that, by integration, results in:

$$\frac{1}{A} - \frac{1}{A_0} = \frac{k_V}{\varepsilon}\left(1 - \frac{KC}{1+KC}\right)t \qquad (15)$$

where *C* is given in equation 12.

Acknowledgements

The authors wish to express their gratitude to the Ministerio de Ciencia y Tecnología project CTQ2006–15456-C04–01 for financial support. E. C. thanks the MICINN for a Fellowship.

References

1. A.B. Descalzo, R. Martínez-Máñez, F. Sancenón, K. Hoffmann, K. Rurack, *Angew. Chem. Int. Ed*. 2006, **45,** 5924-5948.
2. Y. Liu, L. Mu, B. Liu, J. Kong, *Chem. Eur. J*. 2005, **11**, 2622-2631. (b) S. Wang, Y. Song, L. Jiang, *J. Photochem. Photobiol. C: Photochem. Rev*. 2007, *8*, 18-29. (c) Y. Umezawa, H. Roki, *Anal. Chem*. 2004, 321A-325A. (d) S.Flink, F.C.J.M. van Veggel,; D.N. Reinhoudt, *Adv. Mater*. 2000, **12**, 1315-1328. (e) G. Cooke, *Angew*. *Chem. Int. Ed*. 2003, **42**, 4860-4870.
3. D. Julthogpiput, Y.H. Lin, J. Teng, E.R. Zubarev, V.V. Tsukruk, *J. Am. Chem. Soc*., 2003, **125**, 15912. (b) D. Julthogpiput, Y.H. Lin, J. Teng, E.R. Zubarev, V.V. Tsukruk, *Langmuir* 2003, **19**, 7832. (c) S. Chia, J. Cao, J.F. Stoddart, J.I. Zink, *Angew. Chem. Int. Ed*., 2001, **40**, 2447. (d) R. Wang, K. Hashimoto, A. Fujishima, M. Chikuni, E. Kojima, A. Kitamura, M. Shimohigoshi, T. Watanabe, *Nature*, 1997, **388**, 341.
4. E. Raphael, P.G. de Genness, *J. Phys. Chem*. 1992, **96**, 4002. (b) M. Ruths, D. Johannsmann, J. Ruhe, W.Knoll, *Macromolecules* 2000, **33**, 3860.
5. J. Klein, E. Kumacheva, D. Mahalu, D. Perahia, L.J. Fetters, *Nature*, 1994, **370**, 634. (b) A. Berman, S. Steinberg, S. Campbell, A. Ulman, Israelachvili, *Tribol. Lett*. 1998, **4**, 43.
6. (a) I.Y. Galaev, B. Mattiasson, *Trends Biotechnol*. 1999, **17**, 335. (b) I.A. Aksay, M.S. Trau, I. Manne, I. Honma, N. Yao, L. Zhou, P. Fenter, P.M. Eisenberger, S.M.; Gruner, *Science*, 1996, **273**, 892.
7. See for instance: (a) A.K. Boal, V.M. Rotello, *J. Am. Chem. Soc*. 1999, **121**, 4914-4915. (b) M.-C Daniel, J. Ruiz, S. Nlate, J. Palumbo, J.-C. Blais, D. Astruc, *Chem. Commun*., 2001, 2000-2001. (c) A.M. Allgeier, C.A. Mirkin, *Angew. Chem. Int. Ed*. 1998, **37**, 894-908. (d) H.M. Goldston, A.N. Scribner, S.A. Trammell, L.M. Tender, *Chem. Commun*. 2002, 416-417. (e) M. Lahav, E. Katz, A. Doron, F. Patolsky, I. Willner, *J. Am. Chem. Soc*. 1999, **121**, 862-863. (f) M.J. Cook, A.-M. Nygard, Z. Wang, D.A. Rusell, *Chem. Commun*. 2002, 1056-1057. (g) K. Kyungpil, W.S. Jeon, J.K- Kang, J.W. Lee, S.Y. Jon, T. Kim, K. Kim, *Angew. Chem. Int. Ed*. 2003, **42,** 2293.
8. See for instance: (a) M. Asakawa, M. Higuchi, G. Mattersteig, T. Nakamura, A.R. Pease, F.M. Raymo, T. Shimizu, J.F. Stoddart, *Adv. Mater*. 2000, **12**, 1099-1102. (b) C.P. Collier, G. Mattersteig, E.W. Wong, Y. Luo, K. Beverly, J. Sampaio, F.M. Raymo, J.F. Stoddart, J.R. Heath, *Science*, 2000, **289**, 1172-1175. (c) C.P. Collier, J.O. Jeppersen, Y. Luo, J. Perkins, E.W. Wong, J.R. Heath, J.F. Stoddart, *J. Am. Chem. Soc*. 2001, **123**, 12632-12641. (d) I. Willner, V. Pardo-Yissar, E. Katz, K.T. Ranjit, *J. Electroanal. Chem*. 2001, **497**, 172-177.
9. P. Bühlmann, H. Aoki, K.P. Xiao, S. Amemiya, K. Tohda, Y. Umezawa, *Electroanal*, 1998, **10**, 1149-1158. M. Sugawara, A. Hirano, P. Bühlmann, Y. Umezawa, *Bull. Chem Soc. Jpn*. 2002, **75**, 187-201.
10. M. Sugawara, K. Kojima, H. Sazawa, Y. Umezawa, *Anal. Chem*. 1987, **59**, 2842-2846.

11. See for instance: (a) M. Tayaka, P. Bühlmann, Y. Umezawa, *Mikrochim. Acta* 1999, **132**, 55. (b) K. Bandyopadhyay, H. Liu, S.-G. Liu L. Echegoyen, *Chem. Commun*. 2000, 141-142. (c) S. Flink, H. Schönherr, G.J. Vancso, F.A.J. Geurts, K.G.C van Leerdam, F.C.J.M. van Veggel, D.N. Reinhoudt, *J. Chem. Soc., Perkin Trans.* 2000, **2**, 2141-2146. (d) Ito, T. *J. Electroanal. Chem*. 2001, *495*, 87-97.
12. See for instance: (a) H. Aoki, Y. Umezawa, *Analyst*, 2003, **128**, 681-685. (b) H. Aoki, Y. Umezawa, *Electroanal*. 2002, **14**, 1405-1410. (c) V.P.Y. Gadzekpo, K.P. Xiao, H. Aoki, P. Bühlmann, Y. Umezawa, *Anal. Chem*. 1999, **71**, 5109-5115. (d) Y. Katayama, Y. Ohuchi, H. Higashi, Y. Kudo, M. Maeda, *Anal. Chem*. 2000, **72**, 4671-4674. (e) H. Aoki, K. Hasegawa, K. Tohda, Y. Umezawa, *Biosens. Bioelectron*. 2003, **18**, 261-267.
13. (a) A.B. Descalzo, D. Jiménez, J. El Haskouri, D. Beltrán, P. Amorós, M.D. Marcos, R. Martínez-Máñez, J. Soto, *Chem. Commun*., 2002, 562-563. (b) AB. Descalzo, D. Jiménez, M.D. Marcos, R. Martínez-Máñez, J. Soto, J. El Haskouri, C. Guillem, D. Beltrán, P. Amorós, M.V. Borrachero, *Adv. Mater*, 2002, **14**, 966-969. (c) G. Rodríguez-López, M.D. Marcos, R. Martínez-Máñez, F. Sancenón, J. Soto, L.A. Villaescusa, D. Beltrán, P. Amorós, *Chem. Commun*., 2004, 2198-2199. (d) M. Comes, M.D. Marcos, R. Martínez-Máñez, F. Sancenón, J. Soto, L.A. Villaescusa, P. Amorós, D. Beltrán, *Adv. Mater*. 2004, **16**, 1783-1786. (e) A.B. Descalzo, K. Rurack, H. Weisshoff, R. Martínez-Máñez, M.D. Marcos, P. Amorós, K. Hoffmann, J. Soto, *J. Am. Chem. Soc*., 2005, **127**, 184-200. (f) M. Comes, G. Rodríguez-López, M.D. Marcos, R. Martínez-Máñez, F. Sancenón, J. Soto, L.A. Villaescusa, P. Amorós, D. Beltrán, *Angew. Chem. Int. Ed*., 2005, **44**, 2918-2922. (g) A.B. Descalzo, M.D. Marcos, R. Martínez-Máñez, J. Soto, D. Beltrán, P. Amorós, J. *Mater. Chem*. 2005, **15**, 2721-2731. (h) S. Basurto, T. Torroba, M. Comes, R. Martínez-Máñez, F. Sancenón, L.A. Villaescusa, P. Amorós, *Org. Lett*. 2005, **7**, 5469-5472. (i) M. Comes, M.D. Marcos, R. Martínez-Máñez, M.C. Millán, J.V. Ros-Lis, F. Sancenón, J. Soto, L.A. Villaescusa, *Chem. Eur. J*. 2006, **12**, 2162-2170 (j) C. Coll, R. Martínez-Máñez, M.D. Marcos, F. Sancenón, J. Soto, *Angew. Chem. Int. Ed*. 2007, **46**, 1675-1678. (k) A.B. Descalzo, M.D. Marcos, C. Monte, R. Martínez-Máñez, K. Rurack, *J. Mater. Chem*. 2007, **17**, 4716-4723.
14. J.V. Ros-Lis, B. García-Acosta, D. Jiménez, R. Martínez-Máñez, F. Sancenón, J. Soto, F. Gonzalvo, M.C. Valldecabres, *J. Am. Chem. Soc*., 2004, **126**, 4064-4065.
15. J. V. Ros-Lis, R. Martínez-Máñez, K. Rurack, F. Sancenón, J. Soto, M. Spieles, *Inorg. Chem.* 2004, **43**, 5183–5185. J. V. Ros-Lis, M. D. Marcos, R. Martínez-Máñez, K. Rurack, J. Soto, *Angew. Chem.* 2005, **117**, 4479–4482; *Angew. Chem. Int. Ed.* 2005, **44**, 4405–4407.
16. D. Jiménez, R. Martínez-Máñez, F. Sancenón, J. V. Ros-Lis, A. Benito, J. Soto, *J. Am. Chem. Soc.* 2003, **125**, 9000–9001; J. V. Ros-Lis, R. Martinéz-Máñez, J. Soto, *Chem. Commun.* 2002, 2248–2249.
17. J. V. Ros-Lis, R. Martínez-Máñez, J. Soto, *Org. Lett.* 2005, **7**, 2337–2339.
18. H.E. Sprenger, W. Ziegenbein, *Angew. Chem. Int. Ed. Engl.*. 1968, **7**, 530.

19. We would also like to point out that that some kind of interaction might occur between certain polyamines and silanol groups of the silica surface. This interaction might also result in a control of the permeability of the squaraine dye to the thiol groups. However we believe that this kind of interaction has a limited effect because the silica surface was reacted with and excess of the reactives **N3TS** and **MPTS** and therefore a very low number of free silanol groups are expected to exist.
20. (a) R.M. Smith, A.E. Martell, *Critical Stability Constants*, ed. R.M. Smith, A.E. Martell, Plenum, New York, 1974-1989. (b) A.E. Martell, R.M. Smith, R.M. Motekaitis, NIST Critical Stability Constants of Metal Complexes Database, Texas A & M University, College Station, 1993.
21. J.M. Lloris, R. Martínez-Máñez, E. Perales, J. Soto, *J. Chem. Res*. 1998, 432-433.
22. See for instance: (a) A. Bianchi, M. Micheloni, P. Paoletti, *Inorg. Chim. Acta*, 1988, **151**, 269-272. (b) V. Král, A. Andrievsky, J.L. Sessler, *J. Chem. Soc., Chem. Commun.*, 1995, 2349-2350. (c) C. De Stefano, C. Foti, A. Gianguzza, O. Giuffrè, S.J. Sammartano, *J. Chem. Soc., Faraday Trans.*, 1996, **92**, 1511-1518. (d) M.T. Albelda, M.A. Bernardo, E. García-España, M.L. Godino-Salido, S.V. Luis, M.J. Melo, F. Pina, C. Soriano, *J. Chem. Soc., Perkin Trans.* **2,** 1999, 2545-2549. (e) F. Sancenón, A. Benito, J.M. Lloris, R. Martínez-Máñez, T. Pardo, J. Soto, *Helv. Chim. Acta*, 2002, **85**, 1505-1516. (f) M.T. Albelda, J. Aguilar, S. Alves, R. Aucejo, P. Diaz, C. Lodeiro, J.C. Lima, E. García-España, F. Pina, C. Soriano, *Helv. Chim. Acta*, 2003, **86,** 3118-3135. (g) J.M. Lloris, R. Martínez-Máñez, M. Padilla-Tosta, T. Pardo, J. Soto, M.J.L. Tendero, *J. Chem. Soc., Dalton Trans.*, 1998, 3657-3662.
23. See for instance: (a) P.D. Beer, J. Cadman, J.M. Lloris, R. Martínez-Máñez, M.E. Padilla-Tosta, T. Pardo, D.K. Smith, J. Soto, *J. Chem. Soc., Dalton Trans.*, 1999, 127-133. (b) J.M. Lloris, R. Martínez-Máñez, M.E. Padilla-Tosta, T. Pardo, J. Soto, E. García-España, J.A. Ramírez, M.I. Burguete, S.V. Luis, E. Sinn, *J. Chem. Soc., Dalton Trans.*, 1999, 1779-1784. (c) J.M. Lloris, R. Martínez-Máñez, M.E. Padilla-Tosta, T. Pardo, J. Soto, *Helv. Chim. Acta*, 1999, **82**, 1445-1453.
24. D. H. Lee, J. H. Im, S. U. Son, Y. K. Chung, J. –I. Hong, *J. Am. Chem. Soc.*, 2003, **125**, 7752-7753
25. S. –H. Li, C. –W. Yu, W. –T. Yuan, J. –G. Xu, *Anal. Sci.*, 2004, **20**, 1375-1377; S. –H. Li, W. –T. Yuan, C. –Q. Zhu, J. –G. Xu, *Anal. Biochem.*, 2004, **331,** 235-242
26. D. Aldakov, P. Anzenbacher Jr., *J. Am. Chem. Soc.*, 2004, **126,** 4752-475.
27. J. Y. Kwon, Y. J. Jang, S. K. Kim, K. –H. Lee, J. S. Kim, J. Yoon, *J. Org. Chem.*, 2004, **69**, 5155-5157
28. E. Quinlan, S. E. Matthews, T. Gunnlaugsson, *J. Org. Chem.*, 2007, **72**, 7497-7503.

Selective Chromo-fluorogenic Sensing of Heparin by using Functionalised Silica Nanoparticles Containing Binding Sites and a Signalling Reporter

Estela Climent, Pilar Calero, María Dolores Marcos, Ramón Martínez-Máñez, Félix Sancenón, and Juan Soto.

Instituto de Reconocimiento Molecular y Desarrollo Tecnológico, Centro Mixto Universidad Politécnica de Valencia-Universidad de Valencia, Spain
Departamento de Química, Universidad Politécnica de Valencia, Camino de Vera s/n, 46022 Valencia, Spain
CIBER de Bioingeniería, Biomateriales y Nanomedicina (CIBER-BNN).

Received: October 7, 2008
Published online: January 9, 2009

*Chemistry a European Journal, **2009**, 15, 1816 – 1820*

An interesting approach for the preparation of novel sensory systems with enhanced properties is the combination of supramolecular and solid state chemistry concepts. In this field, the anchoring of molecular entities onto pre-organised structures results in the preparation of advanced hybrid systems that show remarkable synergic effects.[1] Prominent examples involving the combination of supramolecular tools with nanoscopic scaffoldings have been reported over the last few years. Among different nanosized solids the use of silica nanoparticles is appealing, owing to its easy preparation, straightforward surface functionalisation and large stability in water.[2] Silica nanoparticles functionalised with organic fluorophores that contain binding sites have been used for the fluorescent recognition of certain metal cations,[3] but anion detection using silica nanoparticles as supports is a scarcely studied field.[4]

Following our interest in the development of novel hybrid organic-inorganic materials as probes[5] we focused our attention towards the preparation of new optical chemosensors for heparin detection. Heparin is a highly sulphated polysaccharide formed by a heterogeneous mixture of diverse chain lengths, which consist of repeating copolymers of 1→4 linked iduronic acid and glucosamine residues in a semi-random order.[6] Heparin has been used extensively as clinical anticoagulant to prevent thrombosis[7] and the close monitoring and control of heparin blood levels during its application is of relevant importance. Several methods for heparin quantification have been traditionally used.[8] Additionally, very recently supramolecular chemistry concepts have been applied in order to prepare chromogenic and fluorogenic chemosensors for the selective detection and quantification of this important polyanion. Thus, colorimetric and fluorimetric displacement assays,[9] fluorescent molecular receptors,[10] organic polymers[11] and simple aggregation–deaggregation protocols using AuNPs have been described.[12]

The new chromo-fluorogenic sensing paradigm we follow herein is shown in Scheme **1**. It involves the use of silica nanoparticles decorated with two different

moieties; thiol groups (R) and polyamines (H). The role of groups R is to react with the squaraine dye (D) through the nucleophilic attack of the thiol group to the electron deficient, central, four-member ring of the squaraine scaffolding. This is known to result in the bleaching of blue squaraine solutions. Additionally H is a suitable host for anion coordination.

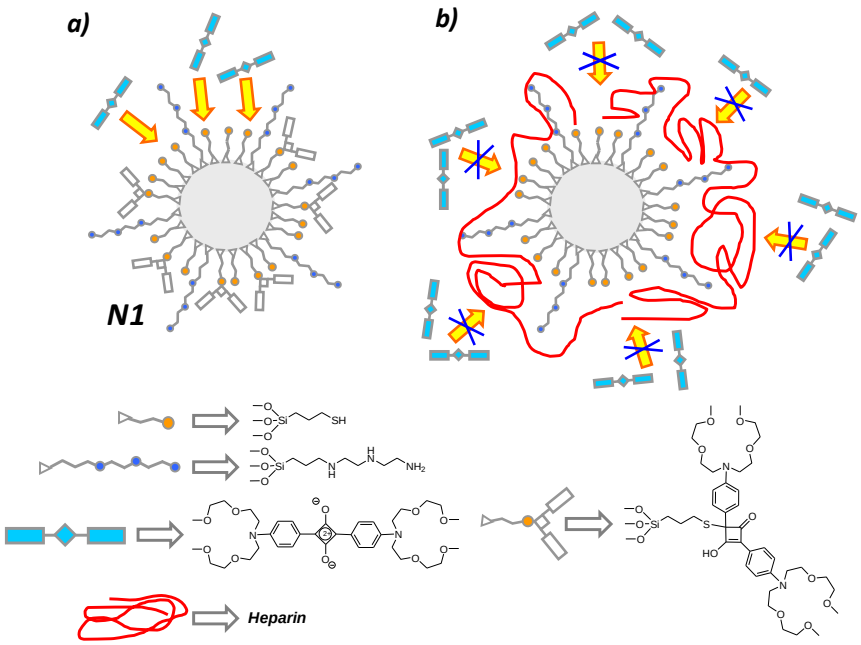

Scheme 1. Colorimetric protocol for heparin signalling. a) bi-functionalised nanoparticles **N1** without the presence of heparin are able to react with squaraine **I**, and b) heparin coordinate with the polyamines on **N1** inhibiting the thiol-squaraine reaction.

The sensing protocol relies in the concept that interaction of H with a suitable guest (G) would inhibit of the reaction between R and D, resulting in a chromo-fluorogenic signalling. In this Scheme the group H is able to control (via coordination or not with suitable guests) mass transport of certain molecules (in our case D) from the solution to the surface of the nanoparticle. Similar procedures have been reported by Umezawa for the electrochemical detection of certain guests.[13]

Squaraines are popular dyes that show favourable spectroscopic properties. These dyes possess typically narrow and very intense absorption bands ($\varepsilon>10^5$) at the red end of the visible spectral window and fluorescence bands of a mirror-image shape with high fluorescence quantum yields $\Phi>0.1$. In fact, attracted by these features, we and others have utilised squaraine derivatives in a number of chemical signalling systems for cations, anions and neutral molecules.[14] Also, squaraines have been used for the development of detection protocols in biological samples.[15] On the other hand, polyamines (and polyammonium groups) are expected to display interactions with charged polysaccharides through hydrogen bonding and electrostatic coulombic attractive forces.

Coated silica nanoparticles **N1** were prepared by using the trialcoxysilyl derivatives mercaptopropyltrimethoxysilane (**MPTS**) and 3-[2-(2-aminoethylamino)ethylamino]propyl-trimethoxysilane (**N3TS**) following reported procedures by Montalti and co-workers (see the Supporting Information).[16] In this synthetic protocol, commercially available silica nanoparticles were heated at 70 °C in a mixture of water/ethanol/acetic acid (1:2:1, v/v/v) in the presence of the coating subunits.

Solid **N1** was characterised using standard procedures. The content of polyamine and thiol were determined by elemental analysis and thermogravimetric measurements and amounts to 0.49 and 2.87 mmol/gSiO_2, respectively. The resulting nanoparticles were characterised by transmission electron microscopy (TEM, see the Supporting Information). The final silica particles have a mean diameter of 20 nm. Analysis of the ^{1}H NMR spectra revealed signal broadening, typical of anchored subunits on nanoparticles. Taking into account the contents and the value of the specific surface of the silica nanoparticle support (195 $m^2\,g^{-1}$), the average coverage on solid **N1** by triamine and thiol groups was 8.80 molecules/nm^2, resulting in an average distance between anchored molecules of about 3.50 Å. By approximation of a single monolayer of subunits on a smooth sphere, a total of 11 000 subunits per nanoparticle are calculated.

One advantage of using silica derivatives as nanoparticles, is the possibility of prepare dispersible stable suspensions. This is especially appealing when using silica supports in sensing protocols because the monitoring of colour or fluorescence changes can be easily made, avoiding the need of filtering as when using micro-metric silica particles. Thus, **N1** nanoparticles were found to form stable suspensions in DMSO containing water up to 50 %. Additionally the squaraine **I** is stable in acetonitrile solutions for weeks without any noticeable decomposition. Consequently, studies were carried out using suspensions **N1** in DMSO to which water containing a certain anion and an acetonitrile solution of **I** were consecutively added. This gives the final water/DMSO/acetonitrile (45:45:10, v/v/v) mixtures in which the following experiments were carried out.

A range of pH values were tested of which pH 7 was selected, because the system displayed a higher selectivity.[17] The studies were carried out in the presence of anions (fluoride, chloride, bromide, iodide, sulfate, phosphate and nitrate), monosaccharides (sucrose, glucose, fructose, arabinose), charged disaccharides (calcium lactobionate) and charged polysaccharides (chondroitin-4-sulfate and heparin).[18] A clear guest control of the squaraine–thiol reaction can be seen in Figure **1**, which plots the absorption at 643 nm (squaraine band) versus time for solutions containing **N1** and **I** at pH 7 in the presence of a certain guest. As it can be seen, the reaction of the dye with the thiols is highly inhibited in the presence of heparin, whereas it is still effective and very fast in the presence of chondroitin-4-sulfate. Other guests (vide infra) display similar reaction profiles to that found for chondroitin-4-sulfate (data not shown). To study the effect of the guest concentration, the following studies were carried out. In a typical assay a DMSO suspension (1.35 mL) of **N1** (80 mg in 150 mL of DMSO) were mixed with water containing a certain concentration of a given anion/saccharide at pH 7 (1.35 mL) and then an acetonitrile solution of squaraine **I** (0.3 mL, $C_{squaraine}$=5×10^{-5} mol dm^{-3}) was added. After 15 min the absorbance of the squaraine band (643 nm) was measured.

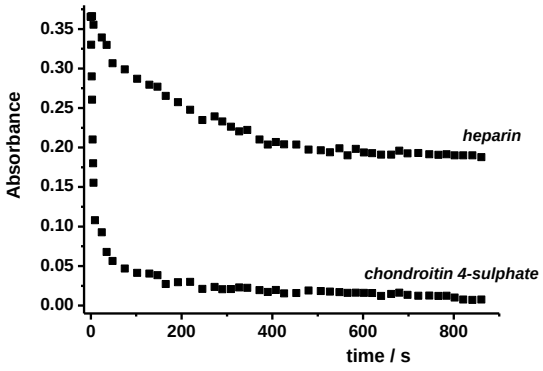

Figure 1. Absorbance at 643 nm (squaraine band) vs. time at pH 7 for mixtures of water/DMSO/acetonitrile (45:45:10, v/v/v) containing **N1**, squaraine **I** and heparin or chondroitin-4-sulfate.

It can be seen how the coordination of heparin to the binding structure (H) results in the modulation of the squaraine-thiol reaction that is function of the heparin concentration (Figure **2**). The charged polysaccharide chondroitin-4-sulfate partially hinders the thiol-squaraine reaction, but only at concentrations higher than 400 μM. The presence of other species; that is, fluoride, chloride, bromide, iodide, sulfate, phosphate, nitrate, lactobionate, sucrose, glucose, fructose and arabinose did not induce any effect even at relatively high concentrations. This full accessibility of squaraine to the thiol-functionalised nanoparticle surface is a consequence of the poor interaction of small anions and mono- and disaccharides with the polyamine network at neutral pH.

The degree of inhibition (heparin > chondroitin-4-sulfate) is clearly related to the anionic charge density of the respective polysaccharide, which suggests that the electrostatic interactions play a dominant role in binding with the polyamine network (H).[19] The overall result is a highly selective colorimetric signalling of heparin, as seen in Figure **2**.

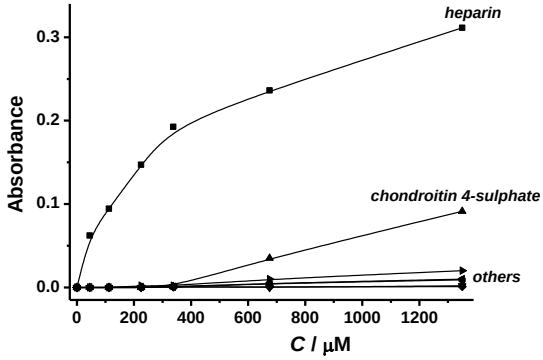

Figure 2. Absorbance at 643 nm (squaraine band) at pH 7 in water/DMSO/acetonitrile (45:45:10, v/v/v) mixtures containing **N1**, squaraine **I** and a certain concentration of heparin, chondroitin-4-sulfate and other guests (fluoride, chloride, bromide, iodide, sulfate, phosphate, nitrate, sucrose, glucose, fructose, arabinose and calcium lactobionate).

By using simple UV-visible measurements a detection limit of ≈50 μM for heparin detection has been achieved. Bearing in mind that a therapeutic dosing level of heparin ranges from 67 μM to 1.7 μM[20] the chromogenic assay would only be able to cover the upper limit. To increase the range of applicability, we made use of the well known fluorescent properties of squaraine **I**. Upon addition of increasing quantities of heparin into different water/DMSO/acetonitrile (45:45:10 v/v/v) suspensions of **N1**, containing **I**, and monitoring the emission band of **I** centred at 679 nm (λ_{exc}=649 nm) the titration curve depicted in Figure **3** was obtained. Using emission measurements a detection limit for heparin as low as 2.0 μM was determined.

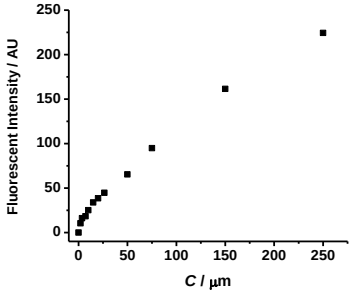

Figure 3. Intensity emission at 679 nm vs. concentration of heparin at pH 7 in water/DMSO/acetonitrile (45:45:10, v/v/v) mixtures containing **N1**, squaraine **I** and a certain heparin concentration.

In relation to the chemical stability of **N1** nanoparticles toward possible thiol oxidation with time, it is important to note that the sensing features remained unaltered for months. Thus a five month old sample of **N1** showed similar recognition features against heparin at pH 7.0 than that found for a freshly prepared sample.

Finally we have made an attempt to quantify the interaction of the binding structure with the guest and have developed a model that is able to describe the observed behaviour in Figures **1** and **2**. The proposed model suggests that the apparent rate of the reaction between the squaraine and the thiols follows a second order kinetics and is proportional to both, (i) the concentration of squaraine dye and (ii) the fraction of binding centres (H) that are not occupied by the corresponding guest at a certain concentration [Eq. (1)]:

$$-\frac{d[Sq]}{dt} = k_v(1-\Theta)[Sq]^2 \qquad (1)$$

in which k_v is the absolute rate constant of the squaraine-thiol reaction, Θ is the number of occupied binding centres at the surface and [Sq] is the squaraine concentration (in mol dm^{-3}). The product $k_v(1-\Theta)$ is the "apparent rate constant" that reflects that the mass transport of the squaraine from the solution to the thiol-functionalised nanoparticle surface is dependent on the interaction between H and G (see Scheme **1**). Our model assumes that the isotherm coverage can be expressed in terms of the Langmuir adsorption constant (K) and the concentration C (in mol dm^{-3}) of the charged polysaccharide at the equilibrium. From these initial hypotheses, the following final Equation (2) used for fitting was obtained:

$$\frac{1}{A}-\frac{1}{A_0} = \frac{k_v}{\varepsilon}\left(1-\frac{KC}{1+KC}\right)t \qquad (2)$$

in which [Eq. (3)]:

$$C = \frac{-(K(\frac{n_M}{V}-C_0)+1)}{2K} + \sqrt{\left(\frac{(K(\frac{n_M}{V}-C_0)+1)}{2K}\right)^2 + \frac{C_0}{K}} \qquad (3)$$

In this equation, A_0 and A are the absorbances of the squaraine band (λ=643 nm) at t=0 and at time t, ε is the molar extinction coefficient of the squaraine **I**, C_0 is the added concentration of charged polysaccharide (in mol dm^{-3}), n_M is the maximum concentration of charged polysaccharide that can be adsorbed in the solid by interaction with the amines and V is the volume (in litres) in which the experiment was carried out. The formalism that leads to the deduction of this equation is given in the Supporting Information.

To determine *kv* (the absolute kinetic rate for the squaraine-thiol reaction on the surface) and *K* (the interaction between a given charged polysaccharide and the polyamines at the surface) the reaction between the solid **N1** and the squaraine **I** was studied by using different concentrations of charged polysaccharides and a fixed concentration of squaraine. *log K* values of 5.55 and 4.38 for heparin and chondroitin-4-sulfate were determined respectively. Log *kv* was found to be 2.88.
Finally, we were concerned with the possibility that the observed effect was not caused by the protocol shown in Scheme **1**, but a result of some simple change in the reactivity of the squaraine dye with the thiol groups anchored on the silica surface in the presence of heparin. To eliminate this possibility we prepared solid **N2**, which is similar to **N1**, but lacking the presence of the binding structure (H in Scheme **1**); that is, **N2** are silica nanoparticles functionalised only with thiol groups. Interestingly this solid shows a very-rapid anion-independent decolouration of the dye, as consequence of the reaction of the squaraine with the SH groups, which indicates that the control of the reactivity observed in Figure **1** is a result of the coordination of the protonated amines (H) with the anionic heparin (G).

In summary, we have applied here a new approach on nanoparticles for the chromo- fluorogenic detection of heparin. The system we show here is one of the few reported heterogeneous molecular probes for anion sensing in water-based solutions. Additionally, this protocol shows enhanced features and displays potential that can not be considered when using classical receptors.[20] For instance, it would be possible to modify with a minimum effort the dye (including

size and charge) and the binding structures (H groups). Additionally, the ratio R/H (see Scheme **1**) can also be easily modulated to give rise to solids with different sensing features and dynamic ranges. Additionally, the anchoring of independent groups on silica nanoparticles in close proximity to the surface support leads to cooperative effects without the need of a direct covalent link between them, avoiding complex synthetic procedures. We also believe that the general protocol shown in Scheme **1** can be of general application to other systems and may lead to new functionalised nanoparticles that show enhanced sensing selective response towards target bio-guests.

Acknowledgements

We thank the Ministerio de Ciencia y Tecnología (project CTQ2006-15456-C04-01) for support. E.C. thanks the Ministerio de Ciencia e Innovación for a FPU Fellowship. P.C. thanks the Ministerio de Ciencia y Tecnología for a Torres Quevedo contract.

References.

1. A. B. Descalzo, R. Martínez-Máñez, F. Sancenón, K. Hoffmann, K. Rurack, *Angew. Chem. Int, Ed.*, **2006**, *45*, 5924-5948; *Angew. Chem.*, **2006**, *118*, 6068-6093.
2. R. Shenhar, V. M. Rotello, *Acc. Chem. Res.*, **2003**, *36*, 549-561; b) C. Beck, W. Härtl, R. Hempelmann, *Angew. Chem. Int. Ed.*, **1999**, *38*, 1297-1300; *Angew. Chem.*, **1999**, *111*, 1380-1382.
3. E. Brasola, F. Mancin, E. Rampazzo, P. Tecilla, U. Tonellato, *Chem. Commun.*, **2003**, 3026-3027; b) E. Rampazzo, E. Brasola, S. Marcuz, F. Mancin, P. Tecilla, U. Tonellato, *J. Mater. Chem.*, **2005**, *15*, 2687-2696; c) P. Teolato, E. Rampazzo, M. Arduini, F. Mancin, P. Tecilla, U. Tonellato, *Chem. Eur. J.*, **2007**, *13*, 2238-2245.
4. P. Calero, E. Aznar, J. M. Lloris, M. D. Marcos, R. Martínez-Máñez, J. V. Ros-Lis, J. Soto, F. Sancenón, *Chem. Commun.*, **2008**, 1668-1670.
5. See for instance: a) J.V. Ros-Lis, R. Casasús, M. Comes, C. Coll, M.D: Marcos, R. Martínez-Mañez, F. Sancenón, J. Soto, P. Amorós, J. El Haskouri, N. Garró, K. Rurack, *Chem. Eur. J*. **2008**, *14*, 8267-8278; b) Comes, M.D. Marcos, R. Martínez-Máñez, F. Sancenón, J. Soto, L.A. Villaescusa, P. Amorós, *Chem. Commun*. **2008**, 3639-3641; c) A.B. Descalzo, M.D: Marcos, C. Monte, R. Martínez-Máñez, K. Rurack, *J. Mater. Chem*. **2007**, *17*, 4716-4723; d) C. Coll, R. Casasús, E. Aznar, M.D: Marcos, R. Martínez-Máñez, F. Sancenón, J. Soto, P. Amorós, *Chem. Commun*. **2007**, 1957-1959; e)

C. Coll, R. Martínez-Máñez, M.D. Marcos, F. Sancenón, J. Soto, *Angew. Chem. Int. Ed*. **2007**, *46*, 1675-1678.

6. J. M. Whitelock, R. V. Iozzo, *Chem. Rev.*, **2005**, *105*, 2745-2764.
7. J. Hirsh, J. E. Dalen, D. Deykin, L. Poller, *Chest*, **1992**, *102*, 337S-352S.
8. See for example: a) N. Ramamurthy, N. Baliga, T. W. Wakefield, P. C. Andrews, V. C. Yang, M. E. Meyerhoff, *Anal. Biochem.*, **1999**, *266*, 116-124; b) B. Boneu, P. de Moreloose, *Semin. Thromb. Hemost.*, **2006**, *32*, 803-809; c) T. –J. Cheng, T. –M. Lin, T. –H. Wu, H. –C. Chang, *Anal. Chim. Acta*, **2001**, *432*, 101-111; d) S. Mathison, E. Bakker, *Anal. Chem.*, **1999**, *71*, 4614-4621; e) S. –C. Ma, V. C. Yang, M. E. Meyerhoff, *Anal. Chem.*, **1992**, *64*, 694-697; f) V. C. Yang, W. –C. Ma, B. Fu, M. E. Meyerhoff, *Anal. Chem.*, **1993**, *65*, 2078-2084; g) N. Ramamurthy, N. Baliga, J. A. Wahr, U. Schaller, V. C. Yang, M. E. Meyerhoff, *Clin. Chem.*, **1998**, *44*, 606-613; h) G. A. Mitchell, R. J. Gargiulo, R. M. Huseby, D. E. Lawson, S. P. Pochron, J. A. Sehuanes, *Thromb. Res.*, **1978**, *13*, 47-52; i) E. Homer, *Thromb. Haemost.*, **1985**, *54*, 29-31.
9. Z. Zhong, E. V. Anslyn, *J. Am. Chem. Soc.*, **2002**, *124*, 9014-9015; b) T. Mecca, G. M. L. Consoli, C. Geraci, R. La Spina, F. Cunsolo, *Org. Biomol. Chem.*, **2006**, *4*, 3763-3768.
10. a) A. T. Wright, Z. Zhong, E. V. Anslyn, *Angew. Chem. Int. Ed.*, **2005**, *44*, 5679-5682; *Angew. Chem.*, **2005**, *117*, 5825-5828; b) S. Wang, Y. –T. Chang, *Chem. Commun.*, **2008**, 1173-1175.
11. W. Sun, H. Bandmann, T. Schrader, *Chem. Eur. J.*, **2007**, *13*, 7701-7707.
12. B. K. Jena, C. R. Raj, *Biosens. Bioelectron*., **2008**, *23*, 1285-1290.
13. See for instance: a) J.V. Ros-Lis, R. Casasús, M. Comes, C. Coll, M.D: Marcos, R. Martínez-Máñez, F. Sancenón, J. Soto, P. Amorós, J. El Haskouri, N. Garó, K. Rurack, *Chem. Eur. J.*, **2008**, *14*, 8267-8278. b) S. Yagi, Y. Hyodo, M. Hirose, H. Nakazumi, Y. Sakarai, A. Ajayaghosh, *Org. Lett*., **2007**, *9*, 6590. c) A. Ajayaghosh, P. Chithra, R. Varghese, *Angew. Chem. Int. Ed*., **2007**, *46*, 230. d) J. V. Ros-Lis, M. D. Marcos, R. Martínez-Máñez, K. Rurack, J. Soto. *Angew. Chem. Int. Ed.*, **2005**, 44, 4405-4407; *Angew. Chem.*, **2005**, *117*, 4479-4482. e) J.V. Ros-Lis, B. García, D. Jiménez, R. Martínez-Máñez, F. Sancenón, J Soto, F. Gonzalvo, M.C. Valldecabres, *J. Am. Chem. Soc*., **2004**, *126*, 4064. f) J. V. Ros-Lis, R. Martínez-Máñez, K. Rurack, F. Sancenón, J. Soto, M. Spieles. *Inorg. Chem.*, **2004**, 43, 5183-5185. g) E. Arunkumar, P. Chithra, A. Ajayaghosh, *J. Am. Chem. Soc*., **2004**, *126*, 6590. h) A. Ajayaghosh, E. Arunkumar, J. Daub, *Angew. Chem. Int. Ed.*, **2002**, *41*, 1766. i) J.V. Ros-Lis, R. Martínez-Máñez, J. Soto, *Chem. Commun*., **2002**, 2248.; j) C.R. Chenthamarakshan, A. Ajayaghosh, *Tetrahedron. Lett*., **1998**, *39*, 1795. k) J. V. Ros-Lis, R. Martínez-Máñez, F. Sancenón, J. Soto, M. Spieles, K. Rurack, *Chem. Eur. J*. **2008**, *14*, 10101-10114.
14. See for instance: a) S. Sreejith, P. Carol, P. Chithra, A. Ajayaghosh, *J. Mat. Chem*., **2008**, *18*, 264-274 and references therein. b) K.D. Volkova, V.B. Kovalska, M.Y. Losytskyy, A. Bento, L.V. Reis, P.F. Santos, P. Almeida, S.M. Yarmoluk, *J. Fluoresc*., **2008**, *18*, 877-882. c) V.S. Jisha, K.T. Arun, M. Hariharan, D. Ramaiah, *J. Am. Chem. Soc*., **2006**, *128*, 6024-6025. d) P.T. Snee, R.C. Somers, G. nair, J.P. Zimmer, M.G. Bawendi, D.G. Nocera, *J. Am. Chem. Soc*., **2006**, *128*, 13320-13321.
15. See for example: a) M. Sugawara, K. Kojima, H. Sazawa, Y. Umezawa, *Anal. Chem*. **1987**, *59*, 2842-2846; b) K. Bandyopadhyay, H. Liu, S. –G. Liu, L. Echegoyen, *Chem. Commun*. **2000**, 141-142; d) S.

Flink, H. Schönherr, G. J. Vancso, F. A. J. Geurts, K. G. C. van Leerdam, F. C. J. M. van Veggel, D. N. Reinhoudt, *J. Chem. Soc., Perkin Trans.* **2000**, *2*, 2141-2146; c) T. Ito, *J. Electroanal. Chem*. **2001**, *495*, 87-97; d) Y. Katayama, Y. Ohuchi, H. Higashi, Y. Kudo, M. Maeda, *Anal. Chem*. **2000**, *72*, 4671-4674; e) H. Aoki, K. Hasegawa, K. Tohda, Y. Umezawa, *Biosens. Bioelectron*. **2003**, *18*, 261-267.

16. M. Montalti, L. Prodi, N. Zacheronni, G. Falini, *J. Am. Chem. Soc.*, **2002**, *124*, 13540-13546.
17. Too basic pHs were avoided in this study in order to stay away from the possible damage of the siliceous matrix at high concentration of hydroxide anions. Also very acidic or basic solutions have been reported to result in a degradation of the squaraine dye **I**.
18. Hyaluronic acid is other relevant negatively charged biopolymer. The formation of a highly dense gel in water-DMSO-acetonitrile 45:45:10 v/v/v mixtures used in this paper prevent the measurement of reliable UV-visible data.
19. I. Capila, R. J. Linhardt, *Angew. Chem. Int. Ed.*, **2002**, *41*, 390-412; *Angew. Chem.*, **2002**, *114*, 426-450.
20. a) J. C. Sauceda, R. M. Duke, M. Nitz, *ChemBioChem*, **2007**, *8*, 391-394; b) K. Gaus, E. A. H. Hall, *Biosens. Bioelectron.*, **1998**, *13*, 1307-1315.
21. See for instance: a) S. L. Wiskur, H. Ait-Haddou, J. J. Lavigne, E. V. Anslyn, *Acc. Chem. Res.*, **2001**, *34*, 963-972; b) V. Amendola, D. Estebán-Gómez, L. Fabbrizzi, M. Licchelli, *Acc. Chem. Res.*, **2006**, *39*, 343-353; c) R. Martínez-Máñez, F. Sancenón, *Chem. Rev.*, **2003**, *103*, 4419-4476; d) P. D. Beer, P. A. Gale, *Angew. Chem. Int. Ed.*, **2001**, *40*, 486-516; *Angew. Chem.*, **2001**, *113*, 502-532; e) V. Amendola, M. Bonizzoni, D. Estebán-Gómez, L. Fabbrizzi, M. Licchelli, F. Sancenón, A. Taglietti, *Coord. Chem. Rev.*, **2006**, *250*, 1451-1470; f) A. T. Wright, E. V. Anslyn, *Chem. Soc. Rev.*, **2006**, *35*, 14-28; g) R. Martínez-Máñez, F. Sancenón, *Coord. Chem. Rev.*, **2006**, *250*, 3081-3093.

Chem. Eur. J., 2009, 1816-1820.

A selective chromo-fluorogenic sensing of heparin using functionalised silica nanoparticles containing binding sites and a signalling reporter.

Supporting Information

Estela Climent, Pilar Calero, María Dolores Marcos, Ramón Martínez-Máñez, Félix Sancenón and Juan Soto

1. Experimental procedures

30 % suspension of ludox silica nanoparticles AS-30 Colloidal Silica were purchased from Sigma-Aldrich and the nanoparticles were used without any further purification. The solvents were absolute grade and were purchased form Scharlab. Anion/saccharide stock solutions ($C_{anion/saccharide}$ = 1 x 10^{-3} mol dm^{-3}) were prepared in water at pH 7. Due to the complexity of heparin and chondroitin-4-sulfate in this research solutions were prepared bearing in mind the molecular weight of the common repeating disaccharide unit (644.2 and 509 g mol^{-1} for

heparin and chondroitin-4-sulfate respectively).[1] Sodium salts of fluoride, chloride, bromide, iodide, sulfate, phosphate and nitrate were purchased from Scharlau. Saccharides sucrose, glucose, fructose and arabinose were purchased from Fluka, calcium lactobionate and chondroitin-4-sulfate were purchased from Sigma-Aldrich and sodium heparin was purchased from Acros Organics. The organosiloxane derivatives 3-[2-(2-aminoethylamino)ethylamino]propyl-trimethoxysilane (**N3TS**) and 3-mercaptopropyltrimethoxysilane (**MPTS**) for the synthesis of the solids **N1** and **N2** were provided by Aldrich.

Thermo-gravimetric analyses were carried out on a TGA/SDTA 851e Mettler Toledo balance. Transmission Electron Microscopy (TEM) images of the particles was obtained with a Philips CM10 operating at 20 KeV. Samples for TEM were prepared by spreading a drop of nanoparticles solution in HEPES onto standard carbon-coated copper grids (200 mesh). SEM microanalyses were obtained using a JEOL 6300 with a detector WDS of Oxford Instruments. UV-visible spectroscopy was carried out with a Lambda 35 UV/Vis Spectrometer (Perkin Elmer Instruments). Fluorescence measurements were carried out with a Felix 32 Analysis Version 1.2 (Build 56) PTI (Photon Technology International) and all solutions for photophysical studies were previously degassed.

2. Preparation of coated silica nanoparticles

Coated silica nanoparticles **N1** were prepared using the corresponding trialcoxysilyl derivatives following reported procedures by Montalti and coworkers.[2] Ludox silica nanoparticles AS-30, 18 ± 2 nm average diameter, (5 mL) were added to a solution containing acetic acid (25 mL), water (25 mL) and ethanol (40 mL). Then a mixture of mercaptopropyltriethoxysilane (**MPTS**, 21.23 mmol) and 3-[2-(2-aminoethylamino)ethylamino]propyl-trimethoxysilane (**M3TS**, 1.42 mmol) were added to the nanoparticle suspension. The crude reaction was heated at 80 ºC for 48 hours, the ethanol was evaporated and then the acetic acid solution neutralized with a saturated solution of sodium hydrogencarbonate. The functionalized nanoparticles (**N1**) were precipitated and isolated by filtration, washed with water and acetone and dried at 70 ºC. This method would allow obtaining a uniform

distribution of both functional groups on the silica surface. Also, and by a similar procedure, nanoparticles functionalized only with the thiol derivative **MPTS** were synthesized (**N2**) as model derivative for the elucidation of the role played by the anionic binding site.

Thermogravimetric analyses were carried out under a flow of air and with a heating rate of 10 ºC/ minute in the 30-1000 ºC interval. The final solid was maintained at 1000 ºC for 30 minutes. In the obtained thermograms of **N1** three clearly defined zones are observed; (i) from 30 ºC to 150 ºC which was assigned to loss of water and organic solvents (0.13 %), (ii) from 150 ºC to 800 ºC which was assigned to the organic matter attached into the nanoparticle surface (28 %) and, finally (iii) from 800º to 1000º C a third step was assigned to condensation of silanol groups (0.14 %). The silica residue amounts to 71.73 %. The diameter of **N1** and **N2** nanoparticles was determined by TEM. TEM images show a very homogenous particle size around 20 nm (see Figure 1) for both materials.

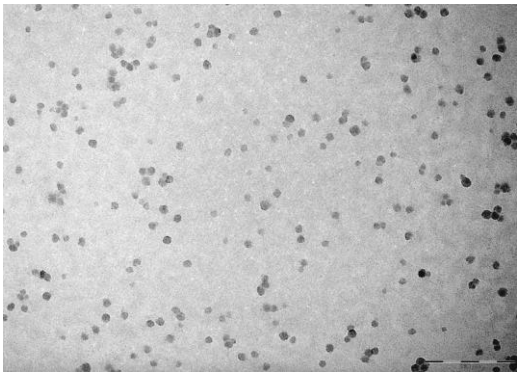

Figure 1. TEM image of hybrid nanoparticles **N1**. The bar corresponds to 200 nm.

3. A model to study the controlled switchable access to the nanoparticles surface.

The kinetic model between squaraine and thiol groups modulated by the interaction between a certain anion in the solution and the binding sites anchored on the silica surface is based on the concept that the rate of the reaction is

proportional both, (i) the concentration of squaraine (Sq) dye and (ii) to the fraction of the free anion binding centers by the corresponding anion at a certain concentration.

$$-\frac{d[Sq]}{dt} = k_v(1-\Theta)[Sq]^2 \qquad (1)$$

where k_v is the rate constant of the Sq-thiol reaction, Θ is the of occupied anion binding centers at the surface and [Sq] is the squaraine concentration (in mol L^{-1}). The interaction of the anions with the binding sites (in this case amines) at the silica surface can be determined using a Langmuir-type analysis. This model assumes that, (i) the anion (the absorbate) forms a monolayer, (ii) there are 0 or 1 molecules adsorbed at each site, (iii) all the binding sites have the same energy and (iv) the interaction between sites is negligible. In Langmuir analysis the isotherm coverage is dependent of both the temperature and the concentration of the adsorbate. If the temperature is fixed, then the coverage is only function of the concentration and the concentration of the anionic guest C:

$$\Theta = \frac{n_A}{n_M} = \frac{KC}{1+KC} \qquad (2)$$

where n_A is he number of moles of the adsorbed anion and n_M the maximum moles of anion that can be adsorbed on the monolayer. Alternatively Θ can be expressed in terms of the Langmuir adsorption constant (*K*) and the concentration *C* (in mol L^{-1}) of the anion at the equilibrium. Taking into account that the total amount of anion (n_0) is the sum of the moles of anion monolayer (n_A) and those remaining in the solution (*n*), i.e.

$$n_0 = n + n_A \qquad (3)$$

then

$$n_A = n_0 - n = n_M\Theta = \frac{n_M KC}{1+KC} \qquad (4)$$

Dividing by the volume of the solution (*V*, in liters), we obtain:

$$C_0 - C = \frac{\frac{n_M}{V}KC}{1+KC} \qquad (5)$$

then

$$KC^2(K(\frac{n_M}{V}-C_0)+1)C-C_0=0 \quad (6)$$

and finally

$$C=\frac{-(K(\frac{n_M}{V}-C_0)+1)}{2K}+\sqrt{\left(\frac{(K(\frac{n_M}{V}-C_0)+1)}{2K}\right)^2+\frac{C_0}{K}} \quad (7)$$

Additionally the reaction between the squaraine dye and the thiol groups in the surface is easily monitored by the decrease of the squaraine blue band at 641 nm. Therefore the concentration of squaraine at any time can be calculated from the simple measurement of the absorbance (A) following the Lambert-Beer law.

$$[Sq]=\frac{A}{\varepsilon} \quad (8)$$

where *A* is the absorbance of the squaraine band at 641 nm and ε is the molar extinction coefficient of the squaraine. Bearing in mind eq 7, 8 and 14 we can write:

$$-\frac{dA}{A^2}=\frac{k_v}{\varepsilon}\left(1-\frac{KC}{1+KC}\right)dt \quad (9)$$

that, by integration, results in:

$$\frac{1}{A}-\frac{1}{A_0}=\frac{k_v}{\varepsilon}\left(1-\frac{KC}{1+KC}\right)t \quad (10)$$

where *C* is given in equation 7.

3. References.

1. A. T. Wright, Z. Zhong, E. V. Anslyn, *Angew. Chem. Int. Ed.*, **2005**, *44*, 5679-5682.
2. M. Montalti, L. Prodi, N. Zacheronni, G. Falini, *J. Am. Chem. Soc.*, 2002, **124**, 13540-13546.

Selective and sensitive chromo-fluorogenic sensing of anionic surfactants in water using functionalised silica nanoparticles.

Estela Climent, Cristina Giménez,
María Dolores Marcos, Ramón Martínez-Máñez,
Félix Sancenón and Juan Soto

Centro de Reconocimiento Molecular y Desarrollo Tecnológico (IDM),
Unidad Mixta Universidad Politécnica de Valencia-Universidad de Valencia, Spain.
Departamento de Química, Universidad Politécnica de Valencia, Camino de Vera s/n, 46022, Valencia, Spain
CIBER de Bioingeniería, Biomateriales y Nanomedicina (CIBER-BBN), Spain

Received 10th March 2011, Accepted 28th April 2011
First published on the web 12th May 2011

Chem. Commun., ***2011****, 47, 6873–6875*

A new chromo-fluorogenic sensing protocol for anionic surfactants in aqueous environments using silica functionalised nanoparticles containing imidazolium and thiol groups has been developed.

Anionic surfactants are among the most common pollutants to be found in both technogenic and natural waters where they can cause serious environmental problems due to foam formation and because they can act as a transfer system to aqueous solution of other pollutants; i.e. petroleum products, oils, pesticides, etc.[1] A number of methods for the determination of these environmentally important species have been reported, such as titrimetry, spectrophotometry, spectrofluorimetry, chromatography, etc.[2] Some of these methods require time-consuming procedures or the use of relatively large amounts of chlorinated solvents that are not readily biodegradable (such as chloroform in the spectrophotometric "Methylene Blue" method). A different approach is the use of ion-selective electrodes, however those still show limitations in their applicability commonly related with signal stability and reproducibility.[3] Because of these restrictions, there is a real need to develop new methods for anionic surfactant sensing in water applicable to a wide range of situations. In this sense, novel selective and sensitive chromo- or fluorogenic methodologies are especially appealing for the design of simple probes for in situ and at site screening applications.[4]

Preparation of advanced sensing systems with enhanced capabilities using supramolecular and nanoscopic solid state chemistry concepts is a research field of interest that has attracted attention recently.[5] In this area, new signalling protocols using functionalized solids containing suitable functional organic groups for instance to enhance recognition or induce a switching mechanism have been reported.[6] Certain particular examples make use of silica nanoparticles prepared via the independent anchoring of functional binding sites and signalling units that have been used for the fluorescent recognition of certain metal cations and anions.[7]

Following our interest in the study of supramolecular functional protocols that come up from the covalent anchoring of organic molecules to solid supports,[8] we focused our attention towards the design of hybrid materials for the straightforward colorimetric detection of anionic surfactants in water without the use of chlorinated solvents using a simple competitive assay based on the controlled access of a dye to functional surfaces.

Scheme 1 shows the proposed chromogenic signalling paradigm. It involves the use of a suitable support (silica nanoparticles) decorated with two different groups, a signalling system (R) that is known to react with a certain dye (D) inducing bleaching, and a binding site (H) able to coordinate with the anionic surfactant (AS). In the absence of AS, the group R reacts with the dye resulting in the decolouration of the solution ("off state"), whereas in the presence of AS the reaction between R and D is partially or totally inhibited resulting in final coloured solutions ("on state"). This very simple signalling paradigm has been recently used for the design of electrochemical and optical sensing systems with very good results.[9]

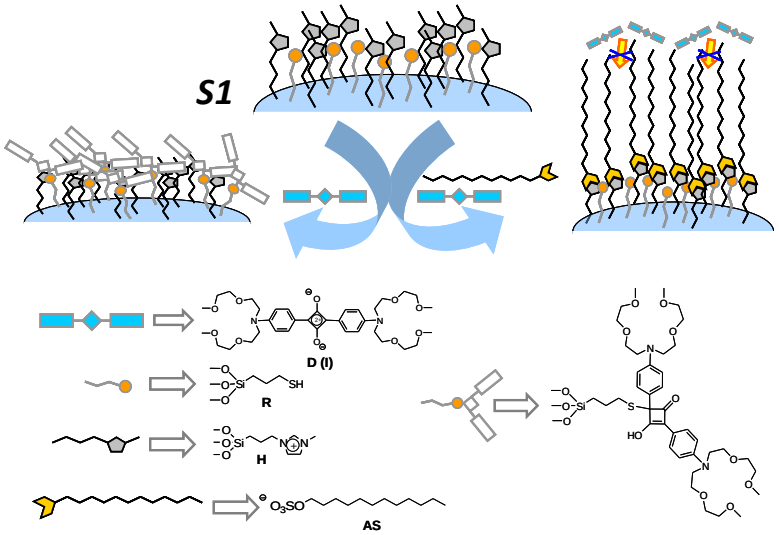

Scheme 1 Sensing paradigm for the chromogenic recognition of anionic surfactants . In the absence of surfactants the dye (D) reacts with R inducing the bleaching of the solution (left). In the presence of certain anionic surfactants (AS) the coordination with the host site (H) induced the inhibition of the reaction between R and D (right).

For this particular case R is a thiol group and D is a squaraine dye. The well-known reaction between thiols and squaraine dyes occurs at room temperature via attack of the nucleophilic thiol group on the electron deficient ring of the squaraine dye resulting in the rupture of the electronic delocalization and a bleaching of the blue squaraine solutions.[10] The designed system is completed by using imidazolium groups as host sites (H) suitable for binding with anionic surfactants. In fact, imidazolium has been widely reported as a suitable coordination site for anions via both electrostatic and hydrogen bonding interactions through $(C–H)^+$ and X^- ionic hydrogen bonds.[11] Additionally, imidazolium groups have been recently used as binding sites for the recognition of anionic surfactants.[12]

The squaraine derivative **I** was synthesised following literature procedures.[13] For the signalling protocol a water/CH_3CN 90:10 v/v mixture was selected due to the poor solubility of squaraine **I** in pure water. Coated silica nanoparticles **S1** were prepared using the known procedures reported by Montalti and coworkers (see ESI) using trialcoxysilyl derivatives 3-(mercaptopropyl)trimethoxysilane (**MPTS**) and N-methyl-N'-propyltrimethoxysilylimidazolium chloride.[14] In a typical reaction silica nanoparticles were heated at 80 °C in a mixture of water/ethanol/acetic acid 1:2:1 in the presence of the coating subunits. Subsequent purification involved the evaporation of the ethanol, neutralization of the acetic acid with ammonium acetate, centrifugation and washings of the nanoparticles with acetone.

Solid **S1** was characterized using standard procedures. The content of thiol (0.49 mmol g^{-1} SiO_2) and imidazolium (2.07 mmol g^{-1} SiO_2) groups was determined by elemental analysis and thermogravimetric studies. The resulting nanoparticles were characterized by transmission electron microscopy (see ESI). Final silica particles show a mean diameter of 17.0 ± 2.6 nm.

In a first step the reactivity of the squaraine **I** with the thiol groups on **S1** was tested at different pH values. A similar bleaching reaction rate was observed in the 3–8 pH range and pH 5.5 was selected for the following studies. In a typical

experiment 1.35 mL of a suspension of **S1** at pH 5.5 (5 mg of **S1** in 10 mL of water) was added to 0.2 mL of an acetonitrile solution of the dye **I** (1.0×10^{-4} M) and the changes in the visible band at 643 nm were monitored versus time. Similar experiments were carried out in the presence of sodium lauryl sulfate (LS) as a representative anionic surfactant at a concentration of 10^{-2} M. For both systems, Fig. 1 shows the absorbance at 643 nm (squaraine band) versus time. An inhibition of the thiol squaraine reaction can be clearly observed for the solution containing LS.

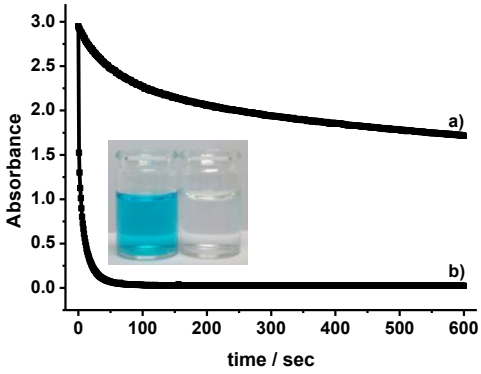

Figure 1. Absorbance of the squaraine dye **I** at 643 nm versus time for; (a)a water/CH_3CN 90:10 v/v suspension of **S1** in the presence of lauryl sulfate (0.01 M) to which squaraine **I** was added; (b) water/CH_3CN 90:10 v/v suspension of **S1** to which squaraine **I** was added. Inset: photograph showing the (a) blue and (b) colourless solutions after 30 s.

Encouraged by this simple colorimetric response, the reactivity of **S1** with squaraine **I** was also studied in the presence of other anionic surfactants; i.e. sodium dodecyl benzenesulfonate (LAS), dodecyl phosphate (DP), sodium tetradecyl sulfate (STS), sodium decyl sulfate (SDeS), sodium octylsulfate (SOS), sodium hexyl sulfate (SHS). Similar studies were also carried out with different carboxylates; i.e. acetate (C2), butyrate (C4), hexanoate (C6), octanoate (C8), decanoate (C10), dodecanoate (C12), myristate (C14), palmitate (C16) and oleate (C18). Also, the chromogenic response was studied in the presence of cationic and neutral surfactants; i.e. cetyltrimethylammonium bromide (CTAB) and tert-octylphenoxypolyethoxyethanol (Tx). The results are summarized in Fig. 2 for a

concentration of the corresponding surfactant of 0.001 M. A high colorimetric response was observed in the presence of anionic surfactants LS and LAS. Also a remarkable response was found in the presence of long chain sulfates (STS) and phosphates (DP), whereas shorter sulfates such as SDeS, SOS and SHS gave a poor response. The chromogenic response in the presence of long chain carboxylates (C18–C10) resembled that observed for sulfate SDeS whereas a complete bleaching was found for shorter carboxylates (C2–C8). Remarkably, the solid gave no response in the presence of neutral (Tx) and cationic surfactants (CTAB).

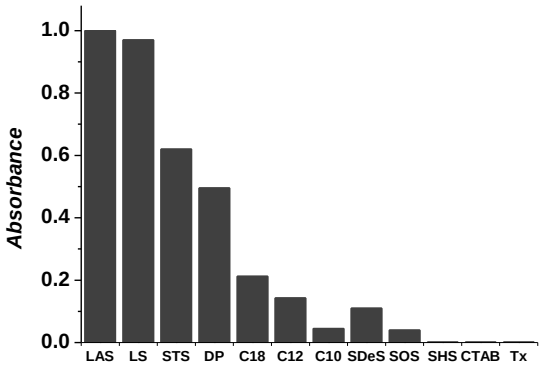

Figure 2. Absorbance at 643 nm (squaraine band) at pH 5.5 after 10 minutes of reaction of the squaraine dye **I** in water/CH_3CN 90:10 v/v with solid **S1** in the presence of certain anionic, cationic, neutral surfactants and carboxylates (C = 0.001 M).

The reactivity of the squaraine **I** with the thiol groups on **S1** was also tested in the presence of the anions sulfate, sulfite, nitrate, chloride, phosphate, bromide, pyrophosphate, carbonate and acetate (C = 0.001 M). Despite some partial response observed for pyrophosphate (similar to that found for SDeS in Fig. 2) the remaining anions were unable to inhibit the reaction between the squaraine dye **I** and thiols on the surface of **S1**. This highly selective colorimetric signalling of anionic surfactants with respect to other cationic, neutral surfactants, long chain carboxylates and inorganic anions in aqueous solutions, based on a control of dye transport (squaraine) from the solution to the solid surface, is quite uncommon

and for instance would have been hardly observable using classical chemosensors. The response of material **S1** as a function of the concentration of LAS is illustrated in Fig. 3 which plots the absorbance of the squaraine dye **I** at 643 nm after the two-step protocol described above. The figure shows that the amount of dye that reacted with the thiol groups at the surface is proportional to the amount of surfactant in the solution. A detection limit of 7.5×10^{-5} M was calculated.

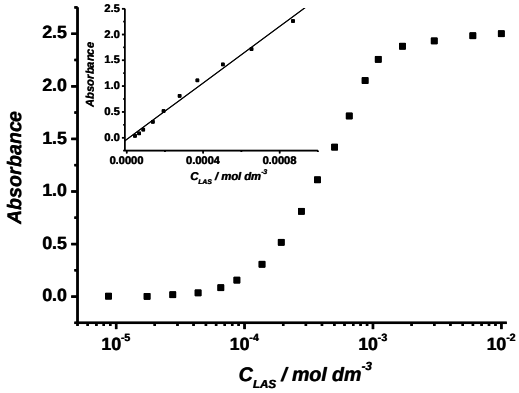

Figure 3. Absorbance of squaraine dye **I** at 643 nm measured for 30 seconds after the two-step protocol described above for suspensions of **S1** and **I** in water/CH_3CN 90:10 v/v as a function of the concentration of LAS .

Finally, in order to verify the feasibility of the developed method, we have prospectively used solid **S1** for the determination of anionic surfactants in water with fine results. In a typical experiment tap water was spiked with 5 and 10 ppm of LAS . Also in order to study the possible interference of carboxylates in the determination of anionic surfactants with **S1**, a mixture containing C18, C16, C10, C4 and C2 and LAS, each one at a concentration of 10 ppm, was prepared. The content of "anionic surfactants" was determined with the hybrid organic–inorganic material **S1** following an addition standard procedure and using the traditional well-known "Methylene Blue" method.[15] Results are shown in Table 1.

Table 1. Determination of anionic surfactants in water

	Metylene Blue method		**Proposed method**	
Added LAS (ppm)	Found (ppm)	R	Found (ppm)	R
5	4.1 ± 0.6	82	4.6 ± 1.2	92
10	9.0 ± 0.7	90	10.7 ± 3.0	107
10[a]	8.1±0.1	81	11.9± 1.9	119

[a]Tap water sample containing 10 ppm of LAS and a mixture of carboxylates (C_{18}, C_{16}, C_{10}, C_4 and C_2) in a concentration of 10 ppm each one.

In summary, a novel and simple approach for the chromogenic sensing of anionic surfactants in water using silica nanoparticles that were functionalised with imidazolium groups as hosts and thiol moieties as reactive sites has been reported. The existence of anionic surfactants in water in the presence of the functionalised silica nanoparticles allows us to control the access of the squaraine dye to the surface of nanoparticles, resulting in a chromo-fluorogenic response. This protocol shows enhanced features and displays a sensing behaviour that is difficult to achieve using classical "binding site–signalling unit" receptors. Additionally the proposed method has been used for the accurate determination of anionic surfactants in water and competes well with current standard techniques. Moreover the method, based on a simple competitive procedure, has allowed us to develop a new undemanding colorimetric "green" procedure for the detection of anionic surfactants without the use of hazardous chlorinated organic solvents.

Financial support from the Spanish Government (project MAT2009-14564-C04-01) and the Generalitat Valencia (project PROMETEO/2009/016) is gratefully acknowledged. E.C. and C.G. thank the MICINN and the UPV for fellowships.

Notes and references

1. E. Liwarska-Bizukojc, *Fresenius Environ. Bull.*, **2009**, *18*, 1666. (b) T. Cserhati, E, Forgacs, G. Oros, *Environ. Int.*, **2002**, *28*, 337.
2. See for example: (a) S. D. Richardson, *Anal. Chem.*, **2007**, *79*, 4295. (b) S. González, D. Barceló, M. Petrovic, *Trends Anal.Chem.*, **2007**, *26*, 116. (c) F. Ventura, P. Voogt, *Comprehensive Anal. Chem.*, **2003**, *40*, 51.
3. (a) J. Sánchez, M. del Valle, *Critical Rev. Anal. Chem.*, **2005**, *35*, 15. (b) M. Gerlache, J. M. Kauffmann, G. Quarin, J. C. Vire, G. A. Bryant, J. M. Talbot, *Talanta*, **1996**, *43*, 507.
4. (a) C. Caltagirone, P. A. Gale, *Chem. Soc. Rev.*, **2009**, *38*, 520. (b) V. Amendola, D. Esteban-Gómez, L. Fabbrizzi, M. Licchelli, *Acc. Chem. Res.*, **2006**, *39*, 343. (c) A. P. de Silva, H. Q. N. Gunaratne, T. Gunnlaugsson, A. J. M. Huxley, C. P. McCoy, J. T. Rademacher, T. E. Rice, *Chem. Rev.*, **1997**, *97*, 1515.
5. R. Martínez-Máñez, F. Sancenón, M. Hecht, M. Biyical, K. Rurack, *Anal. Bioanal. Chem.*, **2011**, *399*, 55-74.
6. See for example: (a) E. Climent, M. D. Marcos, R. Martínez-Máñez, F. Sancenón, K. Rurack, J. Soto, P. Amorós, *Angew. Chem. Int. Ed.*, **2009**, *48*, 8519. (b) R. Casasús, E. Aznar, M. D. Marcos, R. Martínez-Máñez, F. Sancenón, J. Soto, P. Amorós, *Angew. Chem. Int. Ed.*, **2006**, *45*, 6661. (c) T. Balaji, S. A. El-Safty, H. Matsunaga, T. Hanaoka, F. Mizukami, *Angew. Chem. Int. Ed.*, **2006**, *45*, 7202. (d) S. A. El-Safty, A. A. Ismail, H. Matsunaga, F. Mizukami, *Chem. Eur. J.*, **2007**, *13*, 9245.
7. (a) E. Brasola, F. Mancin, E. Rampazzo, P. Tecilla, U. Tonellato, *Chem. Commun.*, **2003**, 3026. (b) E. Rampazzo, E. Brasola, S. Marcuz, F. Mancin, P. Tecilla, U. Tonellato, *J. Mater. Chem.*, **2005**, *16*, 2687.
8. (a) A. B. Descalzo, R. Martínez-Máñez, F. Sancenón, K. Hoffmann, K. Rurack, *Angew. Chem. Int. Ed.*, **2006**, *45*, 5924. (b) B. G. Trewyn, I. I. Slowing, S. Giri, H. –T. Chen, V. S. –Y. Lin, *Acc. Chem. Res.*, **2007**, *40*, 846.
9. See for example: (a) E. Climent, R. Casasús, M. D. Marcos, R. Martínez-Máñez, F. Sancenón, J. Soto, *Chem. Commun.*, **2008**, 6531. (b) E. Climent, P. Calero, M. D. Marcos, R. Martínez-Máñez, F. Sancenón, J. Soto, *Chem. Eur. J.*, **2009**, *15*, 1816. (c) E. Climent, A. Martí, S. Royo, R. Martínez-Máñez, M. D. Marcos, F. Sancenón, J. Soto, A. M. Costero, S. Gil, M. Parra, *Angew. Chem. Int. Ed.*, **2010**, *49*, 5945. (d) V. P. Y. Gadzekpo, K. P. Xiao, H. Aoki, P. Bühlmann, Y. Umezawa, *Anal. Chem.*, **1999**, *71*, 5109. (e) V. P. Y. Gadzekpo, P. Bühlmann, K. P. Xiao, H. Aoki, Y. Umezawa, *Anal. Chim. Acta*, **2000**, *411*, 163.
10. J. V. Ros-Lis, B. García, D. Jiménez, R. Martínez-Máñez, F. Sancenón, J. Soto, F. Gonzalvo, M. C. Valldecabres, *J. Am. Chem. Soc.*, **2004**, *126*, 4064.
11. (a) J. Yoon, S. K. Kim, N. J. Singh, K. S. Kim, *Chem. Soc. Rev.*, **2006**, *35*, 355. (b) Z. Xu, S. K. Kim, J. Yoon, *Chem. Soc. Rev.*, **2010**, *39*, 1457.

12. C. Coll, R. Martínez-Máñez, M. D. Marcos, F. Sancenón, J. Soto, *Angew. Chem. Int. Ed.*, **2007**, *46*, 1675.
13. J. V. Ros-Lis, R. Martínez-Máñez, F. Sancenón, J. Soto, M. Spieles, K. Rurack, *Chem. Eur. J.*, **2008**, *14*, 10101.
14. M. Montalti, L. Prodi, N. Zaccheroni, G. Falini, *J. Am. Chem. Soc.*, **2002**, *124*, 13540.
15. *Standard Methods for the Examination of Water and Wastewater* (Eds.: L. S. Clesceri, A. E. Greenberg, A. D. Eaton), 20th Ed., American Public Health Association, Washington, DC, **1999**, pp. (5-44)-(5-51).

Chem. Commun, 2011, 47, 6873-6875

Selective and sensitive chromo-fluorogenic sensing of anionic surfactants in water using functionalised silica nanoparticles.

Supporting Information

Estela Climent, Cristina Giménez, María Dolores Marcos, Ramón Martínez-Máñez, Felix Sancenón and Juan Soto

1. Experimental procedures

Chemicals

30 % suspension of ludox silica nanoparticles AS-30 Colloidal Silica were purchased from Sigma-Aldrich and the nanoparticles were used without any further purification. The solvents were absolute grade and were purchased form Scharlab. Anions chloride, bromide, sulfate, nitrite, nitrate, phosphate, pyrophosphate and carbonate solutions were prepared from sodium salts purchased from Scharlau. Sodium lauryl sulphate (LS, $CH_3(CH_2)_{11}OSO_3Na$) was purchased from Merck. Sodium tetradecyl sulfate (STS, $CH_3(CH_2)_{13}OSO_3Na$), sodium decyl sulfate (SDeS) and sodium hexyl sulfate (SHS) were purchased from Acros Organics, mono-*n*-dodecyl phosphate (DP) was purchased from Lancaster, sodium dodecyl benzenesulfonate (LAS) was obtained from Fluka and sodium octyl sulfate (SOS) was purchased from Chempur. The cationic surfactant

hexadecyltrimethylamonium bromide (CTAB, $CH_3(CH_2)_{15}N(CH_3)_3Br$) was provided by Fluka. *t*-Octylphenoxypolyethoxyethanol (Tx) surfactant was purchased from Sigma-Aldrich. Methylene Blue (MB) was purchased from Riedel-de Haen. Sodium acetate, sodium butyrate, sodium hexanoate, sodium octanoate, sodium decanoate, sodium dodecanoate, myristic acid, sodium palmitate and sodium oleate were obtained from Sigma Aldrich. Chemical structures for all surfactants and carboxylates are showed in Figure SI-1.

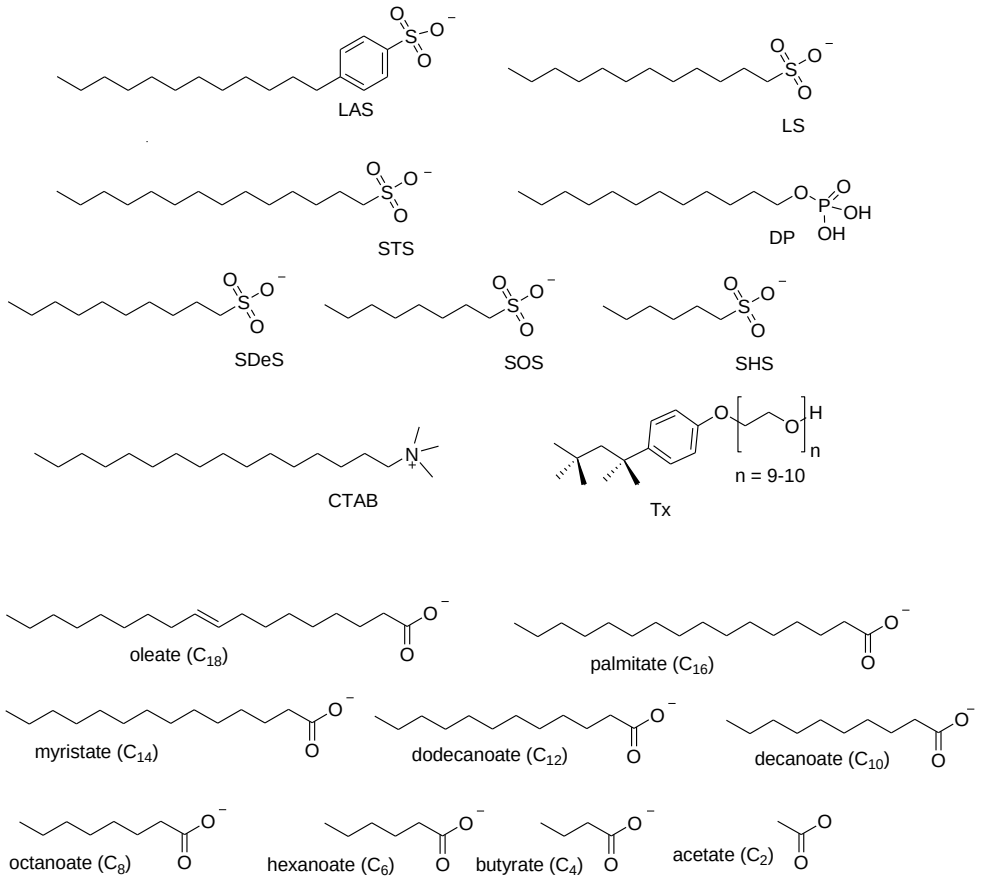

Figure SI-1. Chemical structures of surfactants and carboxylates tested.

For the imidazolium derivative, *N*-methylimidazole was provided by Acros Organics and 3-(chloropropyl)trimethoxysilane was purchased from Fluka. The spectroscopic inhibitor, 3-(mercaptopropyl)triethoxysilane (**MPTS**) for the synthesis of the solid **S1** was provided by Aldrich.

General Techniques

TG analysis, transmission electron microscopy, elemental analysis, nuclear magnetic resonance, UV-visible spectroscopy and fluorescence spectroscopy techniques were employed to characterize the materials. Thermo-gravimetric analysis were carried out on a TGA/SDTA 851e Mettler Toledo equipment, using an oxidant atmosphere (Air, 80 mL/min) with a heating program consisting on a heating ramp of 10 °C per minute from 393 K to 1273 K and an isothermal heating step at this temperature during 30 minutes. Transmission Electron Microscopy (TEM) images of the particles were obtained with a Philips CM10 operating at 20 KeV. Samples for TEM were prepared by spreading a drop of nanoparticles solution in H_2O onto standard carbon-coated copper grids (200 mesh). UV-visible spectroscopy was carried out with a Lambda 35 UV/Vis Spectrometer Perkin Elmer Instruments. ^{1}H and ^{13}C nuclear magnetic resonance (NMR) spectra were acquired with Varian 300 spectrometer (Sunnyvale, CA, USA).

Synthesis of N-methyl-N'-propyltrimethoxysilylimidazolium chloride

The *N*-methyl-*N*'-propyltrimethoxysilylimidazolium chloride was prepared as follows. A mixture of *N*-methylimidazole (6.6 g, 80 mmol) and 3-(chloropropyl)trimethoxysilane (15.9 g, 80 mmol) were stirred in a dry 100 ml flask under nitrogen flow at 95 ºC for 24 h. After cooling at room temperature, the resulting liquid product was washed with ether. The final compound was obtained as a yellow liquid. ^{1}H NMR (DMSO-D6): δ (ppm) = 0.55 (m, 2H, –C*H*$_2$–Si–), 1.81 (m, 2H, C*H*$_2$–CH$_2$–Si–), 3.46 (s, 9H, C*H*$_3$–O–), 3.83 (s, 3H, –N–C*H*$_3$), 4.11 (t, 2H,–N–C*H*$_2$–CH$_2$–), 7.69 (d, 1H, Me–N–C*H*–CH–), 7.75 (d, 1H,CH–C*H*–N–CH$_2$–), 9.11 (s, 1H, N–C*H*–N–). ^{13}C NMR (DMSO-D6): δ (ppm) = 5.4 (–*C*H$_2$–Si–), 23.4 (–*C*H$_2$–CH$_2$–Si–), 35.7 (*C*H$_3$–O–), 50.1 (–N–*C*H$_3$), 50.9 (–N–*C*H$_2$–) 122.2 (–CH–*C*H–N–CH$_2$–), 123.6 (CH$_3$–N–*C*H–CH–), 136.6 (–N–*C*H–N–).

2. Preparation, characterization and use of functionalised silica nanoparticles S1.

Coated silica nanoparticles **S1** were prepared using the corresponding trialcoxysilyl derivatives following reported procedures by Montalti and coworkers. Ludox silica nanoparticles AS-30, 17 nm average diameter, (12 mL) were added to a solution containing acetic acid (60 mL), water (60 mL) and ethanol (100 mL). Then a mixture of 3-(mercaptopropyl)trimethoxysilane (**MPTS**, 2.5 mmol) and N-methyl-N'-propyltrimethoxysilylimidazolium chloride (12.5 mmol) were added to the nanoparticle suspension. The crude reaction was heated at 80 ºC for 48 hours, the ethanol was evaporated and then the acetic acid solution neutralized with a saturated solution of ammonium acetate. The solvent was removed and nanoparticles were washed with acetone. The functionalised nanoparticles (**S1**) were precipitated and isolated by filtration, washed with water and acetone and dried at 70 ºC.

Thermogravimetric analyses were carried out under a flow of air and with a heating rate of 10 ºC/ minute in the 30-1000 ºC interval. The final solid was maintained at 1000 ºC for 30 minutes. In the obtained thermograms of **S1** three clearly defined zones are observed; (i) from 30 ºC to 150 ºC which was assigned to loss of water and organic solvents (6.11 %), (ii) from 150 ºC to 800 ºC which was assigned to the organic matter attached into the nanoparticle surface (25.11 %) and, finally (iii) from 800º to 1000º C a third step was assigned to condensation of silanol groups (0.16 %). The silica residue amounts to 68.6 %. The diameter of **S1** nanoparticles was determined by TEM that shows a very homogenous particle size of 17.0 ± 2.6 nm.

Solid **S1** contains 2.07 mmol of imidazolium per gram of SiO_2. A further characterization of the interaction of the solid **S1** with the anionic surfactant LAS can be estimated from Figure 3 that shows that the saturation of the calibration curve was observed at a LAS concentration of 1.8×10^{-3} mol dm^{-3}. From the amount of nanoparticles used in these experiments the saturation of the curve corresponds to a 1:1 molar ratio between imidazolium binding sites and LAS

molecules. This indicated that each imidazolium cation coordinates with one molecule of LAS most likely resulting in the formation of a highly regular hydrophobic monolayer on the surface of the **S1** nanoparticles.

Signalling experiments using nanoparticles **S1** were carried out at pH 5.5. The pH was fixed using diluted HCl or NaOH solutions when appropriate.

2. Determination of methylmercury using capped mesoporous inorganic materials.

2.1 **Introduction**

As we have reported above in the general introduction, most of the hybrid systems that have been described respond to stimuli such as light, pH or redox reactions. There are few examples able to induce a control release in response to small molecules or anions. However, the design of such systems for certain chemical species may be interesting for the development of new protocols of recognition, and also for the design of complex functional materials controlled by the presence of target chemicals. In connection with this field, the combination of mesoporous supports with processes involving coordination or reactions between certain species is a promising starting point for the application of supramolecular ideas in the design of new nanoscale devices, and a method for carrying molecular and supramolecular concepts into new advances in the field of nanoscience. In relation to this, organic-inorganic hybrid materials that are controlled by small species have a dual function: They are able to produce a mass transport control and, on the other hand, they can also be used as highly selective and sensitive probe systems.

Bearing these concepts in mind, in this chapter we report a new organic-inorganic hybrid material functionalised with a squaraine derivative able to respond to the precence of methylmercury.

2.2 **Mercury species and their bioacumulation.**

Mercury is present in nature in several different geochemical forms, including elemental mercury Hg(0), ionic (or oxidized) mercury Hg(II), and in several organic forms, the most important of which is methylmercury (CH_3Hg^+). Methylmercury is the form most readily incorporated into biological tissues and most toxic to humans. This form of mercury, can accumulate up the food chain in aquatic systems and lead to high concentrations of methylmercury in predatory fish, which, when consumed by humans, can result in an increased risk of adverse effects in highly exposed or sensitive populations.

In the past, methylmercury was produced directly and indirectly as part of several industrial processes such as the manufacture of acetaldehyde. Currently there are few anthropogenic sources of methylmercury pollution other than as an indirect consequence of the burning of wastes containing inorganic mercury and from the burning of fossil fuels. Despite of these few anthropogenic sorcues, an amount of at least 138 tones/year are released to the atmosphere only in the United States.[1] In addition, natural sources produces also a release of mercury to the atmosphere, such as volcanoes, forest fires and weathering of mercury-bearing rocks.[2] Once in the atmosphere, mercury is widely disseminated and can circulate for years, accounting for its wide-spread distribution.

Mercury is a globally dispersed contaminant, and its presence is a problem when the rate of natural formation of methylmercury from inorganic mercury is greater

[1] U. S. Environmental Protection Agency, 1997, "Mercury study report to congress, Volume II: An inventory of anthropogenic mercury emissions in the United States", table ES-3, sum of Utility boilers and Commercial/industrial boilers. Report: EPA-452/R-97-004.

[2] Tewalt, S. J.; Bragg, L. J.; Finkelman, R. B., 2005, Mercury in U.S. coal. Abundance, distribution, and modes of occurrence, U.S. Geological Survey Fact Sheet 095-01. Access-date=January 12, 2006.

than the reverse reaction. The atmosphere contains the three principal forms of mercury, but inorganic divalent mercury Hg(II) is the dominant form. Once in surface water, mercury enters a complex cycle in which one form can be converted to another. The action of anaerobic organisms that live in aquatic systems (lakes, rivers, oceans, etc.) converts inorganic mercury to methylmercury in the natural environment. The conversion of inorganic mercury to methylmercury is important for two reasons: (1) it is much more toxic than inorganic mercury, and (2) organisms require considerably longer times to eliminate it. Due to this, it is biomagnified in aquatic food chains from bacteria, to plankton and fishes. At each step in the food chain, the concentration of methylmercury in the organism increases, due to the fact that it has a half-life of about 72 days in aquatic organisms. This induces that levels of this species in fishes is a million times higher than the ammounts in the water.

The concentration of mercury in any given fish depends on the species, the age and size of the fish and the type of water body in which it is found. In general, fishes such as shark, swordfish, species of tuna, walleye, largemouth bass, and northern pike have higher levels of methylmercury than herbivorous fish or smaller fish such as tilapia, and herring.[3]

People are exposed to methylmercury almost entirely by eating contaminated fish and wildlife that are at the top of aquatic foodchains. The usual amount of mercury found is at levels of anywhere between 0.01 ppm to 0.5 ppm, although in larger fish, such as swordfish or shark, and even some larger tuna, the levels can be elevated to regions of 1.0 ppm, which is the Food and Drug Administration (FDA's) limit for human consumption.

Due to positive charge of the methylmercury species, it readily combines with anions such as chloride (Cl^-), hydroxide (OH^-) and nitrate (NO_3^-). On the other hand, it also has very high affinity for sulfur-containing compounds, particularly

[3] D.J. Hoffman, B.A. Rattner, G.A. Burton, J. Cairns, *Handbook of Ecotoxicology*, 2nd ed. Boca Raton, Florida, CRC Press, 409-463.

the thiol (-SH) groups, forming a covalent bond. Due to this, in the body it is normaly found complexed with free cysteine and with proteins and peptides containing that amino acid. The methylmercuric-cysteinyl complex is recognized by amino acid transporting proteins, and it is transported freely throughout the body, crossing the blood–brain barrier and also the placenta, where it is absorbed by the developing fetus.

2.3 Squaraine-thiol derivative: An ideal reactive receptor unit for mercury species.

As have been menctioned above, mercury species have a high affinity to thiol moieties. Bearing in mind these facts, our research group reported a thiol-functionalized mesoporous hybrid MCM-41-type material (UVM-7 material) containing a squaraine-thiol derivative grafted on its surface, employing the same squaraine and the same thiol groups that we have employed in chapter 1.[4] As we have explained above, this squaraine shows a blue absorption band at ca. 640 nm, losing color and fluorescent propierties upon its transformation to 2,4-bis(4-dialkylaminophenyl)-3-hydroxy-4-alkylsulfanylcyclobut-2-enone upon reaction with thiol groups. Bearing this mind these facts, the authors employed this hybrid material as a chemodosimeter for Hg^{2+} ions. Reaction of Hg^{2+} with thiol moiety, induced a release of the free squaraine dye from the pores to the solution. A selective response of this hybrid material to Hg^{2+} ions was found, and the presence of other thiophilic cations such as Pb^{2+} and Cd^{2+} only yielded very low dye release at relatively high concentrations of 1 mM. Figure 2.1 shows a schematic representation of the Hg^{2+} detection protocol using this hybrid material.

[4] J. V. Ros-Lis, R. Casasús, M. Comes, C. Coll, M. D. Marcos, R. Martínez-Máñez, F. Sancenón, J. Soto, P. Amorós, J. El. Haskouri, N. Garró, and K. Rurack, *Chem. Eur. J.*, 2008, **14**, 8267.

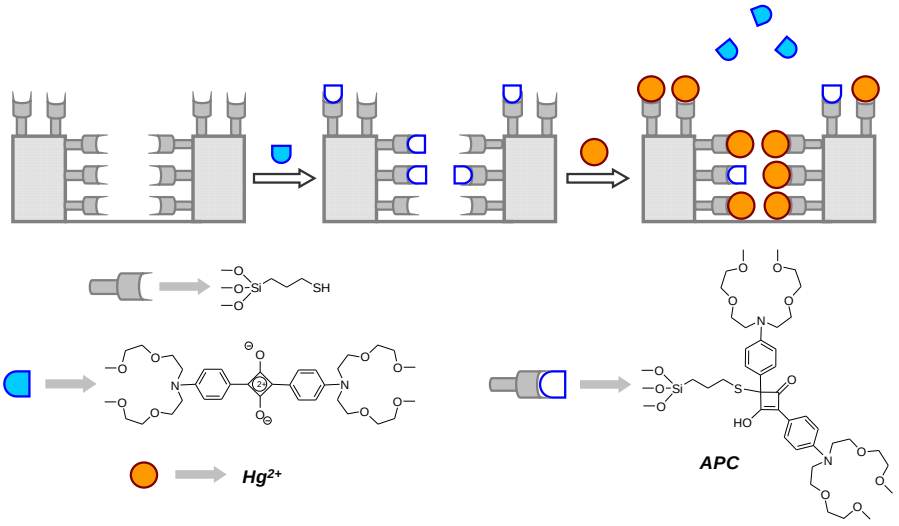

Figure 2.1.- Sheme of the preparation of the hybrid material for the sensing of Hg^{2+}.

2.4 **Objectives.**

Taking into account this mechanism, and also bearing in mind the importance of methylmercury detection, we aimed to design a hybrid material for the detection of this potentially dangerous cation.

In the following section will be presented in detail the preparation of this hybrid material and its application for the selective and sensitive detection of methylmercury.

A method for the determination of methylmercury in real samples using organically capped mesoporous inorganic materials capable of signal amplification

Estela Climent,[a,b,c] María Dolores Marcos,[a,b,c] Ramón Martínez-Máñez,[a,b,c] Félix Sancenón,[a,b,c] Juan Soto,[a,b,c] Knut Rurack,[d] and Pedro Amorós.[e]

[a] Instituto de Reconocimiento Molecular y Desarrollo Tecnológico.
Centro Mixto Universidad Politécnica de Valencia – Universidad de Valencia.
[b] Departamento de Química, Universidad Politécnica de Valencia
Camino de Vera s/n, 46022, Valencia, Spain.
[c] CIBER de Bioingeniería, Biomateriales y Nanomedicina (CIBER-BBN)
[d] Bundesanstalt für Materialforschung und –prüfung, Div. I.5, BAM
Richard-Willstätter-Strasse 11, D-12489 Berlin, Germany.
[e] Institut de Ciència del Materials (ICMUV), Universitat de València. P.O. Box 2085, E-46071 València, Spain.

Received: July 30, 2009
Published online: October 2, 2009

Angewandte Chemie International Edition,
***2009**, 48, 8519 – 8522*

Mercury exists in the environment in a variety of compounds, and the toxicity depends on the chemical species.[1,2] Organomercury derivatives, especially methylmercury (CH_3Hg^+), are more toxic than inorganic or elemental mercury. Methylmercury is rarely emitted anthropogenically, but usually formed naturally through biomethylation of mercury, often of anthropogenic origin. Methylmercury subsequently bio-accumulates through the food chain, for example in the tissue of fish,[3] in which methylmercury concentrations are frequently found that exceed the maximum levels recommended by the Environmental Protection Agency (EPA) and the World Health Organization (WHO) for human consumption (0.1 and 0.23 μg (kg body weight)$^{-1}$ day^{-1}).[4] Methylmercury exposure in adults has been linked to cardiovascular diseases, autoimmune effects, hearing impairment, blindness, and death.[1] In a number of cases, mercury intoxication is related to the consumption of fish.[5]

Several analytical methods have been described for the determination of methylmercury in biological samples. For example, gas chromatography (GC) with electron capture detection (ECD)[6] or inductively coupled plasma mass spectrometry (ICP-MS)[7] and high performance liquid chromatography (HPLC) with elemental[8] or ICP-MS[9] detection have been extensively used. As an alternative to these technically sophisticated methods, which require a laboratory setting, the development of more simple procedures for in situ and rapid screening applications that are based on optical,[10] electrochemical,[11] or gravimetric[12] procedures have recently received considerable attention; these methods involve in part biological species as active sensing elements.[13]

Regarding the development of chromo- and fluorogenic indication systems for mercury derivatives, a large number of examples have been reported for the inorganic form (Hg^{2+}),[14–17] but few studies have targeted CH_3Hg^+.[18] Furthermore, most of these studies were unable to discriminate between Hg^{2+} and CH_3Hg^+ and did not involve the determination of the analyte(s) in relevant samples or matrices such as fish.[19]

Chemically, the great majority of the reported approaches rely on indicator molecules that either bind[14, 17a] or react[15, 17b] with Hg^{2+} to yield the desired change in color or fluorescence. Only very recently, alternative procedures involving organic, inorganic, or hybrid materials have been proposed, which are promising in their performance.[16] Our interest in the latter type of materials motivated us to explore bioinspired strategies toward new signaling models. For mercury indication, we combined our experience in Hg^{2+} sensing[17] and supramolecular hybrid materials design[20] and developed an organically capped mesoporous inorganic material for selective CH_3Hg^+ determination through signal amplification.

Inspired by gated ion channels and pumps, the proposed sensing mechanism relies on the opening of a pore that is controlled by the interaction of a certain molecular stimulus (the target species, CH_3Hg^+) at the receptors that close the gate.[21] Although this reaction itself can already induce an optical response, a second process is implemented in the system that leads to strong signal amplification: the pores of the hybrid are loaded with a large amount of dye molecules, which are only liberated upon analyte-induced opening of the pores. To date, apart from a few examples of analyte-induced pore blockage,[22] pore-opening methods for sensing applications have not been reported.[23]

The sensing procedure is shown in Scheme **1**. The inorganic support is a calcined MCM-41 mesoporous solid that features homogeneous porosity, facile surface functionalization, inertness, and a high loading capacity.[24] The solid is first loaded with a dye (safranine O) and is then capped with 2,4-bis(4-dialkylaminophenyl)-3-hydroxy-4-alkylsulfanylcyclobut-2-enone (APC) groups. The APC moieties are obtained in situ by a nucleophilic addition reaction between mercaptopropyl groups previously attached to the silica surface and the squaraine derivative **I**.[25] Once reacted, the bulky APC groups significantly inhibit dye release by closing the pores.[26] As we have previously shown, APC moieties can react with mercury, resulting in the coordination of the cation to the thiol group and liberation of the restored squaraine chromophore.[17b, 27] This concept suggests that the system

should work equally well with thiophilic CH_3Hg^+ as a "key" to unlock the "gate" (Scheme **1**).

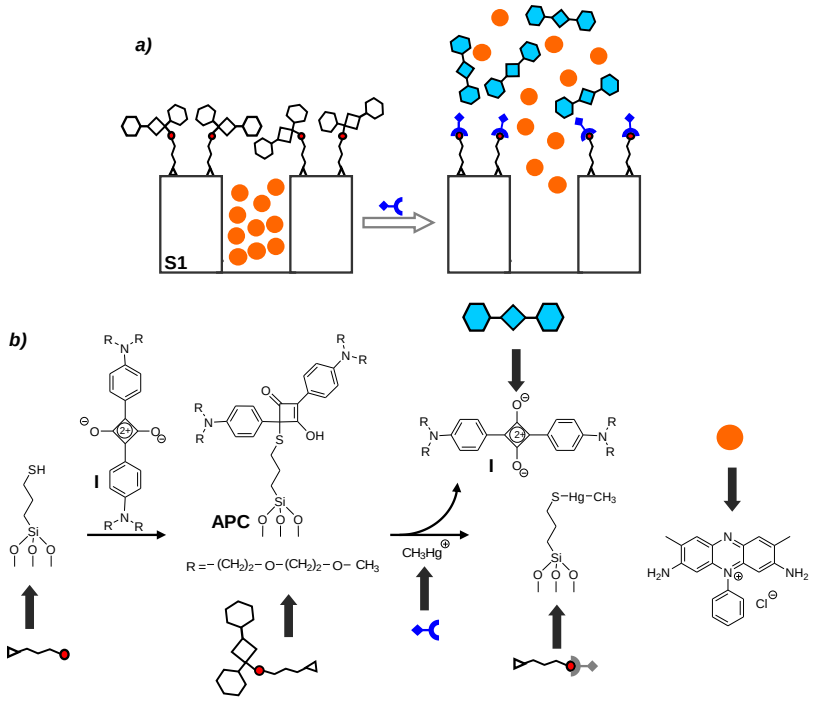

Scheme 1. a) Chromogenic detection of methylmercury ions using solid **S1** with safranine molecules (black circles) entrapped by APC groups (gray). b) Molecular basis of the capping (APC formation) and methylmercury-promoted uncapping steps (release of squaraine).

The mesoporous support was prepared following known procedures.[31] The MCM-41 structure of the starting material was confirmed by X-ray diffraction (Figure **1**) and TEM (see the Supporting Information). The N_2 adsorption–desorption isotherms showed a typical type IV curve, with a specific surface area of 1249 $m^2 g^{-1}$, a narrow pore-size distribution, and an average pore diameter of 2.5 nm. The inorganic scaffold was loaded with safranine O as the reporter dye, and the surface of the mesoporous support was then functionalized with (3-mercaptopropyl)trimethoxysilane (**MPTS**). This sequence ensures that **MPTS** diffusion into the pores is hampered and that functionalization occurs primarily at the outer surface. The capped material **S1** was then obtained by reaction of the thiol groups with **I** in 1:5 v/v acetonitrile/CHES buffer pH 9.6 solution (see the

Supporting Information). Figure **1** shows the powder X-ray pattern of **S1** with the expected features of the MCM-41 phase, indicating that after the filling of the pores and the functionalization of the surface, the mesoporous structure still remains unaltered. The mesoporous structure of **S1** is also clearly observed in the TEM image (Figure **2**). From thermogravimetric and elemental analysis, a content of 0.032 mmol g^{-1} SiO_2 of thio-derivatives and 0.47 mmol g^{-1} SiO_2 of safranine were found.

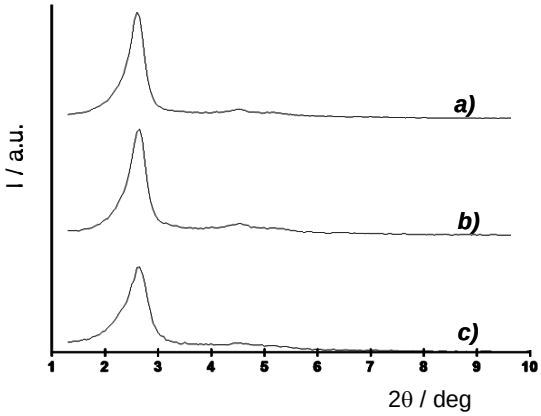

Figure 1. Powder X-ray patterns of (a) MCM-41 as synthesized, (b) calcined MCM-41, and (c) **S1** hybrid material.

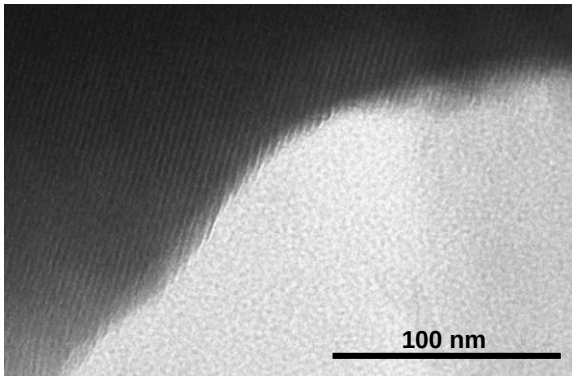

Figure 2. TEM image of solid **S1**, showing typical features of the hexagonal MCM-41 matrix.

Studies on the methylmercury-induced uncapping were carried out in acetonitrile/toluene 4:1 v/v. This solvent mixture was chosen because it fulfils two purposes: it achieves rather tight pore closure,[26] and this mixture is suitable for adopting the AOAC-approved discrimination between CH_3Hg^+ and Hg^{2+} by lipophilicity partitioning and thus the design of a protocol for the determination of CH_3Hg^+ in real samples. Furthermore, CH_3Hg^+ can be readily obtained from fish tissue by extraction in toluene, and acetonitrile promotes the solubility of the safranine dye upon release. In a typical preliminary experiment, **S1** was suspended in acetonitrile/toluene 4:1 v/v in the presence of 1.5 ppm CH_3Hg^+ and the suspension was stirred for 5 min (until maximum delivery of the safranine dye was observed). The delivery was monitored through the absorption band of safranine at 523 nm. Figure **3** shows that in the absence of CH_3Hg^+, some release of the entrapped dye is observed. However, the safranine band is significantly enhanced in the presence of 1.5 ppm of CH_3Hg^+, which is ascribed to the uncapping process upon reaction of CH_3Hg^+ with APC moieties.

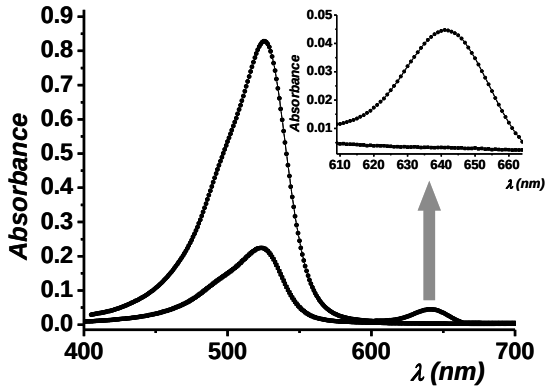

Figure 3. The absorption band of safranine (523 nm) in mixtures of acetonitrile/toluene 4:1 v/v in the presence of 1.5 ppm of CH_3Hg^+ (– – –) and in the absence of CH_3Hg^+ (—). Inset: The region of squaraine absorption in the presence (– – –) and absence (—) of CH_3Hg^+.

One of the key advantages of gated and loaded porous materials is their inherent signal amplification. Only very few analyte molecules, such as CH_3Hg^+, reacting at the pore openings are necessary to release a large number of signaling units (safranine) that were stored in the ensemble. In the present case, signal

amplification is directly evident from a comparison of the ratios of the safranine band at 523 nm and the squaraine band at 641 nm (Figure **3**). Taking into account the molar absorption coefficients of both dyes the removal of one APC group, that is, formation of one squaraine molecule, results in the delivery of about 200 safranine molecules.

Figure **4** shows typical spectrophoto- and fluorometric titration curves for safranine release. The increase in intensity of both the absorption and emission of safranine is proportional to the concentration of CH_3Hg^+, which is in agreement with the uncapping described above. The chromogenic indication reaction allows the detection of CH_3Hg^+ down to 0.5 ppm, and the use of standard fluorometric methods reduces the detection limit to less than 2 ppb.

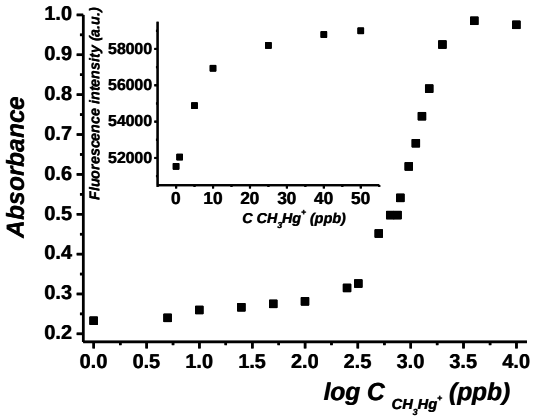

Figure 4. Spectrophotometric titration curves for safranine release monitored at 523 nm in acetonitrile/toluene 4:1 v/v in the presence of increasing amounts of CH_3Hg^+. Inset: Corresponding titration curve obtained from the emission intensities at 560 nm (λ_{exc}=523 nm).

Based on this promising proof-of-principle, we extended our studies to real samples and attempted to achieve discrimination of CH_3Hg^+ from Hg^{2+} by lipophilicity partitioning. Approved analytical protocols rely on the selective extraction of CH_3Hg^+ from fish samples after treatment of the tissue with acid and toluene. To test the sensing ability of **S1**, a certified material of tuna fish ERM-

CE464 with a known content of 5.50±0.1 mg kg^{-1} CH_3Hg^+ was used. The extraction of methylmercury from the sample was carried out following the standard method proposed by the AOAC, namely, a mild acidic digestion of the sample followed by toluene extraction (see the Supporting Information).[28] The final toluene extract (5 mL) was then mixed with 20 mL of acetonitrile containing 10 mg of **S1**. The suspension was removed with a Teflon filter, and the fluorescence of safranine upon excitation at 523 nm was recorded. Following this procedure, the concentration of CH_3Hg^+ in the certified material was determined to be 5.69±0.50 mg kg^{-1} of CH_3Hg^+ (*N*=3 measurements) using a standard addition method, that corroborated well with the certified content. As a control experiment, the same procedure was carried out with samples of ERM-CE464 additionally spiked with 9.0 mg kg^{-1} of Hg^{2+}. Remarkably, a very similar response of **S1** was found in this case when compared with neat ERM-CE464 samples that lack inorganic mercury; that is, **S1** can selectively indicate 5.5 mg kg^{-1} CH_3Hg^+ and discriminate against Hg^{2+}. To assess the potential interference by other species, ERM-CE464 samples were also spiked with 40 mg kg^{-1} of the cations Na^+, K^+, Ca^{2+}, Mg^{2+},Cu^{2+}, Ni^{2+}, Zn^{2+}, Ag^+, Pb^{2+}, Cd^{2+}, Au^{3+}, and Tl^+ (as chloride, nitrate, or perchlorate salts) and with various organic species (sodium lauryl sulphate, cysteine, and histamine at 40 mg kg^{-1} and ethanol, heptylamine, and hexanethiol at 8 mg kg^{-1}); none of these species affected the response of **S1** toward CH_3Hg^+.

In conclusion, we have prepared a new capped mesoporous hybrid material that allows the selective chromo- and fluorogenic determination of methylmercury. The material was designed bearing in mind the affinity of thiophilic CH_3Hg^+ toward the capping APC groups. Signal amplification was implemented into the system by use of safranine O. The use of lipophilicity partitioning guaranteed the required selectivity for CH_3Hg^+, which has not yet been accomplished for other low-cost and time-effective sensory methods, whilst reaching comparable sensitivity in the ppb range.[11–13] This sensitivity is related to the signal amplification features of this method. Although laboratory-based ultra-trace techniques reach lower detection limits in the ppt range,[29] the method proposed herein competes well with current standard techniques[6–9] and with integrated instruments[30] with respect to

detection limits and recovery rates for CH_3Hg^+ determination in fish matrices. The versatility and simplicity of the approach becomes obvious when considering that **S1** can be embedded into a hydrophobic sensing matrix, which can, for example, be dipped into the suspended and digested fish sample, thus extracting and indicating the lipophilic target species. Finally, the system can easily be adopted for ratiometric detection schemes, for example by assessing the fluorescence of safranine upon excitation with 488 or 532 nm and by monitoring the squaraine emission upon 633 or 638 nm excitation, that is, with common laser or LED light sources. We believe that these modular functionalized gated hybrid materials hold great promise for the development of new chromo- and fluorogenic sensing protocols.

References.

1. Toxicological Profile for Mercury, Agency for Toxic Substances and Disease Registry (ATSDR), Atlanta, GA, USA, **1999**.
2. P. B. Tchounwou, W. K. Ayensu in Metal Ions in Biology and Medicine, Vol. 8 (Eds.: M. A. Cser, I. S. Laszlo, J. C. Etienne, Y. Maymard, J. A. Centeno, L. Khassanova, P. Collery, J. Libbey), *Eurotext*, Paris, **2004**, pp. 8.
3. R. Ebinghaus, H. Hintelmann, R. D. Wilken, Fresenius, *J. Anal. Chem.*, **1994**, *350*, 21.
4. K. R. Mahaffey, R. P. Clickner, C. C. Bodurow, *Environ. Health Perspect*., **2004**, *112*, 562.
5. S. Díez, S. Delgado, I. Aguilera, J. Astray, B. Pérez-Gómez, M. Torrent, J. Sunyer, J. M. Bayona, *Arch. Environ. Contam. Toxicol*., **2009**, *56*, 615.
6. J. Marrugo-Negrete, J. O. Verbel, E. L. Ceballos, L. N. Benitez, *Environ. Geochem. Health*, **2008**, *30*, 21.
7. L. Yang, Z. Mester, R. E. Sturgeon, *J. Anal. At. Spectrom*. **2003**, *18*, 431.
8. E. Ramalhosa, S. Río Segade, E. Pereira, C. Vale, A. Duarte, *J. Anal. At. Spectrom*., **2001**, *16*, 643.
9. L. H. Reyes, G. M. M. Rahman, H. M. S. Kingston, *Anal. Chim. Acta*, **2009**, *631*, 121.
10. Oehme, O. S. Wolfbeis, *Mikrochim. Acta*, **1997**, *126*, 177.
11. F. Ribeiro, M. M. M. Neto, M. M. Rocha, I. T. E. Fonseca, *Anal. Chim. Acta*, **2006**, 579, 227.
12. H.-F. Ji, Y. Zhang, V. V. Purushotham, S. Kondu, B. Ramachandran, T. Thundat, D. T. Haynie, *Analyst*, **2005**, *130*, 1577.
13. a) Ivask, K. Hakkila, M. Virta, *Anal. Chem.,* **2001**, *73*, 5168.; b) S. Han, M. Zhu, Z. Yuan, X. Li, *Biosens. Bioelectron.*, **2001**, *16*, 9.

14. a) E. M. Nolan, S. J. Lippard, *J. Am. Chem. Soc.,* **2003**, *125*, 14270; b) S. Yoon, E. W. Miller, Q. He, P. H. Do, C. J. Chang, Angew. Chem. Int. Ed. **2007**, *46*, 6658.
15. a) Y.-K. Yang, K.-J. Yook, J. Tae, *J. Am. Chem. Soc.,* **2005**, *127*, 16760; b) Y. Zhao, Z. Lin, C. He, H. Wu, C. Duan, *Inorg. Chem.*, **2006**, 45, 10013.
16. a) E. Palomares, R. Vilar, J. R. Durrant, *Chem. Commun.,* **2004**, *362*; b) H. Wang, Y. Wang, J. Jin, R. Yang, *Anal. Chem.,* **2008**, *80*, 9021.; c) C. Wang, J. Zhao, Y. Wang, N. Lou, Q. Ma, X. Su, *Sens. Actuators B*, **2009**, *139*, 476.
17. a) A. B. Descalzo, R. Martínez-Máñez, R. Radeglia, K. Rurack, J. Soto, *J. Am. Chem. Soc.,* **2003**, *125*, 3418; b) J. V. Ros-Lis, M. D. Marcos, R. Martínez-Mañez, K. Rurack, J. Soto, *Angew. Chem. Int. Ed.,* **2005**, *44*, 4405.
18. a) H. Wang, W.-H. Chan, *Tetrahedron*, **2007**, *63*, 8825; b) O. del Campo, A. Carbayo, J. V. Cuevas, A. Muñoz, G. García-Herbosa, D. Moreno, E. Ballesteros, S. Basurto, T. Gómez, T. Torroba, *Chem. Commun.,* **2008**, 4576; c) F. Song, S. Watanabe, P. E. Floreancig, K. Koide, *J. Am. Chem. Soc.,* **2008**, 130, 16460; d) M. Santra, D. Ryu, A. Chatterjee, S.-K. Ko, I. Shin, K. H. Ahn, *Chem. Commun.*, **2009**, 2115.
19. a) O. Brümmer, J. J. La Clair, K. D. Janda, *Bioorg. Med. Chem.,* **2001**, *9*, 1067; b) S. Yoon, A. E. Albers, A. P. Wong, C. J. Chang, *J. Am. Chem. Soc.*, **2005,** *127*, 16030.
20. K. Rurack, R. Martínez-Máñez, *in Nanomaterials: Inorganic and Bioinorganic Perspectives* (Eds.: C. M. Lukehart, R. A. Scott), Wiley, **2009**.
21. a) A. B. Descalzo, R. Martínez-Máñez, F. Sancenón, K. Hoffmann, K. Rurack, *Angew. Chem. Int. Ed.,* **2006**, *45*, 5924; b) S. Saha, K. C. F. Leung, T. D. Nguyen, J. F. Stoddart, J. I. Zink, *Adv. Funct. Mater.,* **2007**, *17*, 685; c) K. Ariga, A. Vinu, J. P. Hill, T. Mori, *Coord. Chem. Rev.,* **2007**, *251*, 2562; c) B. G. Trewyn, I. I. Slowing, S. Giri, H. T. Chen, V. S.-Y. Lin, *Acc. Chem. Res.*, **2007**, *40*, 846.
22. a) R. Casasús, E. Aznar, M. D. Marcos, R. Martínez-Máñez, F. Sancenón, J. Soto, P. Amorós, *Angew. Chem. Int. Ed.*, **2006**, *45*, 6661; b) C. Coll, R. Casasús, E. Aznar, M. D. Marcos, R. Martínez-Máñez, F. Sancenón, J. Soto, P. Amorós, *Chem. Commun.*, **2007**, 1957; c) E. Aznar, C. Coll, M. D. Marcos, R. Martínez-Máñez, F. Sancenón, J. Soto, P. Amoros, J. Cano, E. Ruiz, *Chem. Eur. J.,* **2009**, *15*, 6877.
23. Several bioinspired gated hybrid nanomaterials that involve pore-opening processes have been developed for delivery applications; see, for example: a) E. Aznar, M. D. Marcos, R. Martinez-Manez, F. Sancenon, J. Soto, P. Amoros, C. Guillem, *J. Am. Chem. Soc.*, **2009**, *131*, 6833.; b) Y. Zhao, B. G. Trewyn, I. I. Slowing, V. S.-Y. Lin, *J. Am. Chem. Soc.*, **2009**, *131*, 8398. However, issues such as detection limits or sensing selectivities have not been addressed in those cases.
24. F. Hoffmann, M. Cornelius, M. Morell, M. Fröba, *Angew. Chem. Int. Ed.,* **2006**, 45, 3216.
25. J. V. Ros-Lis, B. García, D. Jiménez, R. Martínez-Máñez, F. Sancenón, J. Soto, F. Gonzalvo, M. C. Valldecabres, *J. Am. Chem. Soc.,* **2004**, *126*, 4064.

26. The pore closing is more efficient with less-polar solvents, which is probably due to solvation effects. In less-polar media, the charged safranine dye prefers to reside in the hydrophilic pores containing a large number of neat silanol groups.
27. J. V. Ros-Lis, R. Casasús, M. Comes, C. Coll, M. D. Marcos, R. Martínez-Máñez, F. Sancenón, J. Soto, P. Amorós, J. El Haskouri, N. Garró, K. Rurack, *Chem. Eur. J.*, **2008**, *14*, 8267.
28. AOAC 1992: Official Methods of Analysis: 988.11. Association of Official Analytical Chemists.
29. J. Chen, H. Chen, X. Jin, H. Chen, *Talanta*, **2009**, *77*, 1381.
30. C. Maggi, M. T. Berducci, J. Bianchi, M. Giani, L. Campanella, *Anal. Chim. Acta*, **2009**, *641*, 32.
31. S. Cabrera, J. El Haskouri, C. Guillem, J. Latorre, A. Beltrán, D. Beltrán, M. D. Marcos, P. Amorós, *Solid State Sci.*, **2000**, *2*, 405.

Angew. Chem. Int. Ed., 2009, 8519-8522.

SUPPORTING INFORMATION

A method for the determination of methylmercury in real samples using organically capped mesoporous inorganic materials capable of signal amplification

Estela Climent, María Dolores Marcos, Ramón Martínez-Máñez, Félix Sancenón, Juan Soto, Knut Rurack, and Pedro Amorós

Chemicals

The chemicals tetraethylorthosilicate (TEOS), n-cetyltrimethylammonium bromide (CTAB), sodium hydroxide (NaOH), triethanolamine ($TEAH_3$), 3-mercaptopropyltriethoxysilane (MPTS) and the dye safranine O were purchased from Aldrich. Squaraine 1 was prepared following a literature procedure.[1] Analytical-grade solvents were purchased from Scharlab (Barcelona, Spain). All the products were used as received.

General Techniques

XRD, TG analysis, elemental analysis, EDX microscopy, N_2 adsorption-desorption, UV/vis and fluorescence spectroscopy techniques were employed to characterize the materials. X-ray measurements were performed on a Seifert 3000TT

diffractometer using Cu-K_α radiation. Thermo-gravimetric analyses were carried out on a TGA/SDTA 851e Mettler Toledo equipment, using an oxidant atmosphere (Air, 80 mL min^{-1}) with a heating program consisting of a heating ramp of 10 °C min^{-1} from 393 K to 1273 K and an isothermal heating step at this temperature during 30 minutes. N_2 adsorption-desorption isotherms were recorded on a Micromeritics ASAP2010 automated sorption analyser. The samples were degassed at 120 ºC in vacuum overnight. The specific surface areas were calculated from the adsorption data in the low pressures range using the BET model. Pore sizes were determined following the BJH method. Fluorescence spectra were recorded on a Felix 32 Analysis Version 1.2 (Build 56) PTI (Photon Technology International) and UV/vis spectra on a Lambda 35 UV/Vis Spectrometer from Perkin Elmer Instruments. ^{1}H and ^{13}C nuclear magnetic resonance (NMR) spectra were acquired with a Varian 300 spectrometer (Sunnyvale, CA, USA).

Synthesis of the mesoporous silica support

The synthesis of the MCM-41-type mesoporous support was carried out following the so-called 'atrane route', a simple preparative technique based on the use of complexes that include triethanolamine ($TEAH_3$) related ligands (i.e. in general 'atranes' and silatranes for the silicon-containing complexes), tetraethylorthosilicate (TEOS) as hydrolytic inorganic precursors and surfactants as porogen species. The molar ratio of the reagents in the mother liquor was fixed to 7 $TEAH_3$: 2 TEOS: 0.52 CTAB: 0.5 NaOH: 180 H_2O. In a typical synthesis leading to the MCM-41 pure silica, CTAB (4.67 g) was added at 118 ºC to a solution of $TEAH_3$ (25.76 g) containing 0.012 mol of NaOH and 0.049 mol of a silatrane derivative (e.g., 11 mL of TEOS were added at 70 ºC to TEA, e.g., in the form of $Si(TEA)(TEAH_2)$, where TEA is the fully deprotonated ligand). Then, 80 mL of deionized water were added under vigorous stirring at 70 ºC. After a few minutes, a white suspension resulted. This mixture was aged at room temperature overnight. The resulting powder was collected by filtration and washed with water. Finally, the solid was dried at 70 ºC (MCM-41 as-synthesized). To prepare

the final porous material (MCM-41), the as-synthesized solid was calcinated at 550 ºC for 5h in order to remove the template.

Synthesis of S1

MCM-41 (1.00 g) and the dye safranine O (0.28 g, 0.8 mmol) were suspended in acetonitrile (50 mL) inside a round-bottomed flask connected to a Dean–Stark (trap) apparatus in an inert atmosphere. The suspension was refluxed (110 ºC) in azeotropic distillation collecting 10 mL in the Dean-Stark in order to remove the adsorbed water. Subsequently, the suspension was stirred for 24 hours at room temperature with the aim to achieve maximum loading of the pores of the MCM-41 scaffolding. Afterwards, 5 mmol of 3-mercaptopropyltriethoxysilane (**MPTS**) were added and the final mixture was stirred for 5.5 h at room temperature. This sequence guarantees that **MPTS** diffusion into the pores is hampered and functionalization occurs primarily at the outer surface. After filtration, the solid was suspended in 120 mL of a mixture of 5:1 v/v CHES-acetonitrile pH 9.6 and the squaraine **I** (6 mL, 1.5 mM in acetonitrile) was added to the suspension, continuing to stir the mixture for 5 minutes. Finally, the solid (**S1**) was filtered off, washed with acetonitrile (100 mL) and dried. Elemental analysis, found: C, 9.58; H, 1.70; N, 2.04; S, 0.14%.

Extraction of methyl mercury from the biological sample

The extraction of methyl mercury from the fish sample was carried out with a standard method proposed by the Association of Official Analytical Chemists (AOAC).[2] Sample preparation was performed by acidic digestion and extraction with toluene. The samples were doped with different amounts of methylmercury in order to obtain a calibration curve by standard addition. A total of 400-500 mg of homogenized sample weighed on an analytic balance was placed in a 10 mL centrifugation tube, 5 mL of acetone were added and the solution was stirred vigorously for 30 seconds. After centrifugation (3500 rev min^{-1}, 5 min), 4 mL acetone were carefully pipetted and discarded. The same procedure was repeated 3 times, twice with the addition of 4 mL acetone and once with 4 mL toluene. The

final extract was then suspended in 0.7 mL of hydrochloric acid (1:1 v/v) and vigorously stirred in order to guarantee a complete digestion of the sample and a maximum yield of methylmercury. Then, 3 mL of toluene were carefully added and the crude mixed for 1 minute to extract the methylmercury from the aqueous phase to the toluene. After centrifugation (3500 rev min^{-1}, 5 min), 3 mL of the toluene phase were carefully pipetted and were transferred to a vial containing anhydrous sodium sulfate (extraction part 1). 3 mL toluene were added subsequently to the test tube containing the extract and the aqueous phase, and the extraction was repeated once more. The toluene phase (extraction part 2) was added to the vial containing the first extract. The combined extracts were left for 1 hour in a freezer at 4 °C and were then used for the methylmercury determination.

5 mL of toluene extracts containing the target cation were mixed with 20 mL of acetonitrile in the presence of 10 mg of solid **S1** in order to prepare a calibration curve. The suspensions were filtered off with a teflon filter and the emission intensity of safranine (λ_{exc} = 523 nm) at 560 nm was measured in the solution. These fluorescence intensities at 560 nm plotted vs. methylmercury concentration yielded the calibration curve depicted in Figure **SI-1**. The content of CH_3Hg^+ in the reference extract was calculated through the difference between the y-intercept of the calibration curve and the residual emission of a blank solution (without the certified material) divided by the slope of the calibration curve.

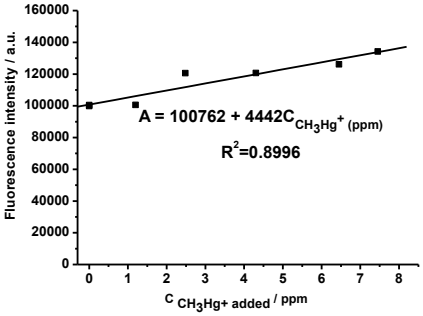

Figure SI-1: Emission intensity of the band of safranine O measured at 560 nm in mixtures of acetonitrile/toluene 4:1 v/v in the presence of increasing amounts of CH_3Hg^+.

Materials Characterization

Solid **S1** was characterized using standard procedures. The thermal analysis of the **S1** solid shows the typical behaviour of functionalised mesoporous materials; i.e. a first weight loss between 25 and 150 ºC related to the solvent evolution, a second step, between 150 and 800 ºC due to the combustion of the organics and a final loss in the 800-1000 ºC range related to the condensation of the silanol groups.

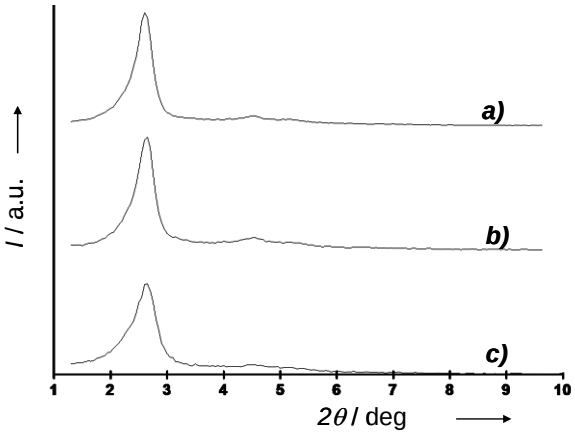

Figure SI-2: X-ray pattern of (a) MCM-41 as synthesized, (b) calcinated MCM-41 and (c) **S1** hybrid material.

Figure **SI-2** shows powder X-ray diffraction patterns of the MCM-41 support and the **S1** functionalised material. The PXRD of siliceous MCM-41 as-synthesized (curve a) shows four low-angle reflections typical of a hexagonal array that can be indexed as (100), (110), (200), and (210) Bragg peaks. A significant displacement of the (100) peak in the XRD powder of the MCM-41 calcinated sample is clearly appreciated in curve b, corresponding to an approximate cell contraction of 5 Å. This displacement and the broadening of the (110) and (200) peaks are related to further condensation of silanol groups during the calcination step. Finally, curve c corresponds to the **S1** XRD pattern. In this case, the loss of the (110) and (200)

reflections is observed, most likely related to a loss of contrast due to the filling of the pore voids with safranine O. Nevertheless, the value and intensity of the (100) peak in this pattern strongly evidences that the loading process with the dye and the further functionalization with the APC derivative have not damaged the mesoporous 3D MCM-41 scaffolding. The presence of the mesoporous structure in the MCM-41 calcinated sample and in the final functionalized solid is also observed from the TEM analysis, in which the typical hexagonal porosity of the MCM-41 matrix can be seen. TEM image of MCM-41 calcinated sample (*a*) and solid **S1** (*b*) displaying the typical hexagonal porosity of the MCM-41 matrix can be observed in Figure **SI-3**.

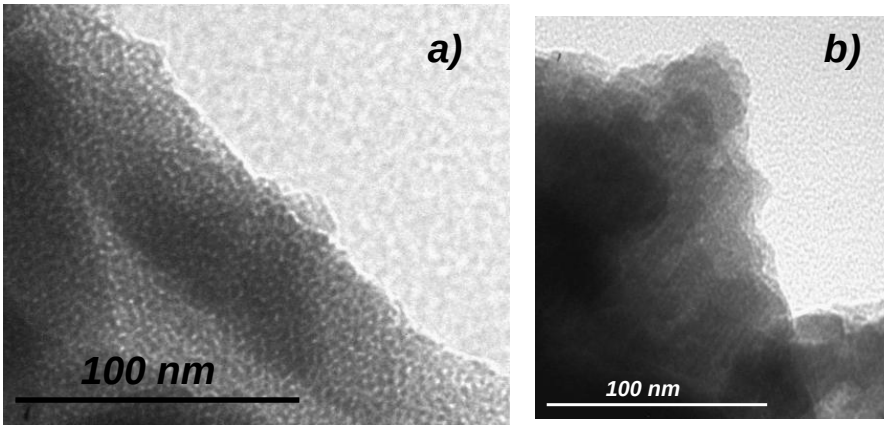

Figure SI-3: TEM images of the MCM-41 mesoporous material showing the typical disordered hexagonal porosity of the MCM-41 matrix (a) and **S1** hybrid material (b).

The N_2 adsorption-desorption isotherms of the MCM-41 calcinated material shows a typical curve for these mesoporous solids; i.e., an adsorption step at an intermediate P/P_0 value 0.3 (see Figure **SI-3** and **SI-4**). This curve corresponds to a type IV isotherm, in which the observed step can be related to the nitrogen condensation inside the mesopores by capillary forces. The absence of a hysteresis loop in this interval and the narrow pore distribution suggest the existence of uniform cylindrical mesopores (0.96 $cm^3 \cdot g^{-1}$). The application of the BET model resulted in a value for the total specific surface area of 1249 $m^2\ g^{-1}$. From the XRD, porosimetry and TEM studies, the a_0 *cell parameter* (39.09 Å), the

pore diameter (2.50 nm) and a value for the *wall thickness* of 14.09 Å can be calculated. The N_2 adsorption-desorption isotherms of **S1** (see Figure **SI-4**) is typical of mesoporous systems with filled mesopores and a significant decrease in the N_2 volume adsorbed is observed (see Table **SI-1**). Solid **S1** presents flat curves, when compared (at the same scale), to those of the MCM-41 parent material, indicating a significant pore blocking, resulting in the absence of appreciable porosity. Similar results have been observed by us in related systems. Moreover, the lack of porosity together with the typical mesoporous-like X-ray powder diffraction profile (showing a characteristic intense peak at low angle values) and the TEM images for **S1** provides direct evidence of the high efficiency of the dye loading.

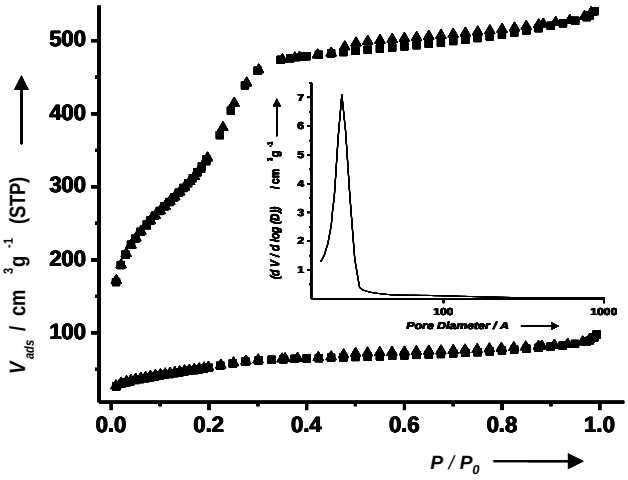

Figure SI-4: Nitrogen adsorption-desorption isotherms for (top) the MCM-41 mesoporous material and (bottom) the dye-loaded and functionalized **S1** material. V_{ADS} is the volume adsorbed ($cm^3\ g^{-1}$). Inset: Pore size distribution for MCM-41 material.

The content of squaraine derivative and dye in **S1** was determined by elemental analysis and thermogravimetric studies. A content of 0.032 and 0.47 mmol g^{-1} SiO_2 of thio-derivatives and safranine were found, respectively. According to a typical range of 50-100 $m^2\ g^{-1}$ for the external surface of MCM-41 solids, and the

content of thio-derivatives (in mmol g^{-1} SiO_2) calculated from the elemental analysis and thermogravimetric measurements, a value of the coverage surface of 0.2-0.4 APC molecules nm^{-2} can be estimated.

Table SI-1. BET specific surface values, pore volumes and pore sizes calculated from the N_2 adsorption-desorption isotherms[a] for selected materials.

	S_{BET} (m^2 g^{-1})	Pore Volume [a] (cm^3 g^{-1})	Pore size [a] (nm)
MCM-41	1249	0.96	2.50
S1	194	0.17	2.30

[a] Volume (V) and diameter (D) of mesopore.

References

[1] J. V. Ros-Lis, R. Martínez-Máñez, F. Sancenón, J. Soto, M. Spieles, K. Rurack, *Chem. Eur. J.*, **2008**, *14*, 10101.

[2] AOAC (1992): Official Methods of Analysis: 988.11. Association of Official Analytical Chemists.

3. Controlled delivery systems using antibody-capped mesoporous nanocontainers

3.1 **Introduction**

In the recent years, scientists have focused their attention in the preparation of functional hybrid materials that mimic objects that perform active tasks in living organisms. Bearing in mind interactions present in nature, an the use of very simple molecules to carry out these interactions, such as amino acids, sugars, nucleobases and certain inorganic materials, scientists have started to develop complex nanometric functional materials that work in a similar fashion than these complex structures in living organisms. Due to this, development of novel biostimuli-responsive hybrid organic-inorganic materials to trigger the release of certain molecules under physiological conditions have became an important field.

As we have explained in the general introduction, some biomolecules, such as enzymes, glucose, or glutathione have been used as stimuli to uncap mesoporous silica materials. Bearing in mind these ideas, our proposal in this chapter was to develop hybrid organic-inorganic mesoporous materials that were triggered using antigen-antibody interactions.

3.1.1 Antigens and antibodies: key molecules in immunoassays.

3.1.1.1 *Antigens.*

The word *antigen* was coined from two words: *antibody* and *generator*. Due to this, an antigen can be defined as "any foreign substance that produces an immune response when it is introduced into the body of a susceptible animal". These species are also called as immunogens, due to its capacity of produce an immune respone. Generally this immune response is involved with the production of antibodies, but sometimes these immune responses are cell mediated, and antibodies are not produced.

Two characteristics in an antigen must be differencied: on the one hand, the immunogenicity of the molecule, that can be defined as the capacity of the molecule to generate an immune response in an organism, and, on the other hand, the antigenicity and specificity of the antigen, wich are related with the recognition of this molecule by certain antibody.

The small site on an antigen to which a complementary antibody may specifically bind is called an *epitope*, and this is usually formed by monosaccharides (from 1 to 6) or amino acid residues that are disposed in the surface of the antigen. Generally antigens are macromolecules of high molecular weight and commonly are proteins or polysaccharides. In addition, polypeptides, lipids, nucleic acids and many other materials can also function as antigens. Antigens are able to produced an immune response when, for instance, they are injected directly to animals. However, smaller molecules (with a molecular weight less than ca. 5000 Da) are poorly immunogenic, and, as consequence, when is required the production of antibodies against these small molecules, these are chemically coupled to a larger carrier protein, such as bovine serum albumin, keyhole limpet hemocyanin (KLH) or other synthetic matrices, in order to be injected and generate more reproducible immune response. These smaller molecules unable to produce an immune response alone, are commonly named as *haptens.* Due to this, immunogens containing smaller molecules are formed by conjugates of hapten-

protein. A variety of molecules such as drugs, simple sugars, amino acids, small peptides, phospholipids, or triglycerides may function as haptens.

All immunochemical methods are based on a highly specific and sensitive reaction between an antigen and an antibody. Due to this, in order to detect small molecules using these methods, is necessary the generation of antibodies for their specific recognition. Thus, in order to generate antibodies for the recognition of small molecules, it is necesary to perform the following steps:

- ✓ Design of small molecules (haptens) with similar chemical structure from analyte containing an appropriate functional group for their coupling with a carrier protein.
- ✓ Synthesis of these small molecules (called haptens).
- ✓ Covalent conjugation of the haptens prepared to the carrier protein in order to prepare the immunogen.
- ✓ Purification of the immunogen, in order to be introduced onto the animal's body.

3.1.1.2 *Design of haptens*

The key step in the development of an immunoassay for small molecules is the hapten design.[1] Thus, in order to obtain a good immune response to small molecules, it is necessary that the haptens designed presented similar features to the target that we want to detect, such as structure, geometry, electronic distribution or their hability to form hydrogen bonds.

In order to facilitate the exposure of the hapten to the immune system, haptens designed must contain a spacer arm, and must be positioned as far away as possible from the recognition site of the hapten. Normally spacer arms contains in their structure a carbon chain, and along it, useful functional groups (such as -

[1] a) M.P. Marco, B.D. Hammock, M.J. Kurth, *J. Org. Chem*, **1993**, 58, 7548. b) Y. H. Liu, M. J. Jin, W. J. Gui, J. L. Cheng, Y. R. Guo, G. N. Zhu, *Anal. Chim. Acta,* **2007***, 591,* 173.

COOH,-OH,-NH_2 or -SH) for covalent attachment to the protein carrier. Normally, the length of the spacer arm is an important factor in the production of antibodies with high affinity for the analyte, and, generally, the sensitivity of the immunoassay can increase by an enhancement of the length of the spacer.[2]

3.1.1.3 *Antibodies obtention: Immunization of animals.*

In order to obtain polyclonal or monoclonal antibodies, an immunization of certain animal is required. The most used animals are mouses, rabbits, goats or chickens. The immunization procedure consists of the injection in an animal of a solution containing the immunogen prepared (hapten covalently bonded to a carrier protein) and an adjuvant (an agent that potents the immune response) repeatedly in suitable doses, in order to achieve a good inmune response. The adjuvant normally accelerates and enhances the antigen-specific immune response.[3]

There are many immunization protocols, with a variable duration. Normally the primary immunization phase usually takes from 1 to 3 months with injections every 15 days, but the entire process normally is produced during 3-6 months. The injection containing the immunogen and the adjuvant is able to produce an immune response. As a consequence, a lot of clones of B cells produced a mixture of antibodies that responds to the immunogen contained in the serum from an immunized animal, named as polyclonal antiserum. Thus, a polyclonal antiserum contains a heterogeneous mixture of antibodies of different classes in arbitrary proportions and with different affinities and selectivities to the analyte for which it has been obtained. Their production is simple and doesn't require a sophisticated equipment or special products, because it is based in the different response of the animals.

[2] a) M. P. Marco, S. Gee, B. D. Hammock, T*rends Anal. Chem.***1995***, 14*, 415. b) F. Szurdoki, H. K. M. Bekheit, M. P. Marco, M. H. Goodrow, B. D. Hammock, *New Frontiers in Agricultural Immunoassays*. D.A. Kurtz, J.H. Skerritt, L. Stanker (Eds.). AOAC, Arlington, VA, 1995, 39.

[3] S. Sasaki, K. Okuda, *Methods in Molecular Medicine*, **2000**, *29*, 241.

On the other hand, it is also possible to obtain monoclonal antibodies, but their obtention is more sophisticated. These antibodies are produced in vitro, employing a single cell clone of B lymphocytes that has been isolated and maintained in culture in the laboratory. These cells are identicals, and, due to this, an homogeneous mixture of immunoglobulins is generated. Their obtention was first described by Georges Kohler and Cesar Milstein, for which they received the Nobel Prize in 1984. The main propierties for monoclonal and polyclonal antibodies are summarized in Table 3.1:

Table 3.1. Main propierties of monoclonal and polyclonal antibodies.

Polyclonal	***Monoclonal***
Heterogeneous mixture of IGs	Homogeneous mixture of IGs
Limited obtention	Non limited obtention
Diferent properties	Same properties
Simple production	Sophisticated production
Obtention in 3 months	Obtention in 6 months

3.1.1.4 *Structure of antibodies.*

Antibodies (also known as an immunoglobulines (Ig)) are gamma globulin proteins that are found mainly in blood. These proteins are synthesized by specialized cells, called plasma cells (which are formed by lymphocytes) when an antigen, a substance foreign to the organism's body, comes in contact with lymphocytes. Their function is to identify and neutralize foreign objects such as bacteria and viruses.

Structurally, the immunoglobulins are formed by multiple polypeptide chains. Their molecular mass is between 150-900 kDa, with a content of carbohydrates between 2 to 15%, and an isoelectric point (pI) between 4.4 and 9.5. These proteins are found, in its soluble form, in blood serum, but are also present in other body fluids, tissues and cells, such as tears, saliva, intestine, milk, eggs, etc.

The antibodies are often visualized as Y-shaped molecules, each containing 4 polypeptides: 2 identical polypeptide units called heavy chains (H) and another 2 called light chains (L), containing each H and L chain an amino-terminal variable (V) region and a carboxyl-terminal constant (C) region. Thus, immunoglobulins are heterogeneous with respect to charge, size, antigenicity, and function, and can be classified into different isotypes or classes, according to the structure of the H and L chains. In human, there are five human H-chain classes: IgM, IgG, IgA, IgD, and IgE. On the other hand, there are two L-chain isotypes named κ and λ. In order to describe an inmoglobulin, an identification of both H and L chains is required.[4] This different isotypes confire an appropriate immune response for each different foreign object: Thus, IgM is the first immunoglobulin that is produced during the primary immune response, whereas IgG, the most abundant immunoglobulin class in the serum (around 80%), are associated with the fixation to macrophages and membrane transport. The content of IgG species onto serum differs depending on some factors. In rabbits, a content of IgG between 1 and 10 mg /mL serum is normally found.[5] IgD and IgE immunoglobulines (active against parasites, acting as a mediator of immediate hypersensitivity) are present in a minimum amounts in normal human serum, whereas no function has been clearly attributed to IgD.[6] Due to the fact that IgG is the most abundant Ig class in the serum and constitutes most of the secondary response to antigens, most immunoassays employs this class of antibodies. IgG contains 3 protein domains, 2 identical fragments, called as Fab fragments and a third domain, called Fc fragment, wich is important in immune system function and regulation.

As we can see, general structure of all antibodies is very similar. However, there is a small region on the protein that is extremely variable, allowing the production of millions of antibodies with slightly different tip structures or antigen binding sites. This region is known as the *hypervariable region*, and is contained onto Fab

[4] C. Janeway, *Immunobiology,* 5th ed. Garland Publishing, **2001**.

[5] R. W. Burry, *Immunocythochemistry*, Ed. Springer**, 2010**.

[6] M. H. Rosner, J. A. Grassman, R. A. Haast, *Environmental Health Perspectives*, **1991**, 94, 131.

fragments. This region allows to antibodies to bind with different targets, named as antigens, using specific binding pockets or regions called paratope. This region (forming a structure analogous to a lock) is specific for one particular epitope (similarly analogous to a key) of an antigen, allowing these two structures to bind together with precision. Figure 3.1 showed a representative scheme of the different parts of an antibody:

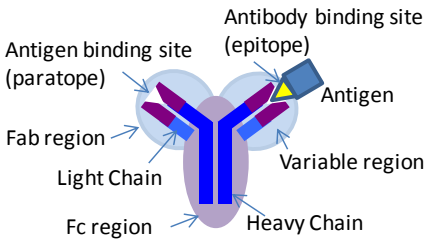

Figure 3.1.- Representative scheme showing the different parts of an antibody

3.1.1.5 *Antigen-antibody binding*

The binding of an antibody with an antigen is produced by non-covalent interactions and, due to this, complex formed is in equilibrium with the free components. The binding pocket of an antibody (paratope region) can accommodate from 6 to 10 amino acids. Due to its specificity, small changes in the antigen structure (such as a single amino acid) can affect the strength of the antibody-antigen interaction. The measure of the strength of the binding is called *affinity*, and it is usually expressed in terms of the concentration of an antibody-antigen complex measured at equilibrium. Typically the ranges found differ from micro to picomolar.[7] High-affinity antibodies shows more stable antibody-antigen complexes, and normally are formed in a shorter period of time. Due to this, high-affinity antibodies are usually preferred in immunochemical techniques.[8]

[7] M. E. Koivunen, R. L. Krogsrud, *Labmedicine*, **2006**, *37*, 490.
[8] M. E. Devey, M. W. Steward, *ELISA and other solid phase immunoassays. Theoretical and practical aspects.* Chichester, UK, John Wiley & Sons, **1988**, 135.

Using the binding explained mechanism, antibodies can discriminate the corresponding antigens from other species, and, with this, can neutralize its target directly (for example, by blocking a part of a microbe that is essential for its invasion and survival).

3.1.2 Immunochemical methods.

In an attempt to develop new detection formats to measure important small molecular weight compounds, scientists have developed analytical methods employing immunological reactions. With this, different immunochemical techniques have been reported, wich offers simple, rapid, robust, sensitive and easily automated methods for routine analysis in clinical laboratories. Thus, employing these techniques is possible to dectect and quantify different compounds at low concentrations in blood, urine, tissues, etc.[9] Most of these immunochemical methods are based on a simple photo-, fluoro-, or luminometric detection, offering fast detection of specific diseases, disease biomarkers, hormones, and pharmaceuticals.[10]

The essential components of antibody-based immunoassay systems are the follow: an antigen that we would like to detect and perhaps quantify; a specific antibody to this antigen; and a system to measure the amount of antigen in a given sample. However, not all assays are antibody-based. Some assays utilize simple enzymatic reactions to detect small molecules or perhaps measure the activity of an enzyme sample. The most common immunoassay systems is the Enzyme Linked Immunosorbent Assays (ELISAs), wich is detailed bellow.

3.1.2.1 *Enzyme Linked Immunosorbent Assay*

In 1971, Peter Perlmann and Eva Engvall at Stockholm University in Sweden, and Anton Schuurs and Bauke van Weemen in the Netherlands independently

[9] a) J. Sherry, *Chemosphere,* **1997**, 34, 1011. b) B. R. Glick, J.J. Pasternak, *Molecular biotechnology, e*d. Am. Soc. for Microbiol., Washington D.C. **1998**.

[10] P. Marco, S. Gee, B. D. Hammock, *Trens in Anal. Chem.*, **1995,** 14, 341.

published papers that presented the fundamental bases of methods to perform ELISA (*Enzyme Linked Immunosorbent Assay*).[11] Nowadays, between all of immunochemical methods reported, ELISA assays represent approximately 90% of all of works.[12] This method is one of the assays most often used in clinical immunochemistry involving either quantitative or qualitative formats, showing detections in solution or in the form of lateral-flow devices like dip-sticks.

The protocol of the ELISA assays for the detection (and quantification) of the presence of the antigen can be performed with a number of modifications to the basic procedure: Antigens from the sample are immobilized on a solid support (usually a polystyrene microtiter plate) in a non-specifically way (via adsorption to the surface) or in a specifically way (via capture by another antibody specific to the same antigen, in a "sandwich" ELISA). After the antigen is immobilized, then a specific antibody is applied over the surface so that it can bind to the antigen, forming a complex. Detection process is produced by the addition of an enzyme that is covalently linked to the antibody (direct format), or can itself be detected by a secondary antibody that is linked to the enzyme (indirect format) through bioconjugation. In the final step, a substance containing the enzyme's substrate is added, and the reaction between the enzyme and the substrate produces a detectable signal, most commonly a color change in the substrate. This visible signal indicates the quantity of antigen in the sample

The most powerful ELISA assay format is the sandwich assay, because it is sensitive and robust. This type of capture assay is called a “sandwich” assay due to the fact that the analyte to be measured is bound between two primary antibodies. For these reason, the analyte must be poseess at least two specific union sites for the corresponding antibodies, and, for these reason, this assay format is employed to detect analites with high molecular weights, such hormones. In addition, this called “sandwich” assay can be direct or indirect:

[11] a) E. Engvall, P. Perlman, *Immunochemistry,* **1971***, 8,* 871, b) B. K. Van Weemen, A. H. Schuurs, *FEBS Letters,* **1971***, 15***,** 232.

[12] J. A. Gabaldón, A. Maquieira, R. Puchades, *Crit. Rev. Food Sci. Nutr,* **1999***, 39*, 519.

when the specific antibody is conjugated to an enzyme, then the assay is called a *direct* sandwich ELISA, whereas the *indirect* sandwich ELISA needs addition of a secondary antibody-labeled with an enzyme in order to produce the signal. Figure 3.2 showed a representation of the common ELISA formats.

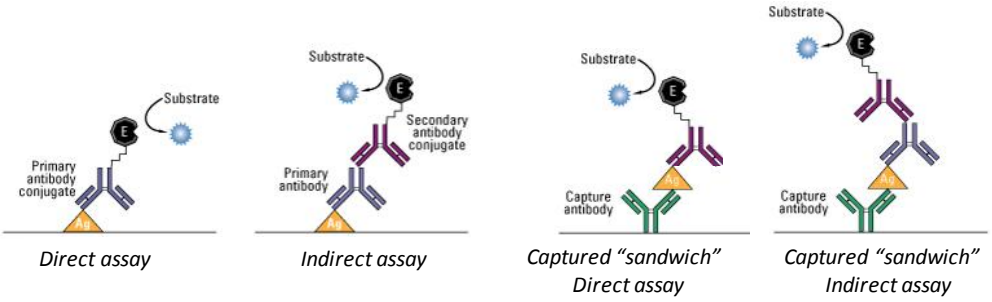

Figure 3.2.- A representation of the common ELISA formats.

When two "matched pair" antibodies are not available for the target, another option is the competitive ELISA, which can use non-purified primary antibodies. It is the most common used assay when only one antibody is available to the antigen of interest or when the target is small, (for example an hapten, wich cannot be bound by two different antibodies). In the *direct* format, the plate is coated with an antibody specific for the analyte. Next, free analyte and enzyme-ligand conjugate are incubated on the coated plate, producing a competition between the free analyte and the ligand-enzyme conjugate for the antibody coated onto the microplate. After washing, the quantity of the enzyme-ligand conjugate bound to the plate is detected after incubation with an appropriate substrate, obtaining an inverse relationship between the signal and the concentration of the analyte in the sample.Thus, the presence of higer amounts of analyte will produce a lower signal.

On the other hand, the competitive assay can be performed in an indirect format: In this case is anchored onto surface a known amount of the analyte, or a derivative analyte, such as an hapten. After washing, addition to the sample of certain amount of analyte and antibody labeled to an enzyme marker will produced a competition between the attached and free antigen for the antibody,

obtaining the same signal behavior as explained before: samples with high antigen concentration will generate a lower signal than those containing low antigen concentration, yielding the inverse correlation between antigen concentration in the sample and color development in the assay. This relationship can then be used to extrapolate antigen concentration in an unknown sample from a standard curve, and with this, it is possible to detect small molecular weight antigens, such as steroids, drugs, lipids or peptides. An schematic representation of the two forms of competitive assay are showed in Figure 3.3.

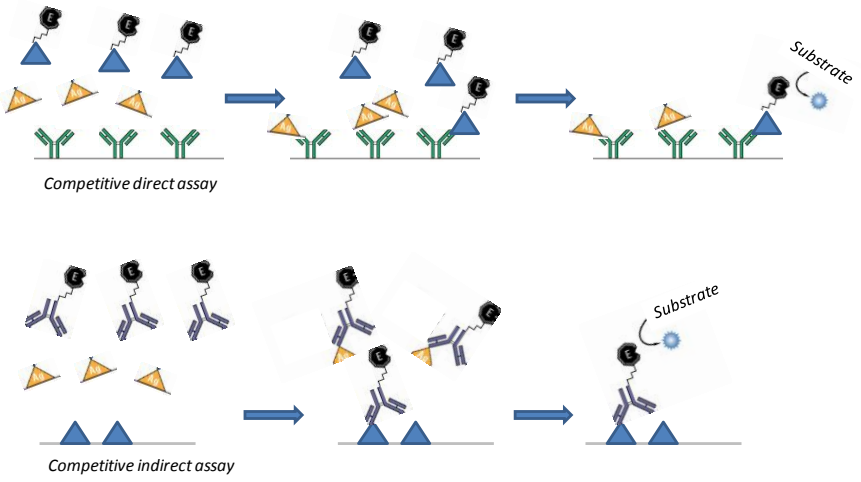

Figure 3.3.- Schematic representation of the direct and indirect competitive ELISA assays.

3.2 **Objectives.**

As we have menctioned before, our proposal in this chapter was to develop hybrid organic-inorganic mesoporous materials that were triggered using antigen-antibody immunological process. In order to carry out this proposal, we used different specific antibody for the corresponding molecules. For this reason, we selected analytes and different antiserums obtained by other research groups through rabbit immunization. Selected analites were sulfathiazole (an antibiotic of the sulfonamides family), finasteride (a 5α-reductase inhibitor) and TATP (an explosive of the family of peroxides).

Specifically, our aim was:

- ✓ Design of new organic-inorganic hybrid materials, which were able to release the cargo entrapped on their pores as a consequence of the immunochemical interaction between an antibody and their corresponding antigen.

- ✓ Synthesis of the new organic-inorganic hybrid materials, employing MCM-41 as inorganic scaffold loaded with a dye and functionalised onto their surface with an appropiate hapten via grafting procedure in order to interact with their corresponding antibody.

- ✓ Characterization of the hybrid materials by using usual techniques in solid state chemistry.

- ✓ Evaluate the release of the dye of the prepared solids in presence of the corresponding antigen, and study the effect of the concentration of trigger.

- ✓ Evaluate the selectivity and sensitivity of each material prepared for each antigen.

The following sections discuss in detail the synthesis of different hybrid materials that are prepared in order to detect different antigens bearing in mind the immunogenical interaction between an antibody and an antigen. Characterization of these materials and studies of the release of the dye in presence of their corresponding analyte are described.

Controlled Delivery Systems Using Antibody-Capped Mesoporous Nanocontainers

Estela Climent,[a,b,c] Andrea Bernardos,[a,b,c] Ramón Martínez-Máñez,[a,b,c] Angel Maquieira,[a,b] María Dolores Marcos,[a,b,c] Núria Pastor-Navarro,[a,b] Félix Sancenón,[a,b,c] Juan Soto,[a,b,c] and Pedro Amorós.[d]

[a] Instituto de Reconocimiento Molecular y Desarrollo Tecnológico. Centro Mixto Universidad Politécnica de Valencia – Universidad de Valencia.

[b] Departamento de Química, Universidad Politécnica de Valencia Camino de Vera s/n, 46022, Valencia, Spain.

[c] Centro de Investigación Biomédica en Red de Bioingeniería, Biomateriales y Nanomedicina (CIBER-BBN)

[d] Institut de Ciència del Materials (ICMUV), Universitat de València. P.O. Box 2085, E-46071 València, Spain

Received: June 3, 2009
Published online: September 9, 2009

Journal of the American Chemical Society,
***2009**, 131, 14075 – 14080*

Abstract

This paper describes the design of new controlled delivery systems consisting of a mesoporous support functionalized on the pore outlets with a certain hapten able to interact with an antibody that acts as a nanoscopic cap. The opening protocol and delivery of the entrapped guest is related by a displacement reaction involving the presence in the solution of the antigen to which the antibody is selective. As a proof-of-the-concept, the solid MCM-41 was selected as support and was loaded with the dye $[Ru(bipy)_3]Cl_2$. Then a suitable derivative of the hapten 4-(4-aminobenzenesulfonylamino)benzoic acid was anchored on the outer surface of the mesoporous support (solid **S1**). Finally the pores were capped with a polyclonal antibody for sulfathiazole (solid **S1-AB**). Delivery of the dye in the presence of a family of sulfonamides was studied in phosphate-buffered saline (PBS; pH 7.5). A selective uncapping of the pores and dye delivery was observed for sulfathiazole. This delivery behavior was compared with that shown by other solids that were prepared as models to assess the effect of the hapten and its interaction with antibody in the dye delivery control in the presence of the antigen.

Introduction

Among the large amount of approximations toward the development of new smart materials, one particularly tempting is the possibility to create stimuli-responsive nanosolids able to react to environmental changes or showing switchable behaviors.[1,2] One appealing application of such systems is the design of functionalized nanocontainers able to deal with cargo delivery under controlled conditions via external triggers.[3] Traditional delivery systems usually rely on simple diffusion-controlled processes or degradation of the nanocarrier,[4] using for instance microcapsules,[5] micelles,[6] vesicles,[7] or liposomes.[8] As an alternative to these materials, silica mesoporous supports (SMP) show unique properties such as large load capacity, biocompatibility, high thermal stability, homogeneous porosity, inertness, and tunable pore sizes with a diameter of ca. 2−10 nm.[9] Moreover, it has been recently demonstrated that it is possible to incorporate in the external surface of SMP functional groups able to be opened or closed at will

for functional control release applications. Specifically, it has been reported that it is possible to design systems able to achieve zero release, which can be fully opened on command via external physical or chemical stimuli. Recently, SMPS-based systems displaying controlled release have been reported that contain different caps such as nanoparticles, nanovalves, and supramolecular frameworks that in most cases use changes in pH,[10] temperature,[11] redox potential,[12,13] light[14] or rely in the presence of small molecules[15] for uncapping the pores.

Despite these examples, the use of SMPS equipped with gatelike scaffoldings for the preparation of real delivery systems is still in its infancy. Thus, in relation to gated systems, some examples still show disadvantages for their potential use in advanced applications such as lack of operational features in aqueous environments, use of difficult-to-apply or complex stimuli, etc. In particular, regardless of very recent reported gated SMPS that can be uncapped by enzymes[16] or can be controlled by certain carbohydrates,[17] there is an almost complete lack of SMPS-based devices designed to trigger cargo release involving biomolecules. In order to advance in this field and as a proof-of-the-concept, we were interested in demonstrating that antibody−antigen interaction could be a powerful switchable method to develop tailor-made SMPS for controlled delivery functions. In particular, and as a part of our interest in the use of inorganic supports for advanced applications,[18] we report here the design of a new controlled delivery system consisting of a mesoporous support functionalized on the pore outlets with a certain hapten able to be recognized by an antibody that acts as a nanoscopic cap. The opening protocol and delivery of the entrapped guest is related to a highly effective displacement reaction involving the presence in the solution of the antigen to which the antibody is selective.

Results and Discussion

Design and Synthesis of the Gated Material

As stated above, the incorporation of gatelike ensembles on mesoporous scaffolds has proved to be a suitable approach for the development of nanoscopic solids for mass transport control and for studying the factors that could influence the design

of gating functions. Apart from molecular and supramolecular models used for the design of gated supports, we were particularly interested in designing systems where delivery could be governed by biomolecules. Thus, our attention was focused on the specific interaction between antibodies and antigens.[19]

The proposed paradigm is depicted in Scheme **1**. In this approach, the external surface of a suitable SMPS is first functionalized with a hapten (solid **S1**) and then the mesopores are capped with a certain antibody that shows good affinity and selectivity toward the anchored hapten via suitable interaction through the two binding IgG regions of the former (solid **S1-AB**). It was expected that the typical size of antibodies (ca. 5.5 nm)[20] would be enough to cap the mesopores in the SMPS. As illustrated in Scheme **1**, the presence in the solution of the corresponding antigen (complementary to the antibody) would induce the uncapping of the pores and release of the entrapped guest. In order to study the functional open/close protocol of the gated ensemble, the dye $[Ru(bipy)_3]^{2+}$ was loaded on the inner mesopores of the MCM-41 solid. Thus, the state of the gatelike system is easily monitored via the emission band of the $[Ru(bipy)_3]^{2+}$ dye at λ = 610 nm (λ_{ex} = 453 nm) in the aqueous phase. Following this procedure, the solid for delivery studies was prepared with MCM-41 solid as the SMPS and sulfathiazole (STZ) as the antigen. Polyclonal sera for STZ were obtained for this target by immunization of female New Zealand rabbits with bovine serum albumin (BSA)−protein conjugates containing the hapten **1**. The same hapten **1** was made to react with 3-aminopropyltrimethoxysilane to furnish **2,** which was anchored on the SMPS surface in order to prepare **S1** (see Supporting Information for details).[21]

Solid **S1** should ideally contain the hapten **1** anchored on the external surface, whereas the dye must be contained in the mesopore channels. Given that in mesoporous systems the inner surface is much larger than the external, the preparation of the solid should be carried out in a programmed fashion. To prepare the organized hybrid material **S1** we made use of a two-step synthetic procedure that has been used recently by other authors and by us to develop responsive gating structures containing a certain cargo in the pores and suitable

switchable ensembles on the pore outlets.[15, 16c] Thus, in a first step, the mesoporous starting scaffold was added to a solution containing a relatively high concentration of $[Ru(bipy)_3]^{2+}$ dye in order to achieve efficient loading of the pores. Then in the same mixture the hapten derivative **2** was added. This is expected to result in final solids where **2** is basically placed on the external surface of the mesoporous silica-based scaffolding because the anchoring reaction of **2** is carried out when the pores are filled with the ruthenium dye. The final yellow/orange solid (**S1**) was filtered, washed with acetonitrile, and dried at 40 °C for 12 h.

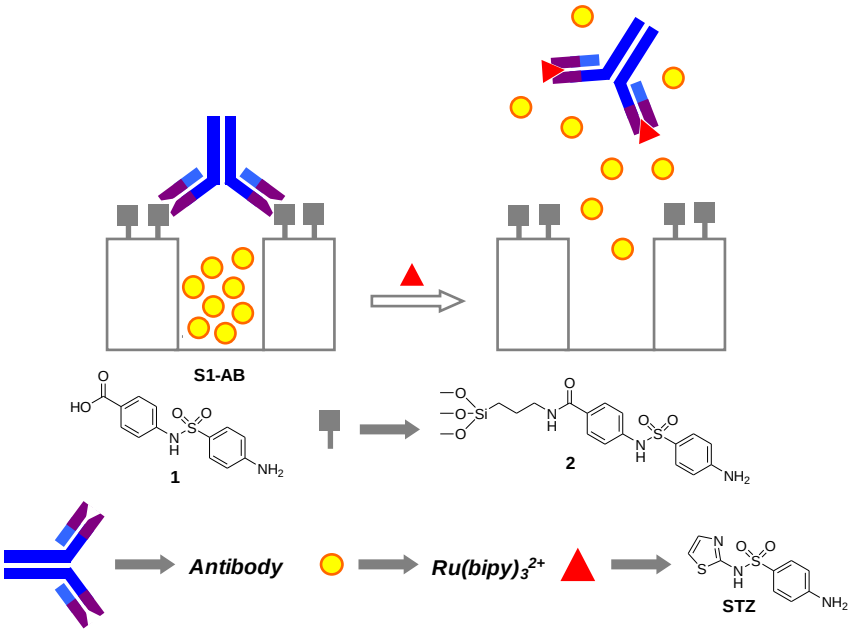

Scheme 1. Schematic representation of gated material **S1** capped with antibody and structures of hapten **1**, hapten derivative **2**, and the antigen sulfathiazole (STZ)

For preparation of the final gated material (**S1-AB**), 400 µg of the SMPS **S1** was suspended in 400 µL of a solution containing the antibody in phosphate-buffered saline (PBS, pH 7.5; see Supporting Information for the exact composition). Optimization of the conditions was performed by checking board titrations with several sera and a range of different serum dilutions (see Supporting Information).

S1-AB was isolated by centrifugation and washed with PBS to eliminate the residual dye and the free antibody.

For the sake of comparison, and as control supports, two additional solids were prepared. One (**S2**) is a material containing only the $[Ru(bipy)_3]^{2+}$ dye on the pore voids, whereas the other (**S3**) contains $[Ru(bipy)_3]^{2+}$ on the mesopores and polyamines on the external surface (see Supporting Information). This second solid, containing amines, was expected to display some interaction with the antibody because sulfathiazole (for which the antibody is selective) also contains an amino group. Both solids will allow assessing the effect that the hapten grafted onto the MCM-41 pores and its interaction with the antibody has in the dye delivery control in the presence of antigen. The procedure to obtain **S2** was the same as described for **S1** but without grafting the hapten **2** on the external surface. Additionally **S3** was prepared, following literature procedures by reaction of dye-loaded MCM-41 with 3-[2-(2-aminoethylamino)ethylamino] propyltrimethoxysilane (**3**) (see Supporting Information).[15b]

Characterization of Materials

Solid **S1** was characterized by standard procedures. Figure **1** shows powder X-ray diffraction (PXRD) patterns of the MCM-41 support and the **S1** functionalized material. The PXRD of siliceous MCM-41 as synthesized (curve a) shows four low-angle reflections typical of a hexagonal array. A significant displacement of the (100) peak in the PXRD powder of the MCM-41 calcined sample (curve b) is clearly appreciated due to condensation of silanol groups during the calcination step. Finally, curve c corresponds to the **S1** PXRD pattern. In this case, all reflections except (100) are lost, most likely related to a change of contrast due to the filling of the pore voids with the ruthenium(II) dye. The value and intensity of the (100) peak in this pattern is strong evidence that the loading process with the dye and the further functionalization with hapten have not damaged the mesoporous scaffolding. The presence of the mesoporous structure in the MCM-41 calcined sample and final functionalized solids is also observed by TEM analysis, in which the typical hexagonal porosity of the MCM-41 matrix can be seen (see Figure **1**).

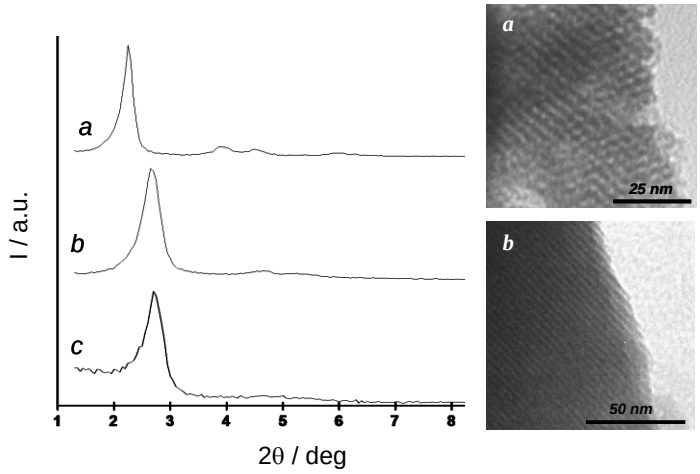

Figure 1. (Left) Powder X-ray patterns of the solids (a) MCM-41 as synthesized, (b) calcined MCM-41, and (c) **S1** containing the dye $[Ru(bipy)_3]^{2+}$ and hapten derivative **2**. (Right) TEM images of (a) calcined MCM-41 sample and (b) solid **S1**, showing the typical hexagonal porosity of the MCM-41 mesoporous matrix.

The N_2 adsorption−desorption isotherms of the MCM-41 calcined material show a typical type IV isotherm in which the observed step can be related to the nitrogen condensation inside the mesopores by capillarity. The absence of a hysteresis loop in this interval and the narrow pore distribution suggest the existence of uniform cylindrical mesopores. Application of the BET model resulted in a value for the total specific surface of 1246 m^2/g. The N_2 adsorption−desorption isotherm of **S1** is typical of mesoporous systems with filled mesopores, and a significant decrease in the N_2 volume adsorbed is observed (see Supporting Information). In fact, this solid presents relatively flat curves when compared (at the same scale) to the MCM-41 material, indicating that there is significant pore blocking. Similar results have been observed for the parent solid **S3** and by us in related systems. BET specific surface values, pore volumes, and pore sizes calculated from the N_2 adsorption−desorption isotherms for MCM-41 and **S1** and **S3** are listed in Table **1** (see Supporting Information for more details).

Table 1. BET specific surface values, pore volumes, and pore sizes calculated from N_2 adsorption−desorption isotherms[a] for selected materials.

	S_{BET} ($m^2\ g^{-1}$)	Pore Volume [a] ($cm^3\ g^{-1}$)	Pore size [a] (nm)
MCM-41	1246	0.85	2.39
S1	291	0.22	2.31
S3	110	0.35	2.18

[a] Volume (*V*) and diameter (*D*) of mesopore.

The content of hapten derivative **2** in **S1**, polyamine in **S3**, and dye in prepared solids, determined by elemental analysis and thermogravimetric and delivery studies, is shown in Table **2**. Further detail for the synthesis and characterization of **S3** is included in Supporting Information.

Table 2. Content (α) of hapten derivative **2** in **S1**, polyamine in **S3**, and dye in prepared solids

Solid	$\alpha_{hapten\ 2}$ (mmol/g SiO_2)	$\alpha_{polyamine\ 3}$ (mmol/g SiO_2)	α_{dye} (mmol/g SiO_2)
S1	0.38	-	0.66
S1-AB	0.38	-	0.12
S2	-	-	0.69
S3	-	0.40	0.60
S3-AB	-	0.40	0.15

When the amount of STZ that induced the observed dye release is taken into account, and with the assumption that two molecules of STZ interact with one antibody molecule (if total occupation is supposed), it can be estimated that **S1-AB** material contains 1.74×10^{18} antibody molecules/g of solid. Additionally, from the typical external surface for a MCM-41 support, this results in an average distance between antibodies of ca. 7.6 nm, a value that is in agreement with the typical effective antibody molecular radius of 5.5 nm. Moreover, from the

antibody and hapten contents, a ratio of 86 hapten molecules/antibody molecules was estimated.

Functional Antigen-Driven Controlled Release

As stated above, we aimed to design delivery systems triggered by a certain antigen by use of antibody-capped mesoporous scaffolds. The uncapping protocol, that is, delivery of the Ru complex from the pore voids to the aqueous solution, was straightforwardly observed via monitoring of the fluorescence band of $[Ru(bipy)_3]^{2+}$ dye centered at 610 nm (λ_{ex} = 453 nm) in the aqueous phase.

To investigate the gating properties, in a typical experiment 250 μL of 1 ppm sulfathiazole in PBS was added to 200 μg of **S1-AB**, and the suspension was stirred in order to establish a competition for the antibody between anchored hapten and free sulfathiazole. Release of the reporter was also determined for solutions of **S1-AB** under similar conditions but in the absence of sulfathiazole. The difference in emission in the presence and absence of STZ is displayed in Figure **2**, which plots the release behavior. The figure shows that solid **S1**-**AB** displays a poor release profile versus time (curve a), whereas the same solid in the presence of 1 ppm STZ (curve b) shows clear delivery of the dye: 95% of the maximum release of the entrapped guest was observed after ca. 2 h. Additionally, the figure also shows how release from the capped system can be triggered on command by adding sulfathiazole (1 ppm) at a certain time (curve c). These experiments demonstrate the real possibility of controlling the cargo delivery in water by use of the antigen for which the antibody capping the mesopores is selective.

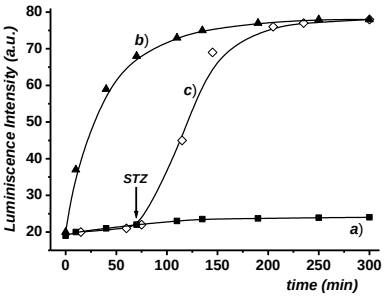

Figure 2. Kinetic release of $[Ru(bipy)_3]^{2+}$ dye from solid **S1-AB** in the absence (a) and presence (b) of 1 ppm sulfathiazole in aqueous PBS (pH 7.5). A third curve (c) shows the release profile of $[Ru(bipy)_3]^{2+}$ complex from **S1-AB** in PBS (pH 7.5) until *t* = 70 min (indicated by the arrow in the figure), when suddenly sulfathiazole (1 ppm) is added to the solution.

Additionally, delivery from **S1-AB** as a function of the concentration of the molecular trigger (sulfathiazole) was studied, and the results are illustrated in Figure **3**. It can be seen that concentrations as low as 100 ppb sulfathiazole were able to start to uncap the mesopores. The figure also shows that the delivered amount of cargo is proportional to the sulfathiazole concentration, displaying a typical noncompetitive immunoassay response curve in agreement with an uncapping protocol due to a displacement of the antibody as indicated in Scheme **1**.[22] Typically the maximum percentage of dye delivery from **S1** in the presence of STZ was over 50−60% of the loaded dye.

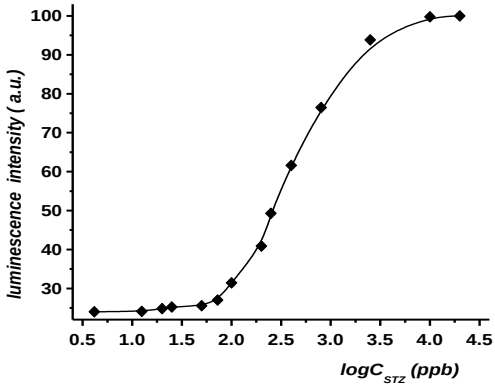

Figure 3. Relative percentage of released $[Ru(bipy)_3]^{2+}$ dye from **S1-AB** as a function of the concentration of sulfathiazole in PBS (pH 7.5) after 2 h of reaction. The amount of released dye was determined through the emission band (λ_{em} = 610 nm) of the $[Ru(bipy)_3]^{2+}$ dye in the solution (λ_{ex} = 453 nm).

Selective Delivery

One of the potential advantages of using antibodies as capping groups is the development of highly selective key-in-lock gating systems. For instance, it is well-known that antibodies can identify and bind only to their unique antigen in mixtures containing a number of different molecules. In order to investigate selectivity in the opening protocol, dye delivery from **S1-AB** was tested in the presence of other molecules very similar to sulfathiazole; that is, a set of sulfonamides (see Supporting Information for the structures). The uncapping

ability of these closely related molecules (at 1 ppm concentration) is shown in Figure **4**, which plots the fluorescence of the dye released from the SMPS **S1-AB** in the presence of different sulfonamides. A very selective uncapping with sulfathiazole was detected, where only the sulfonamides sulfamethizole (SMT) and sulfamerazine (SMR) show certain cross-reactivity with **S1-AB**.[23]

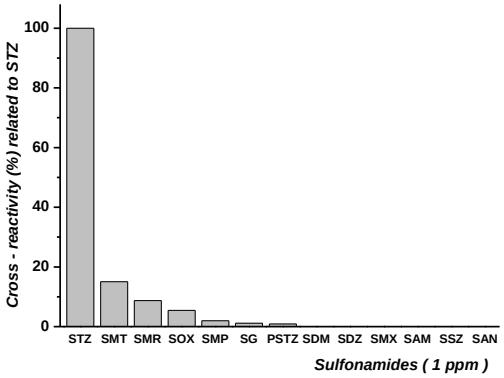

Figure 4. Relative release of $[Ru(bipy)_3]^{2+}$ from **S1-AB** in the presence of 1 ppm of certain molecules (sulfonamides) in PBS (pH 7.5) after 2 h of reaction. From left to right: sulfathiazole (STZ), sulfamethizole (SMT), sulfamerazine (SMR), sulfisoxazole (SOX), sulfamethoxypyridazine (SMP), sulfaguanidine (SG), N^4-phthalylsulfathiazole (PSTZ), sulfadimethoxine (SDM), sulfadiazine (SDZ), sulfamethoxazole (SMX), sulfacetamide (SAM), sulfasalazine (SSZ), and sulfanilamide (SAN). The structures of these sulfonamides used in the cross-reactivity studies are shown in Supporting Information.

In addition to these delivery studies with **S1-AB**, further control experiments were carried out with solids **S2** and **S3** in order to evaluate the effect of the anchored hapten on the selective delivery process. Both solids **S2** and **S3** contain the ruthenium dye in the mesopores. Solid **S2** does not have any additional functionalization; **S3** contains amino moieties on the external surface (see Supporting Information for details). As stated above, due to the presence also of an amino group in sulfathiazole, some kind of interaction between the polyamines anchored on **S3** and the antibody was expected.

Aqueous suspensions at pH 7.5 of solids **S2** and **S3** alone showed fast dye release; however, dye delivery was strongly inhibited when **S2** was in the presence of the antibody due to an unspecific adsorption process of the antibody on the surface of **S2**, most likely through interactions with the silanol groups on the SMPS. Most importantly, the addition of sulfathiazole to this **S2-AB** material resulted in no cargo delivery even when large amounts of sulfathiazole were added (up to 50 ppm). In relation to **S3**, addition of the antibody to this solid resulted in the preparation of solid **S3-AB** (analogous to **S1-AB**). The gating properties of this new solid were studied in 250 μL of a solution containing PBS and 200 μg of **S3-AB**, and the release behavior as a function of time in the presence and absence of STZ is displayed in Figure **5** (left). The figure shows that solid **S3**-**AB** displays a rather important release in the absence of sulfathiazole (curve a) in contrast with the low delivery of the dye observed for **S1-AB** (see Figure **2** curve a). This different behavior is most likely due to much poorer interaction of the antibody with the polyamines in **S3-AB** than with the hapten anchored on **S1-AB**. Additionally, from Figure **5** (left) it is also apparent that the presence of sulfathiazole (1 ppm) enhances the delivery of the dye from the **S3-AB** solid (curve b). Much more important in terms of selectivity are the results observed when solid **S3-AB** is tested in the presence of a family of sulfonamides. Figure **5** (right) shows the relative release (with respect to STZ) of the dye from **S3-AB** in the presence of a concentration of 0.5 ppm of these chemicals in PBS (pH 7.5). A clear unselective uncapping process, as effective in many cases as that found with sulfathiazole, was observed for most of the molecules tested.[24] This behavior heavily contrasts with that found under similar conditions with the hapten-containing solid **S1-AB** (see Figure **4**). The behavior shown by **S2** and **S3** draws attention to the role played by the anchored hapten groups in the gating mechanism; that is, the hapten in **S1** inhibits the unspecific attachment of the antibody on the mesoporous surface (as occurs in **S2**) and allows at the same time a very selective uncapping protocol to take place in the presence of the target antigen (in contrast with **S3**).

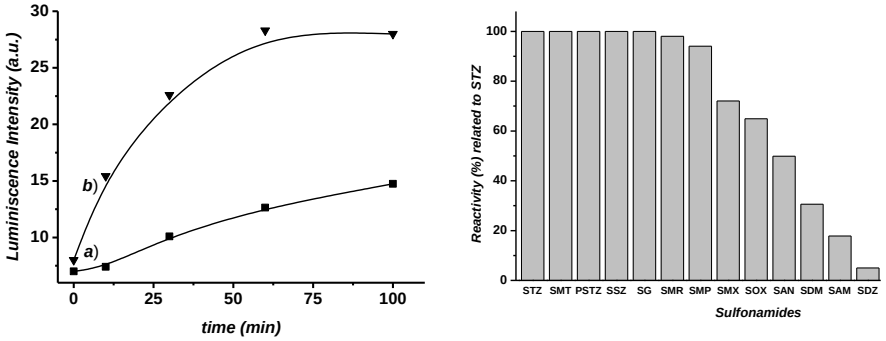

Figure 5. (Left) Kinetic release of $[Ru(bipy)_3]^{2+}$ dye from solid **S3-AB** in the absence (a) and presence (b) of 1 ppm sulfathiazole in PBS (pH 7.5). (Right) Relative release of $[Ru(bipy)_3]^{2+}$ from **S3-AB** in the presence of 0.5 ppm of certain sulfonamides (see Supporting Information for structures) in PBS (pH 7.5) after 2 h of reaction.

Conclusions

In conclusion, we have demonstrated, as a proof-of-the-concept and for the first time, that the use of antibodies as gatekeepers on the surface of SMPS provides a suitable method for the design of delivery systems able to selectively release entrapped guests in the presence of target molecules (antigen) to which the antibody binds selectively. It is advisible to note that this paradigm relies on a different approach, not previously used, and therefore it displays new possibilities for modulation that cannot be considered in other systems. In particular, we believe that gated SMPS based on the use of antibodies may be a promising route for the development of custom-made controlled-delivery nanodevices specifically triggered by target molecular guests. The possibility of including this antibody gating protocol on diverse supports, the potential delivery of different cargos, and the opportunity to select antibodies or similar bioreceptors for a countless amount of possible antigens makes this approach highly appealing for a very wide range of delivery applications in different fields.

Acknowledgments

We express our gratitude to the Spanish Ministerio de Ciencia y Tecnología (Projects CTQ2006-15456-C04-01, CB07/01/2012, CTQ2007-64735-AR07, and MAT2009-14564-C04-01) for their support. E.C. and A. B. are grateful to the

Spanish Ministerio de Ciencia e Innovación and to the Polytechnic University of Valencia for a grant.

References

1. Ariga, K., Vinu, A., Hill, J. P. and Mori, T. *Coord. Chem. Rev*. **2007**, *251*, 2562
2. Katz, E. and Willner, I. *Angew. Chem., Int. Ed*. **2004**, *43*, 6042
3. Descalzo, A. B., Martínez-Máñez, R., Sancenón, F., Hoffmann, K. and Rurack, K. Angew. Chem., Int. Ed. **2006**, *45*, 5924.
4. (a) Puoci, F., Iemma, F. and Picci, N. *Curr. Drug Delivery* **2008**, *5*, 85, (b) Siepmann, F., Siepmann, J., Walther, M., MacRae, R. and Bodmeier, R. *J. Controlled Release* **2008**, *125*, 1.
5. Hamidi, M., Azadi, A. and Rafiei, P. *Adv. Drug Delivery Rev*. **2008**, *17*, 1638
6. Pouton, C. W. and Porter, C. J. H. *Adv. Drug Delivery Rev.* **2008***, 17*, 625
7. Rijcken, C. J. F., Soga, O., Hennink, W. E. and van Nostrum, C. F. *J. Controlled Release* **2007***, 120*, 131
8. Andresen, T. L., Jensen, S. S. and Jorgensen, K. Prog. *Lipid Res.* **2005,** *44*, 69
9. (a) Beck, J. S., Vartuli, J. C., Roth, W. J., Leonowicz, M. E., Kresge, C. T., Schmitt, K. D., Chu, C. T.-W., Olson, D. H., Sheppard, E. W., McCullen, S. B., Higgins, J. B. and Schlenker, J. L. *J. Am. Chem. Soc.* **1992***, 114*, 10834 (b) Wright, A. P. and Davis, M. E. *Chem. Rev.* **2002***, 102*, 3589 (c) Kickelbick, G. Angew. Chem., Int. Ed. 2004, 43, 3102– 3104 (d) Stein, A. *Adv. Mater.* **2003***, 15*, 763.
10. (a) Casasús, R., Marcos, M. D., Martínez-Máñez, R., Ros-Lis, J. V., Soto, J., Villaescusa, L. A., Amorós, P., Beltrán, D., Guillem, C. and Latorre, J. *J. Am. Chem. Soc.* **2004***, 126*, 8612.; (b) Casasús, R., Climent, E., Marcos, M. D., Martínez-Máñez, R., Sancenón, F., Soto, J., Amorós, P., Cano, J. and Ruiz, E. *J. Am. Chem. Soc.* **2008***, 130*, 1903 (c) Bernardos, A., Aznar, E., Coll, C., Martínez-Máñez, R., Barat, J. M., Marcos, M. D., Sancenón, F. and Soto, J. *J. Controlled Release* **2008***, 131*, 181 (d) Yang, Q., Wang, S., Fan, P., Wang, L., Di, Y., Lin, K. and Xiao, F.-S. *Chem. Mater.* **2005***, 17*, 5999 (e) Nguyen, T. D., Leung, K. C.-F., Liong, M., Pentecost, C. D., Stoddart, J. F. and Zink, J. I. *Org. Lett.* **2006***, 8*, 3363 (f) Leung, K. C.-F., Nguyen, T. D., Stoddart, J. F. and Zink, J. I. *Chem. Mater.* **2006,** *18*, 5919 (g) Angelos, S., Yang, Y.-W., Patel, K., Stoddart, J. F. and Zink, J. I. *Angew. Chem., Int. Ed.* **2008**, *47*, 2222 (h) Khashab, N. M., Trabolsi, A., Lau, Y. A., Ambrogio, M. W., Friedman, D. C., Khatib, H. A., Zink, J. I. and Stoddart, J. F. Eur. *J. Org. Chem.* **2009**, 1669 (i) Park, C., Oh, K., Lee, S. C. and Kim, C. *Angew. Chem., Int. Ed.* **2007**, *46*, 1455.
11. Fu, Q., Rao, G. V. R., Ista, L. K., Wu, Y., Andrzejewski, B. P., Sklar, L. A., Ward, T. L. and López, G. P. *Adv. Mater.* **2003***, 15*, 1262.
12. (a) Trewyn, B. G., Giri, S., Slowing, I. I. and Lin, V. S.-Y. *Chem. Commun.* **2007***,* 3236. (b) Trewyn, B. G., Slowing, I. I., Giri, S., Chen, H.-T. and Lin, V. S.-Y. *Acc. Chem. Res*. **2007**, *40*, 846 (c) Lai, C.-Y., Trewyn, B. G., Jeftinija, D. M., Jeftinija, K., Xu, S., Jeftinija, S. and Lin, V. S.-Y. *J. Am. Chem. Soc.* **2003***, 125*, 4451 (d) Torney, F., Trewyn, B. G., Lin, V. S.-Y. and Wang, K. *Nat.*

Nanotechnol. **2007***, 2*, 295 (e) Radu, D. R., Lai, C.-Y., Jeftinija, K., Rowe, E. W., Jeftinija, S. and Lin, V. S.-Y. *J. Am. Chem. Soc.* **2004***, 126*, 13216 (f) Giri, S., Trewyn, B. G., Stellmaker, M. P. and Lin, V. S.-Y. *Angew. Chem., Int. Ed.* **2005***, 44*, 5038 (g) Slowing, I. I., Trewyn, B. G. and Lin, V. S.-Y. *J. Am. Chem. Soc.* **2007***, 129*, 8845 (h) Slowing, I. I., Trewyn, B. G., Giri, S. and Lin, V. S.-Y. *Adv. Funct. Mater.* **2007,** *17*, 1225 (i) Montera, R., Vivero-Escoto, J., Slowing, I. I., Garrone, E., Onida, B. and Lin, V. S.-Y. *Chem. Commun*. **2009**, 3219.

13. (a) Zhao, Y., Trewyn, B. G., Slowing, I. I. and Lin, V. S.-Y. *J. Am. Chem. Soc.* **2009***, 131*, 8398. (b) Hernandez, R., Tseng, H.-R., Wong, J. W., Stoddart, J. F. and Zink, J. I. *J. Am. Chem. Soc.* **2004***, 126*, 3370 (c) Nguyen, T. D., Tseng, H.-R., Celeste, P. C., Flood, A. H., Liu, Y., Stoddart, J. F. and Zink, J. I. *Proc. Natl. Acad. Sci. U.S.A.* **2005***, 102*, 10029 (d) Nguyen, T. D., Liu, Y., Saha, S., Leung, K. C.-F., Stoddart, J. F. and Zink, J. I. *J. Am. Chem. Soc.* **2007***, 129*, 626. (e) Nguyen, T. D., Leung, K. C.-F., Liong, M., Liu, Y., Stoddart, J. F. and Zink, J. I. *Adv. Funct. Mater.* **2007***, 17,* 2101 (f) Fujiwara, M., Terashima, S., Endo, Y., Shiokawa, K. and Ohue, H. *Chem. Commun.* **2006**, 4635 (g) Liu, R., Zhao, X., Wu, T. and Feng, P. J. *Am. Chem. Soc.* **2008***, 130*, 14418.
14. (a) Mal, N. K., Fujiwara, M. and Tanaka, Y. *Nature* **2003,** *421*, 350 (b) Mal, N. K., Fujiwara, M., Tanaka, Y., Taguchi, T. and Matsukata, M. *Chem. Mater.* **2003***, 15*, 3385 (c) Zhu, Y. and Fujiwara, M. *Angew. Chem., Int. Ed.* **2007***, 46*, 2241 (d) Lu, J., Choi, E., Tamanoi, F. and Zink, J. I. *Small* **2008***, 4*, 421– 426 (e) Angelos, S., Choi, E., Vögtle, F., De Cola, L. and Zink, J. I. *J. Phys. Chem. C* **2007***, 111*, 6589 (f) Liu, N., Dunphy, D., Atanassov, P., Bunge, S. D., Chen, Z., López, G. P., Boyle, T. J. and Brinker, C. J. *Nano Lett.* **2004***, 4*, 551 (g) Ferris, D. P., Zhao, Y.-L., Khashab, N. M., Khatib, H. A., Stoddart, J. F. and Zink, J. I. *J. Am. Chem. Soc.* **2009***, 131*, 1686 (h) Aznar, E., Casasús, R., García-Acosta, B., Marcos, M. D., Martínez-Máñez, R., Sancenón, F., Soto, J. and Amorós, P. *Adv. Mater.* **2007***, 19*, 2228 (i) Vivero-Escoto, J. L., Slowing, I. I., Wu, C.-Y. and Lin, V. S.-Y. *J. Am. Chem. Soc.* **2009***, 131*, 3462 (j) Aznar, E., Marcos, M. D., Martínez-Máñez, R., Sancenón, F., Soto, J., Amorós, P. and Guillem, C. *J. Am. Chem. Soc.* **2009***, 131*, 6833
15. (a) Coll, C., Casasús, R., Aznar, E., Marcos, M. D., Martínez-Máñez, R., Sancenón, F., Soto, J. and Amorós, P. *Chem. Commun.* **2007**, 1957 (b) Casasús, R., Aznar, E., Marcos, M. D., Martínez-Máñez, R., Sancenón, F., Soto, J. and Amorós, P. *Angew. Chem., Int. Ed.* **2006***, 45*, 6661 (c) Aznar, E., Coll, C., Marcos, M. D., Martínez-Máñez, R., Sancenón, F., Soto, J., Amorós, P., Cano, J. and Ruiz, E. *Chem. Eur. J.* **2009***, 15*, 6877.
16. (a) Patel, K., Angelos, S., Dichtel, W. R., Coskun, A., Yang, Y.-W., Zink, J. I. and Stoddart, J. F. *J. Am. Chem. Soc.* **2008***, 130*, 2382 (b) Schlossbauer, A., Kecht, J. and Bein, T. *Angew. Chem., Int. Ed.* **2009***, 48*, 3092. (c) Bernardos, A., Aznar, E., Marcos, M. D., Martínez-Máñez, R., Sancenón, F., Soto, J., Barat, J. M. and Amorós, P. *Angew. Chem., Int. Ed.* **2009***, 48*, 5884.
17. Zhao, Y., Trewyn, B. G., Slowing, I. I. and Lin, V. S.-Y. *J. Am. Chem. Soc.* **2009***, 131*, 8398
18. (a) Climent, E., Calero, P., Marcos, M. D., Martínez-Máñez, R., Sancenón, F. and Soto, *J. Chem. Eur. J.* **2009***, 15*, 1816 (b) Ros-Lis, J. V., Casasús, R., Comes, M., Coll, C., Marcos, M. D., Martínez-Máñez, R., Sancenón, F., Soto, J., Amorós, P., El Haskouri, J., Garró, N. and Rurack, K. *Chem. Eur. J.* **2008***, 14*, 8267 (c) Comes, M., Marcos, M. D., Martínez-Máñez, R., Sancenón, F., Soto, J., Villaescusa, L. A. and Amorós, P. *Chem. Commun.* **2008**, 3639 (d) Calero, P., Aznar, E.,

Lloris, J. M., Marcos, M. D., Martínez-Máñez, R., Ros-Lis, J. V., Soto, J. and Sancenón, F. *Chem. Commun.* **2008**, 1668.

19. Diamandis, E. P. and Christopoulus, T. K.. Eds.; *Immunoassay*; Academic Press: San Diego, CA, **1996**.
20. (a) Silverton, E. W., Navia, M. A. and Davies, D. R. *Proc. Natl. Acad. Sci. U.S.A.* **1977***, 74*, 5140. (b) Francis, G. E. and Delgado, C., Eds.; *Methods in Molecular Medicine*, Vol. *25*. Drug Targeting: Strategies, Principles, and Applications; Humana Press, Inc.: Totowa, NJ, **2007**.
21. Langone, J. and van Vunakis, H. *Methods Enzymol*. **1982**, *84*, 628.
22. Additionally, although this report deals primarily with the demonstration that it is possible to develop controlled delivery systems using antibody-capped mesoporous nanocontainers, the fact that cargo delivery is proportional to sulfathiazole (antigen) concentration opens the possibility of developing novel label-free immunoassay paradigms where the properties of the reporter (the cargo) could easily be selected at will. Using this concept, further analytical-oriented studies will be carried out in due course. Also the development of displacement one-step analytical formats is very promising because this immunoassay type usually shows higher sensitivity than the corresponding competitive format. See, for instance, González-Techera, A., Vanrell, L., Last, J., Hammock, B. D. and González-Sapienza, G. *Anal. Chem.* **2007***, 79*, 7799.
23. Although this first example shows a relatively high selective trigger of the cargo delivery, it is important to note that even more selective systems could be prepared using monoclonal antibodies or genetically engineered antibodies. See, for instance, Liddell, E. Antibodies. Chapter 8 in The Immunoassay Handbook, 3th ed.; Elsevier: Amsterdam, **2005**.
24. It might be important to note that **S3-AB** or similar systems could be suitable for the development of gating systems that could be opened by similar species such as a set of sulfonamides.

J. Am. Chem. Soc., 2009, 131, 14075-14080

SUPPORTING INFORMATION

Controlled Delivery Systems Using Antibody-Capped Mesoporous Nanocontainers

Estela Climent, Andrea Bernardos, Ramón Martínez-Máñez, Angel Maquieira, María Dolores Marcos, Núria Pastor-Navarro, Félix Sancenón, Juan Soto, and Pedro Amorós.

Chemicals

The chemicals tetraethylorthosilicate (TEOS), *n*-cetyltrimethylammonium bromide (CTAB), sodium hydroxide (NaOH), triethanolamine ($TEAH_3$), *N*-hydroxysuccinimide (NHS) and *N*,*N'*-dicyclohexylcarbodiimide (DCC) and tris(2,2'bipyridyl)ruthenium(II) chloride hexahydrate ($[Ru(bipy)_3]Cl_2 \cdot 6H_2O$) were provided by Aldrich. The sulfonamides N^4-phthalylsulfathiazole (PSTZ), sulfacetamide (SAM), sulfadiazine (SDZ), sulfaguanidine (SG), sulfamerazine (SMR), sulfamethizole (SMT), sulfamethoxazole (SMX), sulfamethoxypyridazine (SMP), sulphanilamide (SAN), sulfasalazine (SSZ), sulfisoxazole (SOX), sulfadimethoxine (SDM), sulfathiazole (STZ), and the chemical reagent for hapten derivative synthesis (3-aminopropyl)trimethoxysilane were also purchased from Fluka–Sigma–Aldrich Quimica (Madrid, Spain). The structures of sulfonamides used for interference studies are shown in Figure **SI-1**. Hapten **1** (4-(4-amino-

benzenesulfonylamino)-benzoic acid) was prepared following literature procedures.[1] Analytical-grade solvents were from Scharlab (Barcelona, Spain). All reactives were used as received.

General Techniques

XRD, TG analysis, elemental analysis, EDX microscopy, N_2 adsorption-desorption and UV-visible spectroscopy techniques were employed to characterize the materials. X-ray measurements were performed on a Seifert 3000TT diffractometer using Cu-K_α radiation. Thermo-gravimetric analysis were carried out on a TGA/SDTA 851e Mettler Toledo equipment, using an oxidant atmosphere (Air, 80 mL/min) with a heating program consisting on a heating ramp of 10 °C per minute from 393 K to 1273 K and an isothermal heating step at this temperature during 30 minutes. N_2 adsorption-desorption isotherms were recorded on a Micromeritics ASAP2010 automated sorption analyser. The samples were degassed at 120ºC in vacuum overnight. The specific surfaces areas were calculated from the adsorption data in the low pressures range using the BET model. Pore size was determined following the BJH method. Fluorescence spectroscopy was carried out on a Felix 32 Analysis Version 1.2 (Build 56) PTI (Photon Technology International) and UV-visible spectroscopy was carried out with a Lambda 35 UV/Vis Spectrometer Perkin Elmer Instruments. ^{1}H and ^{13}C nuclear magnetic resonance (NMR) spectra were acquired with Varian 300 spectrometer (Sunnyvale, CA, USA).

Buffer solutions

Phosphate-buffered saline 1x (PBS; 8.03 mmol L^{-1} Na_2HPO_4, 1.46 mmol L^{-1} KH_2PO_4, 137 mmol L^{-1} NaCl, 2.73 mmol L^{-1} KCl, pH 7.5) was used for controlled release experiences and cross-reactivity studies.

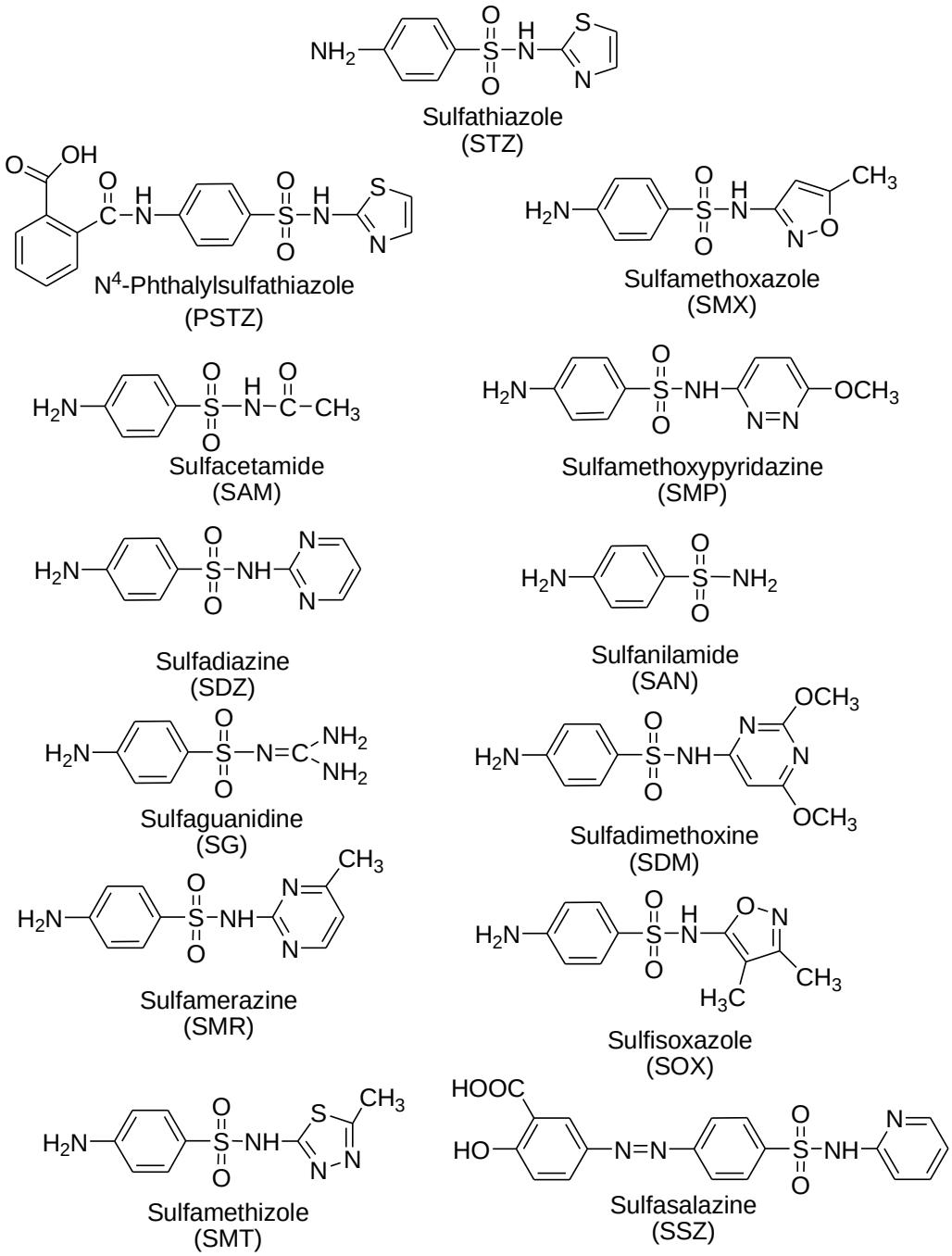

Figure SI-1: Structures of the sulfonamides used for cross-reactivity studies.

Polyclonal-based antibodies for sulfathiazole.

The specific polyclonal-based antibodies for sulfathiazole were obtained by using a procedure described previously.[1] For immunizing purposes the hapten **1** was covalently attached through its carboxylic acid moiety to the lysine residues of BSA using a modification of the active-ester method.[2] The conjugation of the hapten to the protein was estimated by measuring the hapten/protein molar ratio accordingly to UV absorbance values (ratios ranging from 20 to 24 were observed). The immunogen (0.20 mg in 0.5 mL of PBS) was suspended in 0.5 mL of Freund's complete adjuvant and injected intramuscularly into two (I and II) female New Zealand white rabbits. The animals were boosted at 21-day intervals with the same immunogen suspended in 0.5 mL Freund's incomplete adjuvant. Ten days after each boost, blood was obtained by bleeding the ear vein of the rabbit. When no titer enhancement was observed whole blood was collected, allowed to coagulate over-night at 4 ^{o}C and the serum was separated by centrifugation. Two sera were obtained (**1**-I and **1**-II).

Synthesis of the silica mesoporous support (SMPS)

The synthesis of the MCM41-type mesoporous support was carried out following the so-called 'atrane route', a simple preparative technique based on the use of complexes that include triethanolamine ($TEAH_3$) related ligands (i.e. in general 'atranes' and silatranes for the silicon-containing complexes), tetraethylorthosilicate (TEOS) as hydrolytic inorganic precursors and surfactants as porogen species. The molar ratio of the reagents in the mother liquor was fixed to 7 $TEAH_3$: 2 TEOS: 0.52 CTAB: 0.5 NaOH: 180 H_2O. In a typical synthesis leading to the MCM-41 pure silica, CTAB (4.67 g) were added at 118 ºC to a solution of $TEAH_3$ (25.76g) containing 0.012 mol of NaOH and 0.049 mol of a silatrane derivative (e.g. 11 mL of TEOS was added at 70 ºC to TEA, e.g., in the form of $Si(TEA)(TEAH_2)$, where TEA is the fully deprotonated ligand). Then, 80 mL of deionized water were added with vigorous stirring at 70 ºC. After few minutes, a white suspension resulted. This mixture was aged at room temperature overnight. The resulting powder was collected by filtration and washed with water. Finally

the solid was dried at 70 ºC (MCM-41 as-synthesized). To prepare the final porous material (MCM-41), the as-synthesized solid was calcined at 550 ºC for 5h in order to remove the template**.**

Synthesis of S2

The control solid **S2** was prepared following the same procedure described for **S1** but without grafting the hapten derivative **2**. The final orange solid (**S2**) was filtered, washed with water and dried at 50 ºC for 12 hours.

Synthesis of S3

The control amino-functionalised solid **S3** was prepared following literature procedures.[3] 1.00 g of activated MCM-41 and 0.6 g of dye tris(2,2'-bipyridyl)ruthenium(II) chloride were suspended in 50 mL of anhydrous acetonitrile inside a round-bottom flask connected to a Dean-Stark in an inert atmosphere. The suspension was refluxed (110 °C) in azeotropic distillation, collecting 10 mL in the trap in order to remove the adsorbed water. Then, the mixture was stirred during 24 hours at room temperature with the aim of achieving maximum loading in the pores of the MCM-41 scaffolding. Afterward an excess of 3-[2-(2-aminoethylamino)-ethylamino]propyl-trimethoxysilane (4.3 mL, 15.0 mmol) was added, and the suspension was stirred for 5.5 h. Finally, the orange solid (**S3**) was filtered off, washed with CH_3CN, and dried at 70 °C for 12h.

Synthesis and optimization of solids S1-AB and S3-AB.

The optimization for the preparation of solid **S1-AB** was carried out by studying the interaction between the hapten anchored onto the surface of solid **S1** and the specific polyclonal-based antibodies for sulfathiazole, portions of 400 μg of the corresponding solid were suspended in 400 μl of serum **1**-I or serum **1**-II (vide ante) in PBS using different dilutions (1/500, 3/400, 1/100, 1/75, 1/50 and 1/10 μl sera / μl PBS (pH 7.5)) and each suspensions was stirred for 3 hours (see text in manuscript). The prepared systems were fractionated in two parts. To one part, 250 μL of a PBS solution were added, and to the other part 250 μL a PBS solution also containing 50 ppm of sulfathiazole, were added. After centrifugation, the

fluorescence $[Ru(bipy)_3]^{2+}$ emission at 610 nm (λ_{ex} = 453 nm) delivered to the solution was measured. Optimum sera dilutions were found to be 1/75 or 1/50 (see Figure **SI-2**). From these studies it was also found that sera **1**-I shows a larger difference in the fluorescence response than sera **1**-II. Solid **S3-AB** was prepared following a similar procedure using 1/75 or 1/50 dilutions. A scheme of the solid **S3-AB** and the displacement assay in the presence of STZ is shown in Scheme **SI-1**.

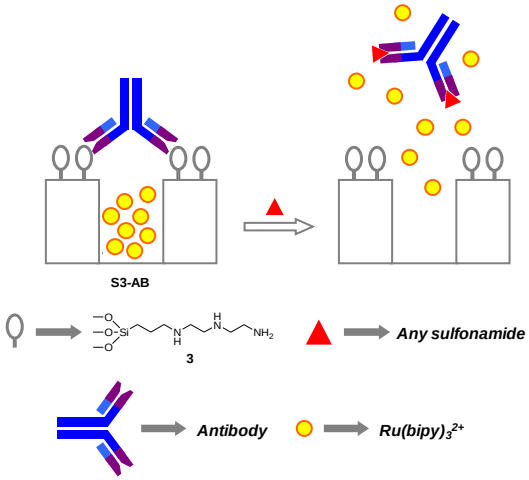

Scheme SI-1.- Schematic representation of the material **S3-AB** capped with an antibody and the reactivity with sulfonamides.

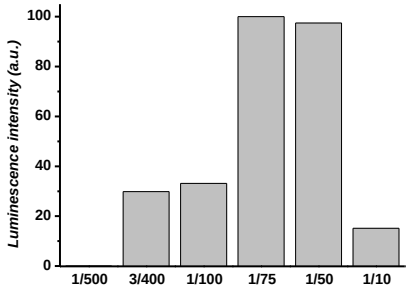

Figure SI-2.- Difference in the release of the dye $[Ru(bipy)_3]^{2+}$ from **S1-AB** solids in the presence and in the absence of sulfathiazole. Several **S1-AB** solids were prepared using different sera dilutions (see text). The data shows the results for sera **1-I**.

Materials Characterization

Solid **S1** was characterized using standard procedures. Figure **1** in the manuscript shows powder X-ray patterns of the MCM-41 support and the **S1** functionalised material. The PXRD of siliceous MCM-41 as-synthesized (curve a) shows four low-angle reflections typical of a hexagonal array that can be indexed as (100), (110), (200), and (210) Bragg peaks. A significant displacement of the (100) peak in the XRD powder of the MCM-41 calcined sample is clearly appreciated in the curve b, corresponding to an approximate cell contraction of 7 Å. This displacement and the broadening of the (110) and (200) peaks are related to further condensation of silanol groups during the calcination step. Finally, curve c corresponds to the **S1** XRD pattern. In this case, the loss of the (110) and (200) reflections is observed, most likely related to a loss of contrast due to the filling of the pore voids with the ruthenium(II) dye. Nevertheless, the value and intensity of the (100) peak in this pattern strongly evidences that the loading process with the dye and the further functionalization with hapten have not damaged the mesoporous 3D MCM-41 scaffolding. The presence of the mesoporous structure in the MCM-41 calcined sample and final functionalized solids is also observed from the TEM analysis (see text). XRD pattern for **S3** also shows with respect to the MCM-41 calcined solid the loss of the (110) and (200) reflections as consequence of the presence of the dye onto the pores (see Figure **SI-3**)

The N_2 adsorption-desorption isotherms of the MCM-41 calcined material shows a typical curve for these mesoporous solids; i.e. an adsorption step at intermediate P/P_0 value 0.3 (see Figure **SI-4**). This curve corresponds to a type IV isotherm, in which the observed step can be related to the nitrogen condensation inside the mesopores by capillarity. The absence of a hysteresis loop in this interval and the narrow pore distribution suggest the existence of uniform cylindrical mesopores (0.85 $cm^3 \cdot g^{-1}$). The application of the BET model resulted in a value for the total specific surface of 1246 m^2/g. From the XRD, porosimetry and TEM studies, the a_0 *cell parameter* (38.29 Å), the *pore diameter* (2.39 nm) and a value for the *wall thickness* of 12.70 Å can be calculated. The N_2 adsorption-desorption isotherms of

S1 (see Figure **SI-4**) is typical of mesoporous systems with filled mesopores and a significant decrease in the N_2 volume adsorbed is observed (see Figure **SI-4**). The same behavior was found for **S3** (not shown). In fact, these solids presents relative flat curves when compared (at the same scale) to those of the MCM-41 parent material, indicating that there is a significant pore blocking resulting in the absence of appreciable porosity. Similar results have been observed by us in related systems. Moreover, the lack of porosity together with the typical mesoporous-like X-ray powder diffraction profile (showing a characteristic intense peak at low angle values) and the TEM images for **S1** and **S3** provides direct evidence of the high efficiency of the dye loading.

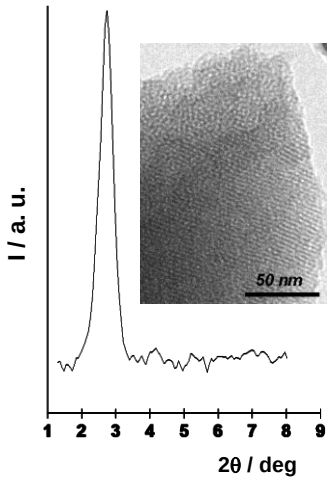

Figure SI-3.- Powder X-ray pattern and TEM image (inset) of the solid **S3**.

The transformation of **S1** to **S1-AB** by the addition of the antibody should not significantly alter the structural order of the mesoporous support. Unfortunately, it was not possible to carry out additional studies (e.g. XRD, N_2 adsorption-desorption techniques) on **S1-AB** due to the very low quantity prepared (in the range of μg) limited by the amount of antibody. However, and despite this lack of complete characterization, the behaviour observed for **S1-AB** is fully consistent with the capping-uncapping procedure described in Scheme **1** (vide infra).

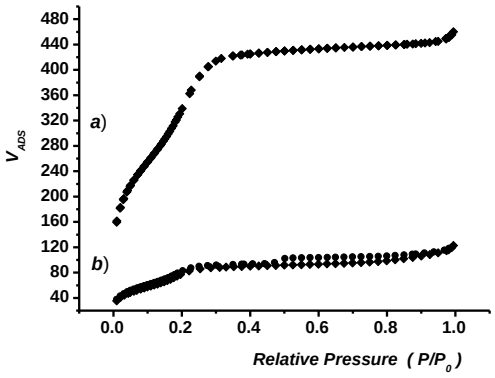

Figure SI-4: Nitrogen adsorption-desorption isotherms for (a) the MCM-41 mesoporous material and (b) the dye-loaded and functionalized **S1** material. V_{ADS} is the volume adsorbed (cm^3/g).

The thermal analysis of the **S1**, **S2** and **S3** solids shows typical behaviour in functionalised mesoporous materials; i.e. a first weight loss between 25 and 150ºC related to the solvent evolution, a second step, between 150 and 800 ºC due to the combustion of the organics and a final loss in the 800 - 1000 ºC range related to the condensation of the silanol groups.

The content of hapten derivative **2** and dye in **S1**, and dye in **S2** and polyamine **3** and dye in **S3** was determined by elemental analysis and thermogravimetric studies. From elemental analysis of C, H, N, S it is possible to determine the amount of hapten **2** and polyamine **3** and dye contained in the materials calculated in millimole per gram of SiO_2 (mmol g^{-1} SiO_2) using equation 1:

$$\alpha_A = \frac{\Delta W_i\% \times 1000}{\Delta W_{SiO_2}\% \times nM_i} \quad (1)$$

where $\Delta Wi\%$ (i = C, N, S) are the weight percentages of carbon, nitrogen or sulphur, M_i is the corresponding atomic weight and n is the number of the corresponding atom type in one molecule. $\Delta WSiO_2\%$ is the inorganic SiO_2 content

in weight percentage. In addition, the content of dye in solid **S1-AB** and **S3-AB** were determined from the dye content in **S1** and **S3** after interaction with the antibody and determining the amount of dye delivered when washing the solids. Also, the amount of dye delivered from **S1-AB** and **S3-AB** in the presence of STZ and other sulfonamides was determined by using values of intensity of the fluorescence bearing in mind that, at low concentrations, relation between concentration and intensity are linear. Values of content are detailed in Table **2** in the manuscript.

Taking into account different amounts of STZ that induced the observed dye release and assuming that two molecules of STZ interacts with one antibody molecule we can estimate that **S1**-**AB** material contains 1.74 x 10^{18} antibody molecules/g of solid. Additionally, and according to a typical external surface for the solid MCM-41 of ca. 100 m^2/g and the antibody content calculated previously, the average surface coverage on solid **S1** by antibody molecules amounts ca. 0.0174 molecules/nm^2. This antibody surface coverage resulted in an average distance between antibody molecules of about 7.6 nm. This value is in agreement with the typical effective antibody molecular radius of about 5.5 nm. Additionally, bearing in mind again a typical value of external surface of MCM-41 solids (ca 100 m^2/g) and the content of hapten (in millimole/g SiO_2) calculated with elemental analysis and thermogravimetric studies, the average surface coverage on solid **S1** by hapten molecules amounts ca. 1.5 molecules/nm^2. With the antibody and hapten contents calculated previously a ratio of ca. 86 hapten molecules / antibody molecules was estimated.

Delivery studies

A certain amount (usually 1 ppm) of sulfathiazole (or other sulfonamides) in 250 μL of a solution containing PBS 1x were added to 200 μg of **S1-AB** or **S3-AB** and the suspension was stirred in order to establish a competition for the antibody between the anchored hapten and the free sulfathiazole. The release of the dye was also determined using solutions of **S1-AB** or **S3-AB** under similar conditions

but in absence of sulfathiazole. Figure **SI-5** shows the emission spectrum (λ_{exc} = 453 nm) of the $[Ru(bipy)_3]^{2+}$ dye from solid **S1-AB** in PBS 1x (pH 7.5) in the absence (a) and in the presence (b) of 1 ppm of sulfathiazole after 2 hours.

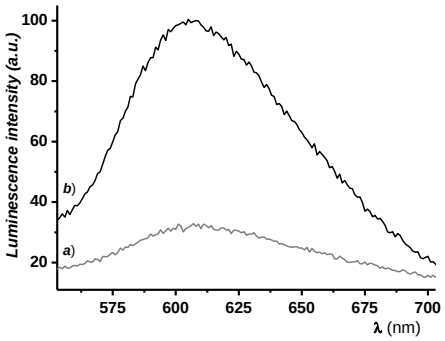

Figure SI-5.- Emission spectrum (λ_{exc} = 453 nm) of the $[Ru(bipy)_3]^{2+}$ dye from solid **S1-AB** in PBS 1x (pH 7.5) in the absence (a) and in the presence (b) of 1 ppm of sulfathiazole after 2 hours.

References

1. Pastor-Navarro, N.; García-Bover, C.; Maquieira, A.; Puchades, R. *Anal. Bioanal Chem*, **2004**, *379*, 1088-1099.
2. J.J Langone, H. van Vunakis, *Methods Enzymol*., **1982**, *84*, 628-640.
3. a) Bernardos, A.; Aznar, E.; Coll, C.; Martínez-Máñez, R.; Barat, J.M.; Marcos, M.D.; Sancenón, F.; Benito, A.; Soto, J. *J. Control Release* **2008**, *131*, 181-189. b) Casasús, R.; Climent, E.; Marcos, M.D.; Martínez-Máñez, R.; Sancenón, F.; Soto, J.; Amorós, P.; Cano, J.; Ruiz, E. *J. Am. Chem. Soc*., **2008**, *130*, 1903-1917.

Antibody-Capped Mesoporous Nanoscopic Materials: Design of a Probe for the Selective Chromo-Fluorogenic Detection of Finasteride

Estela Climent,[a,b,c] Ramón Martínez-Máñez,[a,b,c] Angel Maquieira,[a,b] Félix Sancenón,[a,b,c] María Dolores Marcos,[a,b,c] Eva María Brun,[a,b] Juan Soto,[a,b,c] and Pedro Amorós.[d]

[a] Instituto de Reconocimiento Molecular y Desarrollo Tecnológico.
Centro Mixto Universidad Politécnica de Valencia – Universidad de Valencia.
[b] Departamento de Química, Universidad Politécnica de Valencia
Camino de Vera s/n, 46022, Valencia, Spain.
[c] Centro de Investigación Biomédica en Red de Bioingeniería, Biomateriales y Nanomedicina (CIBER-BBN)
[d] Institut de Ciència del Materials (ICMUV), Universitat de València. P.O. Box 2085, E-46071 València, Spain

Received: October 23, 2011

Chemistry Open, ***2012****, 1, in press*
DOI: 10.1002/open.201100008

Abstract

The synthesis of capped mesoporous silica nanoparticles (MSN) conjugated with an antibody (AB) as a gatekeeper has been carried out in order to obtain a delivery system able to release a entrapped cargo (dye) in the presence of a target molecule (antigen) to which the conjugated antibody binds selectively. In particular, MSN loaded with rhodamine B and functionalized on the external surface with a suitable derivative of *N*-(*t*-butyl)-3-oxo-(5α,17β)-4-aza-androst-1-ene-17-carboxamide (finasteride) have been prepared (**S1**). The addition of polyclonal antibodies against finasteride induced capping of the pores due to the interaction with the anchored hapten-like finasteride derivative to give a MSN-hapten-AB nanoparticle **S1-AB**. It was found that the addition of capped material **S1-AB** to water solutions containing finasteride resulted in displacement of the antibody, pore uncapping and entrapped-dye release. The response of the gated material is highly selective, and only finasteride, among other steroids, was able to induce a significant uncapping process. Compared with finasteride, the finasteride metabolite was able to release 17 % of the dye, whereas the exogen steroids testosterone, metenolone and 16-β-hydroxystanozolol only induced very little release of rhodamine B (lower than 10%) from aqueous suspensions containing sensing solid **S1-AB**. A detection limit as low as 20 ppb was found for the fluorimetric detection of finasteride. In order to evaluate a possible application of the material for label-free detection of finasteride, the capped material was isolated and stored to give final sensing solid **S1-AB-i**. It was found to display a similar behavior towards finasteride as to that shown by freshly prepared **S1-AB**; even after a period of two months, no significant loss of selectivity or sensitivity was noted. Moreover, to study the application for the detection of finasteride in biological samples, this "aged" material, **S1-AB-i**, was tested using commercially available blank urine as matrix. Samples containing 70 and 90% blank urine were spiked with a defined amount of finasteride, and the concentration was determined using capped **S1-AB-i**. Recovery ranges from 94% to 118% were reached.

Introduction

The design of delivery systems able to selectively release entrapped guests in the presence of target molecules is a new research field that has recently attracted great attention.[1] Traditional delivery systems are based on organic polymers that usually release their cargo through diffusion-controlled processes or degradation of the polymeric matrix.[2] As an alternative, in recent years, silica mesoporous supports have been used as inorganic scaffolds for the storage and controlled release of drugs and organic molecules. The unique properties of mesoporous silica materials, such as the presence of ordered tailor-made mesopores with stable structures, large surface areas, bio-compatibility and the possibility to include gate-like scaffoldings on the external surface for the design of nanodevices for on-command delivery applications, make these solids suitable supports for the development of carriers for cargo delivery.[3] In these systems, mass transport can be controlled using molecular and supramolecular interactions or suitable physical stimuli.[4] In particular, delivery of the cargo in gated materials have been reported using changes in pH,[5] temperature,[6] redox potential,[7] light,[8] and the presence of small molecules.[9] However, despite these interesting examples, some of the described systems show disadvantages for their potential use in advanced applications, such as a lack of function in aqueous environments and the use of complex stimuli for mass transport control. Moreover, examples of controlled guest release in response to small molecules or biomolecules are still very rare. One of the most frequently used types of biomolecules for the development of gated hybrid materials are enzymes. The wide collection of available enzymes that can selectively catalyze a large number of different chemical reactions makes these systems very appealing for the design of sensitive and specific mesoporous silica nanoparticles (MSN)-based nanodevices.[10] Also, in this field we and others have reported the use of oligonucleotides for the design of gated MSN for delivery applications.[11]

Furthermore, it is apparent from the literature that most of the reported gated materials have been designed toward the development of advanced drug-delivery systems, but very few examples of pore-blockage or pore-opening protocols for

sensing applications have been reported.[9] However, the design of such systems able to respond to the presence of target molecules is an attractive approach for the development of new sensing paradigms. The protocol involves the use of selective molecular recognition events that control the gate-like scaffolding. The addition of the solid to a solution containing the target molecule induces pore opening and delivery of a suitable dye. If the opening and dye release is a consequence of a selective interaction, the recognition event is translated into a selective optical response. This approach separates the recognition protocols from the signaling event making sensing independent of the stoichiometry of the host-guest complex and, in some cases, simultaneously displaying features of signal amplification.

Given our interest in the development of advanced bio-inspired strategies on inorganic materials for sensing applications using biomolecules, we recently combined the use of antigen-antibody interactions with the preparation of capped MSN able to selectively deliver an entrapped dye in the presence of sulfathiazole.[12] In particular, we believe that the use of antibodies could be a promising approach for the design of custom-made nanodevices for controlled delivery specifically triggered by target guests. The possibility of selecting antibodies for a countless number of antigens, including low molecular weight targets, makes this approach highly appealing for a wide range of applications. Additionally, this approach opens the possibility of developing novel label-free immunoassay paradigms in which the properties of the reporter (cargo) could be selected at will. Inspired by these previous results, we report herein the preparation of antibody-capped MSN for the selective fluorogenic signaling of finasteride, a substance used in sport doping.

Results and Discussion

Design and synthesis of gated MSN

The incorporation of gate-like ensembles on mesoporous scaffolds has proven to be a suitable approach for the development of nanoscopic solids for mass-transport control and for studying the factors that could influence the design of

gating functions. Additionally, as stated above, very few examples have been reported that use capped materials for the design of new sensing concepts. Moreover, in this particular field, the use of antibodies or other biomolecules as "biological keys" opens a wide range of possible opportunities for the design of new sensing protocols. In this study, we selected MSN from the MCM-41 family as the support. This is a suitable inorganic matrix that displays several appropriate characteristics, such as homogeneous porosity, high inertness and ease of functionalisation. Moreover, MCM-41 materials usually contain mesopores in the 2-3 nm range, which allows a rapid uptake and release of selected guests.

We focused our attention on the potential detection of finasteride, a 5α-reductase inhibitor. Finasteride is known to convert testosterone to the more potent androgen 5α-dihydrotestosterone, a class of drug that is used therapeutically to prevent prostate cancer, treat benign prostatic hyperplasia and male baldness. It has been reported that administration of inhibitors of 5α-reductase, such as finasteride, can complicate the evaluation of steroid profiles in sport doping control, causing erroneous results. The reason lies in the suppression of production and renal excretion of 5α-reduced metabolites of anabolic steroids that can produce false-negative doping-control results. In a previous work, an enzyme-linked immunosorbent assay for the detection of finasteride was reported.[13] In this work, a collection of immunoreagents and antiserum were obtained from which we selected the best hapten--antiserum pair for the development of an antibody-capped mesoporous hybrid nanomaterial for the fluorimetric detection of finasteride (see below).

Scheme 1 shows the proposed paradigm using the gated support. Nanoparticles of mesoporous MCM-41 are first loaded with a fluorophore (rhodamine B), then, the external surfaces of the nanoparticles are functionalized with hapten-like derivative **II** to give solid **S1**. Finally the mesopores are capped with finasteride antibodies (AB) via interactions of the two binding IgG regions of the antibody with anchored **II**, giving solid **S1-AB**. Addition of the correspondent antigen, finasteride, induces uncapping of the pores and release of the entrapped

fluorophore. The uncapping process is easily monitored by measuring the emission intensity of rhodamine B at 580 nm (λ_{exc}=555 nm) in the aqueous phase.

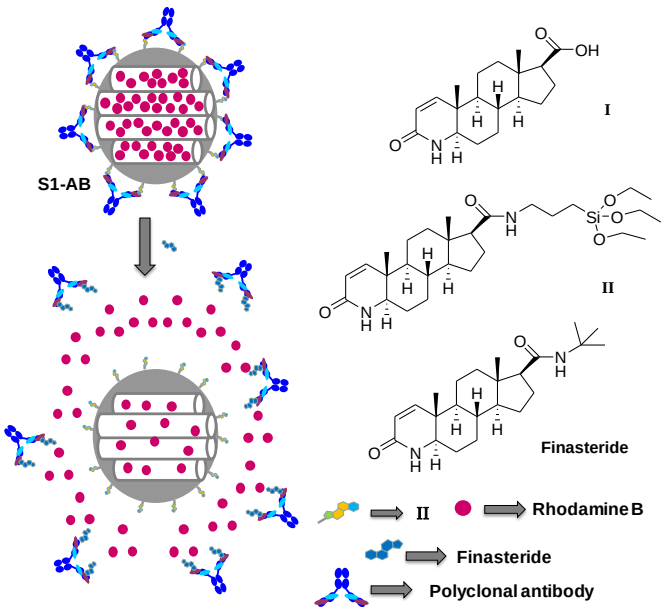

Scheme 1. Representation of the gated material **S1-AB** capped with an antibody, the products (**I**) and (**II**) and the antigen finasteride.

For the preparation of solid **S1**, the hapten-like molecule **I** was selected. Capped materials obtained from **I** (via anchorage of silyl derivative **II**) proved to give a suitable response in terms of time and sensitivity (see below). Compound **II** was readily obtained through reaction of **I** with (3-aminopropyl)triethoxysilane. To prepare the final hybrid material **S1**, we made use of a two-step synthetic procedure. First, the mesoporous starting scaffold was added to a solution containing a high concentration of rhodamine B in order to reach an efficient loading of the pores. Second, organosilane derivative **II** was added. During the grafting of **II**, a high concentration of rhodamine B was contained in the solution, which inhibits diffusion of the dye from the pores into the solution and simultaneously hampers the entrance of **II** into the pores. Moreover, it has been reported that the reaction of organosilane derivatives with siliceous surfaces is usually quicker than diffusion processes from the pores.[9a-c] These features lead to

the reasonable assumption that rhodamine B is captured within the mesopores and derivative **II** is anchored on the external surface of the final nanoparticles. Purple solid **S1** was isolated by filtration, washed with acetonitrile and dried at 35°C for 12 h. Solid **S2** containing rhodamine B within the pores, but lacking derivative **II** was also prepared as a control.

Capping optimization with the specific polyclonal antibodies for finasteride was carried out by stirring solid **S1** (1 mg) for one hour in different aqueous dilutions of serum **I** (0.5 mL, pH 7.4; dilutions of 2.5:100, 1.25:100, 0.625:100 or 0.3125:100). After the capping process, the aqueous phase was removed by centrifugation, and the solid was washed twice to remove residual dye from the uncapped pores. The final material was suspended in water (0.025 mg mL^{-1}; pH 7.4), and the kinetic release of rhodamine B was measured by monitoring the fluorescence emission at 580 nm (λ_{exc}=555 nm). The most effective capping was observed with a 1.25:100 dilution of serum **I**. Lower proportions of serum showed only partial capping of the pores, which was reflected in significant rhodamine B release.

Characterization of the hybrid materials

The prepared solids were characterized using standard techniques. Figure 1 shows powder X-ray diffraction (PXRD) patterns of synthesized MCM-41, calcined MCM-41, and **S1**. The PXRD of synthesized, siliceous nanoparticulated MCM-41 (Figure 1a) shows the typical four low-angle reflections attributed to a hexagonal array that index as (100), (110), (200), and (210) Bragg peaks. From the PXRD data of synthesized MCM-41, a d100 spacing of 40.93 Å was calculated. A significant displacement of the (100) peak in the PXRD of the calcined nanoparticulated MCM-41 was found corresponding to an approximate cell contraction of 2 Å (Figure1b). This displacement and broadening of the (110) and (200) peaks are related to further condensation of silanol groups during the calcination step. Figure1c shows the PXRD patterns for solid **S1**. In this curve, the reflections (110) and (200) are less intense, most likely due to a reduction in contrast as a consequence of the pore loading with the dye and the functionalization with derivative 2. Nevertheless, the clear presence of the (100) peak in the PXRD

patterns indicates that the process of pore loading with rhodamine B and the additional functionalization with **II** did not modify the mesoporous structure of the MCM-41 support to a large extent.

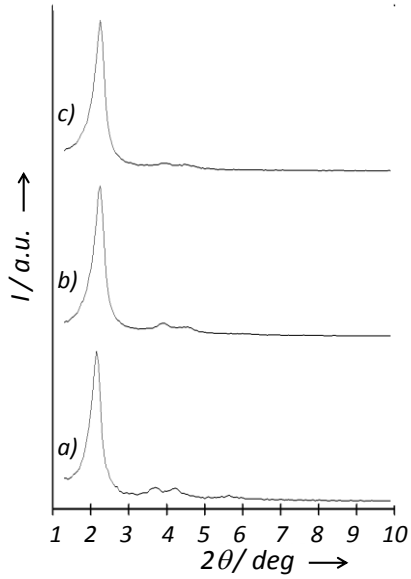

Figure 1. Powder X-ray patterns of the solids (a) MCM-41 as synthesized (b) calcined MCM-41 and (c) solid **S1** containing the dye Rhodamine B and product **II**.

The mesoporous structure of the functionalized solid **S1** and the capped material **S1-AB** was also confirmed using transmission electron microscopy (TEM) analysis. The synthesized MCM-41 support was obtained as spherical particles with diameters ranging from 80 to 150 nm. Figure 2 shows TEM images for **S1** and **S1-AB**. In both cases, the typical hexagonal porosity and channels of the MCM-41 matrix as alternate black and white stripes are observed.

The N_2 adsorption--desorption isotherm of the calcined nanoparticulated MCM-41 is shown in Figure 3a. A typical curve for mesoporous solids consisting of an adsorption step at intermediate P/P_0 values (0.25-0.4) is observed. This curve corresponds to a type IV isotherm, in which the observed step indicates nitrogen condensation inside the mesopores. In the solids, the existence of uniform

cylindrical mesopores (pore diameter of 2.62 nm and pore volume of 0.88 $cm^3\ g^{-1}$, calculated using the Barret, Joyner and Halenda (BJH) model on the adsorption branch of the isotherm) is suggested by the absence of a hysteresis loop in this interval and the narrow BJH pore distribution (Table 1). The application of the Brunauer, Emmett and Teller (BET) model resulted in a value of 1053.4 $m^2\ g^{-1}$ for the total specific surface.

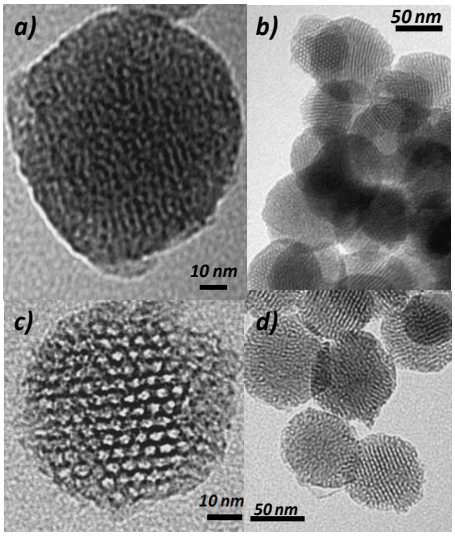

Figure 2. TEM images of solid **S1-AB** (a), solid **S1** (b) and calcined MCM-41 sample (c and d) showing the typical hexagonal porosity of the MCM-41 mesoporous matrix.

From the PXRD, porosimetry and TEM studies, the a_0 *cell parameter* (4.57 nm), *pore diameter* (2.62 nm), and value for the *wall thickness* (1.95 nm) were calculated. In addition to this adsorption step associated to the micelle generated mesopores, a second feature appears in the isotherm at a high relative pressure (P/P_0>0.85). This adsorption corresponds to the filling of the large voids among the particles (pore diameter of 36.4 nm and pore volume of 0.42 $cm^3\ g^{-1}$, calculated by using the BJH model) and therefore must be considered as a textural-like porosity. The N_2 adsorption-desorption isotherm of **S1** is shown in Figure 3b. Solid **S1** presents a similar adsorption-desorption isotherm to the one observed with calcined MCM-41. However, the specific surface and pore volume of **S1** is reduced by ~50 %, that is, a BJH mesopore volume of 0.44 $cm^3 g^{-1}$ and

surface area of 625.2 m^2g^{-1} were calculated. This decrease in volume of adsorbed N_2 and in pore size is ascribed to the presence of the dye and anchored derivative **II** on the external surface of **S1**. The moderate decrease on the specific surface area and pore volume in **S1** is most likely due to the fact that the pores are not completely closed. Additionally, the textural porosity is preserved strongly suggesting that dye molecules are placed inside the mesopores and not in the interparticle porosity.

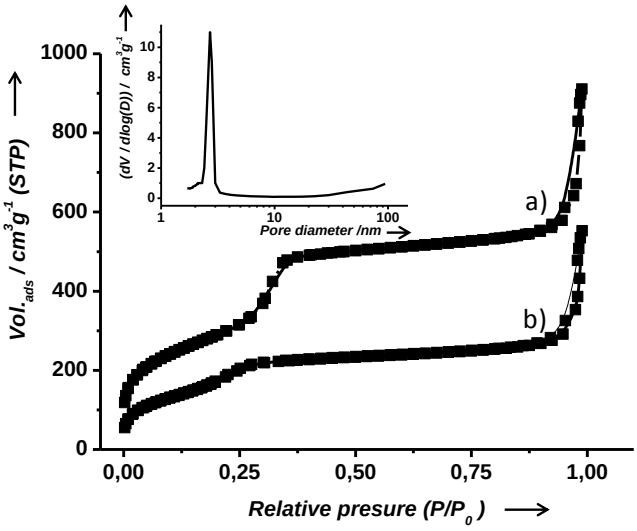

Figure 3. Adsorption-desorption isotherms for (a) **MCM-41** MSN and (b) dye-loaded and functionalized **S1** material. Inset: Pore size distribution of **MCM-41** mesoporous material.

As described above, the transformation of **S1** to **S1-AB** by the addition of antibody does not significantly alter the structural order of the mesoporous support based on TEM images of this solid. Unfortunately, it was not possible to carry out additional PXRD or N_2 adsorption-desorption studies on **S1-AB** due to the small amount of material prepared. However, despite this lack of complete characterization, the behavior of **S1-AB** is fully consistent with the capping-uncapping procedure described in Scheme 1 (see below).

Table 1. BET specific surface values, pore volumes and pore sizes calculated from the N_2 adsorption-desorption isotherms for selected materials.

Solid	S_{BET} ($m^2\ g^{-1}$)	**Pore Volume** ($cm^3\ g^{-1}$)	**Pore size** (nm)
MCM-41	1053.4	0.88	2.62
S1	625.2	0.44	2.33
S3	110	0.35	2.18

The quantity of derivative **II** and dye in **S1** and dye in **S2** was determined by elemental analysis and thermogravimetric studies. The thermal analysis of **S1** and **S2** shows a typical behavior of functionalized mesoporous materials, that is, an initial weight loss between 25 and 150°C related to solvent evaporation, a second loss between 150 and 800°C due to the combustion of organic material, and a final loss in the 800-1000°C range related to the condensation of the silanol groups. The dye content in solid **S1-AB** was determined from the difference between the amount measured for **S1** and the amount released into the aqueous washing fractions of the solid after interaction with the antibody (Table 2).

With the aim of estimating the amount of antibody in solid **S1-AB**, concentrations of immunoglobulin G (IgG, the most abundant type of antibody in plasma) were measured in serum **I** and in the aqueous solutions after the capping process by measuring the absorbance at 280 nm. Considering an average molecular weight (MW) of 150 kDa and the specific molar extinction coefficient of immunoglobulin, a concentration in serum **I** of 5.3 mg mL^{-1} was found. Taking into account the absorbance measurements, an estimated 87% of the antibodies were incorporated in **S1-AB** when a serum dilution of 1.25 : 100 was used. With this data and the known concentration of IgG in serum **I**, it can be estimated that one gram of **S1-AB** contains 1.16×10^{17} immunoglobulin molecules. Additionally, considering the typical external surface of an MCM-41 support, an average distance between two immunoglobulin molecules of $\sim$ 17 nm is calculated (for

details, see the Supporting Information). The amounts of compound **II**, antibody and rhodamine B in **S1**, **S1-AB** and **S2** are shown in Table 2.

Table 2. Content of product **II**, dye and IgG in mmol per gram of solid for **S1, S1-AB** and **S2.**

Solid	*Product II*	*Rhodamine B*	*IgG*
S1	0.275	0.389	----
S1-AB	0.275	0.298	0.0001926
S2	----	0.403	----

Functional antigen-driven controlled release

Several experiments were carried out in order to study the antigen-responsive controlled-release protocol using capped material **S1-AB** and finasteride as a trigger. The uncapping protocol, that is, the delivery of the entrapped dye from the pore voids to the aqueous solution, was observed with ease by monitoring the emission band of rhodamine B centered at 580 nm (λ_{exc}=555 nm) in the aqueous phase. In a typical experiment, a suspension of **S1-AB** (0.2 mL, 2 mg mL^{-1}) was diluted with water (9.8 mL, pH 7.4) containing finasteride (130 ppm). A corresponding experiment was carried out under similar conditions using **S1-AB** but in the absence of finasteride. At a given time point, 1 mL of each suspension was filtered, and the emission of rhodamine B was measured at 580 nm.

From the kinetic-release curves shown in Figure 4, it can be seen that solid **S1-AB** was unable to release rhodamine B in the absence of finasteride, whereas in the presence of the antigen a remarkable delivery of the dye was found (Figure 4a and b). In this case, maximum delivery of dye was achieved after approximately 15 min. The release of rhodamine B was a direct consequence of the displacement process of the antibody from the outer surface of **S1-AB** induced by the presence of free finasteride. The observed uncapping process is caused by the stronger interaction of finasteride with the capping antibody compared with the interaction of the antibody and grafted **II**. In fact, when the same experiment is repeated in the presence of compound **I** instead of finasteride, only 23 % dye

release is observed (compared with the amount of dye released in the presence of finasteride, i.e., 100 %).

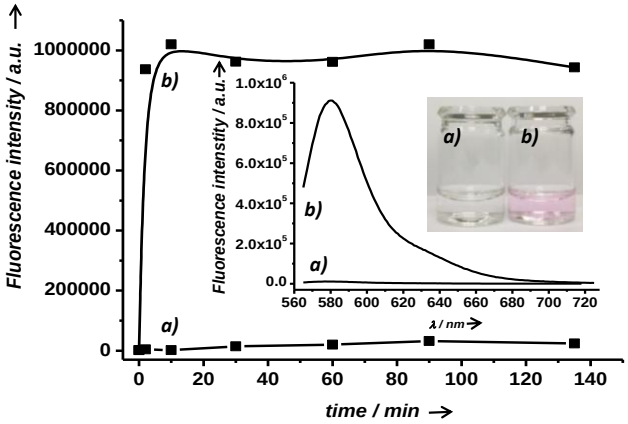

Figure 4. Fluorescence intensity of rhodamine B released measured at 580 nm (excitation at 555 nm) versus time from **S1-AB** solids in water at pH 7.4, in the absence (a) and in presence of 130 ppm of finasteride (b). Inset: Fluorescence spectra of solution containing rhodamine B after filtration in absence (a) and in presence of finasteride (b) at 2 min. The fluorescence of the dye was measured after the suspension filtration (0.45 μm teflon filters). A photograph showing the colorimetric response is also shown.

Similar kinetic experiments with **S1-AB** using lower amounts of finasteride were carried out. In those cases, a lower amount of dye was released (rhodamine B delivery was proportional to the concentration, see below), and overall slower delivery kinetics were found. Finally, a release time of 75 min was selected for further experiments in order to reach a maximum dye delivery for all tested finasteride concentrations.

Figure 5 shows the fluorescence intensity of rhodamine B released from solid **S1-AB** measured in water (pH 7.4) as a function of the concentration of finasteride. The delivered amount of cargo is proportional to finasteride concentration displaying a typical noncompetitive immunoassay response curve, which is in accordance with an uncapping protocol based on the displacement of the antibody, as indicated above. From these studies, a detection limit for finasteride of 20 ppb was calculated.

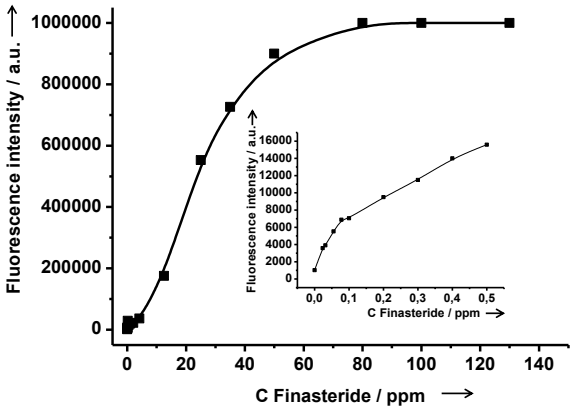

Figure 5. Fluorescence intensity of rhodamine B released from **S1-AB** solid measured at 580 nm (λ_{ex} = 555 nm) in water at pH 7.4 as a function of the concentration of finasteride at 75 min. The fluorescence of the dye was measured after filtration. The inset shows rhodamine B release for low concentration range of finasteride.

Selectivity studies

It is well-known that antibodies can ideally identify and bind only to their unique antigen in complex mixtures. This property allows the design of highly selective capping systems that can ideally be opened using a unique "molecular key". In order to investigate the selectivity in the opening protocol of our system, dye delivery from solid **S1-AB** was tested in the presence of other exogen steroids that produce similar effects to finasteride. The uncapping ability of these closely related molecules (at 1 ppm) is shown in Figure 6, which displays the fluorescence of the released dye from **S1-AB** after 75 min in the presence of the steroids finasteride, finasteride metabolite, testosterone, metenolone, 16-β-hydroxystanozolol, dutasteride, oxandrolone, 1-testosterone, androstanolone, or testosterone glucuronide (for chemical structures, see the Supporting Information). A very selective uncapping process in the presence of finasteride was observed. Only finasteride metabolite is able to release 17% of the dye (relative to finasteride), whereas the exogen steroids testosterone, metenolone and 16-β-hydroxystanozolol induced a very small release of rhodamine B (lower than 10 %) from aqueous suspensions of the sensing solid **S1-AB**.

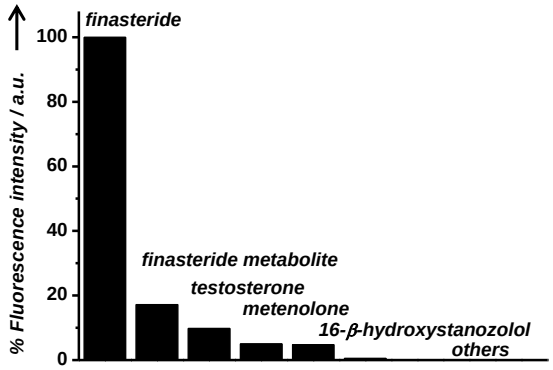

Figure 6. Emission intensity measured (%) at 580 nm (excitation at 555 nm) of rhodamine B released from **S1-AB** in water at pH 7.4 in presence of exogen steroids finasteride, dutasteride, finasteride metabolite, metenolone, oxandrolone, 16-β-hydroxystanozolol, 1-testosterone, androstanolone (DHT), testosterone and testosterone glucuronide (all at 1ppm concentration). The fluorescence of the dye was measured after filtration of the corresponding suspensions.

In addition to these delivery studies with **S1-AB**, further control experiments were carried out using solid **S2**, in order to evaluate the effect on the selective delivery process of the anchored hapten. Unlike **S1-AB**, solid **S2** contains rhodamine B in its mesopores but does not have any additional functionalization. Aqueous suspensions of solid **S2** (pH 7.5) alone showed a fast dye release. However in the presence of antibody, dye delivery was strongly inhibited due to unspecific adsorption of the antibody onto the surface of **S2**, most likely through interactions with the silanol groups on the silica mesoporous supports (SMPS). Very importantly, the addition of finasteride to **S2-AB** did not lead to cargo delivery, even when large amounts of finasteride were added (up to 200 ppm).

Storage of the sensing material and assays with urine standard

In order to improve the properties of **S1-AB** for a potential application in the detection of finasteride, we tried to isolate and store solid **S1-AB**. The final sensing material (**S1-AB-i**) was prepared from **S1-AB**, which was further dried in vacuo overnight and then stored at 4°C. It was found that, even after a period of two months, stored solid **S1-AB-i** showed a similar sensing behavior toward

finasteride as that shown by freshly prepared **S1-AB** without significant loss of selectivity or sensitivity.

Moreover, in order to study the possible application in the detection of finasteride in biological samples, **S1-AB-i** was tested using commercially available blank urine as matrix. In a first step, the tolerance of the solids to urine was studied. In a typical experiment, **S1-AB-i** (0.45 mg) was suspended in urine (5 mL), and the suspension was then diluted with varying amounts of water (pH 7.4). Following this procedure, calibration curves for finasteride containing 50, 70 and 90% urine were obtained, and a similar linear range for all three tested dilutions was found. Moreover, it was confirmed that the results using solid **S1-AB-i** were similar to those obtained for **S1-AB**. In a second step, urine samples containing 70 and 90% urine were spiked with finasteride, and the concentrations were determined using the previously obtained calibration curve. The results found are shown in Table 3. Target analyte spike recoveries in the range of 94-118 % were achieved.

Table 3. Finasteride concentrations in samples containing 70% and 90% of urine determined using solid **S1-AB-i**.

% Urine Added	C Finasteride added (ppb)	C Finasteride found (ppb)	Recovery %
70	33.3	35.57 ± 2.56	106.7
70	66.6	62.92 ± 2.03	94.4
90	30	35.38 ± 1.17	117.9
90	60	58.57 ± 1.84	97.6

Conclusion

In summary, the use of antibodies as gatekeepers on the surface of MSN provides a suitable tool for the design of delivery systems able to release entrapped guests in the presence of target molecules (antigen) to which an antibody binds selectively. In this work, we prepared MSN loaded with rhodamine B and functionalized with a suitable derivative of finasteride on their external surface.

Addition of polyclonal antibodies for finasteride induced the capping of the pores due to the interaction with the anchored hapten-like derivative. This material was used for the fluorimetric recognition of finasteride and is one of the few examples that use a capped system and opening protocols for chemosensing applications. It was found that addition of the capped material to water solutions containing finasteride resulted in a displacement of the antibody, uncapping of the pores and release of the entrapped dye. The response of this gated material is highly selective, and only finasteride, among other steroids, was able to trigger dye delivery. A detection limit as low as 20 ppb was found for the fluorimetric detection of finasteride. Although this detection limit is higher than the value obtained using an enzyme-linked immunosorbent assay (ELISA, 0.01 ppb),[13] we believe that gated SMPS based on the use of antibodies could be a promising route for the development of custom-made, controlled-delivery nanodevices specifically triggered by target molecular guests. The possibility of including antibodies as caps on diverse supports, the choice of the cargo molecule (e.g., various dyes and fluorophores), and the potential design of nanoparticles containing two or more different loaded signaling molecules capped with their corresponding antibodies open the door to the design of new multiplex label-free immunoassay protocols. Further studies in this field are ongoing. It is important to note that the use of capped nanoparticles introduces two remarkable advantages into the immunoassay developed format. One is the direct displayed response, which means that increasing the target concentration in samples results in an increase of the analytical signal. Secondly, for this format it is not necessary to synthesize the typical tracers used in ELISA or other immunoassay-labeled formats. In a wider context, this work suggests that the combination of SMPS with suitable binding sites is an excellent starting point for applying the versatility of supramolecular ideas to the design of nanoscopic devices, which is a promising approach for bringing molecular and supramolecular concepts to new advances in the field of nanoscience.

Experimental Section

General techniques

Powder X-ray diffraction (PXRD) and thermogravimetric analysis (TGA), elemental analysis, transmission electron microscopy (TEM), N_2 adsorption--desorption, NMR, UV-visible (UV-vis) and fluorescence spectroscopy were employed to characterize the synthesized materials. PXRD measurements were performed on a D8 Advance diffractometer using Cu Kα radiation (Philips, Amsterdam, The Netherlands). Thermogravimetric analyses were carried out on a TGA/SDTA 851e balance (Mettler Toledo, Columbus, OH, USA), using an oxidizing atmosphere (air, 80 mL min^{-1}) with a heating program: gradient of 393-1273 K at 10 °C min^{-1}, followed by an isothermal heating step at 1273 °C for 30 min. TEM images were obtained with a 100 kV CM10 microscope (Philips). N_2 adsorption-desorption isotherms were recorded with an ASAP2010 automated sorption analyzer (Micromeritics, Norcross, GA, USA). The samples were degassed at 120°C in vacuo overnight. The specific surface areas were calculated from the adsorption data in the low pressure range using the Brunauer, Emmett and Teller (BET) model. Pore size was determined following the Barret, Joyner and Halenda (BJH) method. ^{1}H and ^{13}C NMR spectra were acquired with a Varian 300 spectrometer (Sunnyvale, CA, USA). UV-vis spectroscopy was carried out using a Lambda 35 spectrometer (PerkinElmer Instruments, Waltham, MA, USA). Fluorescence spectroscopy was carried out on a Felix 32 Analysis version 1.2 (Build 56, Photon Technology International, Birmingham, NJ, USA). The polyclonal-based antibodies for finasteride were obtained according to Ref. 13.

Chemicals

Tetraethylorthosilicate (TEOS), *N*-cetyltrimethylammonium bromide (CTAB), NaOH, (3-aminopropyl)triethoxysilane, rhodamine B, finasteride, chemical reagents for hapten derivative synthesis (*N,N*′-dicyclohexylcarbodiimide and *N*-methylsuccinimide), bovine serum albumin (BSA), complete and incomplete Freund's adjuvant and Tween 20 were purchased from Sigma-Aldrich Química (Madrid, Spain). Dutasteride was purchased from AK Scientific (Union City, CA,

USA). (5α-17β)-3-Oxo-4-aza-androst-1-ene-17-carboxylic acid (**I**) was purchased from Steraloids Inc. (Newport, USA). Keyhole limpet hemocyanin (KLH) was purchased from Pierce Biotechnology (Rockford, IL, USA). Phosphate-buffered saline (PBS, pH 7.4, 20 mm) was prepared containing the following salts: Na_2HPO_4 (16.06 mmol L^{-1}), KH_2PO_4 (2.92 mmol L^{-1}), NaCl (274 mmol L^{-1}) and KCl (5.46 mmol L^{-1}). PBS (20 mmol L^{-1}) was supplemented with Tween 20 (0.05%) to give Tween 20-containing PBS (PBST). All products were used as received.

Synthesis

*N-(3-triethoxysillyl(propyl))-3-oxo-(5α,17β)-4-aza-androst-1-ene-17-carboxamide (**II**).*

A modification of the active ester method for the amidation reaction between compound **I** and (3-aminopropyl)triethoxysilane was used.[1] A mixture of *N*-hydroxysuccinimide (NHS, 90.6 mg, 0.79 mmol) and *N,N'*-dicyclohexylcarbodiimide (DCC, 162.4 mg, 0.79 mmol) in anhyd *N,N*-dimethylformamide (DMF, 1.0 mL) was added to a solution of **I** (238.06 mg, 0.75 mmol) in anhydrous DMF (4 mL). The mixture was stirred at room temperature for 20 h, and precipitated dicyclohexylurea (DCU, white solid) was removed by centrifugation. (3-Aminopropyl)triethoxysilane (150 µL, 0.7 mmol) was added to the solution, and the reaction mixture was stirred at room temperature for 24 h. The solvent was evaporated in vacuo to give a yellow sticky oil. In order to eliminate traces of DCU, CH_2Cl_2 (1 mL) was added, and the solution was filtered through a short silica gel column. The final product **II** was isolated as a colorless oil (0.302 g, 0.58 mmol, 83%): ^{1}H NMR (300 MHz, $CDCl_3$): δ=0.61 (t, 2H, CH_2Si), 0.96 (s, 3H, CH_3C), 1.21 (t, 9H, $SiOCH_2CH_3$), 1.24-2.11 (m, 22H), 3.25 (t, 2H, $NHCH_2CH_2CH_2Si$), 3.80 (q, 6H, CH_3CH_2OSi), 5.78 (d, 1H, COCHC=CH), 6.78 ppm (d, 1H, COCHC=CH); ^{13}C NMR (75 MHz, $CHCl_3$): δ=7.3 (CH_2Si), 11.9 (CH_3), 13.0 (CH_2CH_2Si) 13.3 (CH_3), 18.2 (3C, CH_3CH_2O), 21.1, 24.9, 25.6, 25.9, 29.4, 30.6, 33.8, 35.3, 36.2, 36.6, 39.4 ($NHCH_2CH_2CH_2Si$), 48.8, 55.5, 58.2 (3C, CH_3CH_2O), 59.5, 122.9 (COCHC=CH), 158.4 (COCHC=CH), 164.9 (CONHCH),173.7 ppm ($CONHCH_2$).

MCM-41 mesoporous nanoparticles.

NaOH (2.00 mol L^{-1}, 3.5 mL) was added to a solution of CTAB (1.00 g, 2.74 mmol) in deionized H_2O (450 mL). After the solution temperature was adjusted to 80 °C, TEOS (5.00 mL, 2.57×10^{-2} mol) was added dropwise to the surfactant solution. The mixture was stirred for 2 h to give a white precipitate. The solid was isolated by centrifugation and washed with deionized H_2O and EtOH and then dried at 60°C for 12h to give MCM-41. In order to remove the template phase, MCM-41 was calcined at 550°C using an oxidizing atmosphere.

*Solid **S1**.*

In a typical synthesis, calcined MCM-41 (0.3 g) and rhodamine B (0.115 g, 0.24 mmol) were suspended in CH_3CN (35 mL) and heated at 120°C in a Dean-Stark apparatus to remove adsorbed H_2O by azeotropic distillation under an inert Ar atmosphere. After removing 10 mL, the suspension was stirred at RT for 24 h for loading of the MCM-41 pores. An excess of compound **II** (0.2 g, 0.384 mmol) in $CHCl_3$ (0.5 mL) was added, and the final mixture was stirred at RT for 5.5 h. Resulting solid **S1** was isolated by filtration, washed with CH_3CN (10 mL) and dried at 38°C for 12 h.

*Solid **S1-AB***

In order to prepare solid **S1-AB** and study the interactions between the anchored hapten **II** and the surface of solid **S1**, and the specific polyclonal-based antibodies for finasteride, portions of solid **S1** (1 mg) were suspended in several aqueous dilutions of serum **I** (0.5 mL, pH 7.4; dilutions: 2.5:100, 1.25:100, 0.625:100, and 0.3125:100). Each suspension was stirred at RT for 1 h. After the capping process, the aq phase was removed by centrifugation to eliminate residual dye and free antibody, and the concentration of immunoglobulin (IgG) in the removed aq phase was measured. Results are shown in Table 4. Taking into account the results shown in Table 2, the ideal aq dilution for the preparation of the final material **S1-AB** was 1.25:100 of serum **I** (pH 7.4). Lower concentrations lead to incomplete pore capping, whereas higher concentrations of serum **I** lead to complete pore capping and undesired antibody adsorption.

Table 4. Content of the serum **I** (ml serum / mL solvent) onto **S1-AB**.

Assay	Serum Added	Serum not retained	% retained onto solid S1-AB	IgG[a] μmol/g solid
1	0.025000	0.0057	77.2	0.3418
2	0.012500	0.0016	86.9	0.1926
3	0.006250	-----	100	0.1107
4	0.003125	-----	100	0.0553

[a]Content calculated taking to account a IgG content of 5.3 mg IgG / mL serum, a typical MW for a immunoglobulin of 150.000 Da and an extinction molar coeficient of 210.000 M^{-1} cm^{-1} at 280 nm.

References

[1] a) V. Cauda, L. Muhlstein, B. Onida, T. Bein, *Microporous Mesoporous Mater.* **2009**, *118*, 435-442. b) S. M. Janib, A. S. Moses, J. A. MacKay, *Adv. Drug. Deliv. Rev.* **2010**, *62*, 1052-1063. K. Greish, *Methods Mol. Biol.* **2010**, *624*, 25–37.

[2] a) K. Hoste, K. De Winne, E. Schacht, Int. J. Pharm. 2004, 277, 119-131. K. Harrison *Biomed. Polym.* **2007**, 33-56. b) L. S. Nair, C.T. Laurenciana, *Prog. Polym. Sci.* **2007**, *32*, 762-798. c) T. Traitel, R. Goldbart, J. Kost, *J. Biomater. Sci., Polym.* Ed. **2008**, *19*, 755-767. d) F. Puoci, F. Iemma, N. Picci, *Curr. Drug Deliv.* **2008**, *5*, 85-96. e) F. Siepmann, J. Siepmann, M. Walther, R. MacRae, R. Bodmeier, R. *J. Control, Release,* **2008**, *125*, 1-15. f) S. Liu, R. Maheshwari, K. L. KIck, *Macromolecules*, **2009**, *42*, 3-13.

[3] a) A.B. Descalzo, R. Martínez-Máñez, F. Sancenón, K. Hoffmann, K. Rurack, *Angew. Chem*, **2006**, *118*, 6068-6093; *Angew. Chem. Int. Ed.*, **2006**, *45*, 5924-5948. b) S. Saha, K.C.F. Leung, N.T. Nguyen, J.F. Stoddart, J.I. Zink, *Adv. Func. Mater.* **2007**, *17*, 685-693. c) B.G. Trewyn, I.I. Slowing, S. Giri, H.T. Chen, V.S.-Y. Lin, *Acc. Chem. Res.,* **2007**, *40*, 846-853. d) I.I. Slowing, J.L. Vivero-Escoto, C.W. Wu, V.S.-Y. Lin, *Adv. Drug Deliv. Rev.* **2008**, *60*, 1278-1288. e) H.L. Tu, V.S.-Y. Lin, H.Y. Lin, Y. Hung, L.W. Lo, Y.F. Chen, C. Y. Mou, *Adv. Mater.* **2009**, *21*, 172 – 177.

[4] a) E. Aznar, R. Martínez-Máñez, F. Sancenón, *Expert Opin. Drug Deliv.* **2009**, *6*, 643-655. b) M. Vallet-Regí, F. Balas, D. Arcos, *Angew. Chem. Int. Ed*. **2007**, *46*, 7548-7558; c) K. Cotí, M. E. Belowich,

M. Liong, M. W. Ambrogio, Y. A. Lau , H. A. Khatib, J. I. Zink, N. M. Khashab, J. F. Stoddart, *Nanoscale* **2009**, *1*, 16-39; d) A. Stein, *Adv. Mater.* **2003**, *15*, 763-775.

[5] a) R. Casasús, M.D. Marcos, R. Martínez-Máñez, J.V. Ros-Lis, J. Soto, L.A. Villaescusa, P. Amorós, D. Beltrán, C. Guillem, J. Latorre, *J. Am. Chem. Soc.* **2004**, *126*, 8612-8613. b) R. Casasús, E. Climent, M.D. Marcos, R. Martínez-Máñez, F. Sancenón, J. Soto, P. Amorós, J. Cano, E. Ruiz, *J. Am. Chem. Soc.* **2008**, *130*, 1903-1917. c) A. Bernardos, E. Aznar, C. Coll, R. Martínez-Máñez, J.M. Barat, M.D. Marcos, F. Sancenón, J. Soto, *J. Control. Release.* **2008**, *131*, 181-189. d) Q. Yang, S. Wang, P. Fan, L. Wang, Y. Di, K. Lin, F.-S Xiao, *Chem. Mater.* **2005**, *17*, 5999-6003. e) T.D. Nguyen, K.C.-F. Leung, M. Liong, C.D. Pentecost, J.F. Stoddart, J.I. Zink, *Org. Lett.* **2006**, *8*, 3363-3366. f) K.C.-F. Leung, T.D. Nguyen, J.F. Stoddart, J.I. Zink, *Chem. Mater.* **2006**, *18*, 5919-5928. g) S. Angelos, Y.-W. Yang, K. Patel, J.F. Stoddart, J.I. Zink, *Angew. Chem.* **2008**, *120*, 2254-2258.; *Angew. Chem. Int. Ed.* **2008**, *47*, 2222-2226. h) N. M. Khashab, A. Trabolsi, Y.A. Lau, M.W. Ambrogio, D.C. Friedman, H.A. Khatib, J.I. Zink, J.F. Stoddart, *Eur. J. Org. Chem.* 2009, 1669-1673. i) C. Park, K. Oh, S. Lee, C. Kim, *Angew. Chem. Int. Ed.* **2007**, *46*, 1455-1457.

[6] Q. Fu, G.V.R. Rao, L.K. Ista, Y. Wu, B.P. Andrzejewski, L.A. Sklar, T.L. Ward, G.P. López, *Adv. Mater.* **2003**, *15*, 1262-1266.

[7] a) B. G. Trewyn, S. Giri, I.I. Slowing, V.S.-Y. Lin, *Chem. Commun.* **2007**, 3236-3245. b) B. G. Trewyn, I.I. Slowing, S. Giri, H.-T. Chen, V.S.-Y. Lin, *Acc. Chem. Res.* **2007**, *40,* 846-853. c) C.-Y. Lai, B.G. Trewyn, D.M. Jeftinija, K. Jeftinija, S. Xu, S. Jeftinija, V.S.-Y. Lin, *J. Am. Chem. Soc.* **2003**, *125*, 4451–4459. d) F. Torney, B.G. Trewyn, V.S.-Y. Lin, K. Wang, Nat. *Nanotechnol.* **2007**, *2,* 295–300. e) D.R. Radu, C.-Y. Lai, K. Jeftinija, E.W. Rowe, S. Jeftinija, V.S.-Y. Lin, *J. Am. Chem. Soc.* **2004**, *126,* 13216–13217. f) S. Giri, B.G. Trewyn, M.P. Stellmaker, V.S.-Y. Lin, *Angew. Chem. Int. Ed.* **2005**, *44,* 5038–5044. g) I.I. Slowing, B.G. Trewyn, V.S.-Y. *J. Am. Chem. Soc.* **2007**, *129*, 8845-8849. h) I.I. Slowing, B.G. Trewyn, S. Giri, V.S.-Y. Lin, *Adv. Funct. Mater.* **2007**, *17*, 1225. i) R. Montera, J. Vivero-Escoto, I.I. Slowing, E. Garrone, B. Onida, V.S.-Y. Lin, *Chem. Commun.* **2009**, 3219-3221.

[8] a) N.K. Mal, M. Fujiwara, Y. Tanaka, *Nature,* **2003**, *421*, 350-353. b) N.K. Mal, M. Fujiwara, Y. Tanaka, T. Taguchi, M. Matsukata, *Chem. Mater.* **2003**, *15*, 3385-3394. c) Y. Zhu, M. Fujiwara, *Angew. Chem. Int. Ed.* **2007**, *46,* 2241-2244. d) D.P. Ferris, Y.-L. Zhao, N.M. Khashab, H.A. Khatib, J.F. Stoddart, J.I. Zink, *J. Am. Chem. Soc.* **2009**, *131*, 1686-1688. e) E. Aznar, R. Casasús, B. García-Acosta, M.D. Marcos, R. Martínez-Máñez, F. Sancenón, J. Soto, P. Amorós, *Adv. Mater.,* **2007**, *19*, 2228-2231. F) E. Aznar, M.D. Marcos, R. Martínez-Máñez, F. Sancenón, J. Soto, P. Amorós, C. Guillem, *J. Am. Chem. Soc.,* **2009**, *131*, 6833-6843.

[9] a) C. Coll, R. Casasús, E. Aznar, M.D. Marcos, R. Martínez-Máñez, F. Sancenón, J. Soto, P. Amorós, *Chem. Commun.* **2007**, 1957-1959. b) R. Casasús, E. Aznar, M.D. Marcos, R. Martínez-Máñez, F. Sancenón, J. Soto, P. Amorós, *Angew. Chem. Int. Ed.* **2006**, *45*, 6661-6664. c) E. Aznar, C. Coll, M.D.

Marcos, R. Martínez-Máñez, F. Sancenón, J. Soto, P. Amorós, J. Cano, E. Ruiz, *Chem. Eur. J.,* **2009***, 15*, 6877-6888. d) E. Climent, M.D. Marcos, R. Martínez-Máñez, F. Sancenón, J. Soto, K. Rurack, P. Amorós, *Angew. Chem. Int. Ed.,* **2009**, *48*, 8519-8522. e) I. Candel, A. Bernardos, E. Climent, M. D. Marcos, R. Martínez-Manez, F. Sancenon, J. Soto, A. Costero, S. Gil, M. Parra, *Chem. Commun.,* **2011***, 47,*8313-8315.

[10] a) K. Patel, S. Angelos, W.R. Dichtel, A. Coskun, Y.-W. Yang, J.I. Zink, J.F. Stoddart, *J. Am. Chem. Soc.* **2008***, 130*, 2382-2383. b) A. Bernardos, E. Aznar, M.D. Marcos, R. Martínez-Máñez, F. Sancenón, J. Soto, J.M. Barat, P. Amorós, *Angew. Chem. Int. Ed.,* **2009**, *48*, 5884-5887. c) A. Schlossbauer, J. Kecht, T. Bein, *Angew. Chem. Int. Ed.,* **2009***, 48,* 3092-3095. d) C. Park, H. Kim, S. Kim, C. Kim, *J. Am. Chem. Soc.,* **2009***, 131*, 16614-16615. e) A. Bernardos, L. Mondragón, E. Aznar, M. D. Marcos, R. Martínez-Máñez, F. Sancenón, J. Soto, J. M. Barat, E. Pérez-Payá, C. Guillem, P. Amorós *ACS Nano,* **2010***, 4*, 6353-6368. f) C. Coll, L. Mondragón, R. Martínez-Máñez, F. Sancenón, M. D. Marcos, J. Soto, P. Amorós, E. Pérez-Payá, *Angew. Chem. Int. Ed.,* **2011***, 50*, 2138-2140. g) J. Liu, X. Du, X. Zhang, Chem*. Eur. J.* **2011***, 17*, 810-815.

[11] a) E. Climent, E. R. Martínez-Mañez, F. Sancenón, M. D. Marcos, J. Soto, A. Maquieira, P. Amorós, *Angew. Chem. Int. Ed.* **2010***, 49*, 7281-7283. b) A. Schossbauer, S. Warncke, P.M.E. Gramlich, J. Kecht, A. Manetto, T. Carell, T. Bein, *Angew. Chem. Int. Ed.* **2010***, 49*, 4734-4737. c) E. Ruiz-Hernández, A. Baeza, and M. Vallet-Regí, *ACS Nano,* **2011***, 5*, 1259-1266.

[12] E. Climent, A. Bernardos, R. Martínez-Máñez, A. Maquieira, M. D. Marcos, N. Pastor- Navarro, R. Puchades, F. Sancenón, J. Soto, P. Amorós, *J. Am. Chem. Soc.* **2009***, 131*, 14075 – 14080.

[13] E.M. Brun, A. Torres, R. Ventura, R. Puchades, Á. Maquieira, *Analytica Chimica Acta*, **2010**, *671*, 70–79.

An antibody-capped mesoporous nanoscopic material as probe for the selective fluorimetric detection of finasteride.

Supporting Information

Estela Climent, Ramón Martínez-Máñez, Ángel Maquieira, Félix Sancenón, María Dolores Marcos, Eva María Brun, Juan Soto, Pedro Amorós.

1.- Chemical structures of steroids tested during selective studies.

Chemical structures of finasteride, dutasteride, finasteride metabolite, metenolone, oxandrolone, 16-β-hydroxystanozolol, 1-testosterone, androstanolone, testosterone and testosterone glucuronide are showed in Figure SI-1.

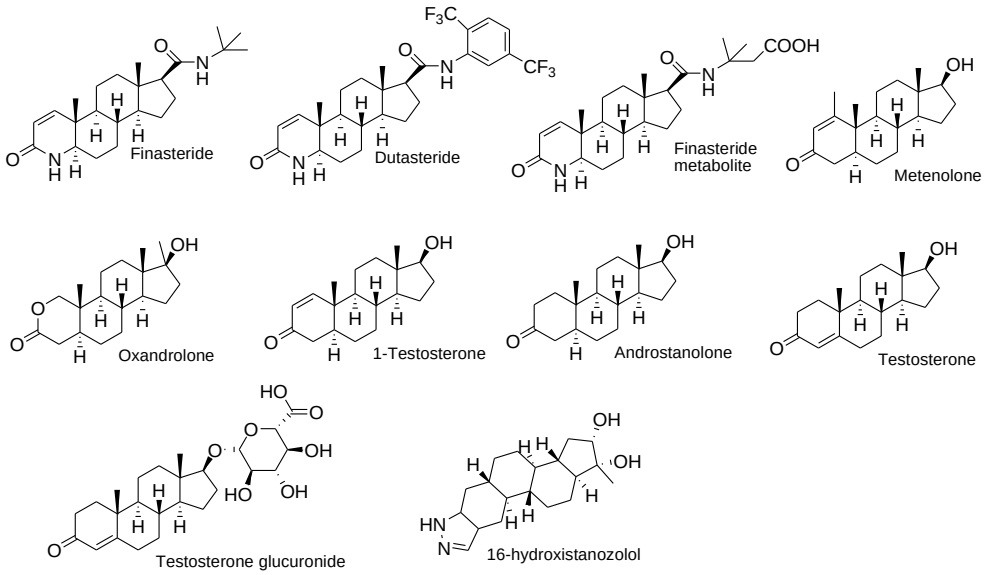

Figure SI-1. Chemical structures of substances tested during studies of selectivity.

Selective and sensitive detection of TATP with antibody-gated dye delivery from mesoporous hybrid nanoparticles in a lateral flow assay

Estela Climent,[1,2] Delia Gröninger,[3] Mandy Hecht,[3] M. Astrid Walter,[4] Ramón Martínez-Máñez,[1,2] Michael G. Weller,[4] Félix Sancenón,[1,2] Pedro Amorós,[5] and Knut Rurack[3]

[1] Centro de Reconocimiento Molecular y Desarrollo Tecnológico (IDM). Unidad mixta Universitat Politècnica de València-Universitat de València. Departamento de Química. Camino de Vera s/n, 46022, Valencia, Spain.
Fax: (+) 34 96 387 93 49. E-mail: rmaez@qim.upv.es

[2] CIBER de Bioingeniería, Biomateriales y Nanomedicina (CIBER-BBN).

[3] Fachbereich 1.9 Sensormaterialien, BAM Bundesanstalt für Materialforschung und – prüfung, Richard-Willstätter-Strasse 11, D-12489 Berlin, Germany.

Fax: (+49) 30 8104 1157. E-mail: knut.rurack@bam.de.

[4] Fachbereich 1.5 Proteinanalytik, BAM Bundesanstalt für Materialforschung und – prüfung, Richard-Willstätter-Strasse 11, D-12489 Berlin, Germany.

[5] Institut de Ciència dels Materials (ICMUV), Universitat de València, P.O. Box 2085, E-46071, Valencia, Spain.

Submitted

Nanoscopic delivery systems have received tremendous attention in recent years, because they can be designed from a large number of materials in a great variety of architectures, enabling a rather precise tailoring and control of their function in a desired location.[1] However, whereas their popularity in drug delivery or related biomedical and pharmaceutical applications is well documented,[2] their breakthrough in the areas of analytical chemistry or sensing is yet to come.[3] The potential of such systems for analytical purposes is nonetheless immediately obvious. Provided that the carrier system is loaded with an indicator and the appropriate detection chemistry is implemented in a way that only the advent of an analyte molecule can trigger delivery, such systems can release a much larger number of indicators than analytes are necessary to induce release, resulting in amplified signalling. The key thus is to equip such systems with a selective gating mechanism that controls the release of the measureable cargo. Few examples have been reported in recent years operating with specific gating chemistries and targeting selected analytes in conventional solution based experiments.[4] A more general approach and its implementation with an actually applicable sensing format has not been realized so far. We report here on the development of such a general approach by designing an antibody-gated dye delivery system and incorporating it with a conventional test strip-based lateral flow assay, finally allowing for small-molecule sensing at ppb level in a fast (2–10 min overall assay time) and easy-to-operate manner.

The model analyte chosen by us here is triacetone triperoxide (TATP). TATP is the prototype of a small-molecule analyte that is difficult to target with supramolecular recognition chemistry, because it lacks functional groups for classical non-covalent binding and is neither particularly polar nor apolar. TATP is also a high-priority analyte because of its popular use in IEDs (improvised explosive devices) for criminal and terrorist activities.[5] Since recent prevention strategies increasingly focus on the tracing of explosives for instance in sewage water to locate IED “bomb factories”,[6] potent on-site sensing systems for the condensed phase are required. However, although various methods for laboratory-based TATP detection in the liquid phase are available, selective and

sensitive portable sensing systems are very scarce.[7] Moreover, a common and severe drawback for TATP detection is that most chemosensing systems rely on the decomposition of TATP and the subsequent detection of one of its precursors, hydrogen peroxide.[8] In fact, most of these tests are not selective for TATP and show a high cross-reactivity against H_2O_2 and other peroxide-based explosives (PBEs).

Our approach for the specific detection of TATP in liquid samples at trace levels with a portable, i.e., handheld and rapidly responding device with straightforward operation is a test strip-based assay with simple fluorescence read-out. Test strip assays for such purposes—especially if neutral small organic molecules unable to influence the optical or redox properties of indicator molecules to a significant extent are concerned—require the integration of signal amplification features. As mentioned above, chemically gated delivery systems are particularly attractive in this regard. Based on our experience in the fields of bio-gated release systems[9] and gated hybrid materials for sensing applications,[4] we designed the ensemble as sketched in Figure 1. Ordered mesoporous silica nanoparticles (MSNs)[10] are used as the nanoscopic support with a defined void structure, high inner surface area and flexible functionalization chemistry. These MSNs are then loaded with the brightly fluorescent indicator dye sulforhodamine B (yielding solid **S0**) and the external surface is subsequently functionalised with a suitable hapten (**S1**). Finally, a TATP-selective polyclonal antibody (**S1-AB**) recently developed by us[11,12] serves as bulky stopper moiety which is attached at the void openings and which efficiently closes the latter. The tailored relay chemistry that connects stopper and support is thus based on non-covalent antibody-antigen interactions and (ideally) only TATP as stimulus should be able to successfully compete with the hapten for the antibody's binding sites, to dislocate the stoppers, to open the voids and to release the entrapped indicator. The latter can be monitored conveniently at excitation wavelengths between 500–570 nm and emission wavelengths between 550–650 nm, covering prominent excitation sources and emission filter windows.

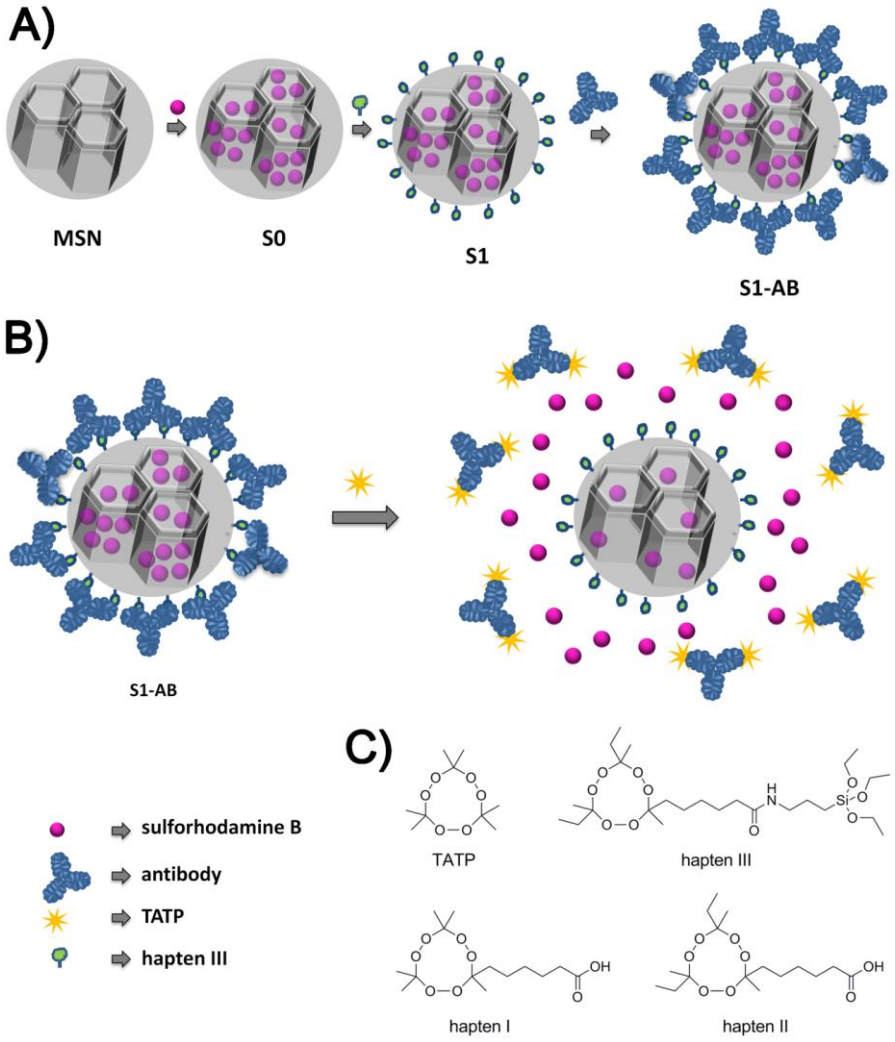

Figure 1. A) Schematic representation of the preparation of gated material **S1-AB** capped with an antibody. B) Sensing scheme of analyte-mediated displacement of the stoppers and dye release. C) Chemical structures of TATP and the hapten derivatives **I–III** employed in this study.

Silica nanoparticles of the mesoporous MCM-41 phase were selected as suitable inorganic support, because they show a high loading capacity, high thermal stability, homogeneous porosity and inertness. The MSNs were prepared along a known procedure with tetraethylorthosilicate (TEOS) as inorganic hydrolytic precursor and hexadecyltrimethylammonium bromide (CTAB) as

porogen.[13] The structure of starting material MSN was confirmed by X-ray diffraction and TEM (Section 7, Supporting Information). The N_2 adsorption-desorption isotherms of the mesoporous nanoparticles showed a typical type IV-curve with a specific surface of 937.6 $m^2\ g^{-1}$, and a pore volume of 0.75 $cm^3\ g^{-1}$. From XRD, porosimetry and TEM studies, the a_0 hexagonal cell parameter (4.56 nm), the pore diameter (2.75 nm) and the wall thickness (1.81 nm) were calculated. Polyclonal sera for TATP were obtained by immunization of 9–12 week old (2–2.5 kg) rabbits with bovine serum albumin (BSA) conjugates containing hapten **I**.[11] The complete synthetic details are given in the Supporting Information.

An important feature when aiming to use the capped hybrid delivery systems in a test strip assay is to obtain a highly selective and sensitive response while guaranteeing fast response times *aka* high delivery rates. Highly selective and sensitive immunological responses are best obtained with high-affinity antibodies. However, such tightly binding receptors are usually characterized by a rather slow off-rate or dissociation constant.[14] Assuming a common on-rate or association constant k_a of $1 \times 10^7\ M^{-1}\ s^{-1}$ for small-molecule hapten–high-affinity antibody interaction,[15,16] our TATP-affine sera with high affinities[11] of $K_0 \sim 1 \times 10^9\ M^{-1}$ are characterized by $k_d \leq 1 \times 10^{-2}\ s^{-1}$, which can be considered as moderate to slow off-rates.[14] Since the affinity of the antibody is even ca. 4-fold higher for **I** as for neat TATP,[11] an alternative hapten had to be developed. We thus opted for the slightly mismatching hapten **II** (Figure 1)[17] and synthesized its reactive precursor **III** to be facilely anchored onto the surface of the mesoporous material. **III** was prepared by reaction of 3-aminopropyltriethoxysilane with **II**. In the next step, MSNs were added to a solution containing a high concentration of sulforhodamine B in order to achieve efficient loading of the pores (solid **S0**) and then **III** was anchored on the external surface to yield **S1**. For the preparation of the final gated sensing material **S1-AB**, 1 mg of **S1** was suspended in 2 mL PBS containing the antibody in phosphate-buffered saline (PBS, pH 7.4) with 0.05% BSA and 345 ppm sulforhodamine B (see Supporting Information). Optimization of the conditions was performed by checking a range of different serum dilutions

(see Supporting Information). **S1-AB** was isolated by centrifugation and washed with PBS. The solid was finally dried in vacuum overnight and stored at 4 °C. The presence of BSA presumably helps in the capping of the pores by the antibodies, further reducing unspecific leaching of the dye from the sensor material. The **S1-AB** nanoparticles were roughly spherical with a diameter of ca. 100 nm (see Supporting Information). The content of hapten derivative **III** and dye in **S1** was determined by elemental and thermogravimetric analysis (TGA), and values of 0.17 and 0.749 mmol (g SiO_2)$^{-1}$ were found. Moreover, a final content of 5.18 × 10^{-4} mmol of antibody per g of SiO_2 was determined for **S1-AB**.

The response of **S1-AB** in the presence of TATP was studied by suspending 0.4 mg of **S1-AB** in 0.8 mL of PBS at pH 7.4 (0.5 mg solid mL^{-1}). This suspension was divided into two aliquots. To assess the effectiveness of pore closure, one fraction was mixed with 2.375 mL PBS containing 5 ppm TATP while the other fraction was only mixed with the same amount of neat PBS. Fractions of both suspensions (0.25 mL) were then centrifuged for certain time intervals (0, 0.25, 0.5, 2 and 5 min) and the amount of released sulforhodamine B was measured fluorometrically. The profiles of delivery kinetics are shown in Figure 2a. It is obvious that the presence of TATP induced a fast opening of the pores with subsequent release of the entrapped dye, whereas virtually no release was observed in the absence of TATP. The maximum delivery of sulforhodamine B from **S1-AB** in the presence of 5 ppm TATP amounted to 25% of the initial content of dye in **S1-AB**. Following a similar procedure, dye delivery from **S1-AB** was studied as a function of the concentration of TATP (Figure 2b). The amount of dye delivered depends on TATP concentration in agreement with a displacement of the antibody from the solid surface upon successful competition of TATP with the binding sites (Figure 1). A closer analysis of the binding isotherms between the particle-bound antibody and TATP according to a Scatchard plot often used to describe protein-ligand binding revealed an apparent equilibrium constant of K = 4.5 × 10^5 M^{-1}, the non-linearity presumably arising from the polyclonality of the sera. Regarding the limit of detection (LOD) of the assay, TATP could be detected down to concentrations as low as 12.5 ppb (for a detailed discussion on binding,

uncertainties and LOD, see Supporting Information). The amount of dye released in the working range of the assay at lower TATP concentrations is ca. 70-times that of antibody displaced, which is a remarkable sign of signal amplification.

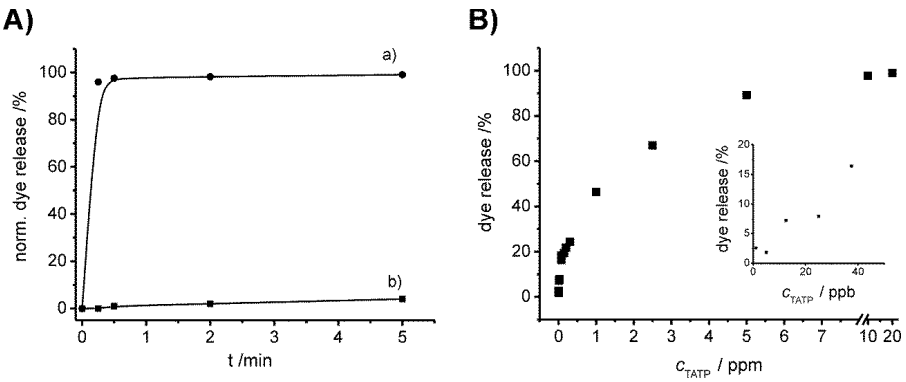

Figure 2. A) Sulforhodamine B release measured by monitoring the fluorescence at 582 nm (λ_{exc} = 564 nm) vs time for **S1-AB** in PBS (pH 7.4), in the absence (b) and the presence of 5 ppm (a) TATP. B) Sulforhodamine B release from **S1-AB** as a function of TATP concentration in PBS (pH 7.4) after 5 min of reaction. The amount of dye released was determined from the emission intensity at 582 nm (with λ_{exc} = 564 nm).

The selectivity of the capped material was studied by monitoring the uncapping process in the presence of other species, in particular of common explosives such as trinitrotoluene (TNT), hexogen (RDX), nitropenta (PETN), octogen (HMX), nitroguanidine (NG) and hexamethylene triperoxide diamine (HMTD), see Figure SI-1, Supporting Information for chemical structures. Furthermore, the synthetic precursors of TATP and **III**, i.e., hydrogen peroxide, acetone and 7-oxooctanoic acid (7-oxo), as well as other synthetic cyclic peroxides, i.e., tri-butanone triperoxide (but-TP), tri-3-pentanone triperoxide (3-pent-TP), tri-2-pentanone triperoxide (2-pent-TP), diacetone diperoxide (DADP), and the structurally related, common crown ether compounds 18-crown-6 and 12-crown-4 were also tested. The uncapping ability of all these compounds at a concentration of 3 ppm is shown in Figure 3. Apparently, from the structurally related compounds, only the analogous (yet in realistic scenarios not relevant) triperoxides but-TP (contains the same triperoxide ring as **III**), 2-pent-TP and 3-

pent-TP were able to partially induce dye release from **S1-AB** nanoparticles. Among the classical explosives only PETN and NG induced a moderate dye delivery. Besides the low detection limit for TATP, the most important feature of the system is its excellent discrimination of TATP against H_2O_2, the cross-reactant most other methods suffer from.

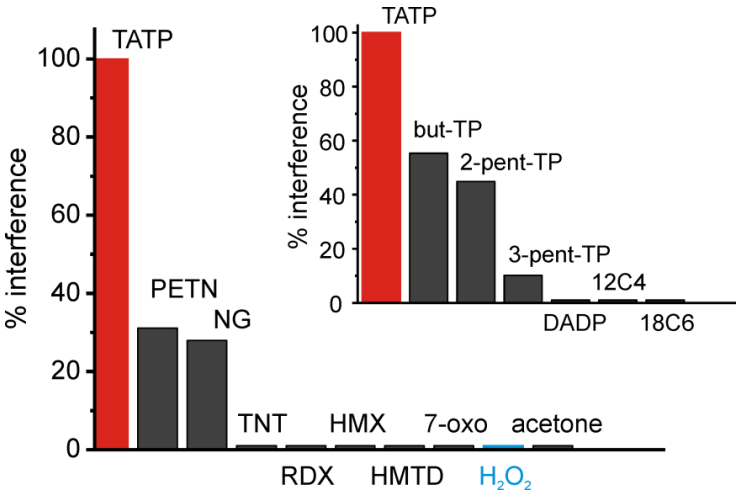

Figure 3. Relative release of sulforhodamine B from **S1-AB** in the presence of 3 ppm of other common explosives and educts of TATP synthesis in PBS (pH 7.4). Inset: Relative release of sulforhodamine B from **S1-AB** in the presence of 3 ppm of selected compounds which are structurally related to TATP. The amount of dye released was determined fluorometrically (λ_{em} = 582 nm, λ_{exc} = 564 nm).

Encouraged by these results and after demonstrating the feasibility of the combination of immunological indication and mesoporous scaffoldings to design antibody-capped mesoporous materials, we proceeded to integrate **S1-AB** with a lateral flow assay for the straightforward on-site detection of TATP. Such assays commonly rely on test strips that carry the (bio)chemical part of the detection system and that, after dipping the test strip into the sample solution and evolution of the flow, develop a colour which can be appreciated by eye. Few such assays are known for the determination of small-molecule analytes of environmental (e.g., atrazine),[18] diagnostic (e.g., morphine)[19] or terroristic (e.g.,

saxitoxin)[20] concern at trace (lower ppb) levels, commonly utilizing antibody–gold nanoparticle (AuNP) conjugates or hapten–protein–AuNP conjugates, partly in combination with gold enhancer solutions. Alternatively, first reports on trace level analysis using quantum dot (QD) conjugates in strip-based assays and handheld fluorescence readers instead of AuNP-based assays have been reported recently.[21] Immanent to both approaches are the facts that such assays are rapid, sensitive, specific, cheap and easy to handle, clear advantages in routine applications by untrained personnel or in emergency cases. However, both AuNP- as well as QD-conjugate assays have a significant drawback, i.e., they require protein conjugates to travel the active distance of the strip which renders them prone to errors due to unspecific binding. As can be deduced from the scheme sketched out in Figure 1, our approach is different. The strip contains also an interaction and a detection zone (Figure 4). However, only the first zone A contains the (bio)chemistry—**S1-AB** (Figure 4a)—that is necessary to generate the response and the second zone B is an arbitrary area at the solvent front in which a signal is collected (Figure 4c). If the investigated sample does not contain the analyte (TATP) no dye release would be observed and no signal would be detected in zone B. However, when TATP is present in the sample, uncapping takes place when the solvent front reaches zone A because of competition between TATP and grafted **III** for the binding sites of the antibody, leading to formation of the more stable TATP-antibody complex, and the liberated dye is transported at the solvent front due to the flow conditions (Figure 4b). Because the scaffold MSNs have been chosen large enough not to be transported by an aqueous flow in the strip's membrane, still capped and uncapped **S1-AB** are both retained at the spot of deposition (Figure 4c, zone A). Depending on the amount of TATP in the sample, the flow transports a certain amount of released dye away from zone A and a fluorescence signal can be detected at the solvent front in zone B.

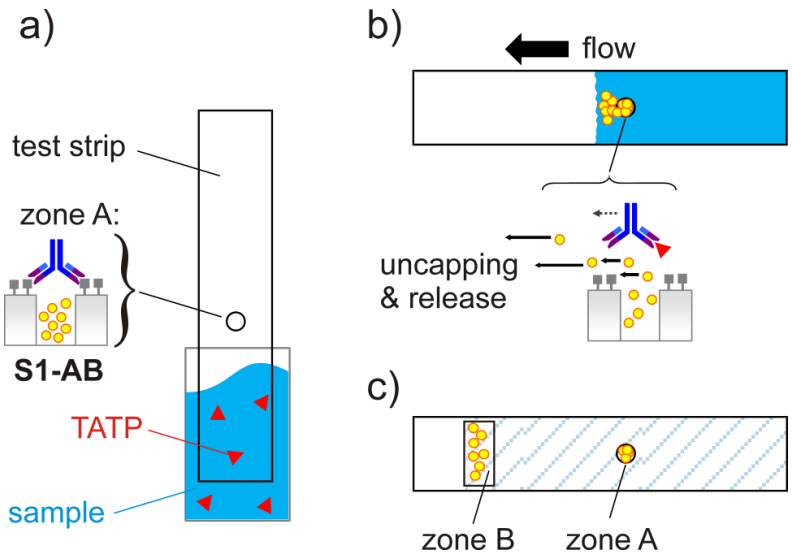

Figure 4. Design and principle of operation of the lateral flow assay: a) **S1-AB** is deposited at zone A so that the strip can be conveniently dipped into the sample; b) the presence of the analyte leads to (partial) uncapping of the pores and release of the dye which is transported at the solvent front; c) after development and drying, zone B contains the amount of dye that corresponds to the amount of analyte in solution and zone A the residual, unreleased dye.

A high-flow nitrocellulose membrane was selected as the support. Strips of 0.5 × 2.5 cm were prepared and **S1-AB** was deposited in 0.5 µL from suspensions of the sensing material (2 mg mL^{-1}) on zone A with a micropipette. The strips were then dipped into buffered solutions containing various amounts of TATP. After 90 s of development, the test strips were dried and the fluorescence was measured using a flow assay reader at 625 nm (λ_{exc} = 520 nm). The drying step is essential since varying amounts of residual liquid on the strip influence the fluorescence of the dye. This step is also the time-limiting step, i.e., when using a hair dryer (in cold air blow mode), the assay can be completed in ca. 2 min (90 s development plus 30 s drying) and when letting the strip dry at room temperature under normal atmosphere, ca. 8 min are required to obtain a stable signal. When the PBS sample solution did not contain TATP, a negligible fluorescence signal was recorded in zone B (Figure 5a). However, when a similar experiment was performed for example with a solution containing 0.5 ppm TATP, a clear signal

was found in zone B (Figure 5b). To the best of our knowledge, this is the first report of a flow assay based on massive indicator release from a nanoscopic chemical container device.

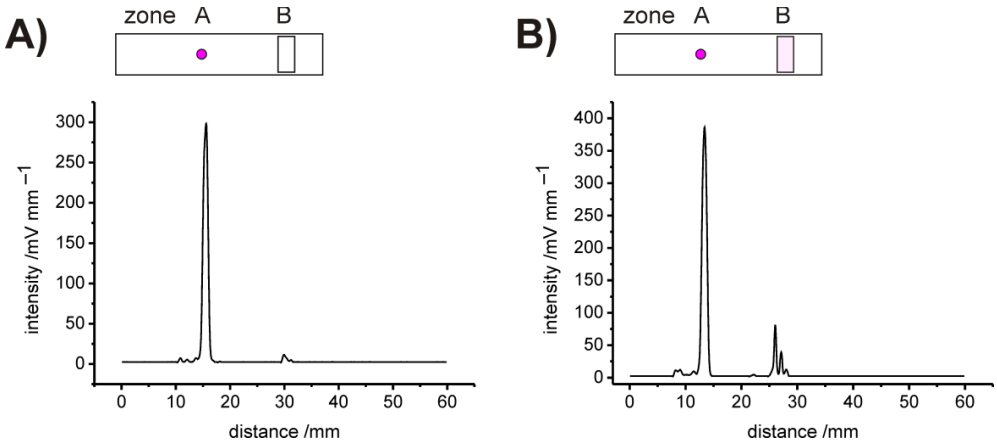

Figure 6. Signal obtained with the fluorescence reader (λ_{exc} = 520 nm, λ_{em} = 625 nm) from dye release in zone B after development of the flow assay in the absence (A) and the presence of 0.5 ppm (B) TATP in PBS buffer (pH 7.4).

Following the same procedure as described above, the effect of TATP concentration in the lateral flow assays was studied. The amount of dye released for each concentration was calculated through the ratio between the area of zone A and the total area of the test strip. A limit of detection of 15 ppb of TATP was determined using this simple procedure (Figure SI-2, Supporting Information). The effect of the educts of the synthesis of TATP, other explosives and other peroxides was also assessed in cross-reactivity studies and the results in terms of selectivity were similar to those observed using **S1-AB** in solution (Figure SI-3, Supporting Information). Moreover, besides the manual deposition procedure described above, we also prepared strips for the assay with an automated dispenser able to deliver droplets of ≤1 nL from suspensions of **S1-AB** (5 mg mL^{-1}) onto the strips; the final volume deposited was 50 nL in these cases. The advantage of this procedure is that an automated and reproducible preparation of the test strips is possible (Figure SI-4, Supporting Information). The same selective uncapping

process in the presence of TATP was observed for these strips with detections limits of 40 ppb. These experiments have shown that the **S1-AB** hybrids are stable enough to be handled in an automated dispensing process using a piezo-driven device. In contrast, due to sedimentation problems of the hybrid nanoparticles in the reservoir, even the use of high-end array spotters did not yield satisfactorily reproducible series of strips (Figure SI-5, Supporting Information). Finally, the strips from both deposition procedures, manual and dispenser, were tested under realistic conditions and were able to detect TATP in tap water (pH 7.4) as well as influent (pH 7.9) and effluent (pH 7.5) water of a sewage treatment plant at lower ppb concentrations, when for instance 0.1 mL of PBS 10X solution are added to 0.9 mL of the sample prior to dipping of the strip. Regarding pH tolerance, the system was tested in the pH range 1–12 and TATP-induced delivery was observed at any pH. However, below pH 4 and above pH 8.5, the delivery rates were reduced, presumably because at acidic pH, TATP starts to decompose and at alkaline pH, the structure of the silica scaffold might be altered.[22] In addition, testing the assay on samples containing ethanol contents of 1–10 % (v/v) revealed that only above 5 %, enhanced release most likely due to accelerated dissociation of the caps is observed (for a detailed description and representative graphs, see Section 9 and Figure SI-6, Supporting Information). Apparently, the strip-based assay is robust enough to accomplish the task of reliably determining TATP in scenarios to locate IED “bomb factories” as described in the Introduction.

In the present work, we have designed and prepared antibody-gated mesoporous silica nanoparticles which are loaded with a sulforhodamine dye and which can be used for the determination of the peroxide-based explosive TATP with a lateral flow fluorescence reader, allowing for detection limits in the lower ppb range. The mechanism of the detection relies on a displacement of the antibody from the surface of the hybrid material because of highly affine antibody–TATP interactions, releasing a much larger number of entrapped dye molecules from the pores as antibodies are displaced. The high selectivity of the antibody is retained in the gated material, allowing for a remarkable discrimination against H_2O_2 here. System design and optimization led to

straightforward integration into a lateral flow assay without further treatment or conditioning of the test strips while guaranteeing remarkably fast overall assay times of ≤ 10 min. Moreover, besides showing a stunning robustness, the inherent architecture of the assay relies on a single step immunochemical reaction, i.e., can dispense with secondary (labelled) antibodies and enables ratiometric signal assessment in the presence of the analyte by simple comparison of the fluorescence signals in two zones. Because of the modularity of the approach, the concept is easily generalisable and applicable for many small-molecule analytes. For instance, assays can be imagined which contain various hybrids of **S1-AB(n)** type for which each material capped with a certain antibody is loaded with a different dye, envisioning multiplexed analysis with such simple assays.

Experimental section

Details of general techniques, reagents employed, synthesis of products, synthesis of solids and full characterization of solids prepared, including figures of Powder X-ray diffraction, TEM analysis and porosimetry isotherms are given in the Supplementary Information.

Acknowledgements

Financial support from the Spanish Government (project MAT2009–14564-C04–01), the Generalitat Valenciana (Spain) (project PROMETEO/2009/016), the Innovationsfonds (BAM/Bundesministerium für Wirtschaft und Technologie) and BAM's PhD Programme (M.A.W.) is gratefully acknowledged. E.C. thanks the Ministerio de Educación (Spain) for a fellowship. We are indebted to J. Schenk, BAM-1.0, for help with the piezo dispenser and S. Fischer and W. Weigel, Scienion AG, Berlin for support with the spotter.

Contributions

K.R., R.M.M. and F.S. conceived the experiments. D.G. synthesized the peroxide-based explosives and haptens. M.A.W., M.G.W. and K.R. designed and optimized the immunochemistry. E.C. performed the materials assembly and delivery experiments. P.A., E.C. and F.S. carried out the characterization of the gated

solids. E.C., R.M.M. and K.R. analysed the data and wrote the paper. All authors discussed the results and commented on the manuscript.

Competing financial interests

The authors declare no competing financial interests.

References

[1] M. Motornov, Y. Roiter, I. Tokarev, S. Minko, *Prog. Polym. Sci.* **2010**, *35*, 174-211; I. I. Slowing, J. L. Vivero-Escoto, C. W. Wu, V. S.-Y. Lin, *Adv. Drug Deliv. Rev.* **2008**, *60*, 1278-1288.

[2] A. S. Hoffman, *J. Control. Release* **2008**, *132*, 153-163.

[3] R. Martínez-Máñez, F. Sancenón, M. Biyikal, M. Hecht, K. Rurack, *J. Mater. Chem.* **2011**, *21*, 12588-12604.

[4] E. Climent, M. D. Marcos, R. Martínez-Máñez, F. Sancenón, J. Soto, K. Rurack, P. Amorós, *Angew. Chem. Int. Ed.* **2009**, *48*, 8519-8522; E. Climent, R. Martínez-Máñez, F. Sancenón, M. D. Marcos, J. Soto, A. Maquieira, P. Amorós, *Angew. Chem. Int. Ed.* **2010**, *49*, 7281-7283.

[5] *Report of the European Security Research Advisory Board ESRAB—Meeting the Challenge: the European Security Research Agenda*, Office for Official Publications of the European Communities, Luxembourg., **2006**, http://ec.europa.eu/enterprise/policies/security/files/esrab_report_en.pdf; *NCTC 2010 Report on Terrorism*, National Counterterrorism Center, Washington, DC, **2011**, http://www.nctc.gov/witsbanner/docs/2010_report_on_terrorism.pdf (see, e.g., Chart 10 - Wounded Victims Grouped by Weapon Type); K. Yeager, *Police Chief* **2011**, *78* (September Issue), 52-55.

[6] H. Doyle, *CommonSense–Development of a Common Sensor platform for the detection of IED bomb factories (Plenary Lecture)*. International Crime Science Conference 2012, London, UK, July 2012.

[7] R. M. Burks, D. S. Hage, *Anal. Bioanal. Chem.* **2009**, *395***,** 301-313; S. Girotti, E. Ferri, E. Maiolini, L. Bolelli, M. D'Elia, D. Coppe, F. S. Romolo, *Anal. Bioanal. Chem.* **2011**, *400*, 313-320; R. Schulte-Ladbeck, P. Kolla, U. Karst, *Analyst* **2002**, *127*, 1152-1154.

[8] M. E. Germain, M. J. Knapp, *Inorg. Chem.* **2008**, *47***,** 9748-9750; S. Malashikhin, N. S. Finney, *J. Am. Chem. Soc.* **2008**, *130***,** 12846-12847; J. C. Sanchez, W. C. Trogler, *J. Mater. Chem.* **2008**, *18***,** 5134-5141.

[9] C. Coll, L. Mondragón, R. Martínez-Máñez, F. Sancenón, M. D. Marcos, J. Soto, P. Amorós and E. Pérez-Payá, *Angew. Chem. Int. Ed.* **2011**, *50*, 2138-2140; E. Climent, A. Bernardos, R. Martínez-Máñez, A. Maquieira, M. D. Marcos, N. Pastor-Navarro, R. Puchades, F. Sancenón, J. Soto, P. Amorós, *J. Am. Chem. Soc.* **2009**, *131*, 14075-14080.

[10] J. S. Beck, J. C. Vartuli, W. J. Roth, M. E. Leonowicz, C. T. Kresge, K. D. Schmitt, C. T. W. Chu, D. H. Olson, E. W. Sheppard, *J. Am. Chem. Soc.* **1992**, *114*, 10834-10843; F. Hoffmann, M. Cornelius, J. Morell, M. Fröba, *Angew. Chem. Int. Ed.* **2006**, *45*, 3216-3251.

[11] M. A. Walter, U. Panne, M. G. Weller, *Biosensors* **2011**, *1*, 93-106.

[12] M. A. Walter, D. Pfeifer, W. Kraus, F. Emmerling, R. J. Schneider, U. Panne, M. G. Weller, *Langmuir* **2010**, *26*, 15418-15423; J. J. Carvalho, M. A. Walter, Y. Baermann-Stapel, M. G. Weller, U. Panne, J. A. Schenk, R. J. Schneider, *In Vivo* **2012**, *26*, 63-70.

[13] S. Cabrera, J. El Haskouri, C. Guillem, J. Latorre, A. Beltrán-Porter, D. Beltrán-Porter, M. D. Marcos, P. Amorós, *Solid State Sci.* **2000**, *2*, 405-420.

[14] M. Stenberg, H. Nygren, *J. Immunol. Methods* **1988**, *113*, 3-15.

[15] T. W. Smith, K. M. Skubitz, *Biochemistry* **1975**, *14***,** 1496-1502.

[16] The values of $k_a \sim 1 \times 10^7$ M^{-1} s^{-1} pertain to interactions of both partners in the liquid phase. For interactions at the solid-liquid interphase when for instance one partner is coupled to a solid support such as a microparticle, k_a values are commonly ca. one order of magnitude smaller, i.e., 1×10^6 M^{-1} s^{-1}, see e.g. [15].

[17] The affinity of the antibody for the parent compound tri-butanone triperoxide (but-TP) is only 4 % compared with neat TATP, see ref. [11].

[18] J. Kaur, K. V. Singh, R. Boro, K. R. Thampi, M. Raje, G. C. Varshney, C. R. Suri, *Environ. Sci. Technol.* **2007**, *41***,** 5028-5036.

[19] S. Gandhi, N. Caplash, P. Sharma, C. R. Suri, *Biosens. Bioelectron.* **2009**, *25*, 502-505.

[20] A. Komano, H. Maruko, H. Sekiguchi, Y. Seto, *Forensic. Toxicol.* **2011**, *29***,** 38-43.

[21] Z. Zou, D. Du, J. Wang, J. N. Smith, C. Timchalk, Y. Li, Y. Lin, *Anal. Chem.* **2010**, *82***,** 5125-5133; Y. Bai, C. Tian, X. Wei, Y. Wang, D. Wang, X. Shi, *RSC Adv.* **2012**, *2***,** 1778-1781.

[22] A. Le-Tuan Phama, D. L. Sedlaka, F. M. Doyle, *Appl. Cat. B. Environm.,* **2012**, *126*, 258– 264.

Selective and sensitive detection of TATP with antibody-gated dye delivery from mesoporous hybrid nanoparticles in a lateral flow assay.

Supplementary Information

Estela Climent, Delia Gröninger, Mandy Hecht, M. Astrid Walter, Ramón Martínez-Máñez, Michael G. Weller, Félix Sancenón, Pedro Amorós, and Knut Rurack.

Figures

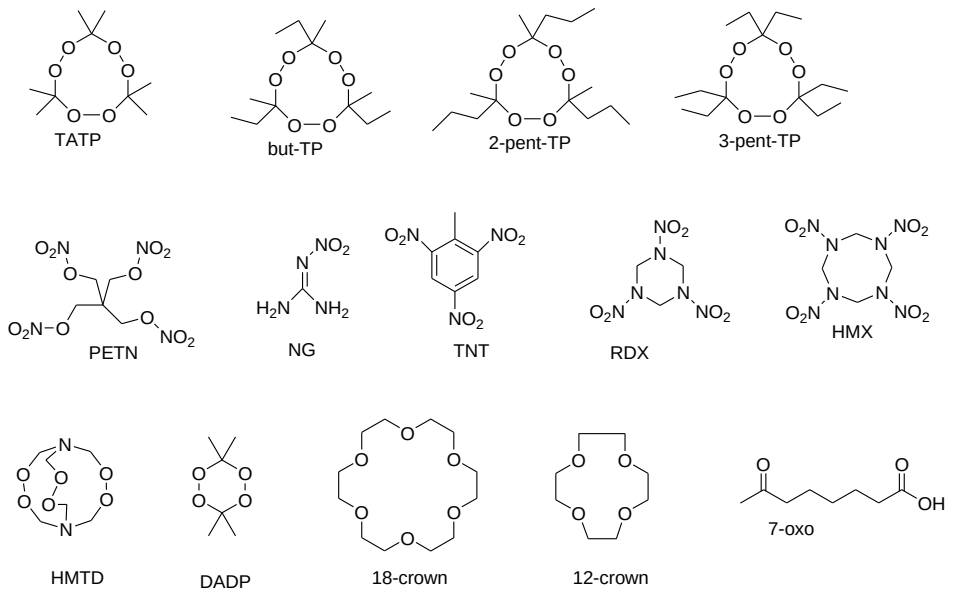

Figure SI-1. Chemical structures of substances tested during cross-reactivity studies.

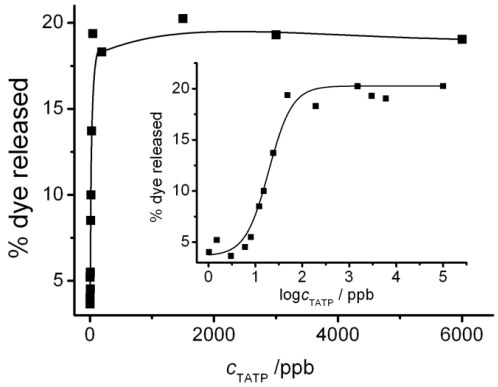

Figure SI-2. Sulforhodamine B release from test strips containing **S1-AB** at zone A in the presence of different amounts of TATP. The amount of release dye was determined through fluorescence at λ_{em} = 620 nm (λ_{exc} = 520 nm).

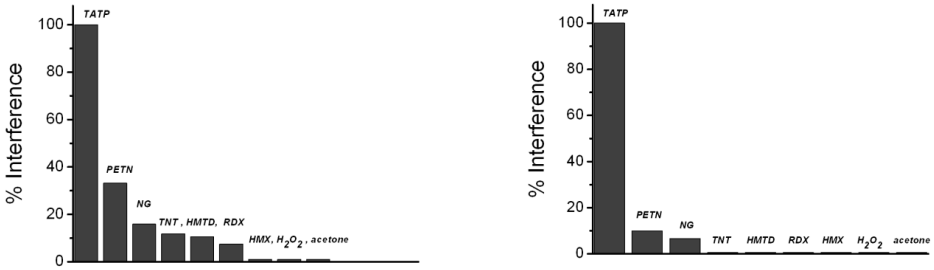

Figure SI-3. Cross-reactivity studies with lateral flow assay and 4 ppm (left) as well as 2 ppm (right) of TATP and potentially interfering compound as indicated in the graphs.

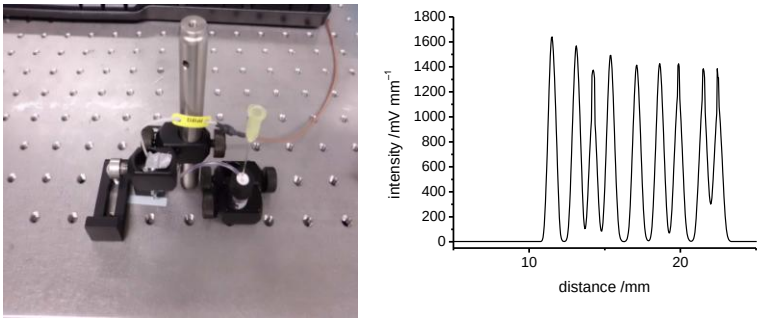

Figure SI-4. Setup for delivering the **S1-AB** suspension onto the strips with a piezo dispenser (left) and reproducibility of the dispensing process with the device (right); 50 × 1 nL droplets were spotted for each of the nine spots onto a single strip (strip was moved manually). Similar results were obtained for a series of strips on which only one spot was delivered.

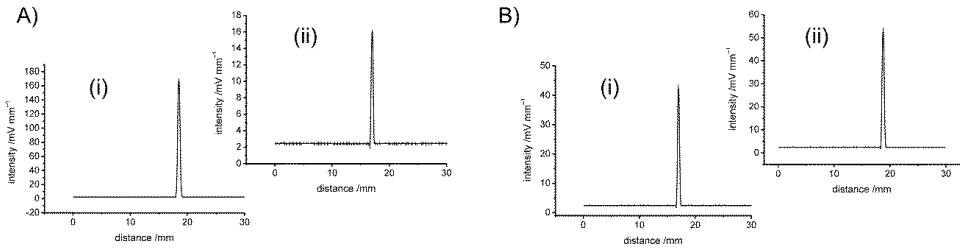

Figure SI-5. Reproducibility of the dispensing process with the spotter. A) First two strips of a series prepared in one run from the same reservoir suspension; on the third strip, virtually no signal was detectable anymore. B) Two strips prepared one by one with renewed stirring of the suspension between spotting of (i) and (ii). It is obvious that constant stirring of the suspension in the reservoir of the spotter is essential for achieving acceptable reproducibility.

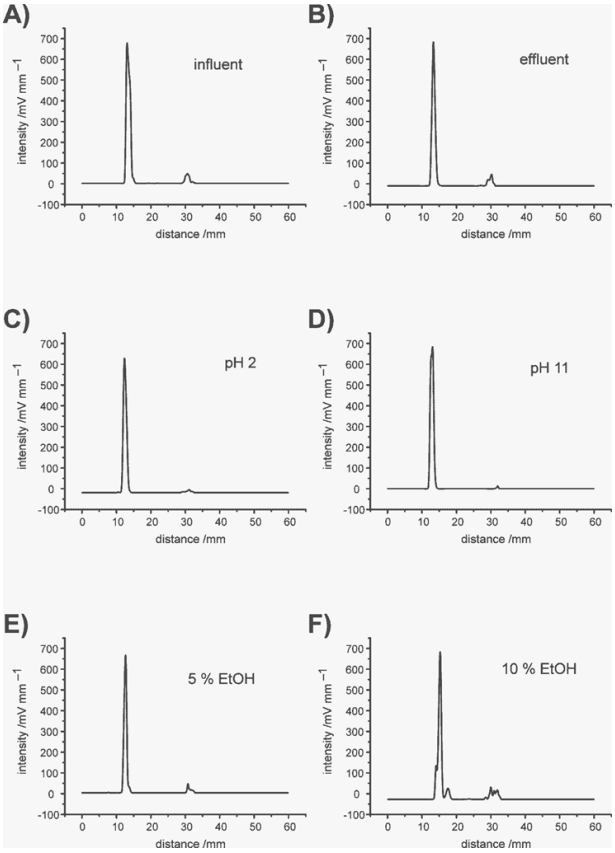

Figure SI-6. Performance evaluation of the strips with A) influent and B) effluent water

1. General techniques

XRD, TGA, elemental analysis, TEM, N_2 adsorption-desorption, NMR, UV-visible spectroscopy and fluorescence spectroscopy techniques were employed to characterize the synthesized materials and test their behaviour toward TATP and other explosives and related peroxides. Powder X-ray measurements were performed on a Philips D8 Advance diffractometer using CuK_α radiation. Thermogravimetric analyses were carried out on a TGA/SDTA 851e Mettler Toledo balance, using an oxidant atmosphere (air, 80 mL min^{-1}) with a heating program consisting of a ramp of 10 °C per minute from 393 to 1273 K and an isothermal heating step at this temperature for 30 min. TEM images were obtained with a 100 kV Philips CM10 microscope. N_2 adsorption-desorption isotherms were recorded with a Micromeritics ASAP2010 automated sorption analyzer. The samples were degassed at 120 °C in vacuum overnight. The specific surface areas were calculated from the adsorption data in the low pressure range using the BET model. Pore size was determined following the BJH method. ^{1}H and ^{13}C nuclear magnetic resonance (NMR) spectra were acquired with a Bruker AV-400 spectrometer. UV-vis spectra were measured with a Specord 210plus from Analytik Jena. Fluorescence spectroscopy measurements were carried out on a Fluoromax4 from HORIBA Scientific, and fluorescence measurements on strips were recorded with an ESE-Quant FL and a universal strip holder from Qiagen. Deposition of the suspended material was performed with a sub-microliter piezoelectric dispenser SPIP from GeSIM GmbH and a sciFLEXARRAYER S11 from Scienion AG.

2 . Reagents

Chemicals and solvents were purchased from Sigma-Aldrich, Merck KGaA and J.T. Baker in the highest quality available. Acetone (picograde) was supplied by LGC Standards. The buffers and solutions were prepared with ultrapure reagent water, which was obtained by running demineralized water (by ion exchange) through a Milli-Q® ultrapure water purification system (Millipore Synthesis A10). The protein

bovine serum albumin (BSA, for immunogen synthesis), fraction V, receptor grade, lyophilized were purchased from Serva.

Buffer solutions. Phosphate-buffered saline (PBS 10X; 70 mmol dm^{-3} Na_2HPO_4, 10 mmol dm^{-3} NaH_2PO_4, 145 mmol dm^{-3} NaCl, pH 7.6), PBS containing 0.05% BSA and sulforhodamine B sodium salt (345 ppm) were used for capping processes, controlled release experiments, interference and competition studies.

Common explosives and compounds structurally similar to TATP. The common explosives PETN, TNT, RDX and HMX were obtained from BAM Division 2.3 Explosives. 12-crown-4 (98%), 18-crown-6 (99.5%) and nitroguanidine (containing ca. 25% water) were purchased from Sigma Aldrich.

Safety Note! *Only highly qualified personnel should work with TATP, other peroxide explosives or other commercial explosives and safety precautions must be strictly adhered to avoid hazardous situations. Furthermore, only small amounts of less than 100 mg should be synthesized and handled. TATP and other peroxides can detonate spontaneously, particularly under impact, friction, static electricity or temperature changes.*

3. Synthesis of TATP, cyclic triperoxides and other explosives

Synthesis of triacetone diperoxide (TATP) was carried out employing the procedure described by Walter et al.[S1]

The other cyclic triperoxides (tri-butanone triperoxide, tri-2-pentanone triperoxide, and tri-3-pentanone triperoxide) were prepared following the same procedure as for TATP synthesis, employing butanone, 2-pentanone and 3-pentanone instead of acetone. The syntheses were carried out by mixing the corresponding ketone (3 mmol) with hydrogen peroxide (1.5 mmol, 30%) and sulfuric acid (0.015 mmol, 2 M) at 0 °C. After 48 h, stock solutions were prepared by dissolving the reaction mixtures completely in 10 mL methanol. Other common explosives such as DADP (diacetone diperoxide) and hexamethylene triperoxide diamine (HMTD) were prepared following procedures described by Dubnikova et al.[S2] and Wierzbicki & Cioffi,[S3] respectively.

4. Synthesis of haptens

Haptens **I** and **II** were prepared following the previously described procedure used to prepare TATP. For the preparation of hapten **I** we used acetone, 7-oxooctanoic acid, hydrogen peroxide and sulphuric acid, whereas for hapten **II** we used butanone instead of acetone.

Hapten III. Hapten derivative **III** was obtained through an amidation reaction between hapten **II** and the alkoxysilane derivative (3-aminopropyl)triethoxysilane using a modification of the active ester method.[S4] In a first step, *N*-hydroxysuccinimide (NHS, 18.89 mg, 0.16 mmol) and *N*,*N'*-dicyclohexylcarbodiimide (DCC, 33.86 mg, 0.16 mmol) were dissolved in anhydrous THF (75 mL). Then the mixture was added to a solution of hapten **II** (50 mg, 0.14 mmol) in anhydrous THF (0.25 mL). The mixture was stirred at room temperature during 5 h, and the white solid formed (dicyclohexylurea) was removed by centrifugation. The mixture was stirred during another 15 h at room temperature and again the white solid formed (dicyclohexylurea) was removed by centrifugation. In a second step, (3-aminopropyl)triethoxysilane (33.53 µL, 0.14 mmol) was added to the solution and the reaction mixture was stirred for 24 h at room temperature. The solvent was evaporated under reduced pressure to give a yellow sticky oil (hapten derivative **III,** 65 mg, 0.12 mmol, yield 82.2 %). ^{1}H NMR ($CDCl_3$): δ = 0.63 (t, 2 H, -*CH*$_2$-Si-), 0.96 (q, 6H, C*H*$_3$CH$_2$-C-) 1.22 (t, 9 H, SiO-*C*H$_2$-*CH*$_3$) 1.22 (m, 2H, -NH-CH$_2$-*CH*$_2$-CH$_2$-Si-), 1.32 (s, 9H, C*H*$_3$-C-) 1.58 (m, 8H, C*H*$_2$-*CH*$_2$-C*H*$_2$-C*H*$_2$-CH$_2$-CO-NH-) 1.84 (m, 4 H, CH$_3$C*H*$_2$-C-), 2.16 (m, 2 H, -CH$_2$-CH$_2$-CH$_2$-CH$_2$-C*H*$_2$-CO-NH-), 3.24 (t, 2H, -NH-*CH*$_2$-CH$_2$-CH$_2$-Si-), 3.81 (s, 6H, CH$_3$-C*H*$_2$-O-Si-). ^{13}C NMR ($CDCl_3$): 7.7, 8.3, 18.1, 18.3, 18.7, 22.8, 23.6, 24.8, 25.4, 25.7, 29.4, 33.7, 41.8, 58.5, 109.5, 109.1, 109,9,173.3. Exact mass (M+1) 554.336; found 554.326.

5. Polyclonal antibodies for TATP

The polyclonal antibodies for TATP were obtained by the procedure described very recently by Walter et al.[S5] For immunizing purposes, hapten **II** was covalently attached, through its carboxylic acid moiety, to the lysine residues of BSA using a modification of the active-ester method. A mean coupling ratio of 14 hapten

molecules per BSA was thus achieved. The TATP-BSA conjugate was employed to immunize two 9–12 week old (2–2.5 kg) rabbits with sub-cutaneous injections, and 11 different sera of each rabbit were obtained. These sera were used to evaluate the titer and affinity maturation of the hapten-specific antibodies via ELISA, and bearing in mind these results, we selected the serum of the boost 11 as the best suited for the preparation of the antibody-capped hybrid materials.[S5]

6. Synthesis of functionalized mesoporous MCM-41 silica nanoparticles

Mesoporous MCM-41 nanoparticles were synthesized by the following procedure: *n*-cetyltrimethylammonium bromide (CTAB, 1.00 g, 2.74 mmol) was first dissolved in deionized water (480 mL). Then, NaOH (3.5 mL, 2.00 mol L^{-1}) in deionized water was added to the CTAB solution, followed by adjusting the solution temperature to 80ºC. TEOS (5.00 mL, $2.57 \cdot 10^{-2}$ mol) was then added dropwise to the surfactant solution. The mixture was stirred for 2 h to give a white precipitate. Finally, the solid product was centrifuged, washed with deionized water and ethanol, and dried at 60 ºC (MCM-41 as-synthesized). To prepare the final porous material (MCM-41), the as-synthesized solid was calcined at 550 ºC using an oxidant atmosphere for 5 h in order to remove the template phase.

Synthesis of S0 and S1. With the aim of loading the maximum amount of dye into the MCM-41 scaffolding, a solution of the dye sulforhodamine B sodium salt (1 mmol L^{-1}) was prepared in acetonitrile. Then, a portion of this solution (44 mL) was added to MCM-41 mesoporous nanoparticles (55 mg), obtaining a suspension with a concentration of dye of 0.8 mmol (g solid)$^{-1}$. The suspension was stirred for 24 h at room temperature. Subsequently, 6 mL of this suspension were centrifuged (10 min at 6000 rpm) and dried at 40 ºC for 12 h, yielding the final solid **S0**. The rest of the suspension (38 mL) were centrifuged (10 min at 6000 rpm) and concentrated in a final volume of 1.5 mL and 0.1 mL of a solution of hapten derivative **III** (0.04 mmol) in dichlorometane were added. The resulting suspension was stirred for 17 h at room temperature. Finally, the suspension was centrifuged (10 min at 6000 rpm), and the solid obtained (**S1**) was washed with

acetonitrile (0.75 mL), isolated by centrifugation, and dried at 35 ºC in vacuum during 12 h.

Synthesis and optimization of S1-AB. In order to determine the necessary amount of antibody for a nearly complete pore capping of **S1**, we prepared solutions of the serum of boost 11 in PBS containing 0.05% BSA and 345 ppm of sulforhodamine B (was added in order to minimize dye release from the pores during the capping process) using different dilutions (1/1000, 1/500, 1/400, 1/200, 1/100) at pH 7.6. Then, 0.15 mg of **S1** was suspended in 0.3 mL of each serum solution and stirred for 1 h at room temperature. Afterwards, the suspensions were centrifuged for 10 min at 9500 rpm. The solids obtained were washed with PBS (4 × 300 μL) in order to eliminate the residual dye from the uncapped mesopores. The prepared solids were separated by centrifugation.

The behaviour of the prepared capped materials was studied by suspending each solid in 300 μL PBS (**S1-AB** suspensions). Then, 50 μL of each suspension of **S1-AB** was diluted with 200 μL PBS and, for each suspension, a kinetic release of sulforhodamine B was recorded by measuring its fluorescence centred at 582 nm (λ_{exc} = 564 nm). An effective capping process was only observed when we used the 1/100 dilution of the serum, whereas dilutions of 1/200 or higher produced ineffective capping. Thus, we selected 1/100 as the optimum serum dilution for the preparation of the final capped material.

Bearing in mind this fact, we prepared the final **S1-AB** as follows: solid **S1** (1 mg) was suspended in PBS containing 0.05% BSA and 345 ppm of sulforhodamine B and serum 11 in a dilution 1/100 (2 mL). The suspension was stirred for 1h at room temperature, followed by centrifugation for 10 min at 9500 rpm. The final solid isolated was washed according to the same procedure as described above, to remove the dye from the uncapped pores (2 mL of PBS in each wash). Finally, the solid was dried in vacuum overnight and stored at 4ºC.

7. Characterization of materials

The prepared solids were characterized using standard techniques. Figure SI-7 (see manuscript) shows powder X-ray patterns of the solids MCM-41 as

synthesized, MCM-41 calcined, and **S1**. Due to the small amount of solid **S1-AB** prepared, PXRD of this material is not shown. The PXRD of nanoparticulate siliceous MCM-41 as-synthesized (curve a) shows the typical low-angle reflections that can be attributed to a hexagonal array that index as (100), (110), and (200) Bragg peaks, and from the XRD data of MCM-41 as-synthesized, a d_{100} spacing of 42.39Å was calculated. XRD powder of the calcined nanoparticulate MCM-41 sample (curve b) shows a significant displacement of the (100) peak corresponding to an approximate cell contraction of 2.89 Å, due to the further condensation of silanol groups during the calcination step. Curve c shows the XRD patterns for solid **S1**. The presence of the (100) peak in the XRD pattern indicates that the process of pore loading with sulforhodamine B and the additional functionalization with hapten **III** did not lead to a significant modification of the mesoporous structure of the MCM-41 support. However, reflections (110) and (200) are less intense, most likely due to a reduction of contrast as a consequence of the dye cargo in the pores and the attachment of **III**. TEM analysis also confirmed the preservation of the mesoporous structure in the functionalized solid **S1,** showing spherical particles with diameters from 80–120 nm, and the typical hexagonal porosity and channels of the MCM-41 matrix as alternating black and white stripes.

The N_2 adsorption-desorption isotherms of the calcined nanoparticulate MCM-41 material and **S1** are shown in Figure SI-8. This curve corresponds to a type IV isotherm, in which the observed step corresponds to nitrogen condensation inside the mesopores, with an adsorption step at intermediate P/P_0 values (0.25–0.4). The application of the BET model resulted in a value of 937.6 $m^2\ g^{-1}$ for the total specific surface, a *pore diameter* of 2.75 nm and *pore volume* of 0.75 $cm^3\ g^{-1}$. From the XRD, porosimetry and TEM studies, the a_0 *cell parameter* (4.56 nm), the pore diameter (2.75 nm), and the value for the wall thickness (1.81 nm) were calculated. The isotherm also shows another adsorption step at high relative pressure ($P/P_0 > 0.85$), which is associated to the filling of the large voids among the particles (pore diameter of 40.11 nm and pore volume of 0.51 $cm^3\ g^{-1}$ calculated by using the BJH model) and which must therefore be considered as

textural porosity. N_2 adsorption-desorption isotherm measurements on **S1-AB** were not carried out due to the low amount of material prepared. However, a further reduction in the specific surface area and pore volume is expected as a consequence of dye entrapment and antibody capping.

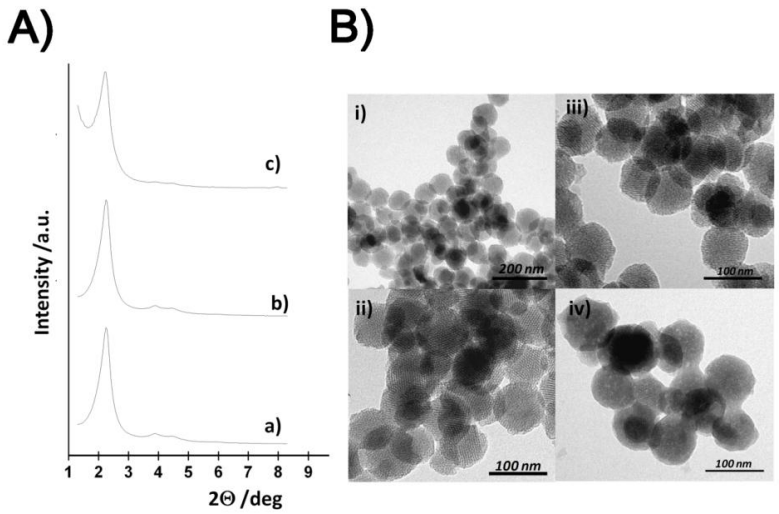

Figure SI-7. A) Powder X-ray patterns of the solids a) MCM-41 as synthesized b) calcined MCM-41 and c) solid **S1** containing the dye sulforhodamine B and hapten **III**. B) TEM images of calcined MCM-41 sample (i) and (ii), solid **S1** (iii) and solid **S1-AB** (iv), showing the typical hexagonal porosity of the MCM-41 mesoporous matrix.

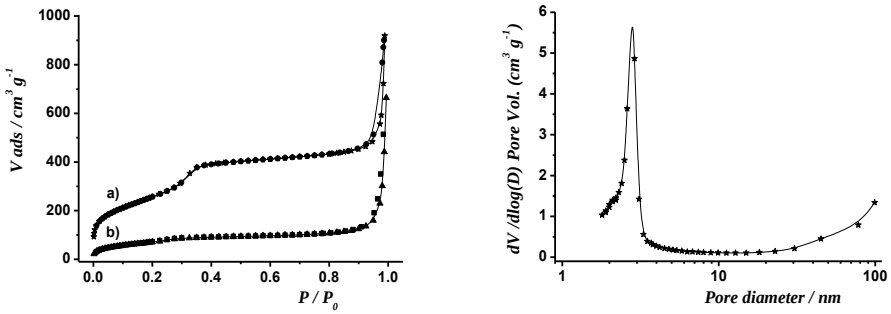

Figure SI-8. Left: Adsorption-desorption isotherms for a) MCM-41 and b) **S1**. Right: Pore size distribution of MCM-41

The content of **III** and dye in **S1** and of dye in **S0** was determined by elemental analysis and thermogravimetric analysis (TGA). In addition, thermogravimetric studies of **S1-AB** allowed us to estimate the antibody content of **S1-AB**. TGA of **S1-AB**, **S1** and **S0** show the typical behaviour of functionalised mesoporous materials; i.e., a first weight loss between 25 and 120 ºC related to the solvent escape, a second step, between 150 and 800 ºC, due to the combustion of the organics and a final loss in the 800–1000 ºC range related to the condensation of the silanol groups. The content of antibody in solid **S1-AB** was determined from TGA measurements, bearing in mind the content of **III** and sulforhodamine B in **S1**. In an indirect approach, we measured the concentration of IgG (immunoglobulin G), the most abundant type of antibody in the plasma, in the serum of boost 11 and in the aqueous solutions after the capping process through monitoring of the absorbance at 280 nm. Serum 11 contains the antibodies and other proteins, and the measurements give us the total content (content of antibody and other proteins). If we consider a typical MW for IgG of 150,000 Da and the corresponding molar absorption coefficient of immunoglobulin, a content of 55.3 mg of total protein (mL serum)$^{-1}$ was found. Taking into account TGA measurements, and assuming that all of the antibodies were incorporated in **S1-AB** when a dilution of serum of 1/100 was used, a content of IgG in the serum of 2.72 mg mL^{-1} was determined. This data is in good agreement with a typical content of IgG in rabbit serum, which ranges from 1–10 mg mL^{-1}.[S6] Contents of antibody, hapten derivative **III** and dye in **S0**, **S1** and **S1-AB** are listed in Table SI-1.

Table SI-1. Content of antibody, hapten derivative **III** and sulforhodamine B in mmol (g SiO_2)$^{-1}$ for **S0, S1** and **S1-AB.**

Solid	Hapten **III**	Sulforhodamine B	Antibody
S0	---	0.777	---
S1	0.170	0.749	---
S1-AB	0.170	0.309	5.18×10^{-4}

8. Antibody-TATP binding studies

According to Scatchard's model (eq. (1)),[S7] the ratio *r* corresponds to the average moles of TATP bound per (total) moles of antibody with ν accounting for the number of binding sites on the antibody, c_f being the free concentration of TATP and *K* the apparent equilibrium constant. If we further assume that TATP can exist in two forms, free and bound with $c_f = c_{total} - c_{bound}$, and that during the analysis the amount of TATP added is always in excess with respect to the amount of antibody present in the suspension so that $c_f >>> c_{bound}$, yielding the simplification $c_f \approx c_{added}$, eq. (1) can be linearized in the form of eq. (2):

$$r = \nu \frac{Kc_f}{1 + Kc_f} \qquad (1)$$

$$\frac{r}{c_f} = \nu K - rK \qquad (2)$$

Figure SI-9 shows the experimental response (symbols) and the fits obtained (solid lines) according to eq. (1) and (2) for $\nu = 1$ and an apparent $K = 4.5 \times 10^5\ M^{-1}$. For polyclonal antibodies as the ones used here, a Scatchard plot as that in Figure SI-7B often deviates from linearity because the binding sites of the antibodies in the sera show a certain heterogeneity and affinity distribution.

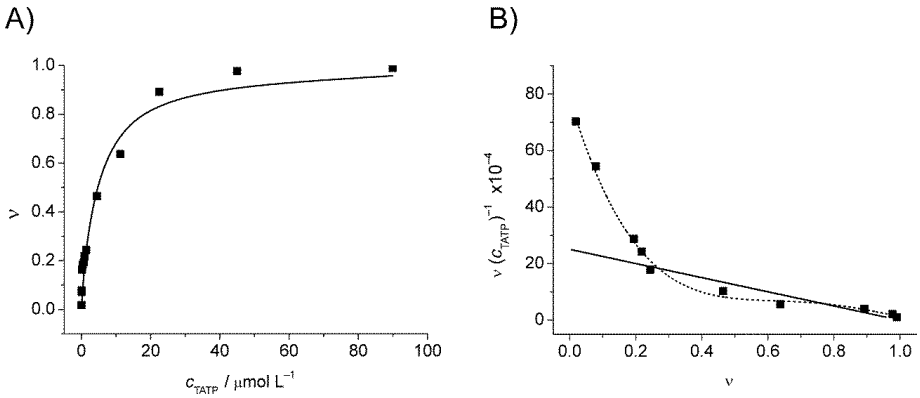

Figure SI-9. A) Binding isotherm of the TATP/**S1-AB** system and corresponding Scatchard plot (B). Fits as black solid line, trend as dotted line in B).

9. Lateral flow assay protocol

Strips of 0.5 × 2.5 cm were prepared and **S1-AB** was dispended (0.5 μL) on zone A from suspensions of the sensing material (2 mg mL^{-1}) with a micropipette (Figure SI-10). The strips were then dipped into the PBS-buffered sample solutions without or with varying concentrations of TATP and let to develop for 90 s. After the test the strips were dried (30 s with hair dryer in cold air blow mode or 8 min at normal room temperature), the fluorescence was measured using a flow assay reader at 625 nm (λ_{exc} = 520 nm). The amount of dye released for each concentration was calculated through the ratio between the fluorescence of zone A and zone B. The results obtained are depicted in Figure SI-2. When strips are developed from solutions containing TATP in a concentration down to 15 ppb, distinct fluorescence signals could be detected in zone B due to the selective uncapping of the pores in the presence of TATP and subsequent sulforhodamine release. In the absence of TATP, no signal was found in zone B. Dye released showed a linear dependence on TATP concentration in the 10–50 ppb range.

Figure SI-10. Photograph of manually dispensed spots (corresponding to zone A).
The tests of real tap water samples spiked with different amounts of TATP were run by measuring off 0.9 mL of spiked sample, adding 100 μL of a PBS 10X solution and running the normal lateral flow assay protocol. Addition of the buffer as aid largely allows the suppression of matrix effects and the determination of TATP down to 75 ppb.

The application of additional commercially available blocking, focussing or conjugation pads as well as the use of Tween as surfactant aid or specific

impregnation of the zone B area with a PBS 10X line had no beneficial effect on the strips' performance. On the contrary, for some of the approaches the flow was reduced, prolonging assay times.

The tests of real water samples spiked with different amounts of TATP were run by measuring off 0.9 mL of spiked sample, adding 100 µL of a PBS 10X solution and running the normal lateral flow assay protocol. Addition of the buffer as aid largely allows the suppression of matrix effects and the determination of TATP down to 75 ppb. The assessment of the interference of pH was tested as follows. Acidic and basic solutions were adjusted to the respective pH with either 0.25 M aqueous HCl solution or 0.1M aqueous KOH solution. Subsequently, 10 µL of TATP stock solution were added to 990 µL of the as-prepared pH solutions and gently shaken for 15min under ambient temperature. These solutions were used in the assay in the same way as the real water samples. For the tolerance tests toward ethanol, solutions containing 1–10 % ethanol were prepared in a similar manner and subjected to the assay also in the same way.

10. Relative measurement uncertainties and limits of detection

Because of the multiplicative and quotient forms of the respective equations and because correlations between the quantities are assumed to be negligible, summation of the squares of the relative uncertainties was performed.[S8]

10.1 Conventional assay

10.1.1 Preparation of suspensions and stock solutions:

a) Weighing of ca. 0.4 mg of **S1-AB** (balance Satorius supermicro Type S4: ± 0.0001 mg); u_{rel}^{w} = 0.025 %

b) Dissolving in 0.8 mL PBS (Eppendorf Reference pipette ± 0.007 mL); u_{rel}^{s} = 0.875 %

c) Weighing of ca. 100 mg of TATP (balance Satorius supermicro Type S4: ± 0.0001 mg); u_{rel}^{W} = 0.0001 %

d) Dissolving in 10 mL MeOH (Eppendorf Reference pipette ± 0.03 mL) for obtaining aTATP stock solution of 10 g L^{-1} in methanol; u_{rel}^{St} = 0.3 %

e) Diluting of stock solution in PBS for obtaining standard TATP solutions of 100 mg L^{-1} and 1.0 µg L^{-1} in PBS (Eppendorf Reference pipette ± 0.001 mL and 0.03 mL); u_{rel}^{d} = 0.3 % and 1 %

f) Preparing TATP standards in PBS (10 mL) from a solution of standard TATP 100 mg L^{-1}, by diluting it in water, starting from 20 mg L^{-1} to 1 µg L^{-1} (Eppendorf Reference pipette ± 0.03 mL) u_{rel}^{d} = 0.3 %

10.1.2 Assay execution and preparation of measurement solutions:

a) Division into aliquots of 0.4 mL (Eppendorf Reference pipette ± 0.006 mL); u_{rel}^{a} = 1.5 %

b) Mixing with 2.375 mL PBS (Eppendorf Reference pipette ± 0.01 mL); u_{rel}^{m} = 0.4 %

c) Fractionation of the suspension (0.25 mL) (Eppendorf Reference pipette ± 0.0035 mL); u_{rel}^{f} = 1.4 %

d) Transfer of the fractions into a 10 mm optical path length quartz cell:[S9] since no dilution step is involved, only contribution from cell length (± 0.01 mm); u_{rel}^{L} = 0.1 %

10.1.3 Fluorescence measurements:

a) Relative uncertainty of the emission spectrum across the respective wavelength range: u_{rel}^{em} ≤ 5 %

b) For the fluorescence intensities at λ_i, the maximum possible error amounts to; $u_{rel}^{em} / F^{\lambda_i}$ ≤ 0.05 %

10.1.4 Experimental standard deviation for replicate measurements: u_{rel}^{r} ≤ 2.6 %

10.1.5 Relative uncertainty:

$$u_{rel}^{ca\,2} = u_{rel}^{w\,2} + u_{rel}^{s\,2} + u_{rel}^{W\,2} + u_{rel}^{St\,2} + u_{rel}^{d\,2} + u_{rel}^{a\,2} + u_{rel}^{m\,2} + u_{rel}^{f\,2} + u_{rel}^{L\,2} + \left(u_{rel}^{em} / F^{\lambda_i} \right)^2 + u_{rel}^{r\,2}$$

$u_{rel}^{ca} \leq 6.3\ \%$

10.2 Lateral flow assay

10.2.1 Preparation of suspensions and stock solutions:

a) Weighing of ca. 2 mg of **S1-AB** (balance Satorius supermicro Type S4: ± 0.0001 mg); u_{rel}^{w} = 0.005 %

b) Dissolving in 1 mL PBS (Eppendorf Reference pipette ± 0.008 mL); u_{rel}^{s} = 0.8 %

c) Weighing of ca. 100 mg of TATP (balance Satorius supermicro Type S4: ± 0.0001 mg); u_{rel}^{W} = 0.0001 %

d) Dissolving in 10 mL MeOH (Eppendorf Reference pipette ± 0.03 mL) for obtaining aTATP stock solution of 10 g L^{-1} in methanol; u_{rel}^{St} = 0.3 %

e) Diluting of stock solution in PBS for obtaining standard TATP solutions of 100 mg L^{-1} and 1.0 µg L^{-1} in PBS (Eppendorf Reference pipette ± 0.001 mL and 0.03 mL); u_{rel}^{d} = 0.3 % and 1 %

f) Preparing TATP standards in PBS (10 mL) from a solution of standard TATP 100 mg L^{-1}, by diluting it in water, starting from 20 mg L^{-1} to 1 µg L^{-1} (Eppendorf Reference pipette ± 0.03 mL) u_{rel}^{d} = 0.3 %

10.2.2 Strip preparation:

a) Deposition of 5 µL of suspension onto the strip (Eppendorf Reference pipette ± 0.0003 mL); u_{rel}^{a} = 6.0 %

10.2.3 Assay execution:

a) Dilution of 0.05 mL TATP stock solution PBS (Eppendorf Reference pipette ± 0.01 mL); u_{rel}^{m} = 0.4 %

10.2.4 Fluorescence measurements: Relative uncertainty of the fluorescence intensities < 1 mV at maximum voltage (2000 mV): $u_{rel}^{em} \leq 5\ \%$

10.2.5 Experimental standard deviation for replicate measurements: $u_{rel}^{r} \leq 1.4\ \%$

10.2.6 Relative uncertainty:

$$u_{rel}^{ca\,2} = u_{rel}^{w\,2} + u_{rel}^{s\,2} + u_{rel}^{W\,2} + u_{rel}^{St\,2} + u_{rel}^{d\,2} + u_{rel}^{a\,2} + u_{rel}^{m\,2} + u_{rel}^{em2} + u_{rel}^{r\,2}$$

$u_{rel}^{ca} \leq 8.0\ \%$

10.3 Limit of detection

For the assessment of the limit of detection (LOD), we adhered to the IUPAC definition[S10]

$$x_{LOD} = \bar{x}_{blank} + 3s_{blank}$$

for which the lowest concentration detectable with >99 % confidence corresponds to a signal x_{LOD} that lies 3-times the standard deviation of blank measurements, s_{blank}, above the mean of the blank measures, $\bar{x}_{blank}$.

References

S1.- M. A. Walter, D. Pfeifer, W. Kraus, F. Emmerling, R. J. Schneider, U. Panne, M. G. Weller, *Langmuir* **2010,** *26*, 15418.

S2.- F. Dubnikova, R. Kosloff, J. Almog, Y. Zeiri, R. Boese, H. Itzhaky, A. Alt, E. Keinan, *J. Am. Chem. Soc.* **2005***, 127,* 1146.

S3.- A. Wierzbicki, E. Cioffi, *J. Phys. Chem. A* **1999,** *103*, 8890.

S4.- J. G. Tatake, M. M. Knapp, C. Ressler, *Bioconjugate Chem.* **1991,** *2*, 124.

S5.- M. A. Walter, U. Panne, M. G. Weller, *Biosensors* **2011***, 1,* 93.

S6.- R. W. Burry, *Immunocytochemistry. A Practical Guide for Biomedical Research,* **2010***,* Springer.

S7.- G. Scatchard, *Ann. N. Y. Acad. Sci.* **1949***, 51,* 660.

S8.- *Joint Committee for Guides in Metrology JCGM*, Paris. *Evaluation of Measurement Data—Guide to the Expression of Uncertainty in Measurement.* 1 Ed **2008**, corrected version **2010**.

S9.- Both, quartz and PMMA cells were used and were found to yield similar results.

S10.- *Limit of detection. IUPAC. Compendium of Chemical Terminology*, 2nd ed. Compiled by A. D. McNaught and A. Wilkinson. Blackwell Scientific Publications, Oxford (1997). XML on-line corrected version: http://goldbook.iupac.org (2006-) created by M. Nic, J. Jirat, B. Kosata; updates compiled by A. Jenkins. ISBN 0-9678550-9-8. doi:10.1351/goldbook.L03540.

4. Controlled Delivery using oligonucleotide-capped mesoporous silica nanoparticles

4.1 **Introduction.**

Progress in bio-molecular chemistry and nanotechnology has resulted recently in fabrication of bio-systems with innovative functions, offering for instance new perspectives for the development of advanced bio-related tools. A key issue in this field is the design of new "smart systems" based in nano-structures showing new fuctionalities using a variety of biomolecules. These systems may find use in many fields, including bio-engineering,[1] bio-sensing,[2] bio-nanotechnology,[3] drug delivery [4] and nanomedicine.[5]

Related with this general subject, in this chapter we report the development of a mesoporous material which has been capped with an oligonucleotide and in which the delivery of the previously entrapped cargo was triggered by the presence of the oligonucleotide complementary strand that induced hibridization between two oligonucleotides.

Before showing in detail the results of our research, in the next section we will display a brief introduction on DNA, its structure, properties and some techniques used for their detection.

---

[1] J. Bath and A. J. Turberfield, *Nat. Nanotechnol.*, **2007**, *2*, 275.

[2] A. P. R. Johnston, A. N. Zelikin and F. Caruso, *Adv. Mater.*, **2007**, *19*, 3727.

[3] R. P. Goodman, I. A. T. Schaap, C. F. Tardin, C. M. Erben, R. M. Berry, C. F. Schmidt and A. J. Turberfield, *Science*, **2005**, *310*, 1661.

[4] M. Nishikawa, S. Rattanakiat, Y. Takakura, *Adv. Drug Delivery Rev.*, **2010**, *62*, 626.

[5] R. Chhabra, J. Sharma, Y. Liu, S. Rinker and H. Yan, *Adv. Drug Delivery Rev.*, **2010**, *62*, 617.

4.1.1 DNA, a key object in life

Nucleic acids (DNA and RNA) are fundamental "molecules of life" as they play essential roles in gene regulation and expression. These molecules contain the genetic instructions used in the development of all known living organisms (with the exception of RNA viruses).

In order to fully understand the function of nucleic acids it is important to have a complete knowledge of its primary and secondary structure. Structure of nucleic acids of single strands show long chains formed by a succession of units called nucleotides, composed each one by a phosphate group, a sugar and a nitrogenous base (nucleobase).

Depending on the sugar, it is possible to diferenciate two types of nucleic acids, ribonucleic acids (RNA, containing ribose as its sugar) and deoxyribonucleic acid, (DNA, wich contains deoxyribose as its sugar). On the other hand, nucleobases are classified into two types: the purines Adenine (A) and Guanine (G), being fused five- and six-membered heterocyclic compounds, and the pyrimidines Cytosine (C) and Thymine (T), containing six-membered rings. A fifth pyrimidine nucleobase, uracil (U), is not usually found in DNA, and normally takes the place of thymine in RNA and differs from thymine by lacking a methyl group on its ring.[6]

Sugar is linked to the nucleobases with a β-glycosidic bond, and, depending on the nucleobases, it takes place between the N-9 of the nucleobase and the C-1' of the sugar in purines and between N-1 of the nucleobase and the C-1' of the sugar in pirimidines, whereas the nucleotides are linked by phosphonate groups through phosphodiester bonds between the third and fifth carbon atoms of adjacent sugar rings.[7] Finally, the asymmetric ends of DNA strands are called the 5' and 3' ends, having the 5' end a terminal phosphate group and the 3' end a terminal hydroxyl group. Normally sequences of nucleotides are written from 5' to 3' termini.

[6] J. Berg, J. Tymoczko, L. Stryer L, *Biochemistry,* **2002***, ed.* W. H. Freeman and Company.

[7] W. Saenger, *Principles of Nucleic Acid Structure*, **1984**, New York. Ed. Springer-Verlag.

A schematic representation of a single strand sequence of a DNA is shown in Figure 4.1.

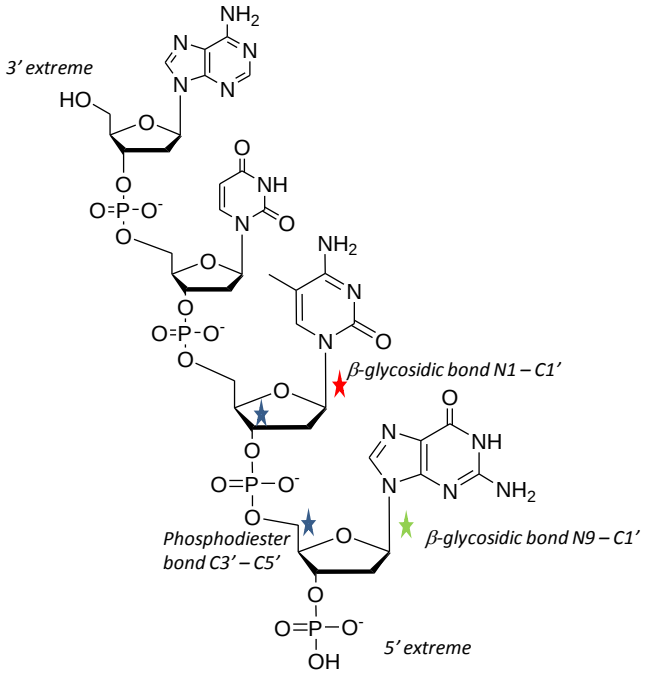

Figure 4.1. A schematic representation of a single strand sequence of DNA named as 5'-GCTA-3'.

As we can see, the primary structure of a nucleic acid comprises its covalent structure and nucleotide sequences. On the other hand, when two complementary strands of nucleic acids interact establishing non-covalent bonds, these strands are able to form a double-stranded molecule, knowing this process as hybridization. James D. Watson and Francis Crick described in 1953 the structure of double helix of DNA, a secondary structure of DNA that comprises two helical shapes. Double helix repeat its structure each 10 nucleotides, showing each base a 34° angle of rotation. Concerning distance values, the structure repeats after 34 Å, showing a diameter of the double helix of approximately 10 Å.[8] On the other hand, the direction of the nucleotides in one strand is opposite to their direction in the other strand, and, due to this, the strands are in a*ntiparallel*

[8] J. D. Watson F. H. C. Crick, *Nature,* **1953,** *171*, 737.

disposition. This property is essential in the processes of DNA replication and transcription.

In the DNA double helix, each type of nucleobase on one strand normally interacts with just one type of nucleobase on the other strand, calling to this phenomenum complementary base pairing. Purines form hydrogen bonds with pyrimidines, and, due to this, A bonds only with T, forming 2 hydrogen bonds, whereas C bonds only with G, forming three hydrogen bonds. As hydrogen bonds are not covalent, they can be broken and rejoined easily, having more stable chains of DNA when a high GC-content is present. A schematic representation of the double helix structure of DNA is shown in Figure 4.2.

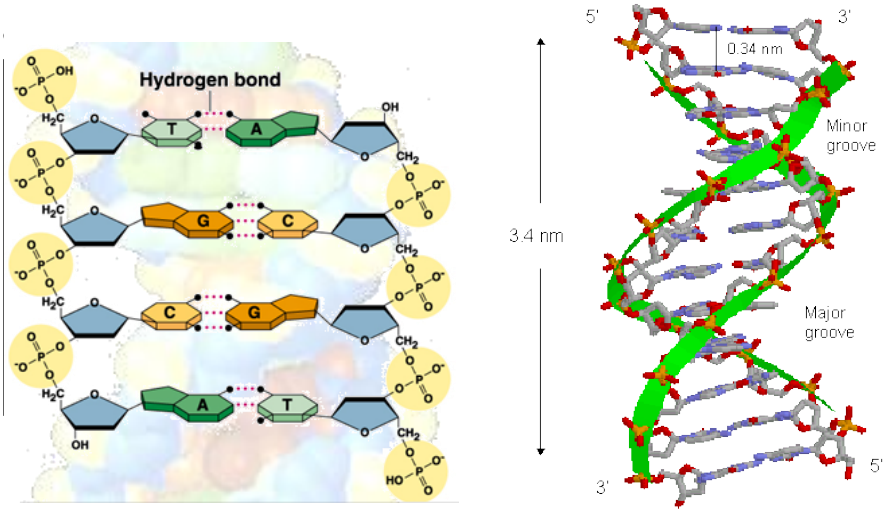

Figure 4.2.- Schematic representation of the structure of DNA double helix form.

Hydrogen bonds stabilized the double helix form, but the base-stacking interactions among the aromatic nucleobases also help to stabilize this structure. Stacking bases interact with each other through van der Waals forces. Despite of the energy associated with a van der Waals interaction is relatively small, a large number of atoms form part in such interactions in a helical structure. Due to this,

the net sum of the energy is quite substantial. In fact, these interactions produced an hipochromic effect: DNA absorbs very strongly at wavelengths close to UV light (around 260 nm), but a single stranded DNA absorb more UV light than that of a double-stranded DNA.[9]

The strength of interaction between two DNA strands can be measured by finding the temperature required to break the hydrogen bonds, called melting temperature or T_m value, wich is the temperature at which 50% of the double-strand DNA molecules (dsDNA) molecules are converted to single-strand (ss) molecules, and depends on ionic strength and the concentration of DNA. Content of CG base pairs also affect to the stability of dsDNA, whereas other important factors are the sequence (formation of base-stacking interactions among the aromatic nucleobases is different in each sequence), length (longer molecules offers more stability) and the stabilization of electrostatic repulsion of the negatively charged phosphate with Mg^{2+} or cationic proteins with abundant Arginine and Lysine residues that stabilizes the double helix.

4.1.2 DNA sensing: Immobilization of DNA onto solid supports.

Due to importance of DNA, scientists have worked in different fields in order to report the interaction of DNA with different molecules,[10] or have focused their attention on DNA sensing through immobilization of DNA onto solids supports, with the aim of prepare diferent materials for DNA diagnostics,[11] biosensors[12] or biochips[13] to investigate and control different reactions and interactions in which DNA is involved.

---

[9] P. Yakovchuk, E. Protozanova, M. D. Frank-Kamenetskii, *Nucleic Acids Res.,* **2006***, 34,* 564

[10] a) S. N. Georgiades, N. H. Abd Karim, K. Suntharalingam, R. Vilar, *Angew. Chem., Int. Ed.*, **2010**, 49, 4020. b) T. Tullius, *Nature*, **2009**, *461*, 1225.

[11] J.-H. Oh and J.-S. Lee, *Chem. Commun.*, **2010**, *46*, 6382.

[12] A. Sassolas, B. D. Leca-Bouvier and L. J. Blum, Chem. Rev., 2008, 108, 109.

[13] a) J. M. Brockman, A. G. Frutos and R. M. Corn, J. Am. Chem. Soc., 1999, 121, 8044. b) S. Singh-Gasson, R. D. Green, Y. Yue, C. Nelson, F. Blattner,M. R. Sussman, F. Cerrina, *Nat. Biotechnol.*, **1999**, *17*, 974. c) G. Hardiman, A. Carmen, *Drug Discovery Ser.*, **2007**, *7*, 1.

The immobilization of DNA includes the selection of a suitable substrate such as glass,[14] silicon,[15] diamond or glassy carbon[16] or gold[17] to which DNA is attached by physical adsorption[18] or covalent immobilization.[19] A number of systems have been reported in this subjet; however, the concept for use nucleic acids to develop bio-responsive controlled release systems is quite recent.

4.1.2.1 *Stimuli controlled release employing nucleic acids*

Thermo-responsive systems

As we have menctioned in the general introduction, Bein et al.[20] described thermo-responsive nanocontainers attaching covalently single-strand DNA (ss-DNA) onto surface of mesoporous silica nanoparticles to cap the pores via hybridization with a biotin-labeled DNA single-strand (Bio-ss-DNA). Additionaly the solid was loaded with fluorescein. The opening of the system was achieved by DNA strand melting at a specific melting temperature. The authors reported two different length oligonucleotides with 15 and 25 base pairs, having melting temperatures of 45ºC and 65ºC, respectively.

Most recently, another thermo-responsive gated material have been reported using a similar mechanism. In this work, Vallet-Regí et al.[21] prepared mesoporous silica nanoparticles loaded with fluorescein and containing in its surface a single-strand DNA. Complementary DNA sequence was attached to magnetic

[14] Y.-H. Rogers, P. Jiang-Baucom, Z.-J. Huang, V. Bogdanov, S.Anderson, M.T. Boyce-Jacino, *Anal.Biochem.*, **1999***, 266*, 23.

[15] a) T. Strother, R. J. Hamers and L. M. Smith, *Nucleic Acids Res.*, **2000**, *28*, 3535. b) T. Bocking, A. Kilian Kristopher, K. Gaus, J. J. Gooding, *Langmuir*, **2006**, *22*, 3494.

[16] W. Yang, O. Auciello, J. E. Butler, W. Cai, J. A. Carlisle, J. E. Gerbi, D. M. Gruen, T. Knickerbocker, T. L. Lasseter, J. N. Russell, L. M. Smith, R. J. Hamers, *Nat. Mater.*, **2003**, *2*, 63.

[17] D. Peelen, L. M. Smith, *Langmuir*, **2005**, *21*, 266

[18] X.-H. Xu, A. J. Bard, *J. Am. Chem. Soc.*, **1995**, *117*, 2627

[19] S. G. Wang, R. Wang, P. J. Sellin, Q. Zhang, Biochem. *Biophys. Res. Commun.*, **2004**, *325*, 1433.

[20] A. Schossbauer, S. Warncke, P. M. E. Gramlich, J. Kecht, A. Manetto, T. Carell, T. Bein, *Angew. Chem. Int. Ed.,* **2010**, *49*, 4734.

[21] E. Ruiz-Hernandez, A. Baeza, M. Vallet-Regi, *ACS Nano,* **2011**, *5*, 1259

nanoparticles (Au-Np-ssDNA). Hybridization between two strands allowed the authors to obtain the capping system. An increase of the melting temperature of the the double-stranded DNA (47ºC, wich corresponds to the upper limit of therapeutic hyperthermia) produced a release of the dye fluorescein. Finally, another DNA-capped material wich was able to respond to temperature and enzyme stimulus was reported by Qu and co-workers.[22] In this case, the authors prepared DNA-MSN conjugates loaded with rhodamine B. Uncapping and cargo release was achieved by thermal denaturation of the DNA duplex, or by addition of the DNase I enzyme.

pH-responsive systems

Formation of hydrogen bonds between doble-strand DNA oligonucleotides can be inhibited at low and high pH values. Based in this concept, Chen et al. employed a single stranded DNA with quadruplex structure to cap the pores of mesoporous silica nanoparticles.[23] At pH 5, the quadruplex structure of DNA inhibited cargo release, whereas at pH 8, cytosine residues are deprotonated, and DNA adopts the single-stranded form, allowing the release of the cargo.

Presence of ions as trigger

Bearing in mind that Hg^{2+} can bind to two thymine bases to form the stable T-Hg^{2+}-T duplex,[24] Zhang et al. developed DNA-functionalized silica nanoparticles for the sensitive and selective detection of Hg^{2+} in aqueous solution.[25] The authors loaded MCM-41 mesoporous silica nanoparticles with fluorescein, and anchored onto surface a single strand ss-DNA, that was able to hybridize with a linker-DNA complementary strand and cap the pore of the dye-trapped silica nanoparticles. In the presence of Hg^{2+}, the Linker-DNA prefered to form the more stable T-Hg^{2+}-T intramolecular duplex structure and therefore dehybridized from the ss-DNA, uncapping the MSN pore to release the dye.

---

[22] C. Chen, J. Geng, F. Pu, X. Yang, J. Ren, X. Qu, *Angew. Chem. Int. Ed.,* **2011**, *50*, 882.

[23] C. Chen, F. Pu, Z. Huang, Z. Liu, J. Ren, X. Qu, *Nucleic Acids Research*, **2011**, *39*, 1638.

[24] T. Li, S. Dong, E. Wang, *Anal. Chem*. **2009**, 81, 2144.

[25] Y. Zhang, Q. Yuan, T. Chen, X. Zhang, Y. Chen, W. Tan, *Anal. Chem.*, **2012**, *84*, 1956.

Using aptamers as taps

The use of aptamer-controlled release systems in mesoporous nanoparticles can be considered an extension of the nucleic acid-based cases. It is well-known that aptamers display biorecognition properties for specific targets that, in addition, can produce a switching of their structure. In particular, Zhu et al.[26] designed mesoporous silica nanoparticles loaded with fluorescein and capped with Au nanoparticles modified with an ATP aptamer (Au-Np-ATP aptamer). Upon addition of ATP, a release of the cargo is observed. This release is produced bearing in mind that Au-Np-ATP aptamer has more affinity for ATP than for the complementary strand. As a consequence, addition of ATP produces a displacement of Au-Np-ATP aptamer from the mesoporous material to solution, uncapping the pores of the mesoporous material and allowing release of fluorescein.

In a similar work, Schäfer and coworkers[27] designed a drug delivery system using silica mesoporous nanoparticles loaded with fluorescein and capped with an ATP aptamer with a hairpin structure. In this case the addition of ATP produced a swiching on the hairpin structure of the aptamer, from the duplex DNA strand to single-stranded DNA structure allowing fluorescein release from the pores to the solution. Figure 4.3 shows a sheme of nucleic acids and aptamer-target interactions that allows cargo controlled release.

[26] C. -L. Zhu, C. –H. Lu, X. –Y. Song, H. –H. Yang, X. –R. Wang, *J. Am. Chem. Soc.*, **2011**, *133*, 1278

[27] V. C. Özalp, T. Schäfer, *Chem. Eur. J.,* **2011**, *17*, 9893.

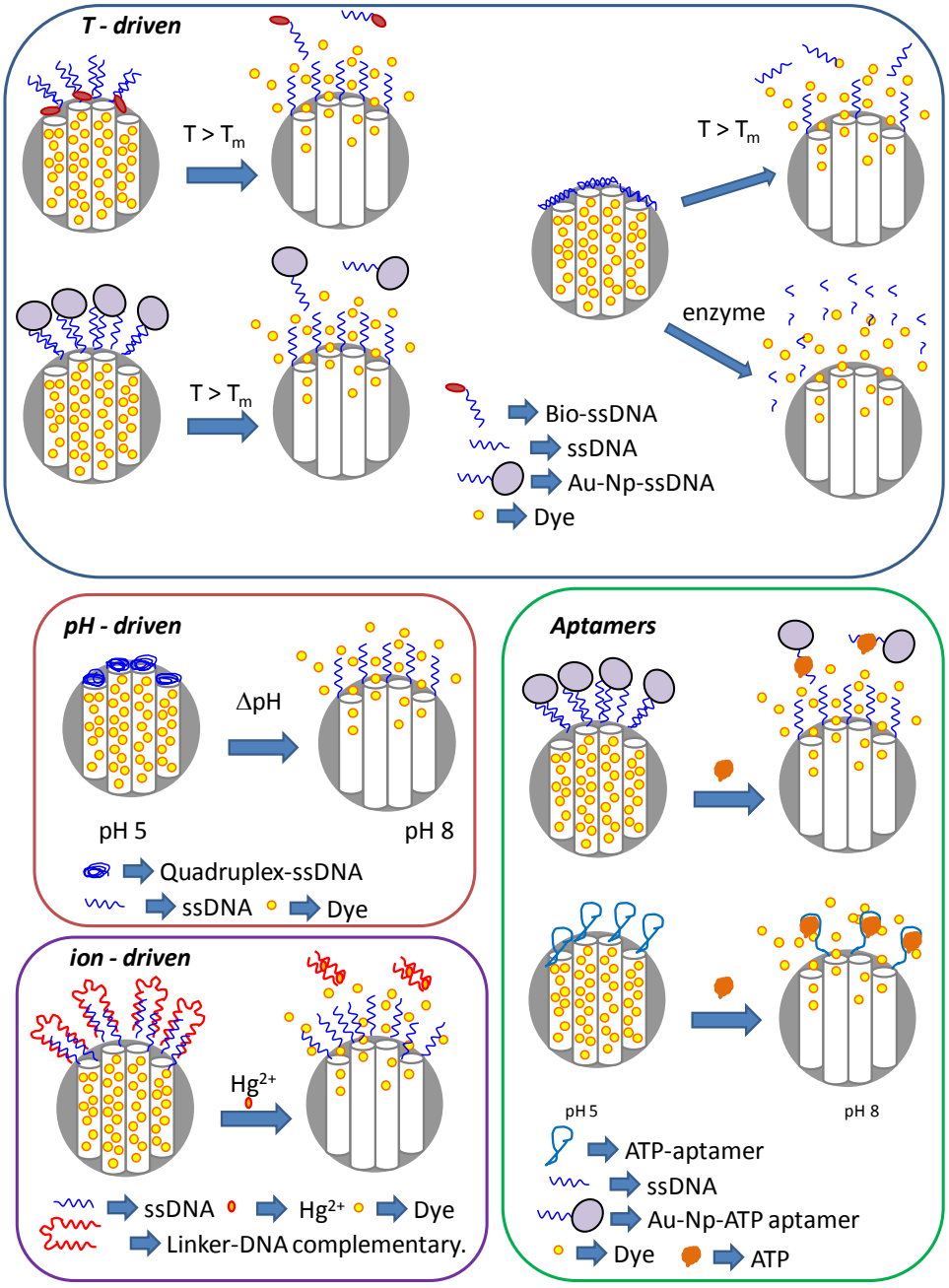

Figure 4.3. Schematic representation of nucleic acids and aptamer-target interaction that allows the controlled release of the entrapped guest.

4.2 **Objectives**

Bearing in mind the importance of nucleic acids, we aimed to develop hybrid organic-inorganic mesoporous materials in which cargo release could be triggered via hybridization between oligonuceotides. In fact when this work was developed there was not any example reporting delivery using nucleotides in mesoporous materials.

Specifically, our aim was:

- ✓ Design of a new organic-inorganic hybrid material able to release the cargo as a consequence of the hybridization of two oligonucleotides.
- ✓ Synthesis of the new organic-inorganic hybrid material using mesoporous silica nanoparticles as inorganic scaffold loaded with a dye and containing, onto their surface, an appropiate group able to interact with the oligonucleotide in order to cap the pores of the mesoporous material.
- ✓ Characterization of the new mesoporous organic-inorganic hybrid materials prepared.
- ✓ Evaluate the release of the dye from the prepared solid in the presence of the complementary oligonucleotide.

Controlled Delivery Using Oligonucleotide-Capped Mesoporous Silica Nanoparticles

Estela Climent,[a,b,c] Ramón Martínez-Máñez, [a,b,c] Félix Sancenón, [a,b,c] María Dolores Marcos, [a,b,c] Juan Soto, [a,b,c] Angel Maquieira, [a,b] and Pedro Amorós. [d]

[a] Instituto de Reconocimiento Molecular y Desarrollo Tecnológico. Centro Mixto Universidad Politécnica de Valencia – Universidad de Valencia.

[b] Departamento de Química, Universidad Politécnica de Valencia Camino de Vera s/n, 46022, Valencia, Spain.

[c] Centro de Investigación Biomédica en Red de Bioingeniería, Biomateriales y Nanomedicina (CIBER-BBN)

[d] Institut de Ciència del Materials (ICMUV), Universitat de València. P.O. Box 2085, E-46071 València, Spain

Received: March 29, 2010
Published online: August 24, 2010

Angewandte Chemie International Edition,

***2010**, 49, 7281 – 7283*

The design of delivery systems with “molecular locks” able to selectively release entrapped guests in the presence of target triggers has attracted great attention recently.[1] As an alternative to traditional polymer-based delivery systems, mesoporous silica supports show unique properties such as a large load capacity, biocompatibility, and potential for the development of gated supports for on-command delivery applications.[2] Recently, mesoporous-silica-based systems displaying controlled release have been reported relying on changes in pH, redox potential, and light for uncapping the pores.[3] However, the use of mesoporous silica supports equipped with gatelike scaffoldings is still an incipient area of research. In particular, despite some recent reported gated mesoporous silica supports that can be uncapped using antigens[4] or enzymes,[5] there is an almost complete lack of mesoporous-silica-based devices designed to trigger cargo release involving biomolecules. Within this context, our interest in the development of gated materials[6] motivated us to explore the possible design of new “bio-gates” able to respond selectively to “key” molecules. We focused our attention on the use of nucleotides.

The proposed paradigm is represented in Scheme **1**. In this work nanoparticles (ca. 100 nm) of mesoporous MCM-41 have been selected as the inorganic scaffold. The MCM-41 support is first loaded with a suitable guest (fluorescein), and then the external surface is functionalized with 3-aminopropyltriethoxysilane (APTS) to give the solid **S1**. Aminopropyl groups are partially charged at neutral pH in water and will interact with negatively charged oligonucleotides, resulting in the closing of the mesopores. The opening protocol will be expected to occur by a highly effective displacement reaction in the presence a target complementary strand; this will result in hybridization of the two oligonucleotides, the uncapping of the pores, and release of the entrapped cargo.

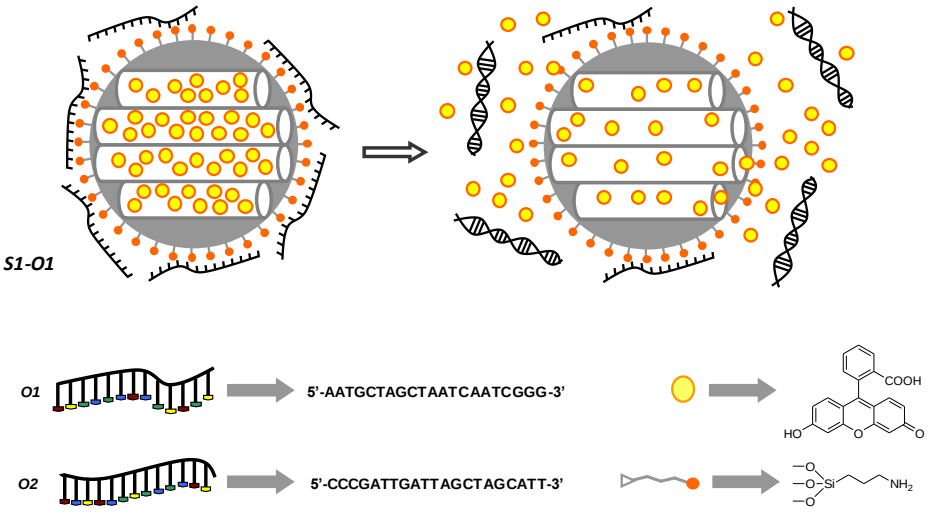

Scheme 1. Representation of the gated material **S1** functionalized with 3-aminopropyltriethoxysilane and capped with a single-stranded oligonucleotide (**O1**). The delivery of the entrapped guest (fluorescein) is selectively accomplished in the presence of the complementary oligonucleotide (**O2**). The sequence of the oligonucleotides **O1** and **O2** is shown.

The mesoporous solid **S1** containing fluorescein in the pore voids and functionalized on the external surface with APTS groups was characterized following standard procedures (see the Supporting Information). The powder X-ray diffraction (XRD) pattern of siliceous MCM-41 nanoparticles as synthesized (Figure **1**, curve a) shows four low-angle reflections typical of a hexagonal array which can be indexed as (100), (110), (200), and (210) Bragg peaks. A significant displacement of the (100) peak in the XRD pattern of the MCM-41 calcined nanoparticles is evident in curve b. Finally, curve c corresponds to the XRD pattern of **S1**. The (100), (110), and (200) peaks are clearly observed strongly suggesting that the dye loading and further functionalization with APTS have not damaged the three-dimensional mesoporous MCM-41 scaffolding.

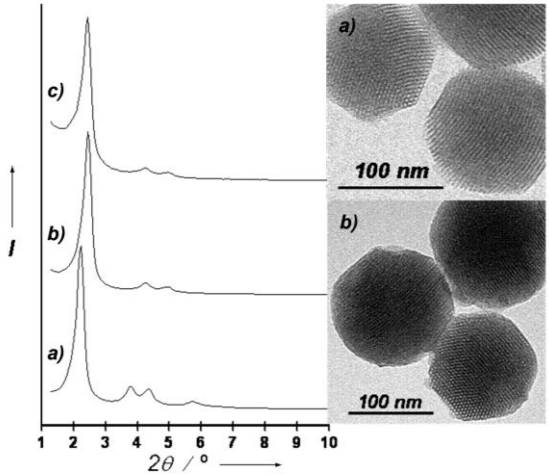

Figure 1. Left: powder X-ray patterns of the solids (a) MCM-41 as synthesized, (b) calcined MCM-41, and (c) solid **S1** containing the dye fluorescein and 3-aminopropyltriethoxysilane. Right: TEM images of calcined MCM-41 sample (a) and solid **S1** (b) showing the typical porosity of the MCM-41 mesoporous matrix.

The N_2 adsorption–desorption isotherms of the calcined MCM-41 nanoparticles show an adsorption step at an intermediate P/P_0 value (0.1–0.3) typical of this type of solid (see the Supporting Information). A pore volume of 0.61 $cm^3\,g^{-1}$ was calculated by using the BJH model on the adsorption branch of the isotherm. The application of the BET model resulted in a value for the total specific surface of 825 $m^2\,g^{-1}$. From the XRD, porosimetry, and TEM studies a pore diameter of 2.41 nm was determined. The N_2 adsorption–desorption isotherm of **S1** is typical of mesoporous systems with filled mesopores, and a significant decrease in the N_2 volume adsorbed and surface area (245 $m^2\,g^{-1}$) was observed.

For the preparation of the gated material **S1-O1**, 500 μg of **S1** was suspended in 500 μL of the hybridization buffer (20 mM Tris-HCl, 37.5 mM $MgCl_2$, pH 7.5)[7] containing the oligonucleotide **O1** (5′-AATGCTAGCTAATCAATCGGG-3′) for a final concentration of 0.026 mmol g^{-1} SiO_2. The final **S1-O1** solid was isolated by

centrifugation and washed with hybridization buffer (2×1 mL) to eliminate the residual fluorescein dye and the free oligonucleotide **O1.**

The quantities of dye and APTS on solid **S1** were determined by elemental analysis and thermogravimetric studies to be 0.078 and 1.98 mmol g^{-1} SiO_2, respectively. Additionally, the amount of oligonucleotide **O1** in solid **S1-O1** was determined by the use of the oligonucleotide **O1'** (5'-AATGCTAGCTAATCAATCGGG-Cy5-3'), which is similar to **O1** but marked with a Cy5 dye; the decrease of the fluorescence emission of **O1'** in solution was measured during the capping process. A content of 0.022 mmol of oligonucleotide per gram of SiO_2 was found.

To investigate the gating properties of **S1-O1**, 500 µg of this solid was suspended in 1 mL of the hybridization buffer, and the suspension was divided into two fractions. A 0.25 mL aliquot of the hybridization buffer was added to the first fraction. The second fraction was treated with 0.25 mL of hybridization buffer containing the target complementary oligonucleotide **O2** (5'-CCCGATTGATTAGCTAGCATT-3') in a concentration of 0.022 mmol g^{-1} SiO_2. In both cases the suspensions were stirred for 3 h at 37 °C. The gating mechanism was monitored through the measurement of the fluorescence emission of the released fluorescein. The delivery profile of fluorescein in the presence and absence of the target oligonucleotide is displayed in Figure **2**. As can be seen, solid **S1-O1** is tightly capped and shows a negligible release of fluorescein (curve a). In contrast, the presence of the complementary oligonucleotide **O2** induced the hybridization between **O1** and **O2**, the opening of the pores, and delivery of the dye (curve c). Curve c also shows that within 90 min more than 95 % of the fluorescein had been released (48 % of the total adsorbed fluorescein in solid **S1-O1**). Additionally, curve b displays the release profile of the fluorescein from **S1-O1** up until *t*=60 min, when suddenly **O2** at a concentration of 0.022 mmol g^{-1} SiO_2 was added to the solution.

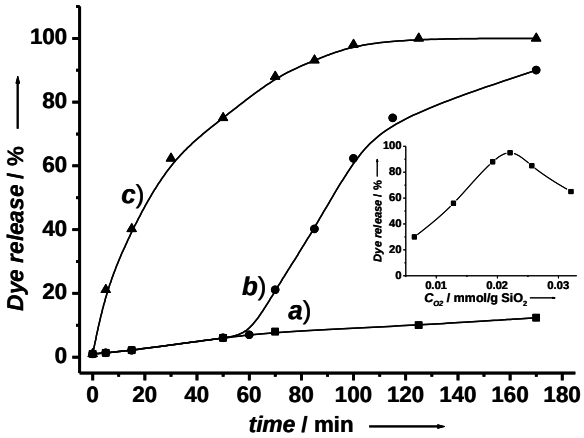

Figure 2. Release of fluorescein from solid **S1-O1** in the absence (a) and in the presence (c) of oligonucleotide **O2** (0.022 mmol g^{-1} SiO_2) in hybridization buffer (20 mM Tris-HCl, 37.5 mM $MgCl_2$, pH 7.5). Curve b shows the release profile of fluorescein from **S1-O1** in hybridization buffer until *t*=60 min when 0.022 mmol of **O2** g^{-1} SiO_2 was added. Inset: Percentage of released fluorescein dye from **S1-O1** as a function of the concentration of **O2** after 70 min of reaction.

The delivery of dye from **S1-O1** was also studied as a function of the amount of the molecular trigger (oligonucleotide **O2**, see inset in Figure **2**). It can be seen that the delivery of the cargo is proportional to the **O2** concentration. The maximum release was observed at an **O2** concentration of 0.022 mmol g^{-1} SiO_2; at higher concentrations the delivery was partially inhibited, most likely because excess **O2** was adsorbed onto the surface of the solid, inducing partial pore capping.

The uncapping mechanism (Scheme **1**) was also confirmed by using solid **S1-O1'** in which the pores had been capped with the Cy5-marked oligonucleotide **O1'**. Solid **S1-O1'** shows a blue coloration due to the Cy5 dye. After addition of the complementary single-strand oligonucleotide **O2** the solid became colorless, and the typical emission band of Cy5 centered at 670 nm (excitation at 649 nm) was observed in the aqueous phase indicating the release to the solution of the **O1'-O2** fragment, and excluding the possibility that double-stranded **O1'-O2** system remained adsorbed on the silica surface.

In order to investigate selectivity in the opening protocol, dye delivery from **S1-O1** was tested in the presence of other oligonucleotides similar to **O2**; that is, **O3** (5'-CCCGATTGATTCTCTAGCATT-3'), a two-base mismatch sequence, and **O4** (5'-CCCGATTGATTGGCTAGCATT-3'), an oligonucleotide with a single-base mismatch sequence. The uncapping ability of **O2**, **O3**, and **O4** (at a concentration of 0.022 mmol g^{-1} SiO_2) as a function of time is displayed in Figure **3**. The results show that only a remarkable release of dye was observed with **O2** (full hybridization with complementary **O1**), whereas the presence of **O3** and **O4** induced a poor uncapping of the pores. Moreover, we observed that the presence of random oligonucleotides did not induce dye delivery.

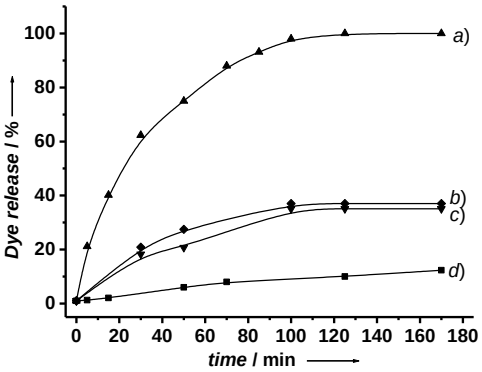

Figure 3. Emission intensity of released fluorescein dye from solid **S1-O1** in hybridization buffer (20 mM Tris-HCl, 37.5 mM $MgCl_2$, pH 7.5) in the presence of oligonucleotide **O2** (a), **O4** (b), and **O3** (c) at concentrations of 0.022 mmol g^{-1} SiO_2, and in the absence of oligonucleotide (d).

In summary, we have demonstrated that the use of oligonucleotides as caps on the surface of mesoporous supports is a suitable method for the preparation of "bio-gated" delivery systems that can be selectively opened in the presence of specific targets (i.e. the complementary oligonucleotide). The possibility of preparing similar systems on different supports and to select and easily synthesize tailor-made oligonucleotides makes this approach of interest in a wide range of timely research fields such as delivery protocols and diagnosis (recognition of certain oligonucleotide chains), and in the design of "keypad-lock-type" systems, which can be activated (opened) only with the correct combination of nucleotides.

References.

1. A.B. Descalzo, R. Martínez-Máñez, F. Sancenón, K. Hoffmann, K. Rurack, *Angew. Chem*. **2006**, *118*, 6068-6093; *Angew. Chem. Int. Ed.* **2006**, *45*, 5924-5948; b) I.I. Slowing, J. L. Vivero-Escoto, C. W. Wu, V. S.-Y Lin, *Adv. Drug Deliv. Rev.* **2008**, *60*, 1278-1288; c) E. Aznar, R. Martínez-Máñez, F. Sancenón, *Expert Opin. Drug Deliv*. **2009**, *6*, 643-655; d) K. Cotí, M. E. Belowich, M. Liong, M. W. Ambrogio, Y. A. Lau, H. A. Khatib, J. I. Zink, N. M. Khashab, J. F. Stoddart, *Nanoscale*, **2009**, *1*, 16-39; d) M. Vallet-Regi, F. Balas D. Arcos *Angew. Chem. Int. Ed*., **2007**, *46*, 7548-7558.
2. A. P. Wright, M. E. Davis, *Chem. Rev.* **2002**, *102*, 3589-3614; b) G. Kickelbick, *Angew. Chem.* **2004***, 116,* 3164-3166*; Angew. Chem. Int. Ed.* **2004**, *43*, 3102-3104; c) A. Stein, *Adv. Mater.* **2003**, *15*, 763-775.
3. For recent examples see for instance: a) R. Liu, Y. Zhang, X. Zhao, A. Agarwal, L.J. Mueller, P. Feng, *J. Am. Chem. Soc*., **2010**, *132*, 1500-1501; b) Y. Zhu, H. Liu, F. Li, Q. Ruan, H. Wang, M. Fujiwara, L. Wang, G. Q. Lu, *J. Am. Chem. Soc*., **2010**, *132*, 1450-1451; c) R. Mortera, J. Vivero-Escoto, I. I. Slowing, E. Garrone, B. Onida, V. S.-Y Lin, *Chem. Commun.* **2009**, 3219-3221; d) Y. Zhao, B. G. Trewyn, I. I. Slowing, V. S.-Y Lin, *J. Am. Chem. Soc*. **2009**, *131*, 8398-8400; e) R. Liu, X. Zhao, T. Wu, P. Feng, *J. Am. Chem. Soc*. **2008**, *130*, 14418-14419; f) F. Torney, B. G. Trewyn, V. S.-Y. Lin, K. Wang, *Nat. Nanotechnol.* **2007**, *2*, 295–300; g) I. I. Slowing, B. G. Trewyn, S. Giri, V. S.-Y Lin, *Adv. Funct. Mater.* **2007**, *17,* 1225-123; h) T. D. Nguyen, Y. Liu, S. Saha, K. C.-F Leung, J. F. Stoddart, J. I. Zink, *J. Am. Chem. Soc*. **2007**, *129*, 626-634; i) T. D. Nguyen, K. C. -F. Leung, M. Liong, Y. Liu, J. F. Stoddart, J. I. Zink, *Adv. Funct. Mater*. **2007**, *17*, 2101-2110.
4. E. Climent, A. Bernardos, R. Martínez-Máñez, A. Maquieira, M. D. Marcos, N. Pastor-Navarro, R. Puchades, F. Sancenón, J. Soto, P. Amorós, *J. Am. Chem. Soc.* **2009**, *131*, 14075-14080.
5. K. Patel, S. Angelos, W. R. Dichtel, A. Coskun, Y. –W. Yang, J. I. Zink, J. F. Stoddart, *J. Am. Chem. Soc.* **2008**, *130*, 2382-2383; b) A. Schlossbauer, J. Kecht, T. Bein, *Angew. Chem.* **2009***, 121,* 3138-3141*; Angew. Chem. Int. Ed.* **2009**, *48*, 3092-3095; c) A. Bernardos, E. Aznar, M. D. Marcos, R. Martínez-Máñez, F. Sancenón, J. Soto, J. M. Barat, P. Amorós, *Angew. Chem.* **2009***, 121,* 5998-6001; *Angew. Chem. Int. Ed*. **2009**, *48*, 5884 –5887; d) C. Park, H. Kim, S. Kim, C. Kim, *J. Am. Chem. Soc.* **2009**, 131, 16614-16615; e) P.D. Thornton, A. Heise, *J. Am. Chem. Soc*., **2010**, *132*, 2024-2028.
6. See for instance: a) R. Casasús, E. Climent, M. D. Marcos, R. Martínez-Máñez, F. Sancenón, J. Soto, P. Amorós, J. Cano, E. Ruiz, *J. Am. Chem. Soc.* **2008**, *130*, 1903-1917; b) C. Coll, R. Casasús, E. Aznar, M. D. Marcos, R. Martínez-Máñez, F. Sancenón, J. Soto, P. Amorós, *Chem. Commun***. 2007,** 1957-1959; c) R. Casasús, E. Aznar, M. D. Marcos, R. Martínez-Máñez, F. Sancenón, J. Soto, P. Amorós, *Angew. Chem.* **2006***, 118*, 6813-6816*; Angew. Chem. Int. Ed.* **2006**, *45*, 6661-6664; d) E. Aznar, C. Coll, M. D. Marcos, R. Martínez-Máñez, F. Sancenón, J. Soto, P. Amorós, J. Cano, E. Ruiz, *Chem. Eur. J*. **2009**, *15*, 6877-6888.
7. L.R. Hilliard, X. Zhao, W. Tan, *Anal. Chim. Acta*, **2002**, *470*, 51-56.

Angew. Chem. Int. Ed., 2010, 49, 7281-7283

Controlled Delivery Using Oligonucleotide-Capped Mesoporous Silica Nanoparticles.

SUPPORTING INFORMATION

Estela Climent, Ramón Martínez-Máñez, Félix Sancenón,
María Dolores Marcos, Juan Soto,
Angel Maquieira, and Pedro Amorós.

Chemicals

The chemicals tetraethylorthosilicate (TEOS), *n*-cetyltrimethylammonium bromide (CTAB), sodium hydroxide (NaOH), triethanolamine ($TEAH_3$), fluorescein, 3-aminopropyltriethoxysilane and the oligonucleotides **O1** (5'-AATGCTAGCTAATCAATCGGG-3'), **O1'** (5'-AATGCTAGCTAATCAATCGGG-Cy5-3'), **O2** (5'-CCCGATTGATTAGCTAGCATT-3'), **O3** (5'- CCCGATTGATTCTCTAGCATT-3'), and **O4** (5'-CCCGATTGATTGGCTAGCATT-3') were provided by Aldrich. Analytical-grade solvents were from Scharlab (Barcelona, Spain). All reactives were used as received.

General Techniques

XRD, TG analysis, elemental analysis, EDX microscopy, N_2 adsorption-desorption and UV-visible spectroscopy techniques were employed to characterize the prepared materials. X-ray measurements were performed on a Seifert 3000TT diffractometer using Cu-K_α radiation. Thermo-gravimetric analysis were carried out on a TGA/SDTA 851e Mettler Toledo equipment, using an oxidant atmosphere (Air, 80 mL/min) with a heating program consisting on a heating ramp of 10 °C per minute from 393 K to 1273 K and an isothermal heating step at this temperature during 30 minutes. N_2 adsorption-desorption isotherms were recorded on a Micromeritics ASAP2010 automated sorption analyser. The samples were degassed at 120ºC in vacuum overnight. The specific surfaces areas were calculated from the adsorption data in the low pressures range using the BET model. Pore size was determined following the BJH method. UV-visible spectroscopy was carried out with a Lambda 35 UV/vis spectrometer (Perkin-Elmer Instruments). Fluorescence spectroscopy was carried out on a Felix 32 Analysis Version 1.2 (Build 56) PTI (Photon Technology International) and UV-visible spectroscopy was carried out with a Lambda 35 UV/Vis Spectrometer Perkin Elmer Instruments.

Buffer solutions

Hybridization buffer consisting in 20 mM Tris-HCl, 37.5 mM $MgCl_2$ (pH 7.5) was used for controlled release experiences.

Synthesis of the silica mesoporous nanoparticles support

The MCM-41 mesoporous nanoparticles were synthesized by the following procedure: *n*-cetyltrimethylammoniumbromide (CTAB, 2.00 g, 5.48 mmol) was first dissolved in 960 mL of deionized water. Then a 7 mL of NaOH 2.00 M in deionized water was added to the CTAB solution, followed by adjusting the solution temperature to 95ºC. TEOS (10.00 mL, 5.14.10-2 mol) was then added dropwise to the surfactant solution. The mixture was allowed stirred for 3 h to give a white precipitate. Finally the solid product was centrifuged, washed with

deionized water and ethanol, and was dried at 60ºC (MCM-41 as-synthesized). To prepare the final porous material (MCM-41), the as-synthesized solid was calcined at 550 ºC using oxidant atmosphere for 5 h in order to remove the template phase.

Synthesis of S1

The amino-functionalised solid **S1** was prepared following literature procedures. 500 mg of calcined MCM-41 and 34.4 mg (0.10 mmol) of dye fluorescein were suspended in 50 mL of anhydrous ethanol inside a round-bottom flask connected to a Dean-Stark in an inert atmosphere. The suspension was refluxed (110 ºC) in azeotropic distillation, collecting 10 mL in the trap in order to remove the adsorbed water. Then, the mixture was stirred during 24 hours at 36ºC with the aim of achieving maximum loading in the pores of the MCM-41 scaffolding. Afterward an excess of 3-aminopropyltriethoxysilane (0.936 mL, 4.0 mmol) was added, and the suspension was stirred for 5.5h. Finally, the yelloy solid (**S1**) was filtered off, washed with ethanol, and dried at 70 ºC for 12h.

Synthesis and optimization of solid S1-O1

The optimization for the preparation of solid **S1-O1** was carried out measuring the decrease of the absorbance of **O1'** (5'-AATGCTAGCTAATCAATCGGG-Cy5-3') in the solution after the capping process. This capping process has been carried out in the presence of different amounts of **O1'**. In order to optimize the necessary amounts of oligonucleotide **O1**, portions of 500 μg of **S1** were suspended in 500 μl of a solution containing the oligonucleotide **O1'** in concentrations of (0.0064, 0.014, 0.019, 0.022, 0.026 and 0.033 mmol oligonucleotide **O1'**/g SiO_2) in hybridization buffer (20 mM Tris-HCl, 37.5 mM $MgCl_2$ at pH 7.5), and each suspension was stirred during 30 min at 37ºC, respectively. The resulting solids were isolated by centrifugation and washed with 2x1 mL of hybridization buffer to eliminate the residual dye and the free oligonucleotide **O1'**. Then, the absorbance of **O1'** in the different solutions were measured. Addition of concentrations as low as 0.019 mmol oligonucleotide **O1'**/g SiO_2 induced a suitable pore blockage. Nevertheless, at concentrations higher than 0.022 mmol oligonucleotide **O1'**/g

SiO_2 a residual value of the absorbance of Cy5 was measured. From this value a content onto the solid of 0.022 mmol oligonucleotide **O1'**/g SiO_2 was found. From these studies it was also found that a concentration of 0.022 mmol oligonucleotide /g SiO_2 was the optimal concentration in order to close all the mesopores of solid **S1**.

With the aim to obtain solid **S1-O1**, 500 μg of **S1** were suspended in 500 μl of a solution containing the oligonucleotide **O1** (5'-AATGCTAGCTAATCAATCGGG-3') in a concentration of 0.022 mmol oligonucleotide/g SiO_2 in hybridization buffer (20 mM Tris-HCl, 37.5 mM $MgCl_2$ pH 7.5), and the suspension was stirred at 37ºC during 30 min. The final **S1-O1** solid was isolated by centrifugation and washed with 2x1 mL of hybridization buffer (pH 7.5) in order to eliminate the residual dye and the free oligonucleotide **O1**.

Materials Characterization

Solid **S1** was characterized using standard procedures. Figure **1** in the manuscript shows powder X-ray patterns of the nanoparticulated MCM-41 support and the **S1** functionalised material. The PXRD of siliceous nanoparticulated MCM-41 as-synthesized (curve a) shows four low-angle reflections typical of a hexagonal array that can be indexed as (100), (110), (200), and (210) Bragg peaks. A significant displacement of the (100) peak in the XRD powder of the nanoparticulated MCM-41 calcined sample is clearly appreciated in the curve b, corresponding to an approximate cell contraction of 4 Å. This displacement and the broadening of the (110) and (200) peaks are related to further condensation of silanol groups during the calcination step. Finally, curve c corresponds to the **S1** XRD pattern. In this case, a slight intensity decrease and a broadening of the (110) and (200) reflections is observed, most likely related to a loss of contrast due to the filling of the pore voids with the fluorescein dye. Nevertheless, the value and intensity of the (100) peak in this pattern strongly evidences that the loading process with the dye and the further functionalization with APTS have not damaged the mesoporous 3D MCM-41 scaffolding. The presence in the final functionalized solids of the mesoporous structure is also confirmed from the TEM analysis, in

which the typical channels of the MCM-41 matrix are visualized as alternate black and white stripes (see Figure **1** in the manuscript). The figure also shows that the prepared MCM-41 and solid **S1** are obtained as spherical particles with diameters ranging from 100 to 200 nm.

The N_2 adsorption-desorption isotherms of the nanoparticulated MCM-41 calcined material shows an adsorption step at intermediate P/P_0 value (0.1-0.3) typical of this solids (see Figure **SI-1**). This step can be related to the nitrogen condensation inside the mesopores by capillarity. The absence of a hysteresis loop in this interval and the narrow BJH pore distribution suggest the existence of uniform cylindrical mesopores with pore volume of 0.61 $cm^3\ g^{-1}$ calculated by using the BJH model on the adsorption branch of the isotherm. The application of the BET model resulted in a value for the total specific surface of 825 m^2/g and a pore volume of 0.63 $cm^3\ g^{-1}$. From the XRD, porosimetry and TEM studies, the a_0 *cell parameter* (4.14 nm), the *pore diameter* (2.41 nm) and a value for the *wall thickness* (1.73 nm) were calculated. In addition to this adsorption step associated to the micelle generated mesopores, a second feature appears in the isotherm at a high relative pressure ($P/P_0 > 0.8$). This adsorption correspond to the filling of the large voids among the particles and present a volume of 0.25 $cm^3\ g^{-1}$ (calculated by using the BJH model) and then must be considered as a textural-like porosity. In this case, the curves show a characteristic H1 hysteresis loop and a wide pore size distribution.

The N_2 adsorption-desorption isotherm of **S1** is typical of mesoporous systems with filled mesopores (see Figure **SI**-**1**), and a significant decrease in the N_2 volume adsorbed and surface area (245 m^2/g) is observed. In fact, this solid shows flat curves when compared (at the same scale) to those of the MCM-41 parent material, this indicates a significant pore blocking and the subsequent absence of appreciable mesoporosity. Additionally, a certain textural porosity is preserved. BET specific surface values, pore volumes, and pore sizes calculated from the N_2 adsorption-desorption isotherms for MCM-41 and **S1** are listed in Table **1**.

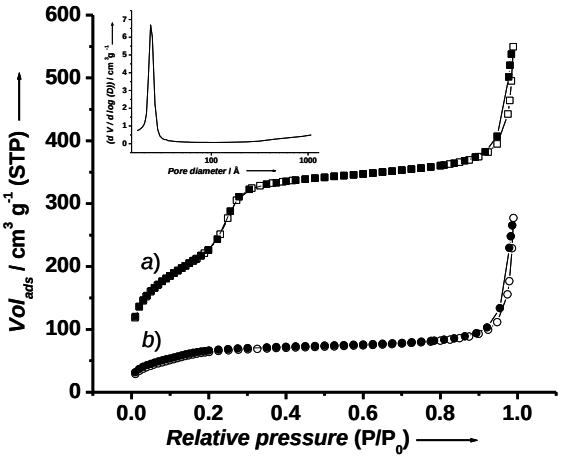

Figure SI-1. Nitrogen adsorption-desorption isotherms for (a) MCM-41 mesoporous material and (b) **S1** material. Inset: Pore size distribution of MCM-41 mesoporous material.

Table 1. BET specific surface values, pore volumes and pore sizes calculated from the N_2 adsorption-desorption isotherms for selected materials.

	S_{BET} ($m^2\ g^{-1}$)	**Pore Volume** [a] ($cm^3\ g^{-1}$)	**Pore size** [a] (nm)
MCM-41	825	0.68	2.41
S1	245	0.24	-

[a] Volume (V) and diameter (D) of mesopore.

The content of 3-aminopropyltriethoxysilane and fluorescein in the prepared solids **S1** and **S1-O1** were determined by elemental analysis, thermogravimetric and delivery studies. The content of dye in solid **S1-O1** was determined from the dye content is **S1** after interaction with the oligonucleotide **O1** by measuring the absorbance of the released fluorescein during the washing process of the solid. Also, the amount of dye delivered from **S1-O1** in the presence of oligonucleotides **O2**, **O3** and **O4** was determined by using the values of the fluorescence intensity bearing in mind that, at low concentrations, the ratio between concentration and intensity is linear. Values of content are detailed in Table **2**.

Table 2. Content of 3-aminopropyltriethoxysilane and fluorescein in the prepared solids **S1** and **S1-O1** in mmol/g SiO_2.

Solid	α_{APTS} (mmol/g SiO_2)	$\alpha_{Fluorescein}$ (mmol/g SiO_2)	α_{O1} (mmol/g SiO_2)
S1	1.98	0.078	-
S1-O1	1.98	0.036	0.022

Taking into account the different amounts of APTS and oligonucleotide **O1** in solid **S1-O1** we can estimate that **S1**-**O1** material contains 1.32 x 10^{19} oligonucleotide molecules/g SiO_2. Additionally, and according to a typical external surface for the solid MCM-41 of ca. 100 m^2/g and the oligonucleotide content calculated previously, the average surface coverage on solid **S1** by oligonucleotide molecules amounts to 0.13 molecules/nm^2. This oligonucleotide surface coverage resulted in an average distance between oligonucleotide molecules of about 2.7 nm. Additionally, if we used a value of 0.43 nm per base for single-stranded oligonucleotide[1] to calculate the length of **O1**, a value of 9 nm was estimated. Bearing in mind again a typical value of external surface of MCM-41 solids (ca. 100 m^2/g) and the content of APTS (in millimole/g SiO_2) calculated with elemental analysis and thermogravimetric studies, the average surface coverage on solid **S1** by APTS molecules amounts to 11.9 molecules/nm^2. With the oligonucleotide and APTS contents calculated previously a ratio of 91.5 APTS molecules / oligonucleotide molecules was estimated.

The ^{29}Si MAS-NMR spectrum of **S1** (Figure **SI**-**2**) confirms that the functionalization with 3-aminopropyltriethoxysilane occurs in a satisfactorily way. Indeed, the incorporation of the aminopropyl arms is probed by the existence of three resolved low-intensity signals in the -75 – -40 ppm δ range, which can be assigned to T^3, T^2 and T^1 silicon sites. In addition, the spectra of **S1** shows three signals centred at ca. -111, -99 and -93 ppm, which can be assigned to Q^4, Q^3 and Q^2 Si environments, respectively. A proportion of T^n sites of ca. 10.3% have been estimated from the NMR data, in very good accordance with the number calculated from elemental analysis and thermogravimetric techniques (10.6%).

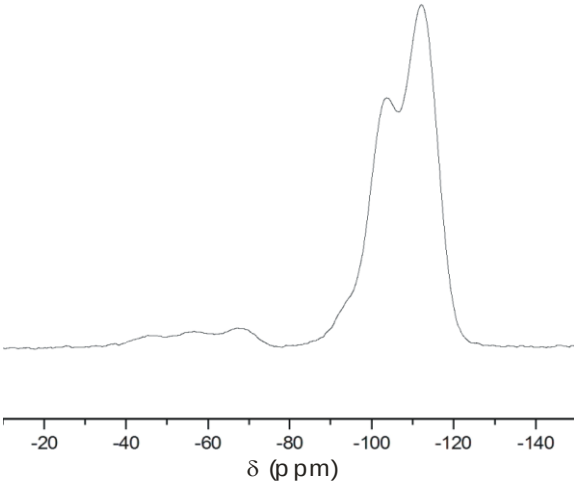

Figure SI-2. ^{29}Si MAS-NMR spectrum of **S1**.

References

1.- Tinland, B.; Pluen, A.; Sturm, J.; Weill, G.; *Macromolecules*, **1997**, *30*, 5763-5765.

5. Conclusions and perspectives

Design of stimuli-responsive nanostructured systems has recently attracted significant attention in areas such as controlled delivery and detection of target chemical species offering a wide range of future particular applications. This thesis has attempted to contribute to this field.

A general introduction showing the principles, perspectives, and recent developments in the field of supramolecular chemistry has been included. The effects induced by the incorporation of molecular entities on solid supports have been explained in order to understand the interactions involving the design of recognition/sensing and controlled release systems. At the end of the introduction a brief description of some significant hybrid materials for these aplications have been included.

The first chapter was focused on the design and preparation of new materials with the ability to control the access to their surface using supramolecular chemistry interactions. Following this concept, several materials for the recognition of certain chemical species have been reported using silica fumed and silica nanoparticles as inorganic supports. The design of the recognition system and the synthesis of the materials have been described. A detailed study of the response of the solids in the presence of target guest was carried out. Detection of pyrophosphate, heparin and anionic surfactants were achieved using these materials.

The remaining three chapters of the thesis focused on the design, synthesis and characterization of new gated hybrid materials. In all cases the materials were loaded with a dye and capped. Upon application of suitable stimuli cargo release was observed. Based in this general concept, in the second chapter we reported the synthesis of a novel probe for methylmercury using a gated hybrid solid that was opened via the strong affinity between this organic cation and thiol moieties. The design, synthesis and sensing features of the material were described. Furthermore, the probe was tested for the detection of methylmercury in extracts of fish tissues.

In the third chapter, three hybrid organic-inorganic mesoporous materials capped with antibodies were prepared and selectively opened in the presence of the corresponding antigens. Following this approach the detection of sulfathiazole (an antibiotic of the sulfonamides family), finasteride (a 5α-reductase inhibitor) and TATP (an explosive) were achieved. It might be interesting to remark that the system able to detect sulfathiazole was the first reported gated mesoporous system using antibodies as caps and the first example that suggested the possible use of such materials for the label-free detection of antigens. Moreover the sensing system for TATP was integrated in a rapid and simple lateral flow test with fluorescence readout.

Finally, the fourth chapter reported the design of a hybrid material in which the release was triggered by hybridisation between complementary oligonucleotides. In a similar way to other systems reported in previous chapters, the design, synthesis and response of the material was described. It might of importance to remark that this was the first reported example that used nucleotides in mesoporous materials for delivery aplications.

In summary, it can be concluded that new hybrid organic-inorganic solids and their application to the design of chromo-fluorogenic probes and controlled delivery systems have been described in this Thesis. It is believed that some of the results obtained here can be of future inspiration for the design of advanced hybrid materials for application in analytical chemistry, biotechnology or in clinical diagnostics.

Conclusiones y perspectivas.

El desarrollo de sólidos híbridos orgánico-inorgánicos funcionales es un campo de investigación relativamente nuevo que ha despertado un gran interés en los últimos años en áreas tales como la liberación controlada y la detección de especies químicas, ofreciendo un amplio rango de posibles aplicaciones. Teniendo esto en cuenta, esta tesis doctoral ha pretendido contribuir a la expansión de esta nueva línea de investigación.

En la introducción general se han presentado los principios, perspectivas y desarrollos recientes en el campo de la Química Supramolecular. Por otro lado se han mostrado los efectos que se producen debido a la incorporación de entidades moleculares sobre soportes sólidos, con la intención de facilitar la comprensión de los procesos de interacción que se producen en los procesos de reconocimiento de especies químicas o durante procesos de liberación controlada. Por otro lado, al final de la introducción se ha realizado una revisión bastante exhaustiva de los sólidos híbridos orgánico-inorgánicos desarrollados recientemente.

El primer capítulo se ha centrado en el diseño y preparación de nuevos materiales con la habilidad controlar el acceso a su superficie empleando interacciones químicas supramoleculares. Así, se han preparado diferentes materiales para el reconocimiento de aniones y surfactantes, empleando silica fumed y nanopartículas de sílice como soportes inorgánicos. En este capítulo se ha descrito el protocolo de reconocimiento y la síntesis de los respectivos materiales. Por otro lado, se ha realizado un estudio detallado de la respuesta de los materiales preparados en la presencia de los analitos a detectar (pirofosfato, heparina y surfactantes aniónicos).

Por otro lado, los ultimos tres capítulos se han centrado en el diseño, sintesis y caracterización de nuevos materiales híbridos con función de puerta molecular. En todos los casos los materiales preparados contienen en su interior un colorante que, mediante la aplicación de un estímulo externo, como la presencia de moléculas pequeñas, es liberado a la disolución. Teniendo en cuenta este concepto, en el segundo capítulo se ha preparado un nuevo material para la

detección de metilmercurio, teniendo en cuenta la afinidad existente entre el metilmercurio y los tioles. En este capitulo se detalla el diseño, la síntesis y la capacidad de detección del material. Además, se han realizado estudios de detección de metilmercurio empleando extractos de tejidos de pescado.

En el tercer capítulo se han preparado tres materiales utilizando anticuerpos como agentes responsables de modular la liberación de forma selectiva en presencia de los correspondientes antígenos. Utilizando estos materiales, se han desarrollado nuevos formatos de detección para los antígenos sulfatiazol (un antibiótico de la familia de las sulfonamidas), finasteride, (un inhibidor de la 5α-reductasa), y TATP (un explosivo). Cabe destacar, que el material preparado capaz de detectar sulfatiazol fue uno de los primeros ejemplos descritos que empleaba biomoleculas (anticuerpos) como agentes modulantes, siendo tambien el primer ejemplo que sugería el posible uso de estos sistemas para la detección sin marcaje de antígenos. Por otro lado, y con la finalidad de intentar mejorar el sistema de detección, el último material preparado, capaz de detectar TATP, se ha integrado en un test de flujo lateral con lector de fluorescencia.

Finalmente, el cuarto capítulo describe el diseño de un nuevo sistema de liberación controlada debido a la hibridación entre oligonucleótidos. Como en el resto de materiales presentados, en este capítulo se detalla el diseño, la síntesis y la respuesta del material. De nuevo, cabe destacar que este material fue el primer ejemplo descrito en que se empleaban oligonucleótidos sobre materiales mesoporosos para aplicaciones de liberación controlada.

En resumen, podemos concluir que en esta tesis se han descrito nuevos materiales híbridos orgánico-inorgánicos que se han aplicado para la detección cromo-fluorogénica de diferentes especies químicas y en procesos de liberación controlada. Alguno de los resultados obtenidos podrían contribuir en el diseño futuro de materiales híbridos para su posible aplicación en la química analítica, biotecnología o en el ámbito del diagnóstico clínico.